BEILSTEIN JOURNAL OF ORGANIC CHEMISTRY

Physical organic chemistry

Edited by John Murphy

Imprint

Beilstein Journal of Organic Chemistry
www.bjoc.org
ISSN 1860-5397
Email: journals-support@beilstein-institut.de

The *Beilstein Journal of Organic Chemistry* is published by the Beilstein-Institut zur Förderung der Chemischen Wissenschaften.

Beilstein-Institut zur Förderung der Chemischen Wissenschaften
Trakehner Straße 7–9
60487 Frankfurt am Main
Germany
www.beilstein-institut.de

Beilstein Journal of Organic Chemistry

Physical organic chemistry

John A. Murphy

Editorial

Open Access

Address:
WestCHEM, Department of Pure and Applied Chemistry, University of Strathclyde, 295 Cathedral Street, Glasgow G1 1XL, U.K

Email:
John A. Murphy - john.murphy@strath.ac.uk

Beilstein J. Org. Chem. **2010,** *6,* 1025.
doi:10.3762/bjoc.6.116

Received: 01 November 2010
Accepted: 01 November 2010
Published: 03 November 2010

Guest Editor: J. Murphy

Physical organic chemistry – the study of the interplay between structure and reactivity in organic molecules – underpins organic chemistry, and we cannot imagine organic chemistry as a subject without knowledge of mechanism and reactivity. It is sometimes thought that the golden age of 'physical organic chemistry' was in the 20th century, when systematic information about mechanism first burst onto the scene. Certainly the impact of early knowledge of mechanism of fundamental aliphatic substitution reactions, among others, was enormous, but our knowledge of reactivity and mechanism has continued to progress and deepen enormously ever since and this has been reflected in a number of Nobel Prizes in Chemistry. In an area of particular interest to me, the transformation of radical chemistry from being an almost impenetrable area to one that can be usefully harnessed even in synthetic applications, has been extraordinary – this transformation has been relatively recent and has been principally dependent on the accurate determination of kinetics of radical reactions.

Applications to complex reactions in biology, polymer chemistry and electronic materials are ever more prevalent, and add to contributions in 'small molecule' chemistry. Novel experimental techniques combined with the revolution in computational chemistry give new impetus to physical organic chemistry and contribute to its continuing importance, an importance that is reflected in the large number of international meetings in physical organic chemistry in the past two years.

I am privileged to act as Guest Editor for this Thematic Series of the Beilstein Journal of Organic Chemistry, and hope that you enjoy the papers that form this issue. I am grateful to the contributors for their contributions.

John A. Murphy

Glasgow, November 2010

Beilstein Journal of Organic Chemistry

Structure and reactivity in neutral organic electron donors derived from 4-dimethylaminopyridine

Jean Garnier[1], Alan R. Kennedy[1], Leonard E. A. Berlouis[1], Andrew T. Turner[2] and John A. Murphy[*1]

Full Research Paper

Open Access

Address:
[1]WestCHEM, Department of Pure and Applied Chemistry, University of Strathclyde, 295 Cathedral Street, Glasgow G1 1XL, U.K. and [2]PR&D Laboratory Building, AstraZeneca, Silk Road Business Park, Charterway, Macclesfield SK10 2NA, United Kingdom

Email:
Jean Garnier - jeangarn@hotmail.com; Alan R. Kennedy - a.r.kennedy@strath.ac.uk; Leonard E. A. Berlouis - l.berlouis@strath.ac.uk; Andrew T. Turner - andrew.t.turner@astrazeneca.com; John A. Murphy* - john.murphy@strath.ac.uk

* Corresponding author

Keywords:
dication; 4-DMAP; electron donor; electron transfer; radical cation; redox; reduction

Beilstein J. Org. Chem. **2010,** *6,* No. 73. doi:10.3762/bjoc.6.73

Received: 27 April 2010
Accepted: 09 June 2010
Published: 05 July 2010

Guest Editor: J. Murphy

Abstract

The effects on the redox properties of modifying the molecular skeleton of neutral bis-2-(4-dimethylamino)pyridinylidene electron donors, derived from 4-dimethylaminopyridine (4-DMAP), have been explored, by varying two parameters: (i) the length of a polymethylene chain linking the two pyridine-derived rings and (ii) the nature of the nitrogen substituents on the 4 and 4′ positions of the precursor pyridines. Restricting the bridge length to two methylene units significantly altered the redox profile, while changes in the nitrogen-substituents at the 4 and 4′ positions led to only slight changes in the redox potentials.

Introduction

Neutral organic compounds **1** and **4**–**10** (Figure 1) have attracted considerable attention as ground-state electron donors [1-38], and many are now being employed as reagents in organic transformations. Such a range of reagents with different redox potentials leads to the expectation of considerable selectivity in their reductions of organic substrates, and evidence is steadily accumulating to support this. Tetrathiafulvalene (TTF, **1**, $E^1_{1/2}$ = 0.37 V; $E^2_{1/2}$ = 0.67 V in DCM vs SCE) [1], one of the weakest of these donors, reduces arenediazonium salts to aryl radicals [2-12], but is not strong enough to react with alkyl and aryl halides. The driving force for its oxidation is the attainment of some degree of aromaticity in the formation of its radical cation salt **2** on the loss of one electron, and full aromaticity in its dication salt **3** on loss of two elec-

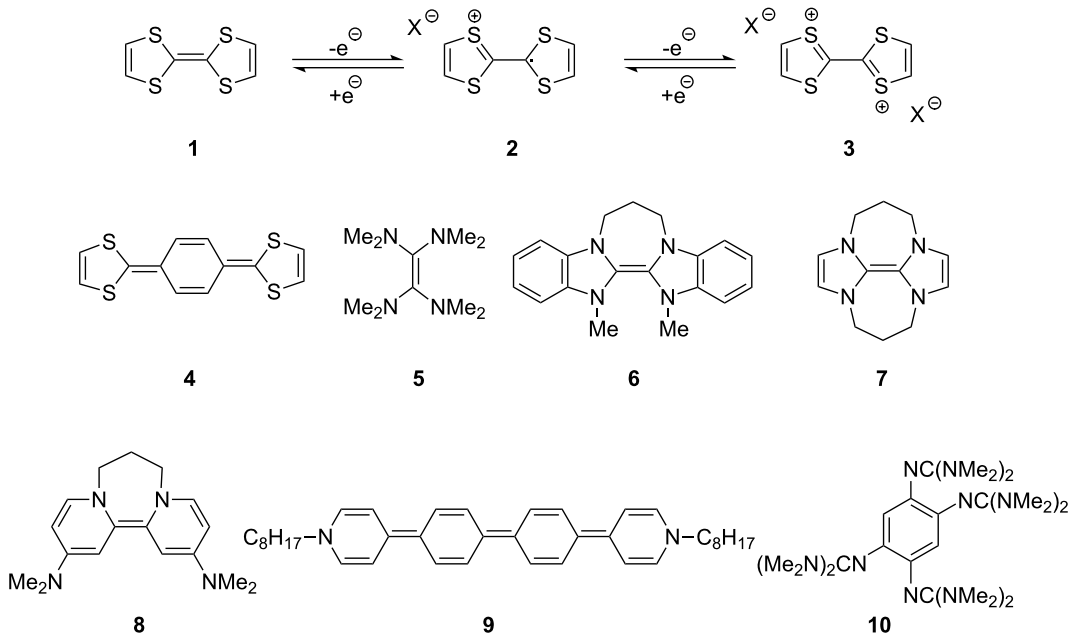

Figure 1: Neutral organic electron donors **1** and **4**–**10**.

trons, as well as the stabilization of both the positive charge and radicals by the lone pairs on the sulfur atoms. The effect of aromatic stabilization is enhanced in the extended analogue **4**; however, unlike TTF, this compound affords only an irreversible oxidation E_p = −0.14 V in MeCN (assuming that the reported value is measured relative to SHE, that would correspond to −0.38 V vs SCE) [13]. Tetrakis-dimethylaminoethene (TDAE, **5**: $E^1_{1/2}$ = −0.78 V; $E^2_{1/2}$ = −0.61 V vs SCE in MeCN) is a stronger reducing agent and converts electron-deficient alkyl bromides to the corresponding anions [14-17] and notably the iodide CF_3–I to trifluoromethyl anion, $^-CF_3$, [15] but is not powerful enough to react with aryl halides. Despite not experiencing any aromatic stabilization on oxidation, the molecule is such a good donor as a result of the ability of the nitrogen atoms in **5** to stabilize both the positive charge and an unpaired electron upon oxidation; this stabilization is greater than is afforded by sulfur in TTF.

Benzimidazole-derived donor **6** ($E^1_{1/2}$ = −0.82 V; $E^2_{1/2}$ = −0.76 V vs SCE in DMF) [18-20], combines the stabilization of positive charge and of an unpaired electron provided by four nitrogens, with aromatic stabilization in its oxidised forms. This exceptional donor has the power to reduce aryl iodides (E^0 = −2.2 V) to aryl radicals, but not to aryl anions [21]. This is paradoxical in view of the standard potential of the second step; E^0 = 0.05 V vs SCE in MeCN for the conversion of an aryl radical to an aryl anion [39]. Whatever about the standard potentials, in practice, the formation of aryl anions is only observed when the electron donor has $E_{1/2}$ = −1 V or is more negative [40]. In line with this, both the imidazole-derived donor **7** ($E_{1/2}$ = −1.20 V vs SCE in DMF) [22-25] and the 4-dimethylaminopyridine (4-DMAP)-derived donor **8** [$E_{1/2}$ (DMF) = −1.69 V vs Fc/Fc^+] [26-29], which would equate to −1.24 V vs SCE [E $(DMF)_{Fc/Fc+}$ = 0.45 V vs SCE] [41] react with aryl iodides to afford aryl anions. As an indication of their enhanced donor properties, these two donors can also cleave appropriate arenesulfonamides [25], aryl alkyl sulfones [25,26], Weinreb amides [28] and acyloin derivatives [29]. They are also prone to transfer two electrons rather than one, with the cyclic voltammogram (c.v.) of **8** showing a single 2-electron reversible redox wave [26] while in donor **7** the potentials of the successive electron transfers are close enough that the c.v. gives the appearance of a single reversible peak, but has a slight shoulder [24]. Molecules **9** ($E_{1/2}$ = −1.00 V vs SCE in DMF) [30-32] and **10** [33,35,37] extend the range of designs of neutral organic electron donors, although we are not aware of them being investigated as yet for the reduction of organic substrates.

In order to design both more potent electron donors, and donors with calibrated and targeted properties, the factors that drive the electron transfer(s) need to be clearly understood, and this paper now probes two factors that could impact on that.

Results and Discussion

Donor **8** has a number of attractive features. It is simply prepared from the reaction of 4-DMAP with 1,3-diiodopropane, followed by treatment of the product with base [26-28]. A wide range of analogues of 4-DMAP, which have been well studied in acylation chemistry [42,43], is already available. This suggests that preparation of analogues of **8** should also be straightforward. Hence, donor **8** was selected as the target for modification. The effect of modifying the length of a polymethylene chain linking the two pyridine-derived rings and the nature of the substituents on the 4- and 4′-positions of those pyridine rings were the points of particular interest. TDAE, **5**, has been used extensively as a two-electron transfer reagent, and many salts that feature its dication have been analysed by X-ray crystallography [44]. In these dications, the two ends of the molecule are twisted extensively to minimize interaction between the two positive charges. It is tempting to think that the degree of twist is linked to the power of the reducing agent. If twisting was not possible, then the driving force for removal of the second electron, for the conversion of the radical cation to the dication, should be diminished. To see if the same twist occurs with our donor **8**, the crystal structure of the disalt **17** was determined [twist (N–C–C–N = 52.5(3) degrees] (Figure 2). The degree of twist is limited by the three-carbon chain – a longer chain should afford greater flexibility and might afford a stronger donor, mirroring the findings of Ames et al. with a different series of compounds [18-20,22]. In contrast, shortening the polymethylene chain as in **14** should constrain rotation of the pyridine rings in the dication **16**, and hence make formation of **16** more difficult. To determine the effect of bridge-length on redox potential, the analogous donors **14** and **15** were prepared in situ and converted to their respective oxidized salts **16** and **18**, as shown in Figure 2, by reaction with iodine. Anion exchange to afford the corresponding hexafluorophosphate salts **16′** and **18′** was then carried out prior to cyclic voltammetry. (The iodide anions were exchanged since iodide ions would be electrochemically active, albeit at more positive potentials than feature in our studies.)

Cyclic voltammetry studies were carried out by adding deoxygenated solutions of the oxidized disalts **16′**–**18′** (rather than the electron donors) to the electrochemical cell and then carrying out the electrochemistry under an inert gas. The donors themselves are highly sensitive to traces of oxygen, and so are less convenient to weigh out than the disalts. All of the cyclic voltammograms showed reversible redox chemistry, featuring the transfer of two electrons, as indicated by calibration with ferrocene/ferrocenium (Fc/Fc^{+}).

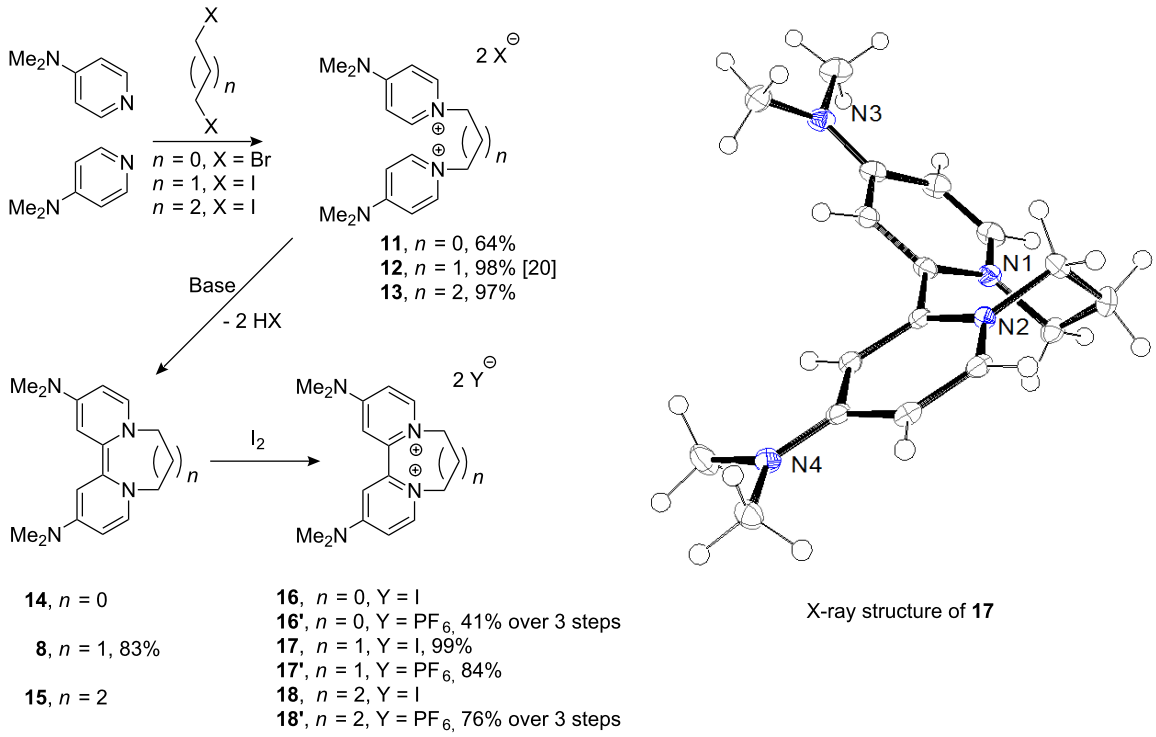

Figure 2: Formation of donors and oxidation to form diiodide salts, together with the ORTEP diagram of diiodide salt **17** (only the cation is shown).

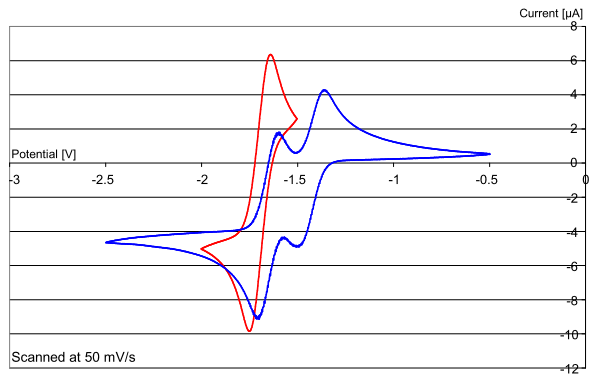

Figure 3: Cyclic voltammograms vs Fc/Fc^+ of **17′** ↔ **8** (red) and **16′** ↔ **14** (blue).

Restricting the bridge length to two carbons made donor **14** a less effective reducing agent (Figure 3) compared to **8**, underlining the importance of flexibility of the inter-ring bond. Here, donor **8** shows a single two-electron wave [$E^1_{1/2}$ (DMF) = −1.24 V vs SCE (calibrated using Fc/Fc^+)], while donor **14** shows two one-electron waves [$E^1_{1/2}$ (DMF) = −1.21 V, and $E^2_{1/2}$ (DMF) = −0.98 V vs SCE (calibrated using Fc/Fc^+)]. The potential for loss of the first electron is similar in both compounds; however, the loss of the second electron from **8** is about 300 mV more negative than from **14**. This indicates a greater driving force for loss of the second electron in **8** than in **14**, consistent with the predicted difficulty in forming **14** as an essentially planar dication, where repulsion between the two charges would be more severe.

In contrast, comparison of the cyclic voltammograms of **18′** and **17′** (Figure 4a) showed only minor differences, with both showing a single wave corresponding to a two-electron reversible process at essentially the same potential (within 10 mV), so the increased flexibility does not benefit the two-electron donor **15** relative to **8**. Taking the idea of flexible rotation between the two halves of the molecule to its limit, we prepared compound **20′** [27] (Figure 5) and determined its cyclic voltammetric behaviour. As shown in Figure 4b, this [$E_{1/2}$ (DMF) = −1.27 V vs SCE (calibrated using Fc/Fc^+)] shows little difference from that of **17′**. [$E_{1/2}$ (DMF) = −1.24 V vs SCE (calibrated using Fc/Fc^+)]. Accordingly, permitting a freer rotation than seen in **17′** by extending the tether between the two pyridine-derived rings does not lead to enhanced donor properties.

The other site of relatively easy variation in **8** was the dialkylamino group. 4-Pyrrolidinopyridine and 4-guanidinopyridine are significantly better catalysts [42,43] in acylation reactions than 4-DMAP. Their effectiveness depends on the delocalization of the electron pair on the 4-substituent into the pyridine ring. Accordingly, the disalts **21** and **22** were prepared from these 4-substituted pyridines [43,45] and converted into their hexafluorophosphates **21′** and **22′**, and then examined by cyclic voltammetry. Each showed a reversible two-electron redox wave (Figure 6). Redox equilibria related to **21** showed that the corresponding donor **23** was a stronger donor than donor **8** by about 90 mV for the transfer of its first electron, while the second electron occurs at the same potential as seen for donor **8**, while **24** transferred both of its electrons at the same potential and was within 10mV of **17′**.

The reactivity of these two donors was also investigated with substrate **27**. Here, **23** and **24** were prepared in situ from **25′** and **26**. This afforded the reductive de-iodination product **28** in good yield (84% when using **25′**, and 68% when using **26**).

These results are in accord with the previous reactions of donor **8**, and show that significantly more powerful donors than **8** cannot be attained simply by altering the tether length between the two pyridine units. Similarly, simple modifications to the

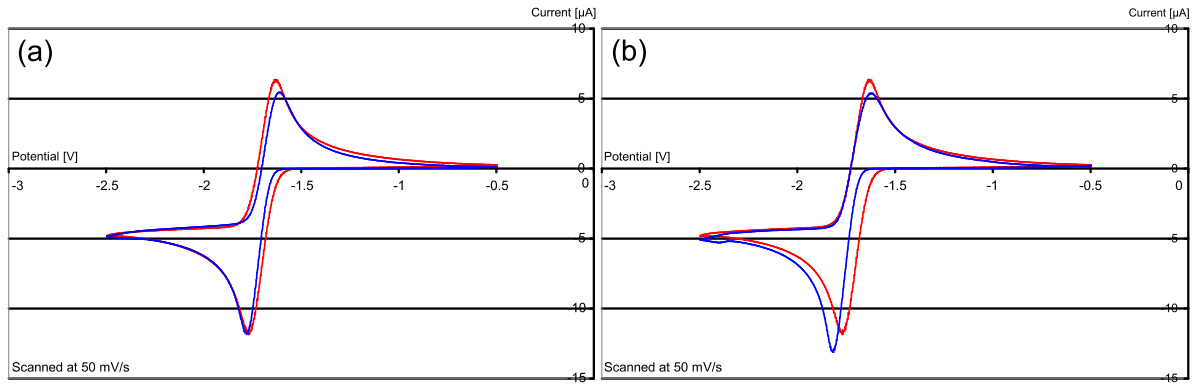

Figure 4: (a) Cyclic voltammograms vs. Fc/Fc^+ of **17′** ↔ **8** (red) and **18′** ↔ **15** (blue) and (b) of **17′** ↔ **8** (red) and **20′** ↔ **19** (blue).

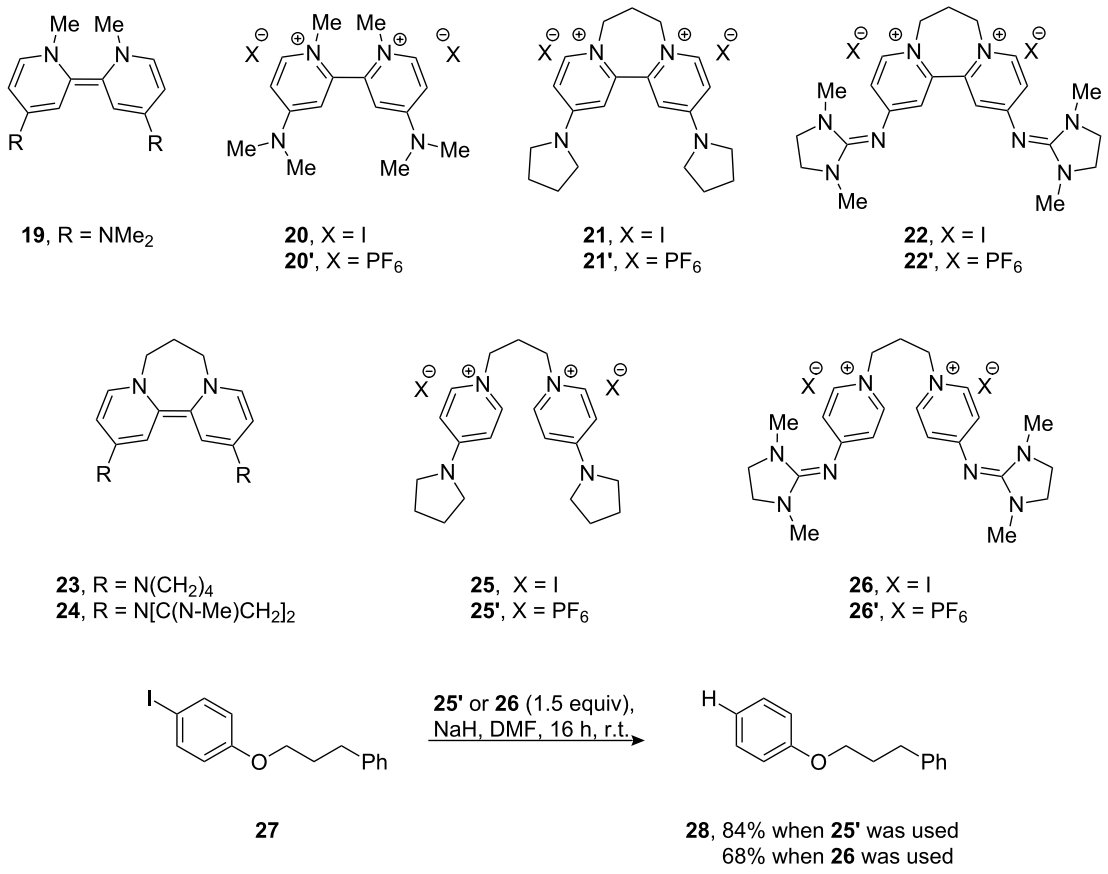

Figure 5: Electron donors, their oxidized dications and their reactions with **27**.

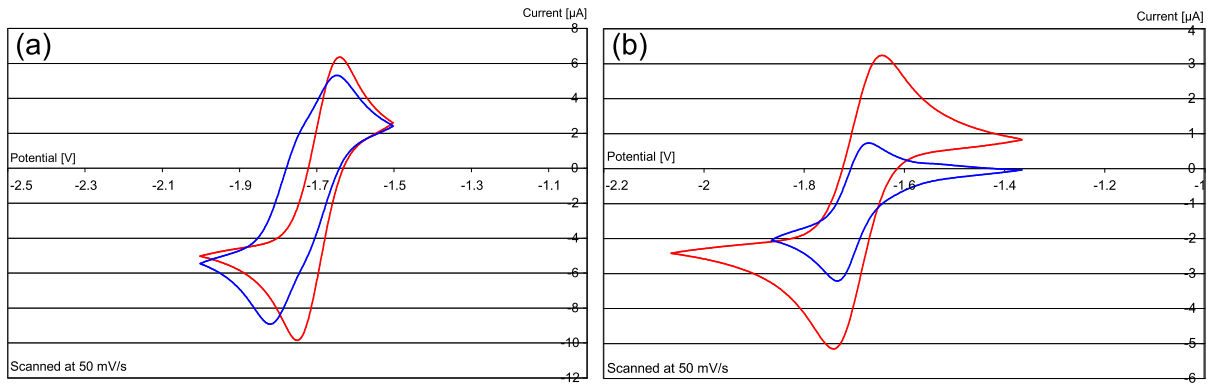

Figure 6: Cyclic voltammograms vs Fc/Fc^+ (a) of **17′** ↔ **8** (red) and **21′** ↔ **23** (blue) and (b) of **17′** ↔ **8** (red) and **22′** ↔ **24** (blue) (at half the concn used for **17′**).

4′-substituent do not lead to very large changes in the redox properties of **8**. [The oxidation potentials of these new donors and the preceding examples mentioned in this paper are tabulated below in Table 1.] These outcomes are already helping our design of new, versatile and more powerful organic electron donors.

Table 1: Oxidation potentials of organic electron donors[a]

Electron Donor	$E^1_{1/2}$	$E^2_{1/2}$	Structure
1[b]	0.37 V	0.67 V	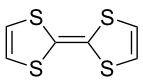
4[c]	−0.38 V(irr)		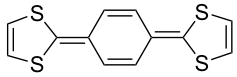
5[c]	−0.78 V	−0.61 V	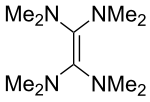
6	−0.82 V	−0.76 V	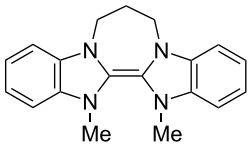
7	−1.20 V[e]		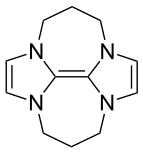
8	−1.24 V[e]		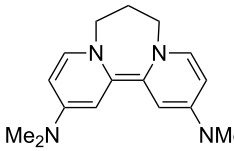
9	−1.00 V[d]		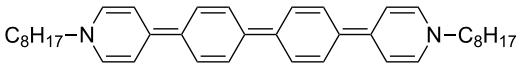
10	−0.32 V[e]		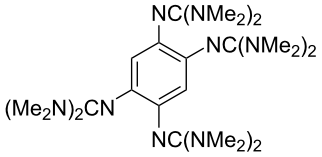
14	−1.21 V	−0.98 V	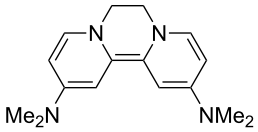
15	−1.23 V[e]		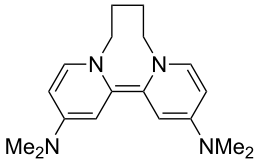
19	−1.27 V[e]		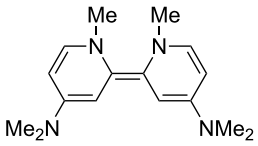

Table 1: Oxidation potentials of organic electron donors[a] (continued)

23	−1.33 V	−1.24 V	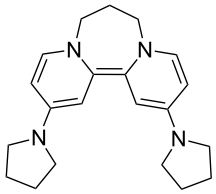
24	−1.24 V[e]		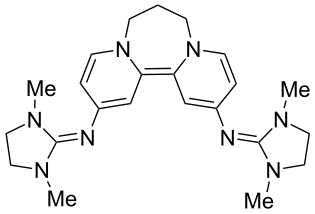

[a]All numbers have been converted for comparison with SCE; all experiments recorded in DMF, except where otherwise stated.
[b]Recorded in DCM.
[c]Recorded in MeCN.
[d]Recorded in THF.
[e]Two-electron wave.

Supporting Information

Supporting Information features detailed information on experimental procedures and compound characterisation.

Supporting Information File 1

Experimental Part
[http://www.beilstein-journals.org/bjoc/content/supplementary/1860-5397-6-73-S1.pdf]

Acknowledgements

We thank EPSRC, University of Strathclyde and AstraZeneca for funding and EPSRC Mass Spectrometry Centre, Swansea for mass spectra. We also thank the National Crystallography Service at Southampton for data collection.

References

1. Segura, J. L.; Martin, N. *Angew. Chem., Int. Ed.* **2001,** *40,* 1372. doi:10.1002/1521-3773(20010417)40:8<1372::AID-ANIE1372>3.0.CO;2-I
2. Murphy, J. A.; Lampard, C.; Lewis, N. *J. Chem. Soc., Chem. Commun.* **1993,** 295. doi:10.1039/C39930000295
3. Begley, M. J.; Murphy, J. A.; Roome, S. J. *Tetrahedron Lett.* **1994,** *35,* 8679. doi:10.1016/S0040-4039(00)78470-X
4. Murphy, J. A.; Fletcher, R. J.; Lampard, C.; Lewis, N. *J. Chem. Soc., Perkin Trans. 1* **1995,** 623. doi:10.1039/P19950000623
5. Murphy, J. A.; Rasheed, F.; Roome, S. J.; Lewis, N. *Chem. Commun.* **1996,** 737. doi:10.1039/CC9960000737
6. Fletcher, R. J.; Hibbs, D. E.; Hursthouse, M.; Lampard, C.; Murphy, J. A.; Roome, S. J. *Chem. Commun.* **1996,** 739. doi:10.1039/CC9960000739
7. Kizil, M.; Lampard, C.; Murphy, J. A. *Tetrahedron Lett.* **1996,** *37,* 2511. doi:10.1016/0040-4039(96)00306-1
8. Murphy, J. A.; Rasheed, F.; Roome, S. J.; Scott, K. A.; Lewis, N. *J. Chem. Soc., Perkin Trans. 1* **1998,** 2331. doi:10.1039/a802971g
9. Fletcher, R.; Kizil, M.; Lampard, C.; Murphy, J. A.; Roome, S. J. *J. Chem. Soc., Perkin Trans. 1* **1998,** 2341. doi:10.1039/a802974a
10. Callaghan, O.; Lampard, C.; Kennedy, A. R.; Murphy, J. A. *Tetrahedron Lett.* **1999,** *40,* 161. doi:10.1016/S0040-4039(98)80047-6
11. Callaghan, O.; Lampard, C.; Kennedy, A. R.; Murphy, J. A. *J. Chem. Soc., Perkin Trans. 1* **1999,** 995. doi:10.1039/a900335e
12. Murphy, J. A. The Radical-Polar Crossover Reaction. In *Radicals in Organic Synthesis, Volume 1: Basic Principles;* Renaud, P.; Sibi, M. P., Eds.; Wiley-VCH: Germany, 2001; pp 298–315.
13. Sato, M.; Lakshmikantham, M. V.; Cava, M. P.; Garito, A. F. *J. Org. Chem.* **1978,** *43,* 2084. doi:10.1021/jo00404a064
14. Burkholder, C.; Dolbier, W. R.; Medebielle, M. *J. Org. Chem.* **1998,** *63,* 5385. doi:10.1021/jo980201+
15. Takechi, N.; Ait-Mohand, S.; Medebielle, M.; Dolbier, W. R., Jr.. *Tetrahedron Lett.* **2002,** *43,* 4317. doi:10.1016/S0040-4039(02)00800-6
16. Since, M.; Terme, T.; Vanelle, P. *Tetrahedron* **2009,** *65,* 6128. doi:10.1016/j.tet.2009.05.036
17. Juspin, J.; Giuglio-Tonolo, G.; Terme, T.; Vanelle, P. *Synthesis* **2010,** 844. doi:10.1055/s-0029-1218590
18. Ames, J. R.; Houghtaling, M. A.; Terrian, D. L.; Mitchell, T. P. *Can. J. Chem.* **1997,** *75,* 28. doi:10.1139/v97-004
19. Shi, Z.; Thummel, R. P. *J. Org. Chem.* **1995,** *60,* 5935. doi:10.1021/jo00123a034
20. Thummel, R. P.; Goulle, V.; Chen, B. *J. Org. Chem.* **1989,** *54,* 3057. doi:10.1021/jo00274a019
21. Murphy, J. A.; Khan, T. A.; Zhou, S. Z.; Thomson, D. W.; Mahesh, M. *Angew. Chem., Int. Ed.* **2005,** *44,* 1356. doi:10.1002/anie.200462038
22. Taton, T. A.; Chen, P. *Angew. Chem.* **1996,** *108,* 1098. doi:10.1002/ange.19961080926
Angew. Chem., Int. Ed. Engl. **1996**, *35*, 1011. doi:10.1002/anie.199610111

23. Hunig, S.; Sheutzov, D.; Schlaf, H. *Justus Liebigs Ann. Chem.* **1973,** *765,* 126.
24. Murphy, J. A.; Zhou, S.-Z.; Thomson, D. W.; Schoenebeck, F.; Mahesh, M.; Park, S. R.; Tuttle, T.; Berlouis, L. E. A. *Angew. Chem., Int. Ed.* **2007,** *46,* 5178. doi:10.1002/anie.200700554
25. Murphy, J. A.; Schoenebeck, F.; Zhou, S.-Z.; Uenoyama, Y.; Miclo, Y.; Tuttle, T. *J. Am. Chem. Soc.* **2007,** *129,* 13368. doi:10.1021/ja074417h
26. Murphy, J. A.; Garnier, J.; Park, S. R.; Schoenebeck, F.; Zhou, S. Z.; Turner, A. T. *Org. Lett.* **2008,** *10,* 1227. doi:10.1021/ol800134g
27. Garnier, J.; Murphy, J.; Zhou, S.-Z.; Turner, A. *Synlett* **2008,** 2127. doi:10.1055/s-2008-1078242
28. Cutulic, S. P. Y.; Murphy, J. A.; Farwaha, H.; Zhou, S.-Z.; Chrystal, E. *Synlett* **2008,** 2132. doi:10.1055/s-2008-1078240
29. Cutulic, S. P. Y.; Findlay, N. J.; Zhou, S.-Z.; Chrystal, E. J. T.; Murphy, J. A. *J. Org. Chem.* **2009,** *74,* 8713. doi:10.1021/jo901815t
30. Porter, W. W.; Vaid, T. P.; Rheingold, A. L. *J. Am. Chem. Soc.* **2005,** *127,* 16559. doi:10.1021/ja053084q
31. Porter, W. W.; Vaid, T. P. *J. Org. Chem.* **2005,** *70,* 5028. doi:10.1021/jo050328g
32. Vaid, T. P.; Lytton-Jean, A. K.; Barnes, B. C. *Chem. Mater.* **2003,** *15,* 4292. doi:10.1021/cm034646c
33. Peters, A.; Kaifer, E.; Himmel, H.-J. *Eur. J. Org. Chem.* **2008,** 5907. doi:10.1002/ejoc.200800900
34. Wang, H. J.; Shi, J.; Fang, M.; Li, Z.; Guo, Q. X. *J. Phys. Org. Chem.* **2010,** *23,* 75. doi:10.1002/poc.1590
35. Peters, A.; Trumm, C.; Reinmuth, M.; Emeljanenko, D.; Kaifer, E.; Himmel, H.-J. *Eur. J. Inorg. Chem.* **2009,** 3791. doi:10.1002/ejic.200900399
36. Lappert, M. F.; Alvarez, S.; Aullon, G.; Fandos, R.; Otero, A.; Rodriguez, A.; Rojas, S.; Terreros, P. *Eur. J. Inorg. Chem.* **2009,** 1851. doi:10.1002/ejic.200801113
37. Vitske, V.; König, C.; Hübner, O.; Kaifer, E.; Himmel, H.-J. *Eur. J. Inorg. Chem.* **2010,** 115. doi:10.1002/ejic.200900724
38. Elbl-Weiser, K.; Krieger, C.; Staab, H. A. *Angew. Chem., Int. Ed. Engl.* **1990,** *29,* 211. doi:10.1002/anie.199002111
39. Andrieux, C. P.; Pinson, J. *J. Am. Chem. Soc.* **2003,** *125,* 14801. doi:10.1021/ja0374574
40. Otero, M. D.; Batanero, B.; Barba, F. *Tetrahedron Lett.* **2006,** *47,* 8215. doi:10.1016/j.tetlet.2006.09.132
41. Connelly, N. G.; Geiger, W. E. *Chem. Rev.* **1996,** *96,* 877. doi:10.1021/cr940053x
42. Spivey, A. C.; Arseniyadis, S. *Angew. Chem., Int. Ed.* **2004,** *43,* 5436. doi:10.1002/anie.200460373
43. Hassner, A.; Krepski, L. R.; Alexanian, V. *Tetrahedron* **1978,** *34,* 2069. doi:10.1016/0040-4020(78)89005-X
44. Bock, H.; Ruppert, K.; Merzweiler, K.; Fenske, D.; Goesmann, H. *Angew. Chem., Int. Ed. Engl.* **1989,** *28,* 1684. doi:10.1002/anie.198916841
45. Narayan, S.; Seelhammer, T.; Gawley, R. E. *Tetrahedron Lett.* **2004,** *45,* 757. doi:10.1016/j.tetlet.2003.11.030

License and Terms

Beilstein Journal of Organic Chemistry

EPR and pulsed ENDOR study of intermediates from reactions of aromatic azides with group 13 metal trichlorides

Giorgio Bencivenni[1], Riccardo Cesari[1], Daniele Nanni[1], Hassane El Mkami[2] and John C. Walton[*3]

Full Research Paper

Open Access

Address:
[1]Dipartimento di Chimica Organica "A. Mangini", Università di Bologna, Viale del Risorgimento 4, Bologna I-40136, Italy, [2]School of Physics and Astronomy, University of St. Andrews, St. Andrews, Fife KY16 9SS, UK and [3]School of Chemistry, University of St. Andrews, EaStChem, St. Andrews, Fife KY16 9ST, UK

Email:
John C. Walton[*] - jcw@st-andrews.ac.uk

* Corresponding author

Keywords:
aluminium; aromatic azides; ENDOR; EPR; gallium; indium

Beilstein J. Org. Chem. **2010,** *6,* 713–725.
doi:10.3762/bjoc.6.84

Received: 17 May 2010
Accepted: 23 July 2010
Published: 09 August 2010

Guest Editor: J. Murphy

Abstract

The reactions of group 13 metal trichlorides with aromatic azides were examined by CW EPR and pulsed ENDOR spectroscopies. Complex EPR spectra were obtained from reactions of aluminium, gallium and indium trichlorides with phenyl azides containing a variety of substituents. Analysis of the spectra showed that 4-methoxy-, 3-methoxy- and 2-methoxyphenyl azides all gave 'dimer' radical cations $[ArNHC_6H_4NH_2]^{+\bullet}$ and trimers $[ArNHC_6H_4NHC_6H_4NH_2]^{+\bullet}$ followed by polymers. 4-Azidobenzonitrile, with its electron-withdrawing substituent, did not react. In general the aromatic azides appeared to react most rapidly with $AlCl_3$ but this reagent tended to generate much polymer. $InCl_3$ was the least reactive group 13 halide. DFT computations of the radical cations provided corroborating evidence and suggested that the unpaired electrons were accommodated in extensive π-delocalised orbitals. A mechanism to account for the reductive conversion of aromatic azides to the corresponding anilines and thence to the dimers and trimers is proposed.

Introduction

The number of applications of indium [1-6], gallium [7-11] and other group 13 metal derivatives, as promoters of radical reactions, has been increasing ever since the original work of Baba and co-workers with dichloroindium hydride [12-16]. Parallel to that, organic azides are increasingly used as sources of N-centred radicals, although most such methods also require organotin hydrides [17-23]. In seeking cleaner, less toxic and more efficient synthetic methodology – not reliant on organotin compounds [24-28] – some of us began investigating the reactions of organic azides with dichloroindium hydride [29],

allylindium dichloride [30], and other group 13 metal derivatives. These reagents smoothly convert aromatic and aliphatic azides into the corresponding amines, γ-azidonitriles into pyrrolidin-2-imines [29], and δ-azidoesters and chlorides into allylated nitrogen heterocycles [30].

To help in elucidating the mechanisms of these reductions, we used CW EPR spectroscopy and attempted to characterise the reactive intermediates in selected reactions involving gallium trichloride. Surprisingly, we found that treatment of phenyl azide and 4-methoxyphenyl azide with gallium trichloride resulted in strong EPR spectra of long-lived paramagnetic species. By combining the results of product analyses with the results of EPR spectroscopy, we were able to show that persistent radical cations of 'dimers' (4-aminodiphenylamines) and 'trimers' (4′-phenylamino-4-aminodiphenylamines) were being formed [31]. We have now broadened the scope of this investigation to aromatic azides with a range of functionality. We report here our findings on the behaviour of aromatic azides when treated with the group 13 trichlorides of gallium, indium and aluminium.

Results and Discussion

Reaction of 4-methoxyphenyl azide (**2**) with group 13 metal chlorides

A set of aromatic azides, each containing an electron-releasing or an electron-withdrawing substituent in the 4-position, was chosen for this study. The position of the substituent was also varied and several other azide types were included (Scheme 1). Each organic azide was reacted with the metal halide in dichloromethane/pentane or acetonitrile solution at rt, and an aliquot (~0.1 mL) was placed in a quartz capillary tube (diam 1 mm), purged with nitrogen for 15 min and transferred to the resonant cavity of an X-band EPR spectrometer. When either $AlCl_3$, or $GaCl_3$ or $InCl_3$ was used, the reaction was accompanied by copious evolution of gas (probably nitrogen) and a deep blue or violet colour usually developed immediately or within a few minutes. In the case of $AlCl_3$ the reactions were very vigorous. Previously, we showed that the main product from the reaction of 4-methoxyphenyl azide **2** with $GaCl_3$ was 4-amino-4′-methoxydiphenylamine (**11b**, Variamine blue), together with traces of anisole, oxidised derivatives (including 4-(4-methoxyphenylamino)phenol, 4-((4-methoxyphenyl)-imino)-cyclohexa-2,5-dienone) and much dark-coloured polymer [31]. The EPR spectrum showed the radical cation of Variamine blue (**11b**$^{+\bullet}$) plus broad signals which we attributed to oligomer and/or polymer radical cations (Scheme 2).

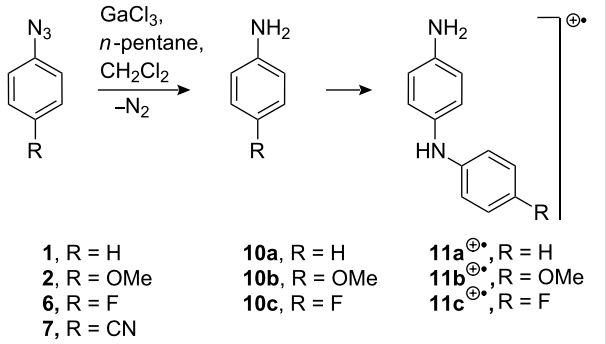

Scheme 2: Reaction of 4-substituted-phenyl azides with $GaCl_3$.

When anhydrous $AlCl_3$ in DCM – instead of the gallium halide – was added to a solution of azide **2**, a vigorous reaction took place. The resulting deep-coloured solution was transferred to the EPR spectrometer and initially the spectrum, Figure 1a, was obtained at 300 K. The broad, poorly resolved signal suggested that the mixture was dominated by polymeric material. However, when the solution was cooled down to 220 K, the well-resolved spectrum, Figure 1b, was obtained. The resolution improvement may be due to the fact that most of the polymer separates from the solution at the lower temperature.

A good computer simulation was achieved by utilising the hyperfine splitting constants (hfs) listed in Table 1. A well-resolved EPR spectrum of **11b**$^{+\bullet}$, generated from **2** with $GaCl_3$, is shown in Figure 1c for comparison. Figure 1d shows the experimental spectrum obtained from treatment of **2** with $InCl_3$, together with the corresponding computer simulation. Although the three EPR spectra appear different at first sight, the hfs derived from the simulations (Table 1) are actually quite similar. The contrasts in the spectral appearances are mainly the result of different line widths with consequently different resolutions. It is evident that the main species in each case is the radical cation **11b**$^{+\bullet}$. The acceptable agreement between the DFT-computed isotropic hfs of **11b**$^{+\bullet}$ (Table 1) and the experimental data provides additional support for this identification.

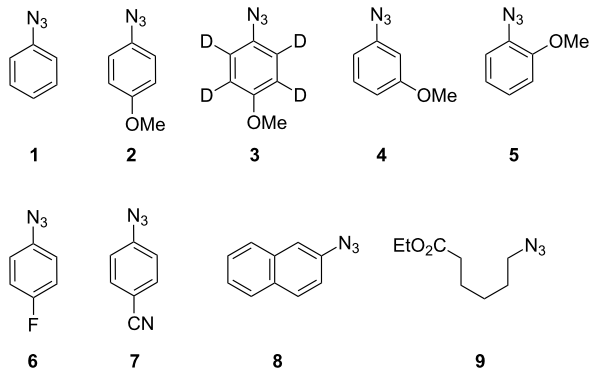

Scheme 1: Organic azides studied.

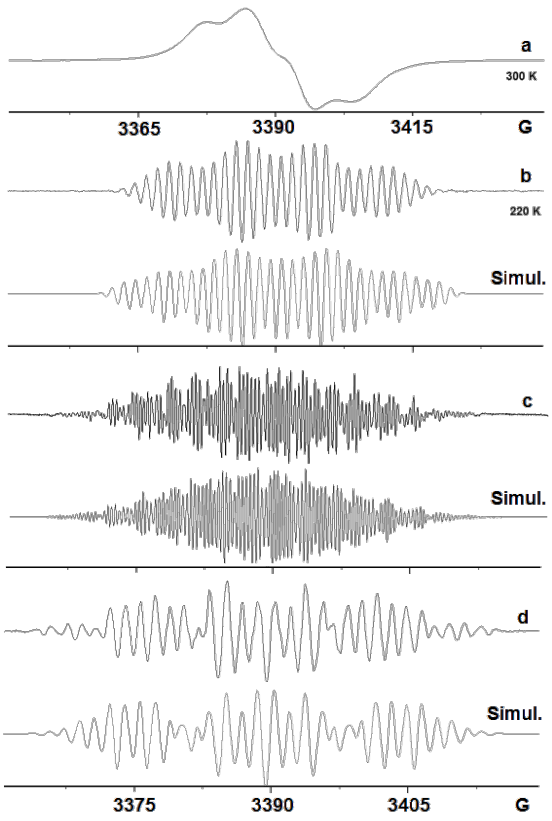

Figure 1: EPR spectra after treatment of azide **2** with MCl_3. (a) $AlCl_3$ in DCM; 1st derivative spectrum at 300 K. (b) $AlCl_3$ in DCM; 2nd derivative spectrum at 220 K; below: computer simulation with the parameters listed in Table 1. (c) $GaCl_3$ in DCM/pentane at 300 K with the computer simulation below. (d) $InCl_3$ in DCM:CH_3CN; 4:1 at 320 K; computer simulation below.

The small differences in the hfs obtained for the different group 13 metal chlorides can probably be attributed to the different counter ions, solvents and temperatures.

The 4-methoxy-tetradeuterio-azide **3** was also treated with $AlCl_3$ in DCM, and the resulting spectrum and simulation are shown in Figure 2.

The unpaired electron interacts with two non-equivalent N-atoms, a single comparatively large H-atom and a pair of equivalent H-atoms. The spectrum obtained previously on treatment of **3** with $GaCl_3$ was better resolved (Table 1) [31]. However, it is clear that the same 'dimer' species was formed with $AlCl_3$, probably having picked up the NH and NH_2 hydrogen atoms from the solvent. The line width of the spectrum with $AlCl_3$ was ca. 0.7 G. Therefore, it is not surprising that hfs from aromatic ring D-atoms were not resolved. Again, differences in the hfs of the spectra from $AlCl_3$ and $GaCl_3$ can be attributed to the different counter ions.

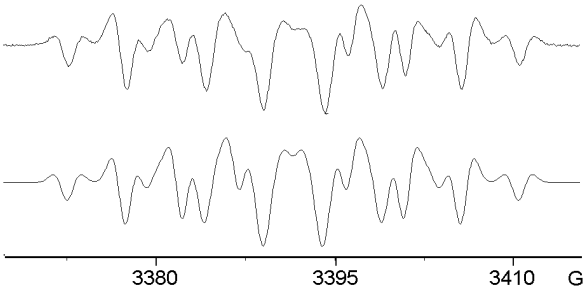

Figure 2: EPR spectrum after treatment of tetra-deuterated azide **3** with $AlCl_3$. Top: 2nd derivative spectrum at 290 K in DCM. Bottom: computer simulation using the hfs from Table 1.

Reactions of phenyl azide and 4-substituted-phenyl azides with group 13 metal chlorides

Azides **1**, **6** and **7** were chosen to vary the electronic properties and leaving group abilities of 4-substituents. We showed previously that treatment of phenyl azide **1** with $GaCl_3$ gave well-resolved spectra of 4-aminodiphenylamine radical cation (**11a**$^{+\bullet}$, the dimer) and of the trimer under different reaction conditions [31]. On treatment with $InCl_3$, **1** gave little sign of reaction. No colour developed and no EPR spectra were obtained. However, a vigorous reaction took place between **1** and $AlCl_3$ with nitrogen evolution and development of a deep blue colour. The EPR spectrum, Figure 3a, was dominated by a broad component, probably due to polyaniline type material, together with some fine structure. The second derivative spectrum at low modulation amplitude discriminated against the broad signal, and spectrum, Figure 3b, was obtained after digitally removing the residual broad component.

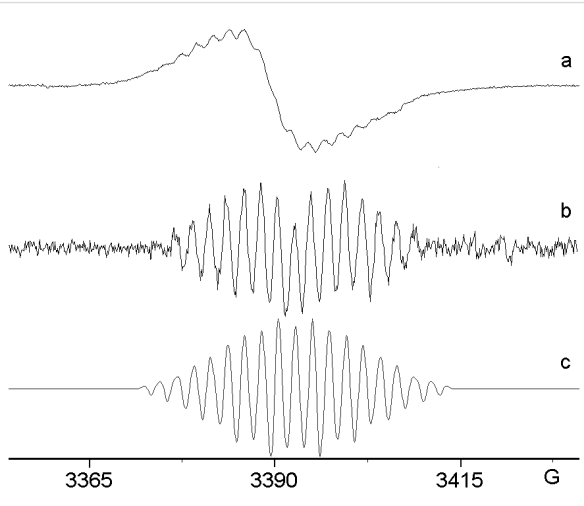

Figure 3: EPR spectra after treatment of azide **1** with $AlCl_3$. (a) 1st derivative spectrum in DCM at 280 K. (b) 2nd derivative spectrum after digital removal of residual broad central component. (c) computer simulation.

Table 1: EPR parameters of 'dimers' $[ArNHC_6H_4NH_2]^{+\bullet}$ from treatment of aryl azides with group 13 metal chlorides.[a]

Precursor	MCl_3/solvent	Radical cation species	1N	1N	(N)H	$(N)H_2$	2H	2H	2H	2H	Other
PhN_3 **1**[b]	$GaCl_3$/DCM	**11a**$^{+\bullet}$	4.9	4.9	6.8	5.6	3.1	2.0	1.0	0.6	1H, 1.0
PhN_3 **1**	$AlCl_3$/DCM, ACN	**11a**$^{+\bullet}$	4.5	4.5	6.3	5.0	2.2				
PhN_3 **1**	DFT[c]	**11a**$^{+\bullet}$	4.3	2.2	−8.4	−4.8	−2.0	−1.8	−1.1	1.0	1H, −2.3
4-$MeOC_6H_4N_3$ **2**	$AlCl_3$/DCM	**11b**$^{+\bullet}$	4.9	4.3	7.3	3.7	1.2	1.2			
4-$MeOC_6H_4N_3$ **2**[d]	$GaCl_3$/DCM	**11b**$^{+\bullet}$	5.2	4.4	7.3	3.8	3.1	2.2	0.8	0.4	
4-$MeOC_6H_4N_3$ **2**	$InCl_3$/DCM 4, ACN 1	**11b**$^{+\bullet}$	5.2	4.0	7.8	3.2	3.2	3.2	1.8		
4-$MeOC_6H_4N_3$ **2**	DFT[c]	**11b**$^{+\bullet}$	4.2	2.0	−8.1	−4.4	−2.0, −1.6	−1.6, −1.4	−0.8	0.2	MeO, 1.2
4-$MeOC_6D_4N_3$ **3**	$AlCl_3$/DCM		5.9	4.8	6.7	4.9	–	–	–	–	
4-$MeOC_6D_4N_3$ **3**[d]	$GaCl_3$/DCM		5.2	4.4	7.1	3.6	0.66, 2D	0.55, 2D			
3-$MeOPhN_3$ **4**[b]	$GaCl_3$/ACN	**17a**$^{+\bullet}$	4.3	–	5.7	5.2, 5.2	5.7, 5.7	5.2, 5.7	–	–	
3-$MeOPhN_3$ **4**	DFT[c]	**17a**$^{+\bullet}$	3.8	1.1	−7.6	−2.3, −2.0	−7.2, −7.3	2.6, −3.4	−2.3, 1.3	−0.9, −0.2	MeO, −0.1
2-$MeOC_6H_4N_3$ **5**	$GaCl_3$/DCM	**17b**$^{+\bullet}$	4.1	4.1	5.5	5.5					
2-$MeOC_6H_4N_3$ **5**	DFT[c]	**17b**$^{+\bullet}$	4.0	1.5	−8.1	−3.9	−3.1, −2.3	−1.5, −1.6	0.8, 0.7	−0.3, 0.1	MeO, 0.8
4-$FC_6H_4N_3$ **6**	$HGaCl_2$/ACN, TES[e]	**11c**$^{+\bullet}$	4.4	3.9	4.0	4.0	2.0	2.0	1.0	0.5	1F, 6.6
4-$FC_6H_4N_3$ **6**	DFT[c]	**11c**$^{+\bullet}$	4.0	2.5	−7.9	−5.5	−1.7	−1.4	−1.4	0.5	4.3[f]
2-$NapN_3$ **8**	$InCl_3$/DCM 4, ACN 1		3.4	3.4	5.6	2.8	2.8 (1H)				

[a]All *g*-factors were 2.0032 ± 0.0005. Assignments of hfs to specific atoms are tentative and are based on the DFT computations. Note that only the magnitudes and not the signs of hfs can be derived from the EPR spectra.
[b]Treatment of PhN_3 and 3-$MeOC_6H_4N_3$ with $InCl_3$ gave only very weak and broad unresolved spectra.
[c]DFT computations: geometries optimised to UB3LYP/6-31+G(d,p) then single point calculations with 6-311++G(d,p) basis.
[d]Data from ref [31].
[e]$HGaCl_2$ prepared from $GaCl_3$ and Et_3SiH (TES). [f]The computed *a*(*F*) varied from 4.3 G, with the 6-311++G(d,p) basis set, to 9.5 G with the DGDZVP basis set.

The hfs were similar to those of **11a**$^{+\bullet}$ (Table 1, entry for **1** with $GaCl_3$) except that the smaller hfs were not resolved. Minor differences in the magnitudes of the hfs can be attributed to the different counter ions. The trimer radical cation was not observed, but clearly a contribution from this species could be hidden under the broad component.

No reaction of 4-azidobenzonitrile **7** with $InCl_3$, $GaCl_3$ or $AlCl_3$ was observed and no paramagnetic species were detected by EPR spectroscopy. It appears the electron-accepting property of the CN group inhibited the coupling process at some stage. It is also worth mentioning that, as expected, aliphatic azides such as ethyl 5-azidopentanoate **9** did not react in the same way either. Treatment of **9** with $InCl_3$ or $GaCl_3$ led to gas evolution but no colour developed and no paramagnetic species could be detected.

Very interesting results were obtained from reactions of 1-azido-4-fluorobenzene (**6**). When **6** was treated with $GaCl_3$ in DCM, a deep blue-violet colour developed and the spectrum was dominated by a broad feature, Figure 4a, although underlying fine structure was evident. When dichlorogallium hydride, prepared from $GaCl_3$ and Et_3SiH in CH_3CN, was used to promote the reaction, a beautifully resolved spectrum resulted, Figure 4b.

The good simulation of this spectrum, Figure 4c, enabled the hfs shown in Table 1 to be determined. Comparison of these hfs

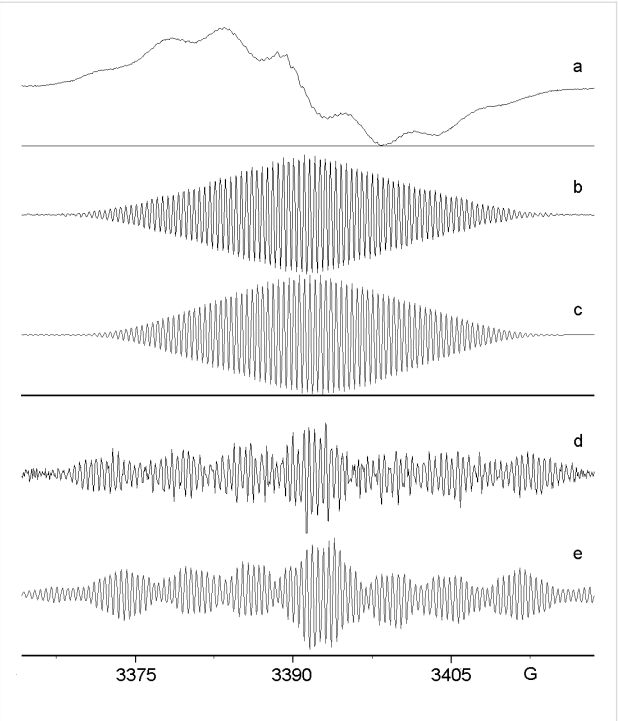

Figure 4: EPR spectra after $GaCl_3$ and $InCl_3$ reactions of azide **6**. (a) 1st derivative spectrum from **6** and $GaCl_3$ in DCM at 300 K. (b) 1st derivative spectrum of dimer (**11c**$^{+\bullet}$) from **6** and $HGaCl_2$ in CH_3CN at 300 K. (c) computer simulation of (b) with hfs of Table 1. (d) 1st derivative spectrum of trimer (**19**$^{+\bullet}$) from **6** and $InCl_3$ in DCM at 300 K. (e) computer simulation of (d) with hfs of Table 2.

with those of the other species in Table 1 supports the identification of this intermediate as the corresponding dimer cation **11c**$^{+\bullet}$, containing a single F-atom. The DFT computation on the dimer hfs gave satisfactory agreement (Table 1), with the possible exception of the *para*-F hfs. However, DFT-computed $a(F)$ values varied from 7.2, to 7.1, to 9.5 and 4.3 G with 6-31G(d), 6-31+G(d,p), DGDZVP and 6-311++G(d,p) basis sets, respectively. This spread indicates the comparative unreliability of the DFT spin density computations for F-atoms in these cations.

Treatment of **6** with $InCl_3$ in DCM led to the usual broad signal from oligomeric and polymeric species superimposed on a spectrum with much narrower lines. On recording the spectrum with a smaller modulation amplitude, and digitally removing the residual broad feature, the spectrum shown in Figure 4d resulted. This is obviously a different species from that of Figure 4b and, after many trials, a satisfactory simulation was obtained, Figure 4e. The derived hfs are presented in Table 2 and they clearly correspond to a trimer, also probably containing a single F-atom, i.e. **19b**$^{+\bullet}$.

It seems clear that the MCl_3 reactions with aromatic azides entail a progression from the aniline $XC_6H_4NH_2$, to the dimer $XC_6H_4NHC_6H_4NH_2$, to the trimer $XC_6H_4NHC_6H_4NH$-$C_6H_4NH_2$, thence to oligomers and eventually polyaniline type polymers $X[C_6H_4NH]_nC_6H_4NH_2$. Some polymer radical cation was always observed by EPR spectroscopy, but whether dimer or trimer or oligomer dominated the spectrum depended on a delicate balance between solvent, metal halide and other factors.

Reactions of 2-methoxy- and 3-methoxyphenyl azides with group 13 metal chlorides

Aromatic azides **4** and **5** were chosen to investigate how the position of the MeO substituent influenced the reaction. Treatment of the 3-methoxy precursor **4** with $InCl_3$ or $HInCl_2$ gave only very weak and broad EPR spectra. However, reaction of **4** with $GaCl_3$ in CH_3CN gave a strong EPR spectrum and the hfs derived from the computer simulation are presented in Table 1. The comparatively large line width (~0.9 G) did not permit the resolution of small hfs from aromatic ring H-atoms. For the same reason, the hfs from the second N-atom were not resolved. However, it is clear that this species is probably a 'dimer' although the connectivity of the angular structure **17a**$^{+\bullet}$ is somewhat different from that of the 4-aminodiphenylamines derived from the 4-substituted phenyl azides (Scheme 3).

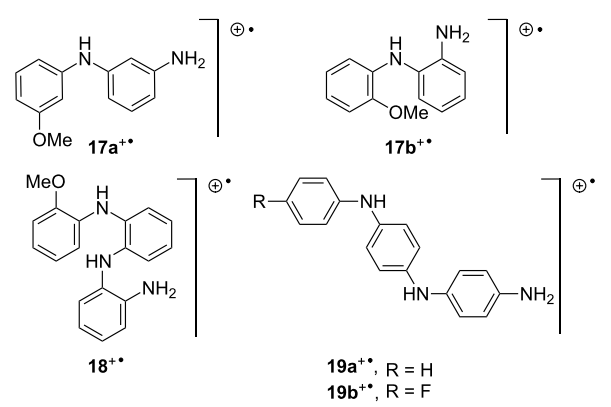

Scheme 3: Dimer and trimer radical cations.

Treatment of the 2-methoxy precursor **5** with $GaCl_3$ in DCM, or with $HGaCl_2$ in CH_3CN, gave essentially the same strong spectrum, see Figure 5a and Supporting Information. The hfs derived from the simulations (Table 1) suggest that this is also a dimer type radical cation **17b**$^{+\bullet}$. However, with the passage of time a central peak began to appear in this spectrum. When **5** was treated with $HGaCl_2$, prepared from $GaCl_3$ and Et_3SiH, the species with a central peak dominated the spectrum, Figure 5b. Treatment of **5** with $InCl_3$ in DCM or with $HInCl_2$ in THF (prepared from $InCl_3$ and DIBAL-H) also gave rise to a spectrum of this same species, Figure 5c. A well-resolved spectrum of this species was obtained by treatment of **5** with

Table 2: EPR hfs of 'trimer' species $\{[ArNH]_2C_6H_4NH_2\}^{+\bullet}$ from treatment of aryl azides with group 13 metal chlorides.[a]

Precursor	MCl_3/solvent or DFT	Trimer radical cation	N	N	$N(H_2)$	$(N)H_2$	(N)H	(N)H	H-rings	Other
PhN_3 **1**[b]	$GaCl_3$/DCM	**19a**$^{+\bullet}$	5.0	4.9	3.0	6.5	4.9	2.1	2.1 (3H) 1.0 (3H)	
PhN_3 **1**	DFT[c]	**19a**$^{+\bullet}$	5.4	3.4	2.0	−3.0	−7.8	−4.8	−1.6 (4H) −1.0 (3H) <±0.6 (6H)	
4-$FC_6H_4N_3$ **6**	$InCl_3$/DCM	**19b**$^{+\bullet}$	5.5	5.5	2.6	6.2	7.2	4.5	2.2 (1H) 1.5 (2H) 0.5 (6H)	2.2 (1F)
4-$FC_6H_4N_3$ **6**	DFT[d]	**19b**$^{+\bullet}$	3.7	2.1	1.5	−3.2	−7.2	−4.2	−1.3 (4H) −0.6 (4H) <0.6 (4H)	1.5 (1F)
2-$MeOC_6H_4N_3$ **5**	$InCl_3$/DCM	**18**$^{+\bullet}$	4.8	4.8	4.8	5.1	5.1	5.1	–	
2-$MeOC_6H_4N_3$ **5**	$HGaCl_2$[e]/CN	**18**$^{+\bullet}$	4.5	4.5	3.0	4.1 1.7	5.5	5.5	1.7 (1H) 0.5 (4H)	
2-$MeOC_6H_4N_3$ **5**	DFT[c]	**18**$^{+\bullet}$	4.4	3.9	1.5	−2.0 −1.6	−6.6	−5.1	−2.0 (1H) −1.7 (2H) −1.1 (1H) <0.7 (8H)	0.4 (CH_3O)

[a]All *g*-factors 2.0032 ± 0.0005, assignments of hfs to specific atoms are tentative and are based on the DFT computations. Note that only the magnitudes and not the signs of hfs can be derived from the EPR spectra. [b]Data from ref [31]. [c]DFT: UB3LYP/6-31G(d). [d]DFT computations: UB3LYP/6-31+G(d,p) then single point calculation with 6-311++G(d,p) basis. [e]$HGaCl_2$ prepared from $GaCl_3$ and Et_3SiH (TES).

$HGaCl_2$ prepared with Et_3SiH in CH_3CN, Figure 5d. The hfs derived from the computer simulation, Figure 5e and Table 2 show the presence of three N-atoms and of four H-atoms with sizeable hfs that can probably be attributed to NH or NH_2 groups. Thus, this species is almost certainly a 'trimer' although this will necessarily have an angular structure **18**$^{+\bullet}$ rather than the linear type structure of the trimers from 4-subsitituted azides such as **19**$^{+\bullet}$ (Scheme 3).

The results from azides **4** and **5** showed that the position of the MeO substituent in the phenyl azides was not critical. The reactions with gallium and indium promoters proceeded along similar lines to that of phenyl and 4-substituted phenyl azides to give dimers, trimers and polymers.

The spectra obtained on treatment of 2-azidonaphthalene **8** with $InCl_3$, $GaCl_3$ and $AlCl_3$ are shown in Figure 6a, Figure 6b and Figure 6c, respectively.

The broad signal in Figure 6c shows that polymerisation dominated the reaction with $AlCl_3$. Similarly, the main broad feature in Figure 6b suggests that polymerisation was again dominant in the reaction with $GaCl_3$. The comparatively well-resolved species observed in the $InCl_3$-promoted reaction, Figure 6a, was well simulated on using the parameters shown in Table 1. The data show that the unpaired electron interacted with two

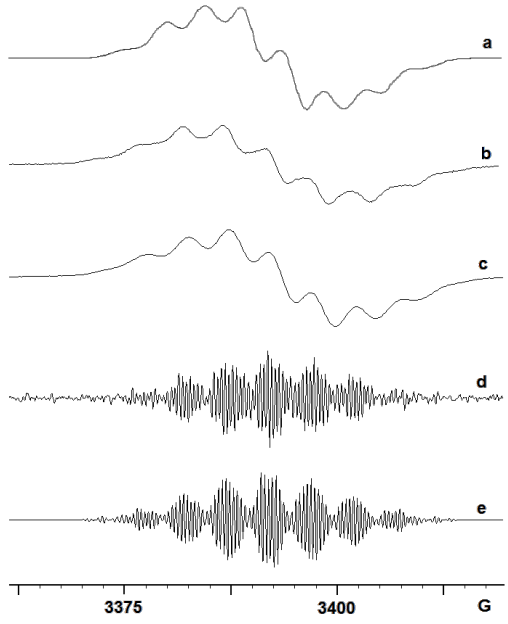

Figure 5: EPR spectra after $GaCl_3$- and $InCl_3$-promoted reactions of 2-methoxyphenyl azide **5**. (a) 1st derivative spectrum of **17b**$^{+\bullet}$ from **5** with $GaCl_3$ in DCM. (b) 1st derivative spectrum of **17b**$^{+\bullet}$ from **5** with $HInCl_2$ in THF at 300 K. (c) 1st derivative spectrum of **18**$^{+\bullet}$ from **5** with $InCl_3$ in DCM at 300 K. (d) 1st derivative spectrum of **18**$^{+\bullet}$ from **5** with $HGaCl_2$ in CH_3CN at 300 K. (e) computer simulation of (d).

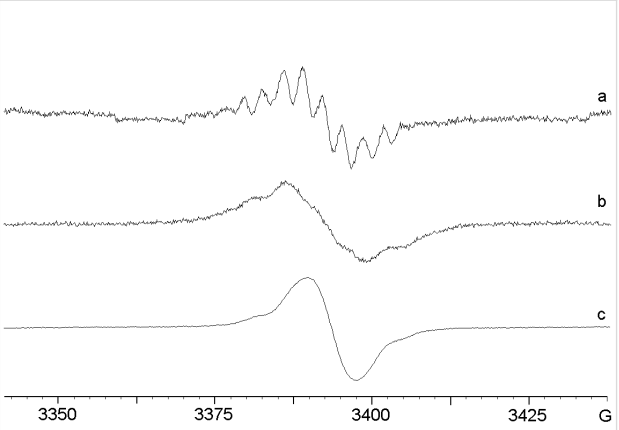

Figure 6: EPR spectra after In-, Ga- and Al-promoted reactions of azide **8**. (a) intermediate from $InCl_3$ treatment of **8** at 260 K in DCM and CH_3CN (4:1). (b) spectrum from $GaCl_3$ treatment of **8** at 300 K in DCM/pentane. (c) spectrum from $AlCl_3$ treatment of **8** at 300 K in DCM.

N-atoms, two (N)H_2 atoms, one (N)H-atom and one other H-atom; other splittings were not resolved. The magnitudes of the hfs are somewhat smaller than those of analogous atoms in the dimer from **1**. This is exactly as would be expected from the greater extent of aromatic delocalisation in a dimer from **8**. Clearly, however, more than one isomer is possible.

Pulse ENDOR spectrum of the intermediate from 4-fluorophenyl azide **6**

Pulsed ENDOR experiments, based on the ESE effect, were carried out on the frozen solution from azide **6** at 50 K. The echo signal was created by the microwave pulse sequence, and an rf pulse was applied during the 'mixing period', which corresponded to the time T in the Davies ENDOR sequence [32]. The rf pulse drove the nuclear spin transitions, which led to a change in the ESE intensity. The ENDOR signal was therefore measured by monitoring the ESE intensity while the rf frequency was varied. In the case of an $S = ½$ system coupled with a nucleus with nuclear spin $I = ½$, the Davies ENDOR spectrum consists of two lines at the nuclear resonance frequencies ν_α and ν_β, which correspond to the transitions associated with the electron spin manifolds $M_s = +½$ and $M_s = -½$, respectively. If the Larmor frequency (ν_n) of the nucleus in question is larger than the hyperfine interaction, then the resonance frequencies are given by:

$$\nu_{\alpha\beta} = |\nu_n \pm ½a_{iso}|. \quad (1)$$

If ν_n is less than $½a_{iso}$, the frequencies are then given by:

$$\nu_{\alpha\beta} = |½a_{iso} \pm \nu_n|. \quad (2)$$

An additional complication arises if the nuclear spin is >½, which adds another term describing the nuclear quadrupole interaction in the above equations [33]. In frozen solution all orientations of the paramagnetic species are observed and therefore an anisotropic ENDOR spectrum is expected. The latter is more complex and requires a detailed understanding of the anisotropy of the system. The above equations are not suitable for such a situation and a more complete resonance condition that considers all the orientations is needed. In the case of a system with $I = ½$ the parameter a_{iso} in Equation 1 and Equation 2 is replaced by A_i (i.e. one of the principal components of the hyperfine tensor).

The Davies ENDOR spectrum from the species derived from the 4-fluoroazide **6** sample at 50 K is shown in Figure 7. The inset shows the ESE-EPR spectrum, with an arrow indicating the magnetic field position at which the ENDOR experiment was performed. The ENDOR spectrum shows powder pattern lineshapes, as expected for frozen solutions, due to the anisotropic hyperfine interactions. Two main features cover the whole spectrum; a powder pattern centred about the ^1H Larmor frequency and a second broad signal located at lower frequency and spread over 8 MHz width.

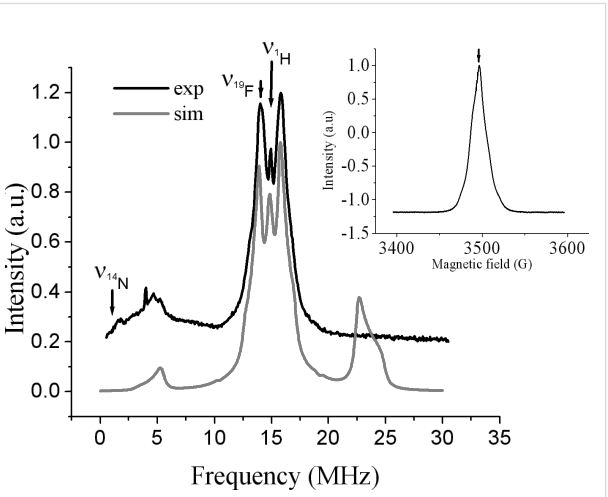

Figure 7: Experimental and simulated Davies ENDOR spectrum after the Ga-promoted reaction of azide **6** recorded at 50 K. The inset shows the field-swept EPR spectrum with an arrow indicating the magnetic field position of the ENDOR experiment.

The lack of resolution encountered in the ENDOR spectrum makes an unequivocal analysis difficult. Therefore, our ENDOR simulation was based mainly on the CW EPR results. A simulated spectrum is displayed in Figure 7, and a deconvoluted version is in the Supporting Information together with one chosen set of ENDOR hyperfine tensor parameters. Almost all the ^1H hyperfine splittings fit well within the ENDOR spectra,

but it is worth noting, as mentioned above, that a satisfactory simulation was only achieved by assuming an anisotropic lineshape of the hyperfine couplings. Extra weak hyperfine couplings, unresolved in the CW EPR, were also included in the simulation. These probably correspond to hyperfine coupling in polymer which was undoubtedly present. The broad feature at low frequency is related to a mixture of fluorine (^{19}F) and nitrogen (^{14}N) contributions. The anisotropy and the unresolved nuclear quadrupole of the nitrogen couplings make the spectra difficult to interpret. Each ^{1}H contributes three sets of peaks to the spectrum times the number of ^{1}H's present. This represents an enormous number of lines in one spectrum. Obviously, they cannot all be assigned from this broad unresolved powder pattern. Almost axial tensors were assumed (see Supporting Information). However, it should be noted that it may well be possible to simulate these spectra with other parameter sets. The experimental Davies ENDOR data support the CW EPR data in confirming the magnitudes of the hyperfine couplings and the nitrogen interactions. Further pulse techniques such as electron spin echo envelope modulation (ESEEM) and its multidimensional extension Hyscore would be required to get more insight into the nitrogen contribution. Regarding the ^{19}F contribution; only the low-frequency part of the ^{19}F coupling fits well with the experimental data. The ^{19}F high-frequency line in our simulation is not consistent with the experimental spectrum, which suggests that the latter might be highly asymmetric. Such situations have been previously reported in other studies where it was shown that this could be related to the relaxation time. Sometimes relaxation processes can lead to a partial saturation in the nuclear transitions such that the observed signal is the result of a transition in one manifold only [34]. Partial saturation may explain the absence of the ^{19}F high-frequency line in our spectrum.

DFT computations of radical cation properties

Quantum chemical calculations were carried out with the Gaussian 03 programme package [35,36]. Density functional theory with the UB3LYP functional was employed. The equilibrium geometries were fully optimised with respect to all geometric variables, no symmetry being assumed either with the 6-31+G(d,p) basis set (dimers) or with the 6-31G(d) basis set (trimers). Isotropic EPR hfs were derived from computed Fermi contact integrals evaluated at the H- and N-nuclei. The hfs were taken directly from the Gaussian output files and are shown in Table 1 and Table 2.

The optimum structures of the radical cations **17a**$^{+\bullet}$ and **17b**$^{+\bullet}$ their associated SOMOs are shown in Figure 8.

The C–NH bond lengths in radical cation **17a**$^{+\bullet}$ (1.40 and 1.38 Å) and **17b**$^{+\bullet}$ (1.38, 1.39 Å) indicated significant double bond character. The CNC angles in **17a**$^{+\bullet}$ and **17b**$^{+\bullet}$ were 128.9 and 131.6°, showing significant widening from trigonal. The aromatic rings in all the structures were twisted significantly out of co-planarity. As might be expected on steric grounds, this increased in the dimers as the substitution site moved from the 4- to the 3- to 2-position. For example, the computed dihedral angles between the rings increased from 26.8 to 30.7 to 39.0 in the series 4-MeO-**11b**$^{+\bullet}$, 3-MeO-**17a**$^{+\bullet}$ and 2-MeO-**17b**$^{+\bullet}$, respectively. It seems that a compromise was reached in which the repulsive steric interaction between substituents of neighbouring rings was balanced against the stabilising effect from conjugation of the π-systems. The SOMOs depicted in Figure 8 show that there was still sufficient orbital overlap in the linear and angular dimer and trimer radical cations to support lengthy π-systems extending over all the rings and N-atoms. This is in accordance with the EPR spectroscopic data, that show extensive delocalisation of the unpaired electron in dimer and trimer radical cations. The computed hfs in Table 1 and Table 2 show reasonable correspondence with the experimentally observed values.

Conclusion

Literature reports show that anilines can easily be oxidised to the corresponding resonance-stabilised radical cations, which can couple with more aniline to afford very persistent radical cation dimers [37,38]. The generation of these radical cations depends critically on the reaction conditions, in particular on the degree of protonation, which can facilitate electron transfer (ET) [39,40]. It has also been reported that electrochemical oxidation of aromatic amines can generate the same radical cations which can polymerise giving oligo- and poly-anilines [41]. In view of the fact that product analyses [31] identified aniline amongst the products from **1** and anisole amongst the products from **2**, it seems probable that the aromatic amines are the precursors of the dimer and trimer species.

A possible mechanism for production of anilines from the aromatic azides is set out in Scheme 4. Coordination of the metal halide to the starting azide should produce the Lewis base–acid adduct **12** that could undergo reduction by ET from more azide to afford, after nitrogen loss, the metal-coordinated aminyl radical **13** together with the $ArN_3^{+\bullet}$ radical cation. Aminyl radical **13** could then abstract an H-atom from solvent RH (or from $HMCl_2$ when the metal hydrides were used) with the production of metal-coordinated amine **14**. The latter can then pick up a proton to produce an aromatic amine and regenerate the metal halide. The reason 4-azidobenzonitrile **7** did not react with any of the group 13 metal chlorides may well be that the ET step **12** → **13** was inhibited by the presence of the electron acceptor CN group.

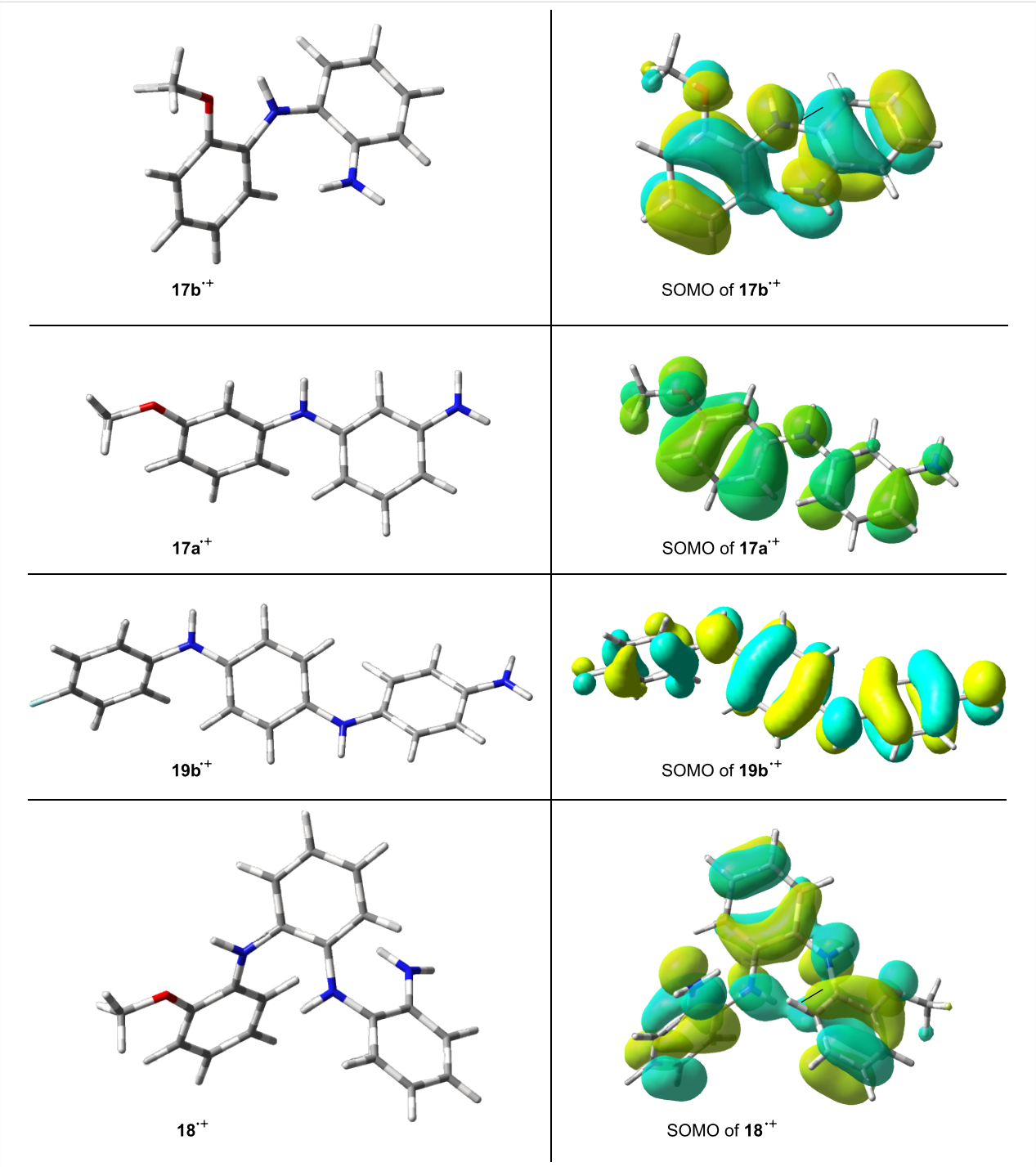

Figure 8: DFT structures and SOMOs for dimer and trimer radical cations.

Several mechanisms have been proposed in the literature for the formation of 'dimers' from anilines. These include [42-44]: (i) initial formation of the radical cation $ArNH_2^{+\bullet}$ which then couples with more aniline and forms the 4-aminodiaryl amine radical cation after loss of HX and (ii) formation of the aniline radical $ArNH^{\bullet}$, which couples with $ArNH_3^{+}$, $ArNH_2$ or $ArNH_2^{+\bullet}$. A plausible mechanism for formation of the dimer and trimer radical cations we observed is shown in Scheme 5 for the case of 2-methoxyaniline.

Ipso attack by radical **13a** on the aniline would lead to the production of delocalised radical **15**. Elimination of $MeOMCl_3^{-}$ would then yield radical **16**, which, on protonation, would afford the observed long-lived dimer radical cations $\mathbf{17}^{+\bullet}$. Of

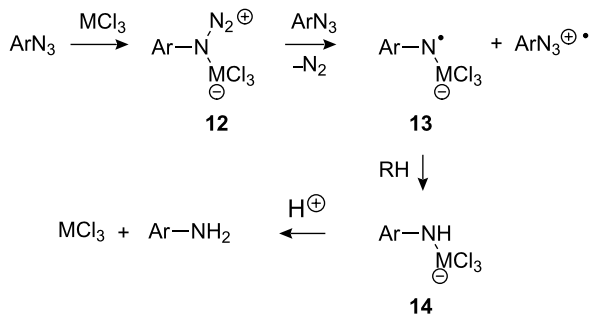

Scheme 4: Possible mechanism of formation of aromatic amines.

course, proton transfer could occur earlier in the reaction, such that coupling takes place with the anilinium cation instead. Trimer $\mathbf{18}^{+\bullet}$ could be produced by coupling of $\mathbf{17}^{+\bullet}$ with more **13a** followed by a similar sequence of steps. The trimer could then grow into oligomer and polymer by a succession of such coupling reactions.

In general, the aromatic azides appeared to react most rapidly with $AlCl_3$ but this reagent tended to generate much polymer. $InCl_3$ was the least reactive group 13 halide such that no reaction was observed with PhN_3 and very little reaction occurred with the 3-methoxyazide **4**. $GaCl_3$ and $HGaCl_2$ were the best promoters. The dimers were the main products from reactions of excess **1** and **2** with $GaCl_3$ such that the process could have synthetic potential. In general, the $GaCl_3$- and $HGaCl_2$-promoted reactions were also best for spectroscopic studies because they gave the most intense and well-resolved spectra of $[ArNHArNH_2]^{+\bullet}$ and/or $\{[ArNH]_2ArNH_2\}^{+\bullet}$ with the narrowest line widths.

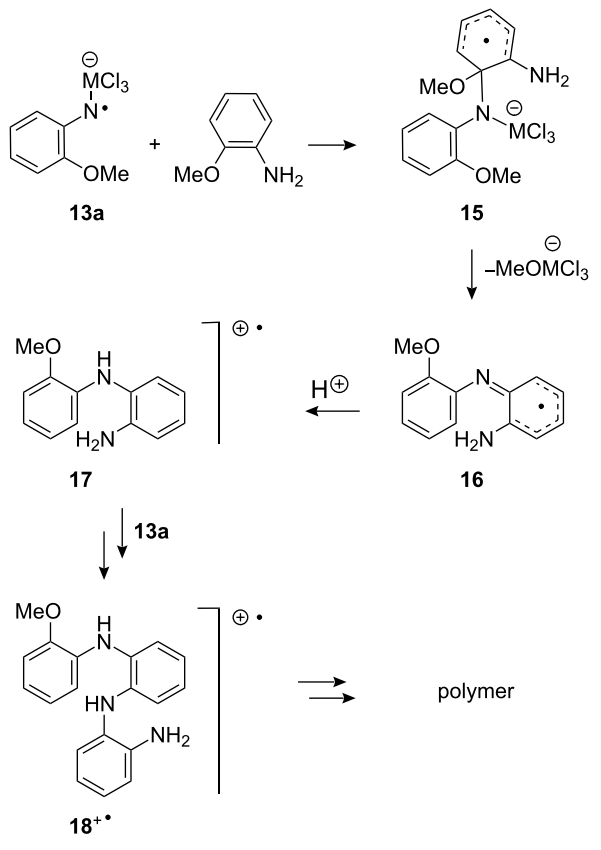

Scheme 5: Possible mechanism for dimer and trimer formation.

Experimental

EPR and ENDOR spectroscopy. EPR spectra were obtained with a Bruker EMX X-Band 10/12 spectrometer fitted with a rectangular ER4122 SP resonant cavity and operating at 9.4 GHz with 100 kHz modulation. An aliquot (~0.1 mL) of the reaction mixture from each aromatic azide and the metal chloride in CH_2Cl_2/pentane or CH_3CN solution was placed in a 1 mm o.d. quartz capillary tube, de-aerated by bubbling nitrogen for 20 min and transferred to the resonant cavity. Spectra were examined at several temperatures but generally best resolution and signal intensity were obtained at around 300 K. Most of the EPR spectra were recorded with 2.0 mW power, 1.0–0.2 G_{pp} modulation intensity and a gain of ~10^6. In all cases where spectra were obtained, hfs were assigned with the aid of computer simulations using the Bruker SimFonia and NIEHS Winsim2002 software packages.

Pulsed EPR and ENDOR were performed using a pulsed EPR X-band spectrometer (Bruker Elexsys E580) equipped with a Dice-ENDOR accessory, a radio frequency (rf) amplifier and a dielectric-ring ENDOR resonator (Bruker EN4118X-MD-4-W1). Samples were maintained at 50 K using liquid helium in an Oxford CF-935 cryostat. Field-swept electron spin echo (ESE) spectra were recorded using a two-pulse ESE sequence while ESE-ENDOR experiments were carried out using Davies three-pulse sequence π-*T*-π/2-τ-π-echo with a selective rf pulse of variable frequency applied during time *T*. The pulse lengths used were 128 and 256 ns for π/2 and π respectively, and 10 μs for the π-rf pulse. ENDOR data were processed and simulated using the EasySpin package (freeware from http://www.easyspin.org/).

DFT calculations. All computations were done with the Gaussian 03W programme package (Version 6.1.0.0) [35]. Geometries were optimised at the UB3LYP/6-31+G(d,p) level [45] (dimers) and the UB3LYP/6-31G(d) level (trimers) and single point calculations at these geometries with a triple zeta quality basis set (6-311++G(d,p)) were used to predict isotropic EPR hfs. The DGTZVP basis set, similar to that recommended by Schäfer et al. [46], was also employed for some computations.

General procedure for the reaction of aryl azides with indium trichloride. The starting azide (1 mmol) was added at 0 °C to an acetonitrile solution of indium trichloride (1.1 mmol) in DCM (4 mL) and stirred for 5 min at 0 °C. Gas was evolved and the solutions took on a dark blue or violet colour. The resulting solutions were rapidly transferred into a quartz capillary tube and purged with nitrogen for few minutes. The tube was sealed and placed in the EPR resonant cavity. Spectra were recorded at several different temperatures. Some samples were photolysed with a 500 W super pressure Hg arc.

General procedure for the reaction of aryl azides with dichloroindium hydride. The starting azide (1 mmol) was added at 0 °C to an acetonitrile solution of dichloroindium hydride (1.1 mmol), generated in situ by stirring under an argon atmosphere anhydrous indium trichloride (243 mg, 1.1 mmol, previously dried by heating at 130 °C under argon for 1 h) and triethylsilane (177 μL, 1.1 mmol) in ACN (4 mL) for 5 min at 0 °C [47]. The resulting solution was rapidly transferred into a quartz capillary tube and nitrogen was bubbled inside for few minutes. The tube was sealed and placed in the EPR cavity. Spectra were recorded at several different temperatures. Some samples were photolysed with a 500 W super pressure Hg arc. Selected samples were given an aqueous work-up with $NaHCO_3$ followed by extraction with diethylether. In each case the corresponding aromatic amine was identified by comparison with literature data.

General procedure for the reaction of aryl azides with $AlCl_3$. Aluminium trichloride (1.1 mmol) was dried under reduced pressure at 25 °C for 1 h. Then DCM (3 mL) was added and a DCM solution of the azide (1 mmol in 1 mL) was introduced at rt. Gas was evolved, sometimes violently, and dark blue or violet colours developed. The resulting solution was then transferred to a capillary quartz tube and purged with nitrogen. The capillary was sealed and several EPR spectra were run at different temperatures. Product analysis was performed by quenching the reaction with an aqueous solution of NaOH and extracting with DCM. The mixtures were analysed by GC–MS and, when possible, by ^{1}H NMR and ^{13}C NMR spectroscopy.

General procedure for the reaction of aryl azides with $GaCl_3$. A pentane solution of gallium trichloride (0.55 mL of 0.5 M; 0.28 mmol) was added under a nitrogen atmosphere to a DCM solution of the azide (0.25 mmol in 4 mL) at rt. Gas was evolved and an intense blue or violet colour developed. The resulting solution was then transferred into a capillary quartz tube and purged with nitrogen. The capillary was sealed, and the sample was analysed by EPR spectroscopy at several different temperatures. Products analysis was performed as above.

Ethyl 5-azidopentanoate (9) [48] was prepared by treatment of the corresponding alkyl bromide with sodium azide in DMSO [49]; IR (ν_{max}, $CHCl_3$), 1718 (CO) and 2092 (N_3) cm^{-1}; ^{1}H NMR (400 MHz) δ 1.24 (t, J = 7.2 Hz, 3H), 1.54–1.77 (m, 4H), 2.32 (t, J = 6.9 Hz, 2H), 3.28 (t, J = 6.6 Hz, 2H), 4.13 (q, J = 7.2 Hz, 2H).

Aromatic azides **1**–**8** were prepared by standard diazotisation of the corresponding anilines followed by treatment with sodium azide, and were identified by comparison with literature data: phenyl azide (**1**) [50], 1-azido-4-methoxybenzene (**2**) [48], 1-azido-3-methoxybenzene (**4**) [51], 1-azido-2-methoxybenzene (**5**) [48], 1-azido-4-fluorobenzene (**6**) [48], 4-azidobenzonitrile (**7**) [52] and 2-azidonaphthalene (**8**) [53]. 2,3,5,6-Tetradeuterio-4-methoxyphenyl azide (**3**) was prepared by diazotisation of 2,3,5,6-tetradeuterio-4-methoxyaniline, derived in turn from the reaction of 3,5-dideuterio-4-methoxyaniline hydrochloride with boiling D_2O for 4 days in a sealed tube [31].

Supporting Information

Supporting information features general procedures, EPR spectra from azides **4** and **5,** deconvolution of ENDOR spectrum from azide **6**, Cartesian coordinates for DFT-computed structures of dimer and trimer radical cations.

Supporting Information File 1

EPR and pulsed ENDOR study of intermediates from reactions of aromatic azides with group 13 metal trichlorides
[http://www.beilstein-journals.org/bjoc/content/supplementary/1860-5397-6-84-S1.pdf]

Acknowledgements

We thank EaStChem and the EPSRC (UK Basic Technology Programme grant GR/S85726/01) for financial assistance. We also acknowledge financial support from MIUR, Italy (2008 PRIN funds for 'Properties and reactivity of free radicals in complex environments and their role in oxidative processes and in organic synthesis').

References

1. Takami, K.; Yorimitsu, H.; Oshima, K. *Org. Lett.* **2002,** *4,* 2993–2995. doi:10.1021/ol026401w

2. Ichinose, Y.; Nozaki, K.; Wakamatsu, K.; Oshima, K.; Utimoto, K. *Tetrahedron Lett.* **1987,** *28,* 3709–3712. doi:10.1016/S0040-4039(00)96363-9
3. Nozaki, K.; Ichinose, Y.; Wakamatsu, K.; Oshima, K.; Utimoto, K. *Bull. Chem. Soc. Jpn.* **1990,** *63,* 2268–2272. doi:10.1246/bcsj.63.2268
4. Taniguchi, M.; Nozaki, K.; Miura, K.; Oshima, K.; Utimoto, K. *Bull. Chem. Soc. Jpn.* **1992,** *65,* 349–353. doi:10.1246/bcsj.65.349
5. Chatgilialoglu, C.; Ballestri, M.; Ferreri, C.; Vecchi, D. *J. Org. Chem.* **1995,** *60,* 3826–3831. doi:10.1021/jo00117a038
6. Schiefer, M.; Reddy, N. D.; Ahn, H.-J.; Stasch, A.; Roesky, H. W.; Schlicker, A. C.; Schmidt, H.-G.; Noltemeyer, M.; Vidovic, D. *Inorg. Chem.* **2003,** *42,* 4970–4976. doi:10.1021/ic0342806
7. Takami, K.; Mikami, S.; Yorimitsu, H.; Shinokubo, H.; Oshima, K. *J. Org. Chem.* **2003,** *68,* 6627–6631. doi:10.1021/jo0344790
8. Mikami, S.; Fujita, K.; Nakamura, T.; Yorimitsu, H.; Shinokubo, H.; Matsubara, S.; Oshima, K. *Org. Lett.* **2001,** *3,* 1853–1855. doi:10.1021/ol015904j
9. Takami, K.; Usugi, S.-I.; Yorimitsu, H.; Oshim, K. *Synthesis* **2005,** *5,* 824–839. doi:10.1055/s-2005-861846
10. Balch, A. L.; Latos-Grazynski, L.; Noll, B. C.; Phillips, S. L. *Inorg. Chem.* **1993,** *32,* 1124–1129. doi:10.1021/ic00059a017
11. Lee, K. E.; Higa, K. T. *J. Organomet. Chem.* **1993,** *449,* 53–59. doi:10.1016/0022-328X(93)80106-L
12. Yasuda, M.; Miyai, T.; Shibata, I.; Baba, A.; Nomura, R.; Matsuda, H. *Tetrahedron Lett.* **1995,** *36,* 9497–9500. doi:10.1016/0040-4039(95)02057-8
13. Miyai, T.; Inoue, K.; Yasuda, M.; Baba, A. *Synlett* **1997,** *6,* 699–700. doi:10.1055/s-1997-3275
14. Miyai, T.; Inoue, K.; Yasuda, M.; Shibata, I.; Baba, A. *Tetrahedron Lett.* **1998,** *39,* 1929–1932. doi:10.1016/S0040-4039(98)00050-1
15. Inoue, K.; Sawada, A.; Shibata, I.; Baba, A. *J. Am. Chem. Soc.* **2002,** *124,* 906–907. doi:10.1021/ja017537c
16. Hayashi, N.; Shibata, I.; Baba, A. *Org. Lett.* **2004,** *6,* 4981–4983. doi:10.1021/ol047849v
17. Benati, L.; Bencivenni, G.; Leardini, R.; Minozzi, M.; Nanni, D.; Scialpi, R.; Spagnolo, P.; Zanardi, G.; Rizzoli, C. *Org. Lett.* **2004,** *6,* 417–420. doi:10.1021/ol036268n
18. Benati, L.; Bencivenni, G.; Leardini, R.; Minozzi, M.; Nanni, D.; Scialpi, R.; Spagnolo, P.; Zanardi, G. *J. Org. Chem.* **2005,** *70,* 3046–3053. doi:10.1021/jo0478095
19. Benati, L.; Bencivenni, G.; Leardini, R.; Minozzi, M.; Nanni, D.; Scialpi, R.; Spagnolo, P.; Zanardi, G. *J. Org. Chem.* **2006,** *71,* 434–437. doi:10.1021/jo0521697
20. Benati, L.; Bencivenni, G.; Leardini, R.; Minozzi, M.; Nanni, D.; Scialpi, R.; Spagnolo, P.; Zanardi, G. *J. Org. Chem.* **2006,** *71,* 5822–5825. doi:10.1021/jo060824k
21. Bencivenni, G.; Lanza, T.; Leardini, R.; Minozzi, M.; Nanni, D.; Spagnolo, P.; Zanardi, G. *J. Org. Chem.* **2008,** *73,* 4721–4724. doi:10.1021/jo800453z
22. Lanza, T.; Leardini, R.; Minozzi, M.; Nanni, D.; Spagnolo, P.; Zanardi, G. *Angew. Chem., Int. Ed.* **2008,** *47,* 9439–9442. doi:10.1002/anie.200804333
23. Minozzi, M.; Nanni, D.; Spagnolo, P. *Chem.–Eur. J.* **2009,** *15,* 7830–7840. doi:10.1002/chem.200802710
24. Baguley, P. A.; Walton, J. C. *Angew. Chem., Int. Ed.* **1998,** *37,* 3072–3082. doi:10.1002/(SICI)1521-3773(19981204)37:22<3072::AID-ANIE3072>3.0.CO;2-9
25. Studer, A.; Amrein, S. *Synthesis* **2002,** *7,* 835–849. doi:10.1055/s-2002-28507
26. Darmency, V.; Renaud, P. *Top. Curr. Chem.* **2006,** *263,* 71–106. doi:10.1007/128_030
27. Walton, J. C. *Top. Curr. Chem.* **2006,** *264,* 163–200. doi:10.1007/128_021
28. Walton, J. C.; Studer, A. *Acc. Chem. Res.* **2005,** *38,* 794–802. doi:10.1021/ar050089j
29. Benati, L.; Bencivenni, G.; Leardini, R.; Nanni, D.; Minozzi, M.; Spagnolo, P.; Scialpi, R.; Zanardi, G. *Org. Lett.* **2006,** *8,* 2499–2502. doi:10.1021/ol0606637
30. Bencivenni, G.; Lanza, T.; Minozzi, M.; Nanni, D.; Spagnolo, P.; Zanardi, G. *Org. Biomol. Chem.* **2010,** *8,* 3444–3450. doi:10.1039/c001848a
31. Bencivenni, G.; Cesari, R.; Nanni, D.; El Mkami, H.; Walton, J. C. *Org. Biomol. Chem.* **2010**. doi:10.1039/C0OB00084A
32. Davies, E. R. *Phys. Lett. A* **1974,** *47,* 1–2. doi:10.1016/0375-9601(74)90078-4
33. Van Doorslaer, S.; Vinck, E. *Phys. Chem. Chem. Phys.* **2007,** *9,* 4620–4638. doi:10.1039/b701568b
34. Epel, B.; Manikandan, P.; Kroneck, P. M. H.; Goldfarb, D. *Appl. Magn. Reson.* **2001,** *21,* 287–297. doi:10.1007/BF03162408
35. *Gaussian 03,* Revision A.1; Gaussian, Inc.: Pittsburgh, PA, 2003.
36. Barone, V. In *Recent Advances in Density Functional Theory;* Chong, D. P., Ed.; World Scientific Publishing Co.: Singapore, 1996. [for the basis set B3LYP/EPRiii//B3LYP/6–31G(d)].
37. Forrester, A. R.; Hay, J. M.; Thomson, R. H. *Organic Chemistry of Stable Free Radicals;* Academic Press: New York, 1968; pp 247–268. Chapter 6.
38. Male, R.; Allendoerfer, R. D. *J. Phys. Chem.* **1988,** *92,* 6237–6240. doi:10.1021/j100333a014
39. Wolf, J. F.; Forbes, C. E.; Gould, S.; Shacklette, L. W. *J. Electrochem. Soc.* **1989,** *136,* 2887–2891. doi:10.1149/1.2096307
40. Wienk, M. M.; Janssen, R. A. J. *J. Am. Chem. Soc.* **1996,** *118,* 10626–10628. doi:10.1021/ja9616591
41. Petr, A.; Dunsch, L. *J. Phys. Chem.* **1996,** *100,* 4867–4872. doi:10.1021/jp952965o
42. Petr, A.; Dunsch, L. *J. Electroanal. Chem.* **1996,** *419,* 55–59. doi:10.1016/S0022-0728(96)04861-9
43. Simon, P.; Farsang, G.; Amatore, C. *J. Electroanal. Chem.* **1997,** *435,* 165–171. doi:10.1016/S0022-0728(97)00284-2
44. Goto, M.; Otsuka, K.; Chen, X.; Tao, Y.; Oyama, M. *J. Phys. Chem. A* **2004,** *108,* 3980–3986. doi:10.1021/jp035579c
45. Becke, A. D. *J. Chem. Phys.* **1993,** *98,* 5648–5652. doi:10.1063/1.464913
46. Schäfer, A.; Horn, H.; Ahlrichs, R. *J. Chem. Phys.* **1992,** *97,* 2571–2577. doi:10.1063/1.463096
47. Hayashi, N.; Shibata, I.; Baba, A. *Org. Lett.* **2004,** *6,* 4981–4983. doi:10.1021/ol047849v
48. Khoukhi, N.; Vaultier, M.; Carrié, R. *Tetrahedron* **1987,** *43,* 1811–1822. doi:10.1016/S0040-4020(01)81492-7
49. L'abbé, G.; Sannen, I.; Dehaen, W. *J. Chem. Soc., Perkin Trans. 1* **1993,** 27–29. doi:10.1039/P19930000027
50. Huber, M.-L.; Pinhey, J. T. *J. Chem. Soc., Perkin Trans. 1* **1990,** 721–722. doi:10.1039/P19900000721
51. Di Nunno, L.; Scilimati, A. *Tetrahedron* **1986,** *42,* 3913–3920. doi:10.1016/S0040-4020(01)87546-3
52. Nicolaides, A.; Enyo, T.; Miura, D.; Tomioka, H. *J. Am. Chem. Soc.* **2001,** *123,* 2628–2636. doi:10.1021/ja003709e
53. Forster, M. O.; Fierz, H. E. *J. Chem. Soc., Trans.* **1907,** *91,* 1942–1953. doi:10.1039/CT9079101942

License and Terms

Beilstein Journal of Organic Chemistry

Kinetic studies and predictions on the hydrolysis and aminolysis of esters of 2-*S*-phosphorylacetates

Milena Trmčić and David R. W. Hodgson*

Full Research Paper

Open Access

Address:
Centre for Bioactive Chemistry, Department of Chemistry, Durham University, Science Laboratories, South Road, Durham DH1 3LE, United Kingdom

Email:
Milena Trmčić - milatrmcic@yahoo.com; David R. W. Hodgson* - d.r.w.hodgson@durham.ac.uk

* Corresponding author

Keywords:
aminolysis; heterobifunctional cross-linker; hydrolysis; kinetics; thiophosphate

Beilstein J. Org. Chem. **2010,** *6,* 732–741.
doi:10.3762/bjoc.6.87

Received: 05 July 2010
Accepted: 07 August 2010
Published: 16 August 2010

Guest Editor: J. Murphy

Abstract

Background: Heterobifunctional cross-linking agents are useful in both protein science and organic synthesis. Aminolysis of reactive esters in aqueous systems is often used in bioconjugation chemistry, but it must compete against hydrolysis processes. Here we study the kinetics of aminolysis and hydrolysis of 2-*S*-phosphorylacetate ester intermediates that result from displacement of bromide by a thiophosphate nucleophile from commonly used bromoacetate ester cross-linking agents.

Results: We found cross-linking between uridine-5′-monophosphorothioate and D-glucosamine using *N*-hydroxybenzotriazole and *N*-hydroxysuccinimde bromoacetates to be ineffective. In order to gain insight into these shortfalls, 2-*S*-(5′-thiophosphoryluridine)acetic acid esters were prepared using *p*-nitrophenyl bromoacetate or *m*-nitrophenyl bromoacetate in combination with uridine-5′-monophosphorothioate. Kinetics of hydrolysis and aminolysis of the resulting *p*- and *m*-nitrophenyl 2-*S*-(5′-thiophosphoryluridine)acetates were determined by monitoring the formation of phenolate ions spectrophotometrically as a function of pH. The *p*- and *m*-nitrophenyl 2-*S*-(5′-thiophosphoryluridine)acetates showed similar reactivity profiles despite the significant difference in the pK_{aH} values of their nitrophenolate leaving groups. Both were more reactive with respect to hydrolysis and aminolysis in comparison to their simple acetate progenitors, but their calculated selectivity towards aminolysis vs hydrolysis, while reasonable, would not lead to clean reactions that do not require purification. Extrapolations of the kinetic data were used to predict leaving group pK_a values that could lead to improved selectivity towards aminolysis while retaining reasonable reaction times.

Conclusions: Both *p*- and *m*-nitrophenyl 2-*S*-(5′-thiophosphoryluridine)acetates show some selectivity towards aminolysis over hydrolysis, with the *m*-nitrophenolate system displaying slightly better selectivity. Extrapolation of the data for hydrolysis and aminolysis of these esters suggests that the use of readily accessible trifluoroethyl 2-*S*-(5′-thiophosphoryluridine)acetate with a leaving group pK_{aH} of 12.4 should afford better selectivity while maintaining reasonable reaction times. Kinetically, *p*- and *m*-nitrophenyl 2-*S*-(5′-thiophosphoryluridine)acetates show similar properties to *o*-nitrophenyl 2-*S*-ethylacetate, and show no evidence for intramolecular catalysis of hydrolysis or aminolysis by the phosphoryl groups.

Introduction

Heterobifunctional cross-linking agents are used widely in protein science for forming covalently-bonded protein-protein complexes [1] and protein-small molecule systems [2]. *S*-Alkylation and *N*-acylation processes are used together extensively as orthogonal methods to effect hetero-cross-linking. *S*-Alkylation processes are not affected by competing hydrolysis, however, *N*-acylation using reactive esters is hampered by competing hydrolysis processes. The aminolysis and hydrolysis of activated esters has been well studied [3], however, the hydrolysis and aminolysis kinetics of 2-*S*-phosphorylacetic acid esters **2**, which are present as intermediates when using 2-bromoacetic acid esters **1** as heterobifunctional cross-linking agents with thiophosphate systems **3** (Scheme 1), have not been investigated.

In this paper we present our findings into the use of bromoacetate-based cross-linking agents with thiophosphate nucleophiles **3**, where our aim was to generate nucleoside-pyrophosphate mimics as potential glycosyl transferase inhibitors under aqueous conditions. Initially, we focus on the use of the bromoacetic acid esters of *N*-hydroxybenzotriazole **1** (R = Bt) and *N*-hydroxysuccinimide **1** (R = NHS) before moving on to studies on the aminolysis and hydrolysis kinetics of *p*- and *m*-nitrophenyl 2-*S*-(5′-thiophosphoryluridine)acetates **7** (R = *p*NP) and **7** (R = *m*NP) with a view towards tuning the leaving group properties of 2-*S*-phosphorylacetic acid esters **2** in such a way as to favour aminolysis over undesired hydrolysis processes. In addition to kinetic studies, we present predictions of leaving group characteristics, based on correlation with literature data, that should allow for improvement in the performance of 2-bromoacetic acid esters **1** as heterobifunctional cross-linking agents, particularly in the context of small-molecule synthetic applications.

Results and Discussion

2-Bromoacetic acid esters **1** were prepared by allowing bromoacetyl bromide to react with the respective *N*-hydroxy species or nitrophenols in the presence of pyridine. After standard aqueous work-up, the products were 70–99% pure as measured by integration of signals in ^{1}H NMR spectra, and were used without further purification. Uridine-5′-monophosphorothioate **4** was prepared using an adaptation of Whitesides' procedure for the thiophosphorylation of adenosine [4]. We performed preliminary studies into thiophosphate-amine cross-linking using both *N*-hydroxybenzotriazole **1** (R = Bt) and *N*-hydroxysuccinimde **1** (R = NHS) esters of bromoacetic acid with thiophosphate **4** and D-glucosamine as a representative thiophosphate and a representative amine, respectively (Scheme 2). A mixed water/MeCN solvent system was employed where the reagents formed homogeneous solutions that we hoped to use for simple kinetic studies. When using the *N*-hydroxybenzotriazole system (leaving group pK_{aH} = 4.60 [5]), we performed several experiments at different pH values and at concentrations of ~0.02 M for all three components. These conditions represented a compromise between the lower concentrations required to maintain a homogeneous solution and the higher concentrations required to favour the bimolecular aminolysis and *S*-bridging-thiophosphate formation processes.

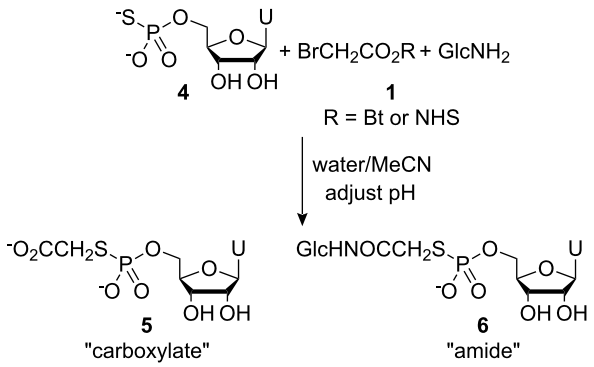

Scheme 2: Cross-linking between thiophosphate **4**, D-glucosamine ($GlcNH_2$) and bromoacetyl-*N*-hydroxybenzotriazole **1** (R = Bt) or bromoacetyl-*N*-hydroxysuccinimide **1(** R = NHS) in water/MeCN.

Product mixtures were resolved by ion exchange chromatography (Supporting Information File 1), and product distributions were assessed by integration of the absorbance-retention time data (Supporting Information File 1, Figure 1). In the most favourable cases (pH 6.08 and 7.80), ~65% of the desired amide product was produced along with ~30% of the "carboxylate" arising through competing hydrolysis processes. Chromatographic separation proved time consuming and resolution of the

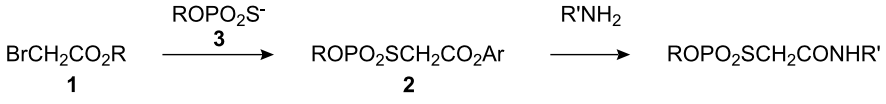

Scheme 1: Use of 2-bromoacetic acid esters as heterobifunctional cross-linking agents.

products was poor, further illustrating the need to improve selectivity and avoid purification steps. Furthermore, the preparation of bromoacetyl-*N*-hydroxybenzotriazole **1** (R = Bt) proved troublesome, and the compound itself was not stable on storage. We next tried the *N*-hydroxysuccinimde system **1** (R = NHS) (leaving group pK_{aH} = 6.0 [6]) where we found that the desired amide product and *N*-hydroxysuccinimde co-eluted in the ion exchange chromatography, and, thus, we did not pursue the use of this system any further.

In order to gain an understanding of the aminolysis vs hydrolysis processes, we re-focused our studies towards activated bromoacetic acid phenyl ester systems that were more readily amenable to kinetic studies via UV–vis spectrophotometry. The 2-bromoacetic acid esters of *p*-nitro- and *m*-nitrophenol were allowed to react with thiophosphate **4** to generate *p*- and *m*-nitrophenyl 2-*S*-(5′-thiophosphoryluridine)acetates **7** (R = *p*NP) and **7** (R = *m*NP) (Scheme 3). In order to obtain simple kinetic data, it was essential to ensure that the nitrophenyl esters **7** (R = *p*NP) and **7** (R = *m*NP) were the only sources of the *p*- and *m*-nitrophenolate ions that were observed spectrophotometrically. With this in mind, thiophosphate **4** was used in excess to ensure complete, rapid consumption of the 2-bromoacetic acid-based phenyl esters **1** (R = *p*NP) and **1** (R = *m*NP) that could also give rise to *p*- and *m*-nitrophenolate ions during their hydrolyses. High concentrations of both thiophosphate **4** and 2-bromoacetic acid esters **1** (R = *p*NP) and **1** (R = *m*NP) were used in order to ensure that the S_N2 reactions between these reagents occurred rapidly with minimal scope for hydrolysis of the esters during synthesis. Material containing 0.2 equiv of unreacted thiophosphate **4** and 1.0 equiv of NaBr by-product was then used for kinetic studies.

Hydrolysis and aminolysis kinetic studies were carried out by observing spectrophotometrically the formation of *p*- or *m*-nitrophenolate ions arising from displacement of these ions from nitrophenyl esters **7** (R = *p*NP) and **7** (R = *m*NP) (Scheme 4).

Hydrolysis studies were performed in a range of buffers of differing pHs and strengths. The formation of *p*- and *m*-nitrophenolate ions was monitored at λ ~ 400 nm, and the spectrophotometric data showed simple exponential rises, confirming pseudo first order behaviour. We only found strong evidence for buffer catalysis when using HEPES and EPPS buffers, and even here, the effect was small (k_{GB} < 0.03 $M^{-1}min^{-1}$ in both cases). In these cases, recorded k_{hydrol} values correspond to extrapolation of experimental measurements over a range of different buffer concentrations, to zero buffer concentration. The fact that little general base assistance was observed is in line with observations of reactions between *p*-nitrophenyl acetate and other relatively non-basic amines [3]. Surprisingly, no evidence for general base catalysis was found with the more basic amine buffers (CHES and CAPS). Observed pseudo first order rate coefficients, k_{hydrol} (Table 1), were plotted as a function of pH (Figure 1), and the data were

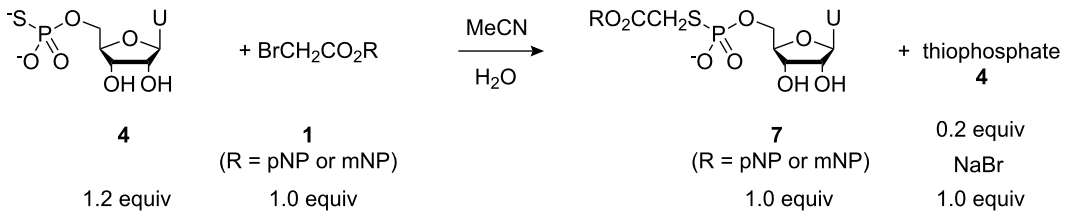

Scheme 3: Ligation of 2-bromoacetic acid esters **1** (R = *p*NP or *m*NP) to thiophosphate **4**.

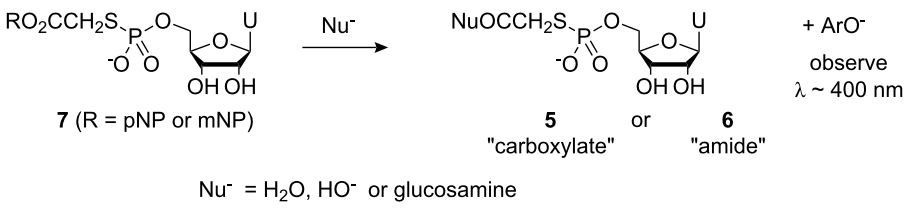

Scheme 4: Displacement of *p*- or *m*-nitrophenolate ions from nitrophenyl esters **7** (R = *p*NP) and **7** (R = *m*NP).

then fitted to a simple kinetic model for water- and hydroxide-promoted hydrolysis, namely,

$$k_{\text{hydrol}} = k_0 + k_{\text{OH}}[\text{OH}^-] \quad (1)$$

where

$$[\text{OH}^-] = 10^{\text{pH}-14} \quad (2)$$

Table 1: Observed kinetic data for the hydrolysis of *p*-nitrophenyl ester **7** (R = *p*NP)[a] and *m*-nitrophenyl ester **7** (R = *m*NP)[b] at 25 °C.

pH	k_{hydrol} (min^{-1})[a]	k_{hydrol} (min^{-1})[b]
10.5	4.59	2.59
10.17	2.79	0.83
9.81	0.68	0.51
9.44	0.36	0.27
9.06	0.18	0.11
8.00	3.0×10^{-2}	2.2×10^{-2}
7.50	1.3×10^{-2}	7.3×10^{-3}
7.10	6.0×10^{-3}	3.7×10^{-3}
6.60	2.0×10^{-3}	8.8×10^{-4}
6.20	1.7×10^{-3}	3.0×10^{-3}
5.20	1.8×10^{-3}	1.2×10^{-3}
4.80	2.1×10^{-3}	1.3×10^{-3}
4.66	1.8×10^{-3}	8.2×10^{-4}

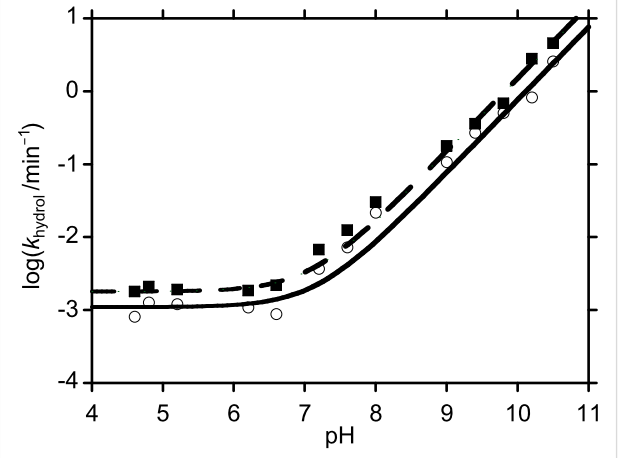

Figure 1: log k_{hydrol} vs pH for the hydrolysis *p*-nitrophenyl ester **7** (R = *p*NP) and *m*-nitrophenyl ester **7** (R = *m*NP) at 25 °C. Squares correspond to data for *p*-nitrophenyl ester **7** (R = *p*NP); circles correspond to data for *m*-nitrophenyl ester **7** (R = *m*NP). The dashed line corresponds to data fitting for *p*-nitrophenyl ester **7** (R = *p*NP) and the solid line corresponds to data fitting for *m*-nitrophenyl ester **7** (R = *m*NP).

The pseudo first order rate coefficients, k_0, for water-promoted hydrolyses of *p*-nitrophenyl ester **7** (R = *p*NP) and *m*-nitrophenyl ester **7** (R = *m*NP) were 1.8×10^{-3} min^{-1} and 1.1×10^{-3} min^{-1}, respectively. The second order rate coefficients for hydroxide-promoted hydrolyses, k_{OH}, for these species were 1.5×10^4 $\text{M}^{-1}\text{min}^{-1}$ and 7.6×10^3 $\text{M}^{-1}\text{min}^{-1}$, respectively.

In order to assess the relative performance of *p*-nitrophenyl ester **7** (R = *p*NP) and *m*-nitrophenyl ester **7** (R = *m*NP) with respect to selective aminolysis in competition with hydrolysis processes, aminolysis studies were performed over a range of pHs. D-Glucosamine was chosen as a model amine system to investigate these properties because of its relatively low pK_{aH} of 7.75 [7]. Thus, even at relatively low pHs, a substantial proportion of the amine will be in its neutral, nucleophilic form. In addition, by structural analogy with ethanolamine, despite D-glucosamine's relatively low basicity, it was still expected to display good nucleophilicity [8]. Observed pseudo first order rate coefficients, k_{aminol} (Table 2), were plotted as a function of pH (Figure 2), and the data were then fitted to the expression.

$$k_{\text{aminol}} = k_0 + k_{\text{OH}}(10^{\text{pH}-14}) + k_{\text{NH}_2}[\text{GlcNH}_2]_{\text{total}}(10^{-\text{p}K_{\text{aH}}} / (10^{-\text{p}K_{\text{aH}}} + 10^{-\text{pH}})) \quad (3)$$

where fixed values for k_0 and k_{OH} determined from the hydrolysis experiments, and a literature value for p$K_{\text{aH}}(\text{GlcNH}_2)$ = 7.75 [7] was used.

Table 2: Observed kinetic data for the aqueous aminolysis and hydrolysis of *p*-nitrophenyl ester **7** (R = *p*NP)[a] and *m*-nitrophenyl ester **7** (R = *m*NP)[b] in the presence of 0.05 M D-glucosamine at 25 °C (n.d. = not determined).

pH	k_{aminol} (min^{-1})[a]	k_{aminol} (min^{-1})[b]
10.17	2.14	n.d.
9.81	2.19	n.d.
9.44	0.89	0.57
9.06	0.49	0.27
8.44	0.37	0.17
8.00	0.20	0.16
7.50	0.13	9.8×10^{-2}
7.10	7.7×10^{-2}	7.1×10^{-2}
6.60	2.2×10^{-2}	1.8×10^{-2}
6.20	8.1×10^{-3}	n.d.
5.88	3.7×10^{-3}	n.d.
5.20	2.3×10^{-3}	n.d.
4.88	2.1×10^{-3}	n.d.

The second order rate coefficients for aminolysis by D-glucosamine, k_{NH2}, for *p*-nitrophenyl ester **7** (R = *p*NP) and *m*-nitrophenyl ester **7** (R = *m*NP) were found to be 6.1 $\text{M}^{-1}\text{min}^{-1}$ and 5.1 $\text{M}^{-1}\text{min}^{-1}$, respectively. These results suggest that the *m*-nitrophenyl ester **7** (R = *m*NP) retains com-

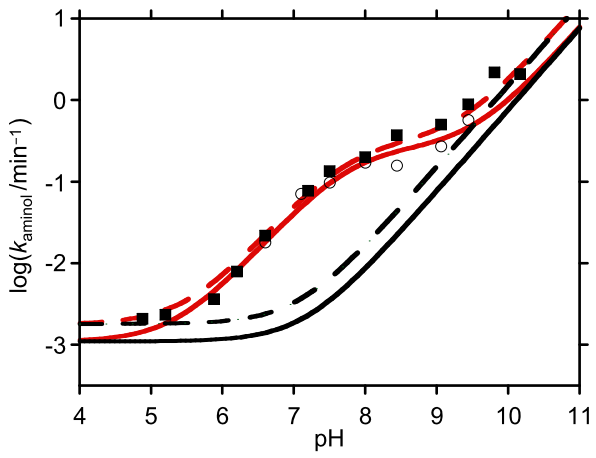

Figure 2: log k_{aminol} vs pH for the combined aminolysis and hydrolysis of *p*-nitrophenyl ester **7** (R = *p*NP) and *m*-nitrophenyl ester **7** (R = *m*NP) in the presence of 0.05 M D-glucosamine at 25 °C. Squares correspond to data for *p*-nitrophenyl ester **7** (R = *p*NP); circles correspond to data for *m*-nitrophenyl ester **7** (R = *m*NP). The dashed black line corresponds to data fitting for the hydrolysis of *p*-nitrophenyl ester **7** (R = *p*NP) and the solid black line corresponds to data fitting for the hydrolysis of *m*-nitrophenyl ester **7** (R = *m*NP) (Figure 1). The dashed red line corresponds to data fitting for the combined aminolysis and hydrolysis of *p*-nitrophenyl ester **7** (R = *p*NP); solid red line corresponds to data fitting for the combined aminolysis and hydrolysis of *m*-nitrophenyl ester **7** (R = *m*NP).

parable reactivity towards aminolysis by D-glucosamine, whereas, it is less susceptible to attack by water and hydroxide ion than the *p*-nitrophenyl ester **7** (R = *p*NP). On this basis, the *m*-nitrophenyl ester **7** (R = *m*NP) would appear to offer better selectivity properties, and, thus, *m*-nitrophenyl 2-bromoacetate **1** (R = *m*NP) represents a potentially more effective heterobifunctional cross-linking agent than *p*-nitrophenyl 2-bromoacetate **1** (R = *p*NP). Our kinetic studies were performed under pseudo first order conditions in order to simplify kinetic analysis. However, with rate coefficient data in hand, we are able to make predictions on the relative selectivity of nitrophenyl esters **7** (R = *p*NP) and **7** (R = *m*NP) towards aminolysis over hydrolysis processes under more realistic conditions where activated ester and amine nucleophile are present at comparable concentrations. The concentrations of reagents in most synthetic laboratory reactions are usually ~0.01–0.05 M with one reagent being present in slight excess. Under standard conditions for bioconjugation processes, these concentrations are usually significantly lower and, consequently, lower yields of amide product are expected. With the more favourable synthetic applications in mind, we have used numerical integration techniques, in combination with the values for the rate coefficients k_0, k_{OH} and k_{NH2}, to predict the relative selectivities of nitrophenyl esters **7** (R = *p*NP) and **7** (R = *m*NP) towards aminolysis by D-glucosamine over hydrolysis (see experimental section for details of these calculations). Our kinetic model is described in Scheme 5.

We chose to employ ester concentrations of 0.05 M and D-glucosamine concentration of 0.055 M that are expected to form homogeneous solutions that are amenable to simple kinetic modelling. Our predictive analyses were performed ~pH 7.4 based on King's approach for predicting the optimal reaction pH for reactions between nucleophiles and reactive electrophiles [9]. The results from this exercise are plotted below (Figure 3 and Figure 4).

For the *p*-nitrophenyl ester **7** (R = *p*NP), pH_{max} was predicted to be 7.41, and 99% consumption of the ester was expected to take ~2 h. Under these conditions, 90% of the ester is expected to be converted to the amide. For the *m*-nitrophenyl ester **7** (R = *m*NP), pH_{max} was predicted to be 7.46, and 99% consumption of the ester was expected to take ~3 h. Under these conditions, 93% of the ester is expected to be converted into the amide. Clearly, these calculations show that selectivity towards amino-

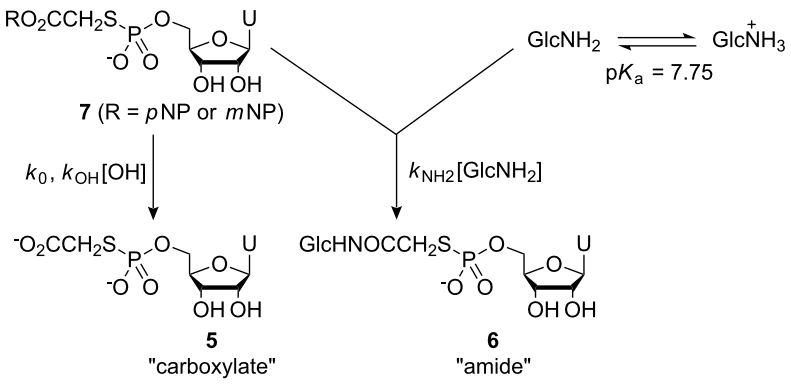

Scheme 5: Kinetic model for competing hydrolysis and aminolysis processes of nitrophenyl esters **7** (R = *p*NP) and **7** (R = *m*NP) in the presence of D-glucosamine.

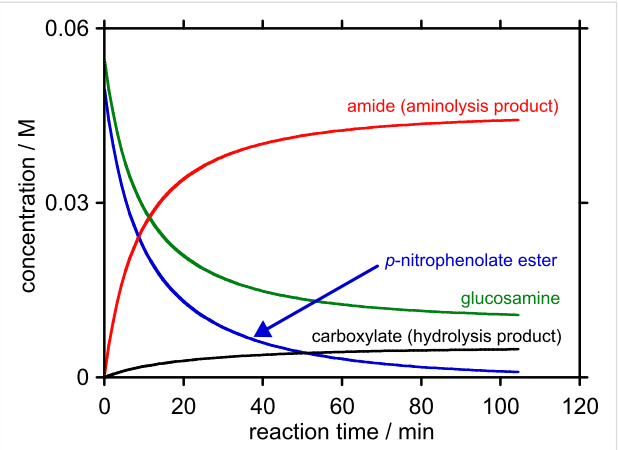

Figure 3: Predicted concentration-time profile for the reaction between starting concentrations of 0.05 M *p*-nitrophenyl ester **7** (R = *p*NP) and 0.055 M D-glucosamine at pH 7.41, 25 °C to 99% consumption of *p*-nitrophenyl ester **7** (R = *p*NP).

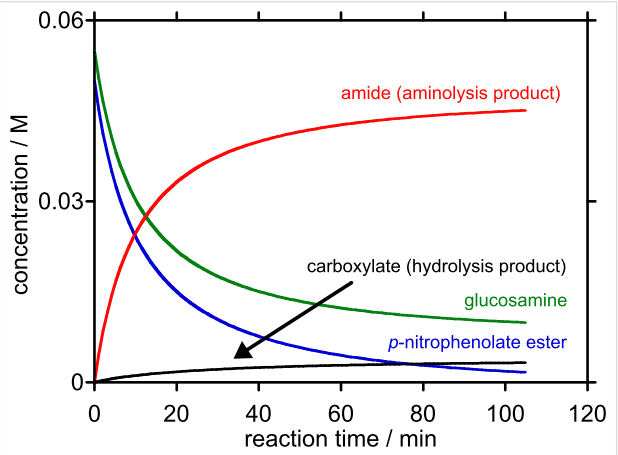

Figure 4: Predicted concentration-time profile for the reaction between starting concentrations of 0.05 M *m*-nitrophenyl ester **7** (R = *m*NP) and 0.055 M D-glucosamine at pH 7.46, 25 °C to 99% consumption of *m*-nitrophenyl ester **7** (R = *m*NP).

lysis needs to be improved before this type of 2-*S*-(5′-thiophosphoryl)acetic acid ester or their bromoacetic acid ester progenitors can be used to provide product mixtures that do not require chromatographic purification. The *m*-nitrophenyl ester **7** (R = *m*NP) shows greater selectivity towards aminolysis than the *p*-nitrophenyl ester **7** (R = *p*NP), and, on this basis, we expect further improvements to be gained through increasing the pK_{aH} of the oxy-anionic leaving group.

By using simple Brønsted relationships, which have been repeatedly shown to be applicable to the hydrolyses and aminolyses of esters [3,10,11], we can estimate the effects that a change in the pK_{aH} of the ester leaving group is likely to have on the values of k_0, k_{OH} and k_{NH2}. Based on the values for k_0, k_{OH} and k_{NH2} determined for the *p*- and *m*-nitrophenyl ester **7** (R = *p*NP) and **7** (R = *m*NP), and the known pK_a values for *p*- and *m*-nitrophenol, which are 7.14 and 8.35, respectively [12], the following Brønsted relationships can be considered:

$$\log k_0 = -1.8\ \mathrm{p}K_{aH} - 1.48 \quad (4)$$

$$\log k_{OH} = -2.5\ \mathrm{p}K_{aH} + 5.93 \quad (5)$$

$$\log k_{NH_2} = -0.064\ \mathrm{p}K_{aH} + 1.24 \quad (6)$$

Studies on phenylacetic acid esters [3] and a range of 2-nitrophenyl 2-substituted acetates [11] show that simple Brønsted behaviour operates for the attack of amine nucleophiles, based on the pK_a of the conjugate acid of the amine (i.e. pK_{aH}). Thus, additional kinetic data from the use of amines other than D-glucosamine could be used to assist predictions of k_{NH2} based on the nature of the amine nucleophile.

Using these Brønsted relationships, together with the starting reagent concentrations of 0.05 M 2-*S*-(5′-thiophosphoryl-uridine)acetic acid ester **7** and 0.055 M glucosamine, we have used numerical methods to predict the ester leaving group pK_{aH} values that are required to afford defined product distributions of aminolysis vs hydrolysis products. The solver function on Microsoft Excel™ was used to determine the pK_{aH} values of (oxy-anionic) leaving groups of 2-*S*-(5′-thiophosphoryl-uridine)acetic acid esters **7** that would be required to obtain given user-defined product distributions when 99% of the starting ester has been consumed. This process was performed for a range of user-defined product distributions over the range of 90–99% aminolysis product. The results from this process are presented in Figure 5.

These predictions rely on the validity of the Brønsted relationships across a broad pK_a range. At higher leaving group pK_a values, one or more of the relationships for k_0, k_{OH} and k_{NH2} may break down. Esters with poorer leaving group (e.g. phenyl acetate) tend to exhibit general species catalysis in their hydrolyses and aminolysis, which will complicate the simple kinetic model that we have used, however, these processs are also expected to exhibit predictable Brønsted behaviour [3,10]. This change in behaviour corresponds to a change in rate determining step from the addition of nucleophile in the case of better leaving groups towards the expulsion of leaving groups in the case of poorer leaving groups. However, very good Brønsted behaviour for the k_{OH} term for acetyl ester hydrolysis has been observed across a very wide leaving group pK_a range [3], thus this term is expected to extrapolate well to higher leaving group pK_{aH} values. Furthermore, log k_0 values usually correlate linearly with log k_{OH} values [10].

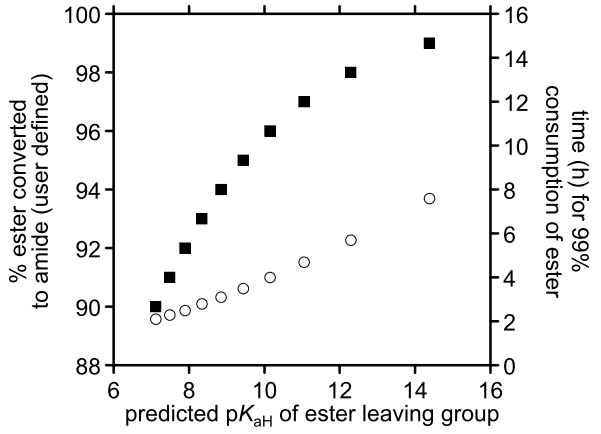

Figure 5: Predicted leaving group pK_{aH} values required for user-defined conversion levels of starting concentrations of 0.05 M 2-*S*-(5′-thiophosphoryluridine)acetic acid ester **7** and 0.055 M D-glucosamine to D-glucosamine amide **6** based on Brønsted extrapolations of k_0, k_{OH} and k_{NH2}. In each case, the calculations proceed to 99% consumption of ester. Squares correspond to % ester converted to amide in relation to pK_{aH} (left hand scale); circles correspond to time taken to attain 99% consumption of the ester with a leaving group of a given pK_{aH}.

In addition, our assumptions rely on a mechanism where the amine nucleophile attacks the ester carbonyl group and displaces the leaving group (Scheme 6A). Given the nature of the thiophosphate group in the 2-position of the ester, we may also consider the possibility of intramolecular nucleophilic catalysis where an oxygen atom of the phosphoryl group displaces the ester leaving group to form a cyclic mixed carboxylic-phosphoric acid anhydride (Scheme 6B) which is then attacked by amine. Alternatively, intramolecular general base catalysis of aminolysis and hydrolysis processes are also conceivable (Scheme 6C).

A comparison of the rate coefficients for the pH-independent hydrolysis of nitrophenyl esters **7** (R = *p*NP) and **7** (R = *m*NP) which were measured as $k_0 = 1.8 \times 10^{-3}$ min^{-1} and 1.1×10^{-3} min^{-1}, respectively with other 2-substituted acetates may provide insight at this point. Holmquist and Bruice have studied the hydrolysis kinetics of 2-nitrophenyl 2-(ethylthio)acetate at 30 °C [10], which is a thioether as opposed to the *S*-bridging-thiophosphates that form the basis of this paper (Figure 6).

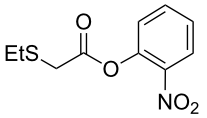

Figure 6: 2-nitrophenyl 2-(ethylthio)acetate.

Whilst we have used *p*-nitrophenyl- and *m*-nitrophenyl esters, and our kinetic studies were performed at 25 °C rather than 30 °C, some analogies with the *o*-nitrophenyl acetate system [10] may be drawn and conclusions may be inferred on the basis of similar leaving group properties of *o*-nitrophenol (pK_{aH} = 7.23 [12]). Rate coefficients for the pH-independent hydrolysis of 2-nitrophenyl 2-(ethylthio)acetate and 2-nitrophenyl acetate were reported in second order form as 1.32×10^{-8} M^{-1}s^{-1} and 1.08×10^{-7} M^{-1}s^{-1}, respectively. In pseudo-first order form these coefficients translate to 4.36×10^{-5} min^{-1} and 3.56×10^{-4} min^{-1}, respectively. When compared with *p*-nitrophenyl acetate, where $k_0 = 3.3 \times 10^{-5}$ min^{-1} at 25 °C [13], *o*-nitrophenyl acetate shows comparable reactivity. On this basis, we would expect 4-nitrophenyl 2-substituted-acetates and 3-nitrophenyl 2-substituted-acetates to show similar reactivity trends to the 2-nitrophenyl 2-substituted-acetates reported by

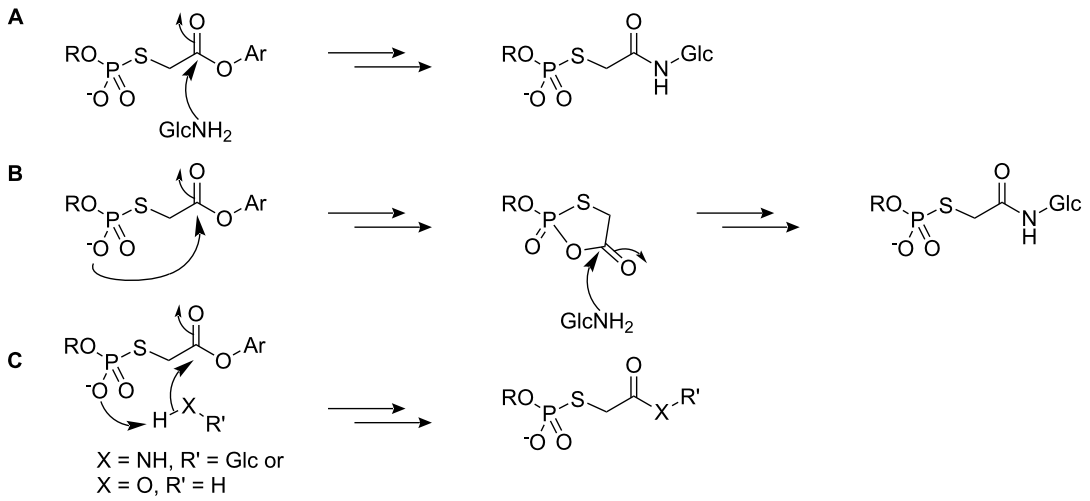

Scheme 6: (A) Direct aminolysis of the ester carbonyl group; (B) intramolecular nucleophilic catalysis of ester cleavage followed by aminolysis of the mixed phosphoric-carboxylic anhydride; (C) intramolecular general base-assisted attack by amine or water.

Holmquist and Bruice [10]. The 2-nitrophenyl 2-(ethylthio)acetate system with $k_0 = 3.56 \times 10^{-4}$ min^{-1} shows comparable, if slightly lower, reactivity to the *p*- and *m*-nitrophenyl esters **7** (R = *p*NP) and **7** (R = *m*NP) with $k_0 = 1.8 \times 10^{-3}$ min^{-1} and 1.1×10^{-3} min^{-1}, respectively. Given these similar values, intramolecular catalysis of the displacement of the phenyl esters in our 2-*S*-thiophosphoryl acetate systems seems unlikely. When considering k_{OH} terms, *p*-nitrophenyl acetate and *o*-nitrophenyl acetate show similar reactivities with k_{OH} = 570 M^{-1}min^{-1} and 1500 M^{-1}min^{-1} (both at 25 °C), respectively, [10,14] which suggests that comparison between *o*-nitrophenyl and *p*- or *m*-nitrophenyl esters should be valid. Again, *p*- and *m*-nitrophenyl esters **7** (R = *p*NP) and **7** (R = *m*NP) with $k_{OH} = 1.5 \times 10^4$ M^{-1}min^{-1} and 7.6×10^3 M^{-1}min^{-1}, respectively, show comparable reactivity to 2-nitrophenyl 2-(ethylthio)acetate ester with $k_{OH} = 1.29 \times 10^4$ M^{-1}min^{-1}. Holmquist and Bruice also performed aminolysis studies on 2-nitrophenyl 2-substituted-acetates [11]. Most salient to our work is a comparison with aminolysis using glycine ethyl ester, with the pK_{aH} of the amine being identical to that of D-glucosamine. Glycine ethyl ester displayed k_{NH2} = 1.1 M^{-1}s^{-1} and 22.6 M^{-1}s^{-1} when used in reactions with 2-nitrophenyl 2-(ethylthio)acetate and 2-nitrophenyl acetate, respectively. In our studies, using D-glucosamine, k_{NH2} values for *p*- and *m*-nitrophenyl esters **7** (R = *p*NP) and **7** (R = *m*NP) were found to be 6.1 M^{-1}min^{-1} and 5.1 M^{-1}min^{-1}, respectively. Although marginally smaller than the value observed for 2-nitrophenyl 2-(ethylthio)acetate, both are similar. The same authors also found a linear correlation between log k_{NH2} and log k_0 over four orders of magnitude in k_0, which supports the idea that extrapolations of k_{NH2} can be made over a reasonably broad range of leaving group pK_{aH} values. Holmquist and Bruice observed that the linear correlation of the aminolysis rate coefficients k_{NH2} was also relatively insensitive to changes in hydrolysis rate coefficients k_0 [11], which is in accord with our observations of relative insensitivity of k_{NH2} to leaving group pK_{aH}.

Conclusion

The esters *p*- and *m*-nitrophenyl esters **7** (R = *p*NP) and **7** (R = *m*NP) both display similar hydrolysis and aminolysis kinetics to 2-nitrophenyl 2-(ethylthio)acetate. The thiophosphoryl group appears to play a spectator role and does not contribute to catalysis in either the hydrolysis or aminolysis processes. Predictive studies suggest that both esters are likely to function as reasonably selective cross-linking agents, however, extrapolations, which appear reasonable in comparison to other acetate ester systems, suggest that an increase in leaving group pK_{aH} to ~12.4 should improve selectively so that chromatographic purification should be avoidable while retaining reasonable reaction times.

Experimental

Uridine-5′-monophosphorothioate **4**

Dry uridine (1 g, 4.1 mmol) was dissolved in freshly distilled triethylphosphate (10 mL) by heating at 50 °C under a nitrogen atmosphere. The flask was then transferred to an ice bath. Ice-cooled 2,6-dimethylpyridine (1.4 mL, 12.3 mmol) and ice-cooled thiophosphoryl chloride (0.75 ml, 7.4 mmol) were added sequentially to the solution and the mixture was stirred for 2 h at 4 °C under a nitrogen atmosphere. The mixture was allowed to warm to room temperature and then poured into petroleum ether (bp 40–60, 300 mL). The white precipitate was allowed to settle, the solvents were decanted and the residual white solid was washed with petroleum ether (2 × 100 mL). Iced water (50 mL) was then added to the solid, and the mixture stirred at 4 °C for 2 h. The solution was adjusted to pH 8 by the addition of potassium hydroxide while warming to room temperature. The solution was extracted successively with diethyl ether (2 × 100 mL) and petroleum ether (bp 40–60, 2 × 100 mL), and the aqueous layer lyophilised for storage. The crude thiophosphate **4** was dissolved in equilibrating buffer (50 mM triethylammonium bicarbonate solution (TEAB) [15], pH 7.6) and loaded using a 50 mL superloop onto a DEAE Sepharose FF column (500 ml bed volume, in a 30 × 5 cm column). Anion exchange chromatography was performed using a linear gradient of triethylammonium bicarbonate solution (50–600 mM) pH 7.6 [15], over 2 h at a flow rate of 30 mL/min using an Äkta Plus chromatography system. Fractions containing the desired product, eluted between 200 and 300 mM of triethylammonium bicarbonate, were combined and lyophilised to give uridine-5′-monophosphorothioate **4** as the bis(triethylammonium) salt. Triethylammonium ions were exchanged for sodium ions by mixing a solution of the bis(triethylammonium) thiophosphate **4** salt (0.6 g from several chromatographic runs) in water (2.5 mL), and a solution of sodium iodide (0.6 g, 4 mmol) in acetone (12.5 mL). Methanol (2.5 mL) and diethyl ether (2.5 mL) were added to assist precipitation. The mixture was centrifuged at 4500 rpm for 10 min and the supernatant liquid decanted. After washing with acetone (2 × 25 mL), the resulting sticky, amorphous pellet was re-dissolved in water and lyophilised to afford a white powder of the disodium salt of uridine-5′-monophosphorothioate **4** (0.3 g, 37%). (Found C, 24.98; H, 3.76; N, 6.38. $C_9H_{11}O_8N_2PSNa_2$ requires C, 24.67; H, 3.91; N, 6.39%); ν_{max} (KBr disk)/cm^{-1} 3220 (OH), 1690 (CO imide), 1270 (PO), 620 (PS); δ_H (500 MHz; D_2O) 7.99 (1H, d, *J* 8.0, 6-C*H*), 5.82 (1H, d, *J* 5.4, 1′-C*H*), 5.79 (1H, d, *J* 8.1, 5-C*H*), 4.24 (1H, t, *J* 5.1, 2′-C*H*), 4.20 (1H, t, *J* 4.5, 3′-C*H*), 4.08–4.12 (1 H, m, 4′-C*H*), 3.82–3.93 (2 H, m, 5′-C*H*); δ_P (160 MHz, D_2O) 44.2; δ_C (125 MHz; D_2O) 167.3 (4-*C*=O), 152.7 (2-*C*=O), 142.3 (6-*C*H), 102.8 (5-*C*H), 88.3 (1′-*C*H), 84.2 (4′-*C*HP), 74.1 (2′-*C*H), 70.3 (3′-*C*H), 63.6 (5′-*C*H$_2$); *m/z* (ES$^-$) 339.0059 (M – H. $C_9H_{12}N_2O_8PS$ requires 339.0057).

p-Nitrophenyl 2-bromoacetate **1** (R = *p*NP)

A solution of pyridine (0.35 mL, 4.3 mmol) in dry DCM (5 mL) was added dropwise to a stirred solution of bromoacetyl bromide (0.38 mL, 4.3 mmol) in dry DCM (5 mL) cooled in an ice bath. Following the careful addition of *p*-nitrophenol (0.6 g, 4.3 mmol), the reaction mixture was stirred for 1 h. Saturated sodium bicarbonate solution (5 mL) was added, the layers were separated, and the organic layer was washed successively with water (2 × 5 mL), hydrochloric acid (0.1 M, 3 × 5 mL) and saturated sodium chloride solution (5 mL). The organic phase was then dried over anhydrous magnesium sulphate and the solvent removed under reduced pressure to give the *p*-nitrophenyl ester (0.752 g, 67%); mp = 72–75 °C (dec); (Found C, 36.94; H, 2.31; N, 5.17. $C_7H_6BrNO_4$ requires C, 36.92; H, 2.31; N, 5.38%); ν_{max} (KBr disc)/cm^{-1} 3110–2963 (CH), 2847 (CH_2), 1770 (ester CO); δ_H (500 MHz; $CDCl_3$) 8.31 (2 H, d, *J* 9.0, C*H*CNO$_2$), 7.34 (2 H, d, *J* 9.3, C*H*CO), 4.08 (2 H, s, CO*CH*$_2$Br); δ_C (125 MHz; $CDCl_3$) 165.2 (*C*=O), 155.1 (*C*O), 145.9 (*C*NO$_2$), 125.6 (NO$_2$C*C*H), 122.4 (*C*HCO), 25.3 (*C*H$_2$Br); *m/z* (EI) 258.9 and 260.9.

m-Nitrophenyl 2-bromoacetate **1** (R = *m*NP)

The procedure for *p*-nitrophenyl 2-bromoacetate **1** (R = *p*NP) was followed except *p*-nitrophenol was replaced by *m*-nitrophenol (0.6 g, 4.3 mmol). After work up, the *m*-nitrophenyl ester was obtained (0.697 g, 62%); mp = 50–53 °C (dec); (Found C, 36.96; H, 2.31; N, 5.39. $C_7H_6BrNO_4$ requires C, 36.92; H, 2.31; N, 5.38%); ν_{max} (KBr disc)/cm^{-1} 3116–3011 (CH), 2864 (CH_2), 1777 (ester CO); δ_H (500 MHz; $CDCl_3$) 8.16 (1 H, d, *J* 8.8, 4-C*H*), 8.05 (1 H, s, 4-C*H*), 7.63 (1 H, t, *J* 8.1, 5-C*H*), 7.53 (1 H, t, *J* 8.2, 6-C*H*), 4.10 (2 H, s, *CH*$_2$Br); δ_C (125 MHz; $CDCl_3$) 165.5 (*C*=O), 150.7 (*C*O), 149.0 (*C*NO$_2$), 130.6 (5-*C*H), 127.8 (6-*C*H), 121.6 (4-*C*H), 117.3 (2-*C*H), 25.2 (*C*H$_2$Br); *m/z* (EI) 258.9 and 260.9.

p- and *m*-Nitrophenyl 2-*S*-(5′-thiophosphoryluridine)acetates **7** (R = *p*NP) and **7** (R = *m*NP) for kinetic studies

The disodium salt of uridine-5′-monophosphorothioate **4** (1 eq, 20 mg, 58.8 μmol) was dissolved in deionised water (0.5 mL) and a solution of *p*- or *m*-nitrophenyl 2-bromoacetate **1** (R = *p*NP) or **1** (R = *m*NP) (0.8 eq, 12 mg, 46 μmol) in acetonitrile (0.5 mL) added. The mixture was stirred for one minute then rapidly frozen in liquid nitrogen followed by lyophilisation to give a light yellow solid of intermediate, *p*- or *m*-nitrophenyl 2-*S*-(5′-thiophosphoryluridine)acetate **7** (R = *p*NP) or **7** (R = *m*NP) (~80% purity by ^{1}H NMR spectroscopy, contaminated with excess uridine-5′-monophosphorothioate **4**). Stock solutions were prepared by dissolving crude *p*- or *m*-nitrophenyl 2-*S*-(5′-thiophosphoryluridine)acetate **7** (R = *p*NP) or **7** (R = *m*NP) (10 mg) in deionised water (3 mL), and this was divided into portions that were frozen in liquid nitrogen. Owing to the instability and crude nature of the nitrophenyl 2-*S*-(5′-thiophosphoryluridine)acetate esters in aqueous solution, only ^{1}H NMR and ES$^-$ analyses were performed. Data for *p*-nitrophenyl 2-*S*-(5′-thiophosphoryluridine)acetate **7** (R = *p*NP) δ_H (500 MHz; D_2O) 8.11 (2 H, d, *J* 9.2, C*H*CNO$_2$), 7.55 (1 H, d, *J* 8.2, 5-C*H*), 7.24 (2H, d, *J* 9.2, *CH*CO), 5.72 (1H, d, *J* 3.9, 1′-C*H*), 5.55 (1H, d, *J* 8.2, 6-*CH*), 4.32–3.91 (5 H, m, 2′–5′-C*H*), 3.7 (2 H, d, *J* 15.4, S*CH*$_2$); δ_P (80 MHz; D_2O) 19.2; *m/z* (ES$^-$) 518.0 (M–H for UMPS-CH_2CO_2-*p*-$C_6H_4NO_2$), 379.1 (M–H for the cyclic hydrolysis product, UMPS$CH_2CO_2^-$).

Hydrolysis studies on *p*- and *m*-nitrophenyl 2-*S*-(5′-thiophosphoryluridine)acetates **7** (R = *p*NP) and **7** (R = *m*NP)

Kinetic measurements were performed by mixing stock solution of the ester (25 μL) with buffer (1.5 mL) to give ~0.1 mM final concentration of ester in the cuvette. The cuvette was inserted into a thermostated (25 °C) compartment of the UV–vis spectrophotometer and the increase in absorbance of *p*- or *m*-nitrophenolate monitored at λ ~ 400 nm. The kinetic data were fitted to the function $A_t = A_0 + A_\infty(1-e^{-k_{obs}\,t})$, and showed clean first order behaviour with observed rate constants k_0.

Aminolysis studies on *p*- and *m*-nitrophenyl 2-*S*-(5′-thiophosphoryluridine)acetates **7** (R = *p*NP) and **7** (R = *m*NP)

D-Glucosamine solution (1.24 M, 60 μL) was mixed with buffer (0.5 M, 1.44 mL) to generate a solution (1.5 mL) with 50 mM final concentration of D-glucosamine in the cuvette. Stock solution of ester was then added, and the kinetics were monitored and analysed as described above.

Buffer preparation for kinetic studies

Buffers were prepared using CAPS (pH 10.5 and 10.17), CHES (pH 9.81, 9.44 and 9.06), EPPS (pH 8.44 and 8.00), HEPES (pH 7.50 and 7.10), MES (pH 6.60, 6.00 and 5.88) and acetate (pH 4.80 and 4.66) systems where pHs were adjusted by the addition of hydrochloric acid or hydroxide solutions. Buffer strengths of 0.05, 0.1, 0.2, 0.3 and 0.5 M were used to check for general species-promoted hydrolysis. All aminolysis studies were performed using 0.5 M buffers in the presence of 0.05 M D-glucosamine.

Data analysis and kinetic predictions

Kinetic data were analysed using Kaleidagraph™. Kinetic predictions were based on Brønsted relationships between observed rate coefficients k_0, k_{OH} and k_{NH2} and the pK_{aH} of the leaving group. Minimisations were performed using the Solver function in Microsoft Excel™. A spreadsheet was constructed

where the reaction was modelled over 1500 time points that were equally spaced to cover 99% consumption of the ester. King's approach towards estimating pH_{max} [9] was adopted in order to ensure that all product distribution estimations were performed at the optimum pH. Minimisations centred on predicting the values of k_0, k_{OH} and k_{NH2} that would lead to a given proportion of the desired amide product, subject to the Brønsted relationship constraints and King's pH_{max} estimation. The Excel™ spreadsheet is available as Supporting Information File 4.

Supporting Information

Supporting information features a PDF document presenting details of studies using the bromoacetyl-OBt system **1** (R = Bt) and bromoacetyl-NHS system **1** (R = NHS), and associated experimental details, as well as Excel™ spreadsheets for the prediction of product outcomes and the optimisation of leaving group pK_{aH} values of 2-*S*-thiophosphate esters with reference to controlling aminolysis over hydrolysis.

Supporting Information File 1

Synthesis and application of bromoacetyl-OBt and NHS systems
[http://www.beilstein-journals.org/bjoc/content/supplementary/1860-5397-6-87-S1.pdf]

Supporting Information File 2

Prediction of product distribution using *p*-nitrophenyl ester **7** (R = *p*NP)
[http://www.beilstein-journals.org/bjoc/content/supplementary/1860-5397-6-87-S2.xls]

Supporting Information File 3

Prediction of product distribution using *m*-nitrophenyl ester **7** (R = *m*NP)
[http://www.beilstein-journals.org/bjoc/content/supplementary/1860-5397-6-87-S3.xls]

Supporting Information File 4

Optimisation of leaving group pK_{aH} values of 2-*S*-thiophosphate esters
[http://www.beilstein-journals.org/bjoc/content/supplementary/1860-5397-6-87-S4.xls]

Acknowledgements

We thank the Department of Chemistry, Durham University for support in the form of a studentship (MT), and the Royal Society for providing funds for the purchase of an ion exchange chromatography system. We thank the referees for constructive comments.

References

1. Hermanson, G. *Bioconjugate Techniques;* Academic Press: San Diego, 1996.
2. Hang, H. C.; Bertozzi, C. R. *Acc. Chem. Res.* **2001,** *34,* 727–736. doi:10.1021/ar9901570
3. Johnson, S. L. *Adv. Phys. Org. Chem.* **1967,** *5,* 237–330. doi:10.1016/S0065-3160(08)60312-3
4. Abril, O.; Crans, D. C.; Whitesides, G. M. *J. Org. Chem.* **1984,** *49,* 1360–1364. doi:10.1021/jo00182a009
5. Carpino, L. A.; Imazumi, H.; Foxman, B. M.; Vela, M. J.; Henklein, P.; El-Faham, A.; Klose, J.; Bienert, M. *Org. Lett.* **2000,** *2,* 2253–2256. doi:10.1021/ol006013z
6. Ames, D. E.; Grey, T. F. *J. Chem. Soc.* **1955,** 631–636. doi:10.1039/jr9550000631
7. Ng, L. T.; Swami, S.; Gordon-Thomson, C. *Radiat. Phys. Chem.* **2006,** *75,* 604–612. doi:10.1016/j.radphyschem.2005.11.006
8. Brotzel, F.; Chu, Y. C.; Mayr, H. *J. Org. Chem.* **2007,** *72,* 3679–3688. doi:10.1021/jo062586z
9. King, J. F.; Rathore, R.; Lam, J. Y. L.; Guo, Z. R.; Klassen, D. F. *J. Am. Chem. Soc.* **1992,** *114,* 3028–3033. doi:10.1021/ja00034a040
10. Holmquist, B.; Bruice, T. C. *J. Am. Chem. Soc.* **1969,** *91,* 2982–2985. doi:10.1021/ja01039a027
11. Holmquist, B.; Bruice, T. C. *J. Am. Chem. Soc.* **1969,** *91,* 2985–2993. doi:10.1021/ja01039a028
12. Jencks, W. P.; Regenstein, J. *CRC Handbook of Biochemistry and Molecular Biolog.;* CRC Press: Cleveland, 1976.
13. Jencks, W. P.; Carriuolo, J. *J. Am. Chem. Soc.* **1960,** *82,* 1778–1786. doi:10.1021/ja01492a058
14. Kirsch, J. F.; Jencks, W. P. *J. Am. Chem. Soc.* **1964,** *86,* 833–837. doi:10.1021/ja01059a018
15. Williams, D. M.; Harris, V. H. In *Organophosphorus reagents: a practical approach in chemistry;* Murphy, P. J., Ed.; OUP: Oxford, 2004.

License and Terms

Beilstein Journal of Organic Chemistry

Catalysis: transition-state molecular recognition?

Ian H. Williams

Commentary

Open Access

Address:
Department of Chemistry, University of Bath, Bath BA2 7AY, United Kingdom

Email:
Ian H. Williams - i.h.williams@bath.ac.uk

Keywords:
catalysis; computational simulation; enzymes; molecular recognition; transition state

Beilstein J. Org. Chem. **2010,** *6,* 1026–1034.
doi:10.3762/bjoc.6.117

Received: 18 August 2010
Accepted: 05 October 2010
Published: 03 November 2010

Guest Editor: J. Murphy

Abstract

The key to understanding the fundamental processes of catalysis is the transition state (TS): indeed, catalysis is a transition-state molecular recognition event. Practical objectives, such as the design of TS analogues as potential drugs, or the design of synthetic catalysts (including catalytic antibodies), require prior knowledge of the TS structure to be mimicked. Examples, both old and new, of computational modelling studies are discussed, which illustrate this fundamental concept. It is shown that reactant binding is intrinsically inhibitory, and that attempts to design catalysts that focus simply upon attractive interactions in a binding site may fail. Free-energy changes along the reaction coordinate for S_N2 methyl transfer catalysed by the enzyme catechol-*O*-methyl transferase are described and compared with those for a model reaction in water, as computed by hybrid quantum-mechanical/molecular-mechanical molecular dynamics simulations. The case is discussed of molecular recognition in a xylanase enzyme that stabilises its sugar substrate in a (normally unfavourable) boat conformation and in which a single-atom mutation affects the free-energy of activation dramatically.

Introduction

"Molecular recognition of transition states" was the title of a paper presented by Kirby [1] at a discussion held in April 1993 on the chemistry of biological molecular recognition; he addressed the fundamental question of how enzymes lower the free energies of the transition states for the reactions they catalyse, with reference to his own elegant experimental studies on catalysis. In March 1991, at a workshop held under the auspices of the Science and Engineering Research Council's Molecular Recognition Initiative, I presented a paper on theoretical modelling of transition states for biochemical processes, which included a computational model for carbonyl reduction catalysed by lactate dehydrogenase [2]. The abstract for this workshop presentation began with the following sentence: The key to understanding of the fundamental processes of catalysis is the transition state; indeed, "catalysis is a transition-state molecular recognition event". The present paper discusses cases of methyl transfer and of glycoside hydrolysis to illustrate and to update the same theme from a computational point of view.

Discussion

The transition state is of strategic importance within the field of chemical reactivity. Owing to its location in the region of the highest energy point on the most accessible route between reactants and products (Figure 1), it commands both the direction and the rate of chemical change. Questions of specificity and catalysis may be answered by knowledge of the structure and properties of the TS.

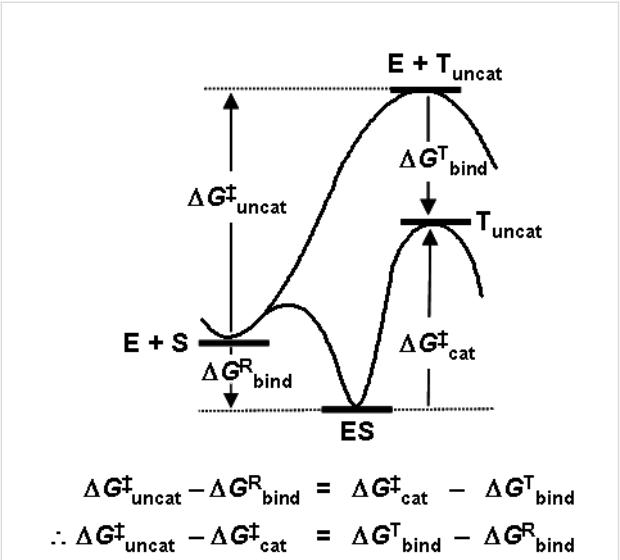

Figure 1: Free energy profiles for reactions of substrate S uncatalysed and catalysed by enzyme E, showing how the barrier height reduction is equal to the binding energy for transition state T offset by the binding energy for the reactant state R.

Computational chemistry provides techniques for the generation and exploration of the multi-dimensional energy surfaces that govern chemical reactivity; energy minima and saddle points can be located and characterised, and the pathways that interconnect them can be determined. A rigorous distinction should be drawn between a TS (corresponding to a bottleneck on a free energy surface) and a transition structure (corresponding to a saddle point on a potential energy surface). The commonly assumed identity between the two terms is often reasonable for small, "simple" systems in vacuum, for which it may be sufficient to model the TS by first finding a transition structure and then evaluating its molecular partition function by QM computations. However, it would be quite wrong to neglect the distinction for "complex" systems, for which the free energy of the TS may not be evaluated using simple analytical expressions for partition functions determined for a single transition structure. Enzyme catalysed reactions in solution are of this nature, and it is necessary to take averages over an extensive sampling of configurational space in order to obtain the changes in free energy that dictate their reactivity.

It was Linus Pauling who suggested that the catalytic activity of enzymes was due to structural complementarity with the TS rather than the reactant state of the substrate [3]: "enzymes are molecules that are complementary in structure to the activated complexes of the reactions they catalyse … [which] would thus lead to a decrease in its energy, and hence to a decrease in the energy of activation" [4]. A corollary to this insight was provided by W. P. (Bill) Jencks, who noted that a catalyst might be synthesised by raising an antibody to a hapten resembling the TS of the reaction to be catalysed: "the combining sites of such antibodies should be complementary to the TS and should cause an acceleration by forcing bound substrates to resemble the TS" [5]. However, the clear logical implications of the notion of TS complementarity for understanding the origins of enzyme catalytic power were described eloquently (but with a friendly tongue in cheek) by R. L. (Dick) Schowen as the "fundamentalist" position in contrast to the "canonical" view of Jencks and others. He asserted that "the entire and sole source of catalytic power is stabilisation of the TS" [6], which implied not only that reactant-state binding interactions were by nature inhibitory and only wasted catalytic power (Figure 1), but also that the particularities of any events occurring along paths between reactants and TS (termed as the "microhistory" of the reaction [7]) are irrelevant to the catalysis itself. Theories within the "canon" of enzyme catalysis tend to omit or at least de-emphasise the TS, focussing instead on some sort of reactive complex en route from reactants to TS. For example, Bruice's "near-attack conformation" concept highlights a particular structure (a "NAC") which behaves as a "turnstile through which the ground state must pass to enter the TS" [8]. One might consider, however, that this amounts to redefinition of the dividing surface between reactants and products as the NAC rather than the TS, but without providing any means for locating and characterising it. In my opinion, the TS is already well defined and continues to serve well as the focus of the present discussion.

Recently, some authors have sought to go "beyond the Pauling paradigm" by noting that "enzymes enter into reactions with substrates and do not merely complement the transition states of the uncatalysed reactions" [9]. The implication seems to be that the notion of TS complementarity and TS stabilisation as the source of enzyme catalytic power ignores any interactions between an enzyme and the substrate in the reactant state. However, careful reading of Pauling's own words reveals that his views on enzymes follow a discussion of structural complementarity between an antibody and its antigen, and that his statement (quoted above) regarding complementarity between an enzyme and the "activated complex" of the catalysed reaction is in turn followed by this sentence [3]: "If the enzyme were completely complementary in structure to the substrate, then no other molecule would be expected to compete success-

fully with the substrate in combining with the enzyme, which in this respect would be similar in behaviour to antibodies; but an enzyme complementary to a strained substrate molecule would attract more strongly to itself a molecule resembling the strained substrate molecule than it would the substrate molecule." This clearly implies a consideration of the relative extent of binding interactions of the reactant state and TS with an enzyme, and of the inhibitory nature of the former.

The essential importance of *preferential* TS stabilisation was absolutely explicit in Schowen's treatment [6]: "A complete understanding of enzyme catalysis … resolves into a characterisation of two binding processes: that for the transition state, which yields a model for catalysis, and that for the reactant state, which yields a model for … inhibitory effects … The differential stabilisation of the transition state (total stabilisation of the transition state minus stabilisation of reactant species) always gives the catalytic acceleration." Recently, Simón and Goodman [10] have astutely observed that an optimal catalyst does not simply maximise TS stabilisation per se, but rather achieves a maximal reduction in barrier height by means of differential stabilisation. The cases discussed below all exemplify TS molecular recognition and stabilisation *relative* to the reactant state.

Catalyst design: preferential TS binding

Methyl group transfer from an electrophile to a nucleophile by an S_N2 mechanism is an archetypal reaction in organic chemistry and an important process in biochemistry. Catechol-*O*-methyl transferase (COMT) catalyses methyl transfer from *S*-adenosylmethionine (SAM) to a catechol (Scheme 1), and this reaction manifests an unusually large inverse secondary kinetic isotope effect as compared with a model, uncatalysed reaction in solution: the isotope effect $V^{CH3}/V^{CD3} = 0.83 \pm 0.05$ for methylation of 3,4-dihydroxyacetophenone with SAM at 37 °C catalysed by COMT was found [11] to be more inverse than the value of $k_{CH3}/k_{CD3} = 0.97 \pm 0.02$ for methylation of methoxide ion by *S*-methyldibenzothiophenium ion at 25 °C in methanol [12]. According to the orthodox view, Schowen and co-workers interpreted these observations in terms of a tighter S_N2 transition state for the COMT-catalysed reaction than for the non-enzymic reaction, and consequently proposed the "compression hypothesis" for enzymic methyl transfer as a possible explanation [13].

As outlined above, the power of any catalyst derives fundamentally from its ability to stabilise the TS relative to the reactant state, as compared with the uncatalysed reaction. This requires effective discrimination between the reactant state and the TS. In the case of methyl transfer, stabilising enzyme-substrate interactions (① in Figure 2) probably do not provide any

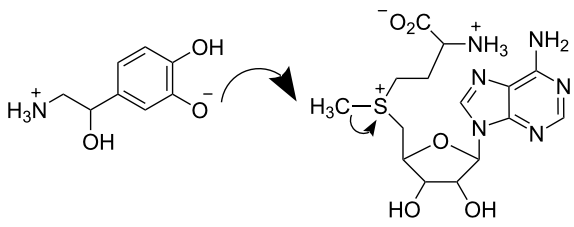

Scheme 1: S_N2 methyl transfer from SAM to catechol catalysed by COMT.

significant degree of discrimination, since the geometrical and electronic changes occurring do not provide sufficient differences; thus

$$\left|\Delta E^{R}_{\text{stabilise}}\right| \approx \left|\Delta E^{T}_{\text{stabilise}}\right| \quad (1)$$

The key proposal of the compression hypothesis is the following: if the TS for S_N2 methyl transfer is more plastic than the reactant state for the catalysed process, then mechanical compression by the enzyme (② in Figure 2) might destabilise the reactants more than the TS. In other words, the energetic penalty for deforming the structure to a given degree is greater for the reactant state than for the TS:

$$\left|\Delta E^{R}_{\text{compress}}\right| > \left|\Delta E^{T}_{\text{compress}}\right| \quad (2)$$

The net effect (③ in Figure 2) is the reduction of the barrier for the catalysed reaction as compared with that for the uncatalysed process:

$$\Delta E^{\ddagger}_{\text{cat}} < \Delta E^{\ddagger}_{\text{uncat}} \quad (3)$$

As a consequence of (intrinsically unfavourable) compression of the S_N2 TS in the enzymic reaction, the enzyme is able to distinguish the TS structurally from the preceding reactant state and the succeeding product state in order to stabilise the TS specifically. Thus, compression may serve to achieve efficient catalysis, with a large V_{max} at the expense of a slight reduction in V_{max}/K_m. The importance for enzyme catalysis of destabilisation as well as binding has also been noted by Jencks [14].

Some years ago I performed an ab initio Hartree–Fock investigation [15], intended to test the validity of the compression hypothesis; this exercise amounted to the computational design of a catalyst for the identity S_N2 methyl transfer from methylammonium to ammonia (Figure 3a). The transition structure for

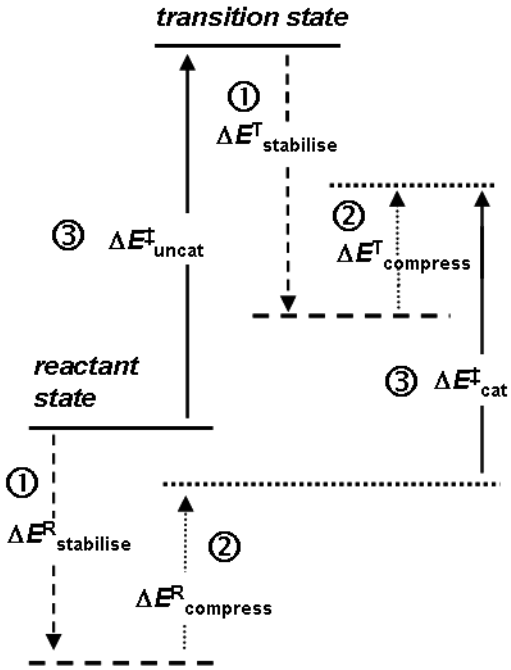

Figure 2: Energetic analysis of the compression hypothesis for enzyme-catalysed methyl transfer.

this reaction has an overall positive charge, and a reasonable strategy for its stabilisation seemed to be to construct an array of point charges, such that each N–H or C–H bond was perfectly aligned with the negative end of a dipole (Figure 3b). However, when both the transition structure and the ion-molecule reactant complex were reoptimised within the frozen array of point charges, it transpired that the stabilisation energy $\Delta E^{R}_{stabilise}$ of the latter was greater than the stabilisation energy $\Delta E^{T}_{stabilise}$ of the former (Figure 3e). Unintentionally, the barrier for S_N2 methyl transfer with the "catalyst" was higher than that without: inhibition, or anti-catalysis, had been achieved. With hindsight, it may be seen from the electrostatic potential of the transition structure (represented by colour on an electron density contour in Figure 3c), that the transferring methyl group is unlikely to interact favourably with the dipoles intended to do so: the electrostatic potential for the transition structure within the catalyst (Figure 3d) appears uniform. The catalyst dipoles interact more strongly with the localised charge on the reactant (or product) ion-molecule complex than with the delocalised charges on the atoms of the transition structure.

However, when a pair of inert-gas atoms (grey spheres in Figure 3d) was placed on the N···C···N axis so as to impose repulsive interactions on both the reactant and transition structures sandwiched between them, the destabilising effect $\Delta E^{R}_{compress}$ on the former could be adjusted (by appropriate

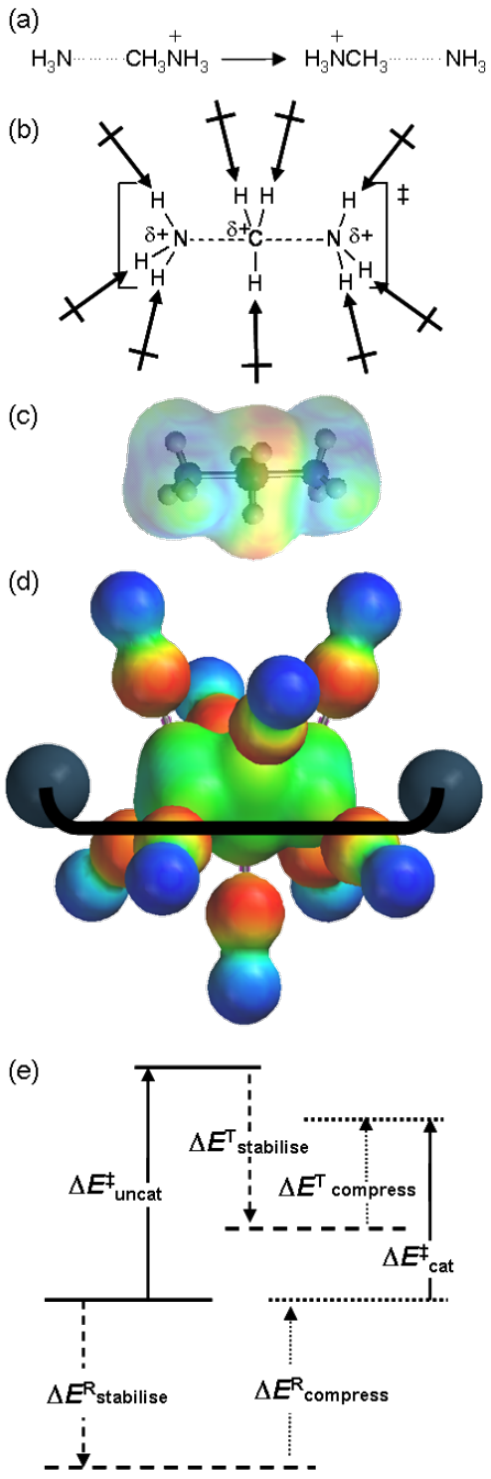

Figure 3: Catalyst design for methyl transfer: (a) the reaction to be catalysed; (b) dipoles favourably aligned with the transition structure; (c) electrostatic potential plotted on the isodensity contour surface of the transition structure; (d) electrostatic potential (on isodensity contour surface) of the complex of the transition structure within a frozen array of dipoles, together with a pair of inert-gas atoms; (e) preferential TS stabilisation as the net result of stabilising (attractive) and destabilising (repulsive, compressing) interactions.

choice of the fixed separation of the inert-gas atoms) to be significantly larger than the destabilising effect $\Delta E^{T}_{compress}$ on the latter. The net effect of the attractive and repulsive components of the catalyst yielded $\Delta E^{‡}_{cat} < \Delta E^{‡}_{uncat}$ (Figure 3e), because the preferential destabilisation of the reactant state by compression outweighed its preferential stabilisation by attractive interactions with the dipole array; alternatively, ΔE^{R}_{bind} (= $\Delta E^{R}_{stabilise} + \Delta E^{R}_{compress}$) < ΔE^{T}_{bind} (= $\Delta E^{T}_{stabilise} + \Delta E^{T}_{compress}$) leading to net TS stabilisation.

Later we proposed [16] a more realistic catalyst design for methyl transfer in the shape of inside-methylated [1.1.1]cryptand (Scheme 2). B3LYP/6-31G* calculations predicted the inter-bridgehead N···N distance in cryptand (b) to be 0.75 Å shorter than in the ion-molecule complex between trimethylamine and tetramethylammonium (a), indicating compression along the N···C···N axis, but more significantly the corresponding difference in the corresponding transition structures was only 0.35 Å. In other words, the change from reactant complex to transition structure was 0.4 Å less for the compressed reaction (b) than for the uncompressed reaction (a); moreover, the potential energy barrier for (b) was 22 kJ mol^{-1} less than for (a), and the α-D_3 KIEs was more inverse (0.91 vs 0.93) for (b) than for (a). These results were consistent with the compression hypothesis for catalysis of methyl transfer.

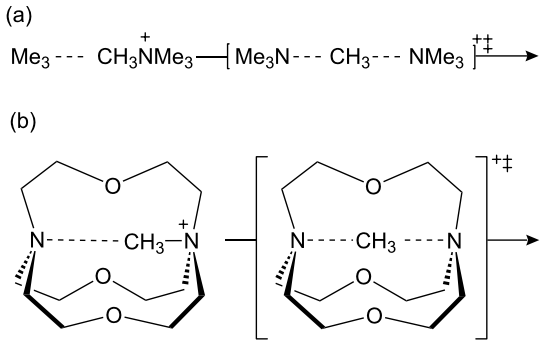

Scheme 2: S_N2 methyl transfer (a) uncatalysed and (b) within a cryptand cavity.

Origin of COMT catalytic power

To assess whether compression actually operates in COMT-catalysed methyl transfer, hybrid QM/MM calculations have been performed at the AM1/MM level [17-19]. The secondary α-D_3 KIE for the COMT-catalysed reaction (Scheme 1) was calculated to be more inverse than for the same reaction in water [18], but this preliminary result was based upon single structures for the reactant complex and transition state of the enzymic and non-enzymic reactions. Recently we performed extensive AM1/OPLS/TIP3P simulations [19] with ensemble averaging to include the effect of thermal fluctuations in the enzyme and solvent environments to obtain a value for the α-D_3 KIE = 0.82 ± 0.05, which is in excellent accord with the experimental value [11] of V^{CH3}/V^{CD3} = 0.83 ± 0.05 for methylation of 3,4-dihydroxyacetophenone with SAM at 37 °C catalysed by COMT. In contrast, we calculated k_{CH3}/k_{CD3} = 0.99 ± 0.16 for methylation of methoxide ion by *S*-methyldibenzothiophenium ion at 25 °C in methanol, as compared with the experimental value [12] of 0.97 ± 0.02. The computational results reproduce the experimental observation of a significantly more inverse value of α-D_3 KIE for enzyme-catalysed than for uncatalysed methyl transfer in solution. However, the average values for the making and breaking bonds between $C_α$ and, respectively, the nucleophile and nucleofuge in the nearly collinear TS for the COMT-catalysed reaction were computed as 2.06 ± 0.02 Å and 2.11 ± 0.01 Å, the sum of which is scarcely different from the sum of the corresponding average bond lengths, 2.18 ± 0.04 Å and 2.00 ± 0.04 Å, for the uncatalysed reaction. Thus the simulations did not provide any structural evidence for compression.

It is instructive to analyse the various energetic contributions to catalysis (Figure 4) by COMT by means of appropriate computer simulations, as was done in an earlier study [17]. (N.B. The terminology and notation employed here differ from that work.) The potential of mean force (PMF), computed from MD simulations at the AM1/CHARMM/TIP3P level with umbrella sampling along a reaction coordinate defined as the difference in bond lengths from $C_α$ to the nucleophile and nucleofuge, predicted a 44 kJ mol^{-1} increase $\Delta G^{‡}_{enz}$ in free energy in going from the enzymic reactant complex ES^{R}_{enz} to the enzymic transition state ES^{T}_{enz} for the COMT-catalysed reaction at 300 K. An analogous PMF for exactly the same reaction occurring in water without COMT yielded a free energy minimum for a solvent-separated ion-pair reactant complex S^{R}_{aq}; if this species were taken as the reference state for both catalysed and uncatalysed reactions, the reduction in barrier height would simply be equal to ΔG^{T}_{bind}, the TS stabilisation. In the published analysis [17], the free energy barrier $\Delta G^{‡}_{aq}$ = 82 kJ mol^{-1} for the uncatalysed reaction in aqueous solution was considered as the sum of two terms: (i) a distortion energy ΔG^{R}_{dist} = 30 kJ mol^{-1} for going from S^{R}_{aq} to a contact ion-pair S^{R}_{enz} in solution having the same geometry as that of the substrate-derived part of the enzymic reactant complex ES^{R}_{enz} and (ii) an activation free energy ΔG^{R}_{act} = 52 kJ mol^{-1} to the transition state S^{T}_{aq}. The sum of ΔG^{R}_{dist} and the interaction energy ΔG^{R}_{int} is equal to the apparent binding energy ΔG^{R}_{bind}. The magnitude of the enzyme catalytic power $\Delta G^{‡}_{aq} - \Delta G^{‡}_{enz}$ = 38 kJ mol^{-1} is equal to the difference in binding energies $\Delta G^{T}_{bind} - \Delta G^{R}_{bind}$ of the enzyme with the TS and the solvent-separated ion-pair, neither of which was evaluated in the simu-

lation. The difference $\Delta G^{R}_{act} - \Delta G^{‡}_{enz}$ = 8 kJ mol^{-1} was considered to quantify the energetic influence of the environment – either protein or water – upon the substrate as it changes from the reactant state to the transition state. However, this analysis lacks consistency in one respect, because, although the structure of S^{R}_{enz} is (by definition) geometrically the same for the substrate in both the enzyme active site and in aqueous solution, the structures of S^{T} in the two different environments are not the same. A fair point of criticism for the concept of TS binding in enzyme catalysis has been that the TS need not be the same for both the catalysed and uncatalysed reactions [8]. Consequently, the previous analysis [17] should be modified by recognising that the apparent binding energy ΔG^{T}_{bind} is the sum of distortion energy ΔG^{T}_{dist} and interaction energy ΔG^{T}_{int}.

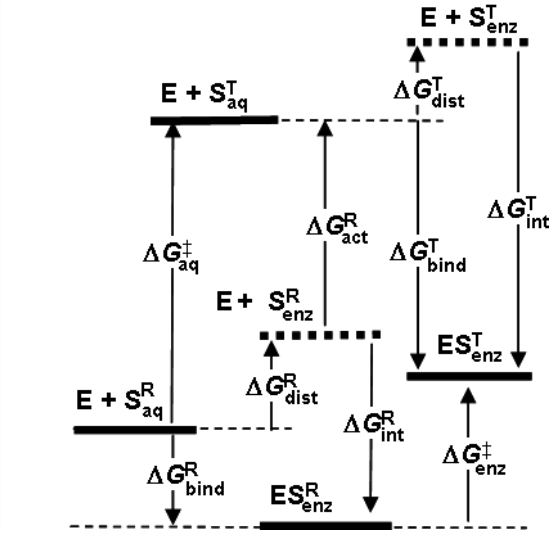

Figure 4: Free energy analysis of COMT catalysis.

The species S^{R}_{enz} in water is well defined and amenable to computational investigation, although experimentally it is transient and may not necessarily correspond to a genuine intermediate. Similarly, species S^{T}_{enz} in water is also well defined and amenable to computational investigation, although – unlike S^{R}_{enz} in water – it was not considered in the previous work [17]. A fair evaluation of the energetic influence of the protein or water environment on the substrate as it changes from the reactant state to the transition state should be made by comparison of $\Delta G^{‡}_{enz}$ with $\Delta G^{R}_{act} + \Delta G^{T}_{dist}$, since in each case the structures are the same. Owing to the structural distortions of both the reactant and transition states in going from aqueous solution into the enzyme active site, the quantity $\Delta G^{T}_{bind} - \Delta G^{R}_{bind}$ is an apparent catalytic power which differs from the intrinsic catalytic power $\Delta G^{T}_{int} - \Delta G^{R}_{int}$ by virtue of the differential distortion energy $\Delta G^{T}_{dist} - \Delta G^{R}_{dist}$.

TS recognition in enzymic glycoside hydrolysis

The *endo*-1,4-β-xylanase (BCX) from *Bacillus circulans* catalyses the hydrolysis of xylan and β-xylobiosides with net retention of anomeric configuration by means of a double displacement mechanism involving a covalent glycosyl-enzyme intermediate. Formation and hydrolysis of this covalent intermediate occur via oxacarbenium ion-like TSs, with the assistance of two key active site glutamic acid residues [20]. Glu78 is deprotonated in the noncovalent enzyme-substrate reactant complex: it attacks the anomeric carbon of the substrate as a nucleophile and displaces the aglycone nucleofuge (Scheme 3). Glu172 is protonated in the reactant complex and plays a dual role of acid/base catalyst: in the glycosylation step it assists formation of the glycosyl-enzyme intermediate by donating a proton to the aglycone of the natural substrate, and in the subsequent deglycosylation step it serves as a base, deprotonating the attacking water molecule. Tyr69 donates a strong hydrogen bond to the nucleophilic oxygen atom (O_{nuc}) of Glu78 in the reactant complex; in the covalent intermediate, this hydrogen bond is weaker, but a stronger interaction is formed between Tyr69 and the ring oxygen (O_{ring}) of the proximal xylose moiety of the xylobioside substrate [21]. The phenolic oxygen (O_Y) of Tyr69 is very important for catalysis, as evidenced by the observation that the Tyr69Phe mutant exhibits no detectable enzyme activity [22], and so it is an intriguing question to investigate the nature of this $O_YH_Y\cdots O_{ring}$ interaction.

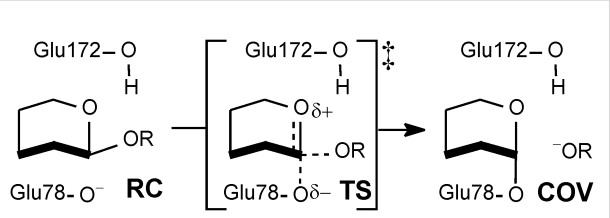

Scheme 3: Formation of glycosyl-enzyme covalent intermediate COV.

MD simulations with the hybrid AM1/OPLS-AA/TIP3P method showed that both $^{4}C_{1}$ chair and $^{2,5}B$ boat conformers of phenyl β-xyloside remained stable in water during the course of 30 ps trajectories, even in the presence of propionate and propionic acid moieties to mimic Glu78 and Glu172 [23]. In contrast, analogous MD simulations for the $^{4}C_{1}$ conformer of the reactant complex of phenyl β-xylobioside with BCX showed spontaneous transformation to the $^{2,5}B$ conformer (Figure 5): the conformational change is accompanied by a marked decrease in the length of the $O_YH_Y\cdots O_{ring}$ hydrogen bond. Moreover, analogous simulations for the Tyr69Phe mutant (lacking O_Y) showed the chair to be stable, thereby confirming the key role of Tyr69 in preferentially stabilising the boat, with

a relative free energy difference of about 20 kJ mol^{-1}, by means of the $O_YH_Y\cdots O_{ring}$ hydrogen bond [23].

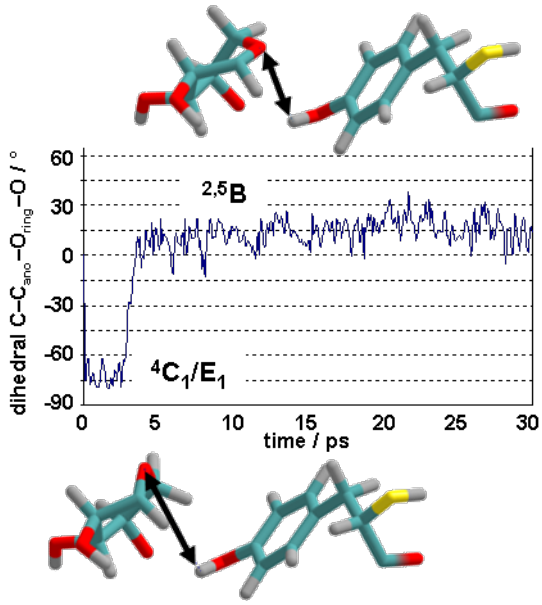

Figure 5: Conformational change of the xylose ring from chair (via envelope) with long $O_YH_Y\cdots O_{ring}$ hydrogen bond to boat with short hydrogen bond, as shown by QM/MM MD simulation in active site of BCX.

A two-dimensional PMF computed for 4-nitrophenyl β-xylobioside (the substrate employed in the experimental kinetics studies) with BCX using the same AM1/OPLS-AA hybrid potential, as a function of coordinates for nucleophilic substitution and proton transfer from Glu172, showed no requirement for protonation of the activated nucleofuge [24]. PMFs, with respect to the nucleophilic substitution reaction coordinate for both the wild-type and the Tyr69Phe mutant, computed with the same QM/MM MD method, revealed a decrease in free energy of activation of about 40 kJ mol^{-1} due to the presence of the single O_Y atom in BCX (Figure 6).

Fluctuations in the hydrogen-bond distances $H_Y\cdots O_{ring}$ (red) and $H_Y\cdots O_{nuc}$ (blue) to the boat conformer of RC, TS and glycosyl-enzyme COV intermediate in the active site of BCX, as determined by 30 ps AM1/OPLS-AA MD trajectories, are shown Figure 7. Averaged over a longer (93 ps) trajectory for RC than shown here, the mean $H_Y\cdots O_{ring}$ distance was significantly shorter (2.47 ± 0.49 Å) than $H_Y\cdots O_{nuc}$ (3.29 ± 0.48 Å). On the other hand, $H_Y\cdots O_{nuc}$ is consistently shorter (1.97 ± 0.14 Å) in the TS than $H_Y\cdots O_{ring}$ (2.39 ± 0.20 Å), indicating that the hydrogen bond between Tyr69 and Glu78 is favoured, although both distances are shorter than in RC. In COV, however, $H_Y\cdots O_{nuc}$ is once more longer than $H_Y\cdots O_{ring}$, indicating that Tyr69 now donates its hydrogen bond exclusively to the xylose ring rather than to Glu78, although the average distance to the latter is similar to that in RC. Thus it appears that stabilisation of the TS is due to the transient presence of a shorter, stronger hydrogen bond to O_{nuc}, which, of course, is absent in the TS for the Tyr69Phe mutant.

Conclusion

Catalysts work by stabilising the TS relative to reactants, but the idea of designing a "catalyst" simply to bind strongly to the TS does not always work. Selective stabilisation of the TS for

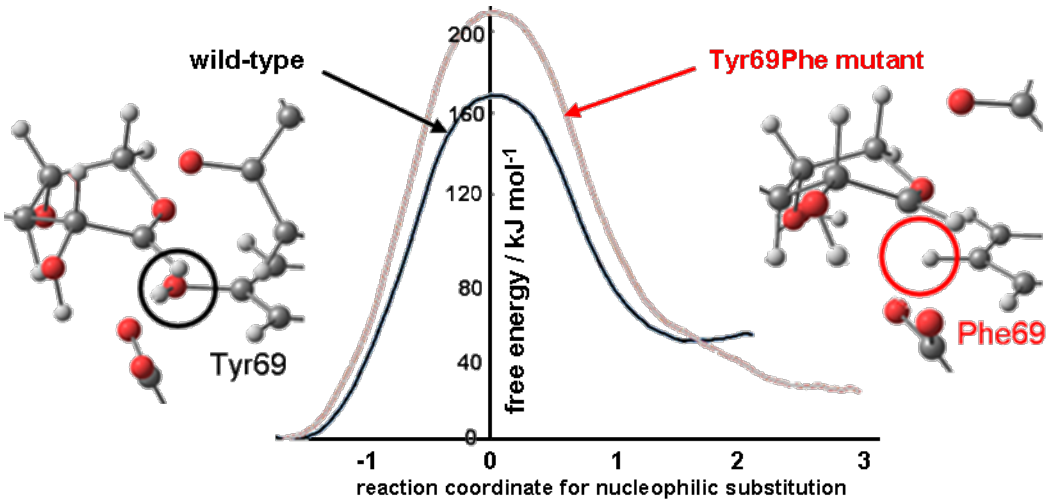

Figure 6: AM1/OPLS potentials of mean force for formation of glycosyl-enzyme covalent intermediate between 4-nitrophenylxylobioside and BCX wild-type (black) and Tyr69Phe mutant (red).

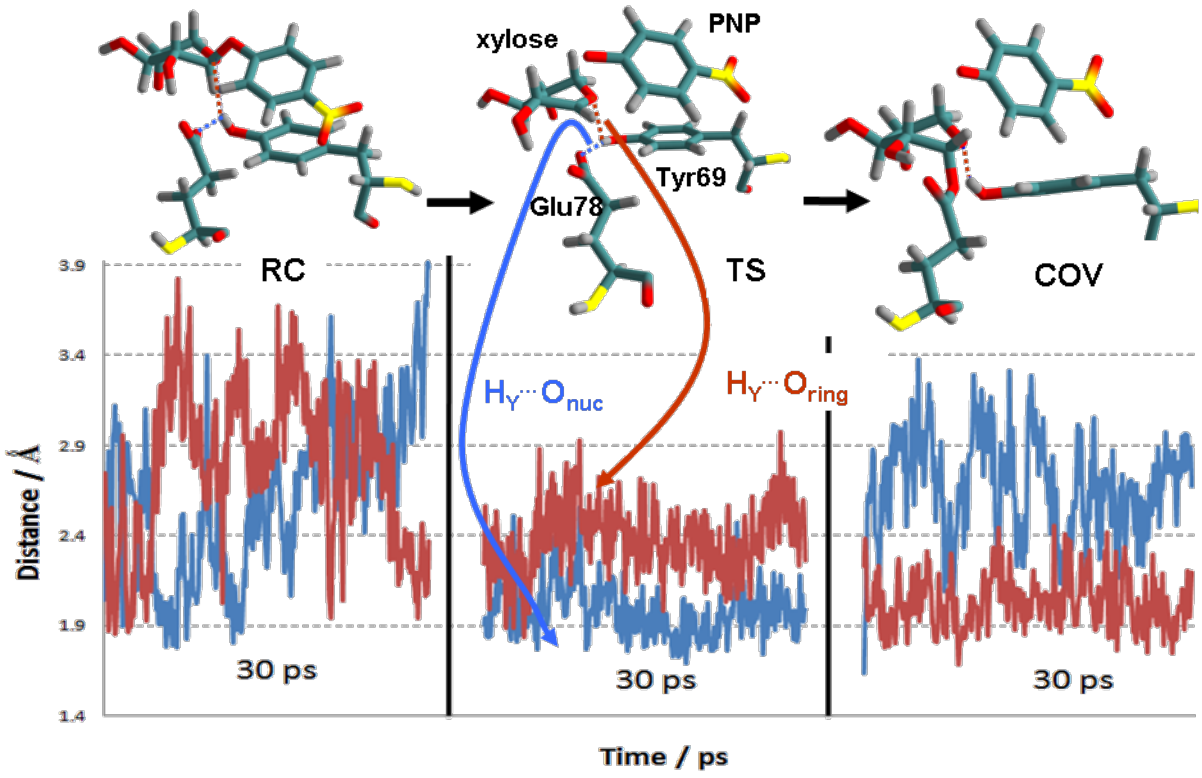

Figure 7: Hydrogen-bond distances $H_Y\cdots O_{ring}$ (red) and $H_Y\cdots O_{nuc}$ (blue) to boat conformer of RC, TS and glycosyl-enzyme COV intermediate, as shown by QM/MM MD simulation in active site of BCX.

methyl transfer could be achieved in principle by means of compression, but in practice COMT catalyses by requiring less reorganisation of the electrostatic environment to go from RC to TS than is needed in aqueous solution, thereby achieving selective stabilisation of TS. The boat conformer of a xyloside substrate is favoured over the chair in the active site of BCX owing to a hydrogen bond from Tyr69 to O_{ring} of xylose, but preferential stabilisation of the TS in the wild-type relative to a Tyr69Phe mutant is achieved by means of a short, strong hydrogen bond from Tyr69 to the enzymic nucleophile. Catalysis is TS molecular recognition, and computational simulation may provide valuable insight into the causes of preferential stabilisation.

Acknowledgements

I am grateful to Professor T. M. Krygowski for the invitation to present this material at the Central European School on Physical Organic Chemistry, Przesiecka, Poland (June 2010), the theme of which was intermolecular interactions and molecular recognition. I also thank my collaborators, former postdocs and students, as named in the literature citations, for their invaluable contributions over many years to computational studies of transition states.

References

1. Kirby, A. J. *Phil. Trans. R. Soc. Lond. A* **1993,** *345,* 67–76. doi:10.1098/rsta.1993.0118
2. Wilkie, J.; Williams, I. H. *J. Am. Chem. Soc.* **1992,** *114,* 5423–5425. doi:10.1021/ja00039a064
3. Pauling, L. *Chem. Eng. News* **1946,** *24,* 1375–1377.
4. Pauling, L. *Nature* **1948,** *161,* 707–709. doi:10.1038/161707a0
5. Jencks, W. P. *Catalysis in Chemistry and Enzymology;* McGraw-Hill: New York, 1969; p 288.
6. Schowen, R. L. In *Transition States of Biochemical Processes;* Gandour, R. D.; Schowen, R. L., Eds.; Plenum Press: New York, 1978.
7. Schowen, R. L. *Proc. Natl. Acad. Sci. U. S. A.* **2003,** *100,* 11931–11932. doi:10.1073/pnas.2235806100
8. Bruice, T. C. *Acc. Chem. Res.* **2002,** *35,* 139–148. doi:10.1021/ar0001665
9. Zhang, X.; Houk, K. N. *Acc. Chem. Res.* **2005,** *38,* 379–385. doi:10.1021/ar040257s
10. Simón, I.; Goodman, J. M. *J. Org. Chem.* **2010,** *75,* 1831–1840. doi:10.1021/jo901503d
11. Hegazi, M. F.; Borchardt, R. T.; Schowen, R. L. *J. Am. Chem. Soc.* **1979,** *101,* 4359–4365. doi:10.1021/ja00509a052
12. Gray, C. H.; Coward, J. K.; Schowen, K. B.; Schowen, R. L. *J. Am. Chem. Soc.* **1979,** *101,* 4351–4358. doi:10.1021/ja00509a051
13. Olsen, J.; Wu, Y.-S.; Borchardt, R. T.; Schowen, R. L. In *Transmethylation;* Usdin, E.; Borchardt, R. T.; Creveling, C. R., Eds.; Elsevier: New York, 1979.

14. Jencks, W. P. *Phil. Trans. R. Soc. Lond. A* **1993,** *345,* 3–10. doi:10.1098/rsta.1993.0112
15. Williams, I. H. *J. Am. Chem. Soc.* **1984,** *106,* 7206–7212. doi:10.1021/ja00335a058
16. Moliner, V.; Williams, I. H. *J. Am. Chem. Soc.* **2000,** *122,* 10895–10902. doi:10.1021/ja001170e
17. Roca, M.; Martí, S.; Andrés, J.; Moliner, V.; Tuñón, I.; Bertrán, J.; Williams, I. H. *J. Am. Chem. Soc.* **2003,** *125,* 7726–7737. doi:10.1021/ja0299497
18. Ruggiero, G. D.; Williams, I. H.; Roca, M.; Moliner, V.; Tuñón, I. *J. Am. Chem. Soc.* **2004,** *126,* 8634–8635. doi:10.1021/ja048055e
19. Kanaan, N.; Ruiz Pernía, J. J.; Williams, I. H. *Chem. Commun.* **2008,** 6114–6116. doi:10.1039/b814212b
20. McIntosh, L. P.; Hand, G.; Johnson, P. E.; Joshi, M. D.; Körner, M.; Plesniak, L. A.; Ziser, L.; Wakarchuk, W. W.; Withers, S. G. *Biochemistry* **1996,** *35,* 9958–9966. doi:10.1021/bi9613234
21. Sidhu, G.; Withers, S. G.; Nguyen, N. T.; McIntosh, L. P.; Ziser, L.; Brayer, G. D. *Biochemistry* **1999,** *38,* 5346–5354. doi:10.1021/bi982946f
22. Wakarchuk, W. W.; Campbell, R. L.; Sung, W. L.; Davoodi, J.; Yaguchi, M. *Protein Sci.* **1994,** *3,* 467–475. doi:10.1002/pro.5560030312
23. Soliman, M. E. S.; Ruggiero, G. D.; Ruiz Pernía, J. J.; Greig, I. R.; Williams, I. H. *Org. Biomol. Chem.* **2009,** *7,* 460–468. doi:10.1039/b814695k
24. Soliman, M. E. S.; Ruiz Pernía, J. J.; Greig, I. R.; Williams, I. H. *Org. Biomol. Chem.* **2009,** *7,* 5236–5244. doi:10.1039/b911644c

License and Terms

Beilstein Journal of Organic Chemistry

β-Hydroxy carbocation intermediates in solvolyses of di- and tetra-hydronaphthalene substrates

Jaya S. Kudavalli and Rory A. More O'Ferrall*

Full Research Paper

Open Access

Address:
School of Chemistry and Chemical Biology, University College Dublin, Belfield, Dublin 4, Ireland

Email:
Jaya S. Kudavalli - kjsnarayana@yahoo.co.in;
Rory A. More O'Ferrall* - rmof@ucd.ie

* Corresponding author

Keywords:
aromaticity; β-hydroxycarbocations; hyperconjugation; solvolysis

Beilstein J. Org. Chem. **2010,** *6,* 1035–1042.
doi:10.3762/bjoc.6.118

Received: 02 September 2010
Accepted: 25 October 2010
Published: 03 November 2010

Guest Editor: J. Murphy

Abstract

Solvolysis of trichloroacetate esters of 2-methoxy-1,2-dihydro-1-naphthols shows a remarkably large difference in rates between the *cis* and *trans* isomers, k_{cis}/k_{trans} = 1800 in aqueous acetonitrile. This mirrors the behaviour of the acid-catalysed dehydration of *cis*- and *trans*-naphthalene-1,2-dihydrodiols to form 2-naphthol, for which k_{cis}/k_{trans} = 440, but contrasts with that for solvolysis of tetrahydronaphthalene substrates, 1-chloro-2-hydroxy-1,2,3,4-tetrahydronaphthalenes, for which k_{cis}/k_{trans} = 0.5. Evidence is presented showing that the *trans* isomer of the dihydro substrates reacts unusually slowly rather than the *cis* isomer unusually rapidly. Comparison of rates of solvolysis of 1-chloro-1,2,3,4-tetrahydronaphthalene and the corresponding (*cis*) substrate with a 2-hydroxy group indicates that a β-OH slows the reaction by nearly 2000-fold, which represents a typical inductive effect characteristic also of *cis*-dihydrodiol substrates. The slow reaction of the *trans*-dihydrodiol substrate is consistent with initial formation of a β-hydroxynaphthalenium carbocation with a conformation in which a C–OH occupies an axial position β to the carbocation centre preventing stabilisation of the carbocation by C–H hyperconjugation, which would occur in the conformation initially formed from the *cis* isomer. It is suggested that C–H hyperconjugation is particularly pronounced for a β-hydroxynaphthalenium ion intermediate because the stability of its no-bond resonance structure reflects the presence of an aromatic naphthol structure.

Introduction

Cis-arenedihydrodiols are products of fermentation of aromatic molecules by mutant strains of soil bacteria containing dioxygenase enzymes such as *Pseudomonas putida* UV4 [1]. A characteristic reaction they undergo is acid-catalysed dehydration to form phenols [2], as illustrated for benzene-1,2-dihydrodiol in Scheme 1.

A surprising finding is that the reactivity of *cis*-dihydrodiols is much greater than that of the synthetically accessible *trans* isomers, e.g., k_{cis}/k_{trans} = 4500 for *cis*- and *trans*-benzene dihydrodiols (**1**), despite the expectation that the two reactions proceed through a common β-hydroxycarbocation intermediate (**2**) [3]. This contrasts with reactions of *cis*- and *trans*-dihydro-

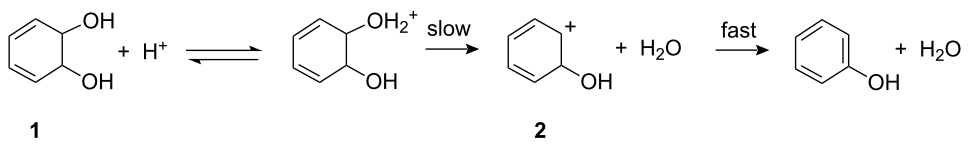

Scheme 1: Mechanism of dehydration of benzene-1,2-dihydrodiol.

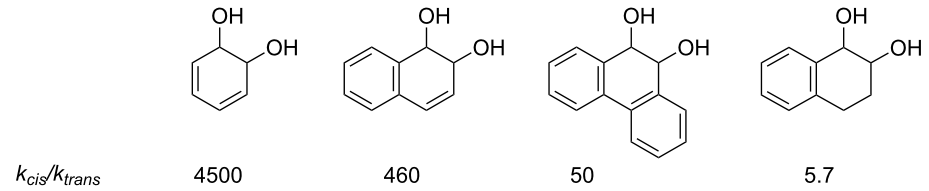

Figure 1: Reactivity ratios for acid-catalyzed reaction of arene dihydrodiols.

diols of non-aromatic double bonds for which only a small advantage for the *cis*-diol is observed. Indeed, the *cis*/*trans* rate ratio decreases regularly as the aromaticity of the double bond decreases, as shown for the dihydrodiols of benzene, naphthalene (1,2), phenanthrene (9,10) and 3,4-dihydronaphthalene in Figure 1 [3].

The purpose of the present work was to determine whether the same differentials apply to solvolysis reactions of dihydrodiol derivatives for which one of the hydroxy groups has been converted to a more reactive leaving group. In the case of benzene dihydrodiol it is hard to functionalise the hydroxy group without triggering aromatisation to phenol, at least in the case of the *cis*-diol. The same is true of the *cis*-1,2-dihydrodiol of naphthalene. However, prior methylation of the 2-hydroxy group of this substrate led to the preparation of *cis*- and *trans*-1-trichloroacetoxy-2-methoxy-1,2-dihydronaphthalenes (**3**) which were stable enough to be isolated and purified (Figure 2). This allowed us to compare a ratio of rate constants for the solvolyses of these two isomers with the corresponding ratio for solvolyses of *cis*-and *trans*-1-chloro-2-hydroxy-1,2,3,4-tetrahydronaphthalene (1-chloro-2-tetralol, **4**), which are similar in structure but lack a 3,4-double bond and yield carbocations which cannot undergo deprotonation to form aromatic products.

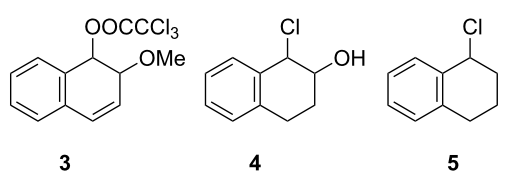

Figure 2: Substrates for solvolysis measurements.

Finally, to allow the influence of the β-hydroxy group on the rate of solvolysis to be assessed, a rate constant for solvolysis of the corresponding tetrahydronaphthalene substrate lacking a β-hydroxy group, namely 1-chloro-1,2,3,4-tetrahydronaphthalene (**5**), has been measured.

Results

Cis- and *trans*-1-trichloroacetoxy-2-methoxy-1,2-dihydro-naphthalenes (3)

Rate constants for solvolyses of *cis*- and *trans*-1-trichloroacetoxy-2-methoxy-1,2-dihydronaphthalene (**3**) were measured spectrophotometrically in aqueous acetonitrile and were recorded for different solvent compositions (Table 1). Addition of the acetonitrile to water solubilised the substrates which are precipitated in pure water. A rate constant in water for the *cis*-substrate was extrapolated from measurements at different solvent compositions plotted as log *k* against Y_{OTs} (Supporting Information File 1, Figure S1) [4,5]. For the *trans* isomer the solvolysis was too slow for measurements over a wide range of solvent compositions and rate constants could conveniently be measured only for 10 and 20% (v/v) acetonitrile. A rate constant in water was crudely extrapolated from the ratio of rate constants for the *cis* and *trans* isomers at these two solvent compositions. Values in water are shown in brackets in Table 1.

In the case of the more slowly reacting *trans* isomer there was a competing hydrolysis of the trichloroacetate ester group to give *trans*-2-methoxy-1,2-dihydro-1-naphthol (**6**-*trans*), as shown in Scheme 2. The fraction of hydrolysis was determined by HPLC and was found to increase with increasing water content and amounted to 67% in 10% acetonitrile.

Surprisingly, 10% of the hydrolysis product was also identified in the products from solvolysis of the *cis*-trichloroacetate

Table 1: Rate constants for solvolysis of *cis*- and *trans*-1-trichloroacetoxy-2-methoxy-1,2-dihydronaphthalene (**3**) in acetonitrile-water mixtures at 25 °C.

% MeCN	$10^3\ k_{obs}(s^{-1})$ *cis*	$10^3\ k_{obs}(s^{-1})$ *trans*	% solvolysis[a] *trans*	Y_{OTs}[b]	k_{cis}/k_{trans}
50	0.63			1.4	
40	0.84			1.8	
30	2.31			2.3	
20	6.75	0.0053[c]	33	3.2	1.28×10^3
10	20.1	0.0122[c]	16	3.7	1.65×10^3
0	(35)	(0.019)[c]		3.9	(~1.8×10^3)

[a]Measured by HPLC. [b]Values interpolated from measurements recorded for solvent mixtures made up by weight from [5] [c]Rate constant for solvolysis corrected for competing hydrolysis.

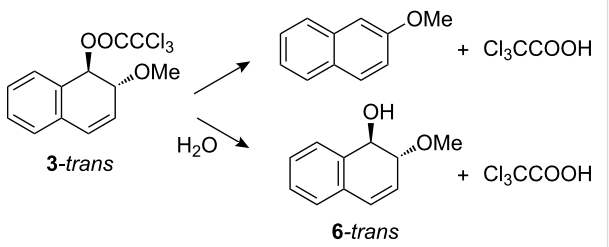

Scheme 2: Products of solvolysis and (ester) hydrolysis of *trans*-1-trichloroacetoxy-2-methoxy-1,2-dihydronaphthalene.

(**3**-*cis*). This was unexpected because the solvolysis of this substrate is more than one thousand times faster than that of its *trans* isomer whereas the rate of hydrolysis should remain practically unchanged. In so far as the hydrolysis product was not present in the reactants and the fraction of hydrolysis was independent of solvent composition, the most likely explanation would seem to be that the hydrolysis is catalysed by the *cis*-methoxy group.

The supplementary data record salt effects for the solvolysis of the *cis*-trichloroacetate ester (**3**-*cis*). For sodium acetate, the rate in 20% acetonitrile increased by a factor of close to two at a concentration of 0.4 M, whilst smaller effects were observed for both sodium perchlorate and sodium azide. A little surprisingly, sodium trichloroacetate showed a small negative salt effect leading approximately to a halving of the rate at a salt concentration of 1 M. This is unlikely to be a common ion effect, because loss of a β-proton from a naphthalenium ion intermediate to form the aromatic product (naphthol) is expected to be too fast [6,7]. This conclusion is confirmed by the lack of saturation of the effect and the normal salt effects observed for sodium acetate and sodium azide, which would be expected to trap a carbocation intermediate more effectively than the trichloroacetate anion. The normal salt effect exerted by the sodium azide also confirms that the solvolysis proceeds via the formation of a carbocation intermediate rather than by an S_N2 mechanism.

1-Chloro- and 1-chloro-2-hydroxy-1,2-tetrahydronaphthalenes

Rate constants for solvolysis of *cis*- and *trans*-1-chloro-2-hydroxy-1,2,3,4-tetrahydronaphthalenes (**4**) were measured in aqueous solution by monitoring small but easily measurable changes in the UV absorbance. Values obtained were 8.1×10^{-3} s^{-1} and 1.6×10^{-2} s^{-1} for the *cis* and *trans* isomers, respectively. Product analyses showed the formation of practically the same ratio of *cis* to *trans* diols from *cis* and *trans* reactants together with a small amount of 2-tetralone. The product distribution for the *trans* isomer is shown in Scheme 3. The corresponding figures for the *cis* isomer are 76% *cis* and 20% *trans* dihydrodiols plus 4% 2-tetralone.

The similarity of the product ratios for *cis* and *trans* isomers argues for a common carbocation intermediate in the solvolysis reactions. The possibility of significant reaction via an epoxide

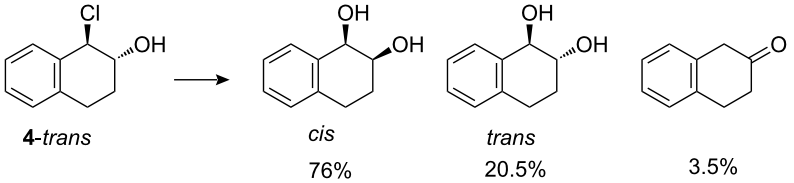

Scheme 3: Products of solvolysis of *trans*-1-chloro-2-hydroxy-1,2,3,4-tetrahydronaphthalene.

intermediate is made unlikely by the predominant formation *cis*-dihydrodiol from the *trans*-chlorohydrin reactant and the formation of similar products from both isomers. Evidence of partial reaction via an epoxide intermediate in buffers at higher pH, which could favour epoxide formation, will be reported elsewhere [8].

For the 1-chlorotetrahydronaphthalene (**5**), solvolysis in water could not be measured directly, but a value of 14 s^{-1} was obtained by extrapolation of a plot of log *k* against Y_{OTs} for aqueous acetonitrile mixtures (Supporting Information File 1, Figure S1). The measured and extrapolated rate constants in water for the five substrates studied are summarised under the appropriate structures in Figure 3.

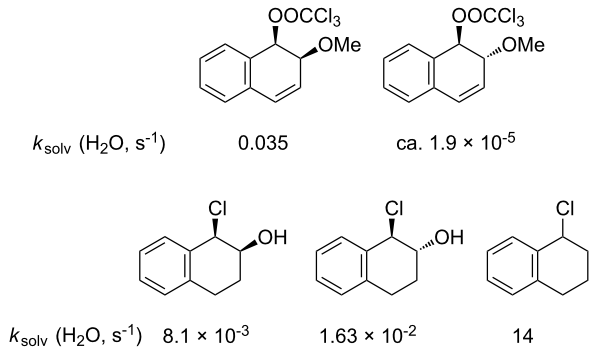

Figure 3: Rate constants for aqueous solvolyses.

Discussion

The major conclusion to be drawn from the measurements described above is that solvolysis of *cis* and *trans* 1-trichloroacetoxy-2-methoxy-1,2-dihydronaphthalenes (**3**) show an even larger advantage for reaction of the *cis* isomer, with k_{cis}/k_{trans} = ~1800, than the acid-catalysed reaction of the corresponding dihydrodiols **7** (k_{cis}/k_{trans} = 440) or the similar 2-methoxy-1,2-dihydronaphthols **8** (k_{cis}/k_{trans} = 415) [8]. Moreover, this advantage is lost for the chlorohydrins of the non-aromatic double bond of 3,4-dihydronaphthalene (as it is for the corresponding dihydrodiol). These measurements are summarised in Figure 4.

It is clear that the β-OH and β-OMe substituents exert a profound influence on the relative reactivity of *cis*- and *trans*-dihydrodiol isomers and their derivatives functionalised at the 1-position when the dihydrodiol is derived from an aromatic double bond. A question that arises is: does this selectivity derive from an unusually reactive *cis* isomer or an unusually unreactive *trans* isomer? Evidence on this point comes from examining the effect of the β-hydroxy group on the rate of reactions of the *cis* and *trans* isomers.

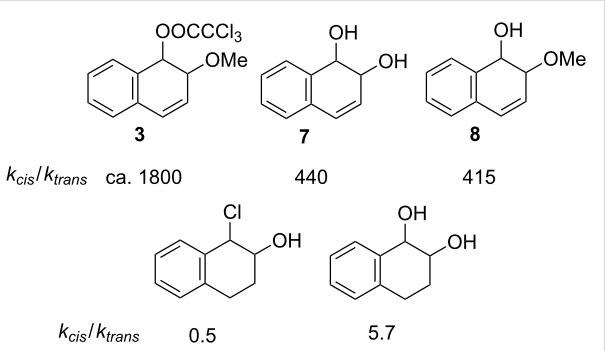

Figure 4: *Cis*/*trans* reactivity ratios for β-hydroxycarbocation forming reactions.

Comparison of rate constants for the aqueous solvolysis of *cis*- and *trans*-1-chloro-2-hydroxy-1,2-dihydronaphthalenes (**4**) with the rate constant for the corresponding substrate lacking a hydroxy group (**5**) in Figure 3 shows that the hydroxy slows the rate by a factor of 860 in the case of the *trans* isomer and 1700 in the case of the *cis*. These rate retardations seem a little large when compared with early estimates of the effect of a β-hydroxy or methoxy group in solvolysis reactions, which gave k_H/k_{OH} ~100 [9-11]. However, for β-oxy substituents it is difficult to separate a rate-retarding (inductive) effect from a competing acceleration arising from participation of oxygen as a neighbouring group [12,13].

As shown in Table 2, more recent estimates of the rate-retarding effect have been based on incorporating oxygen into a structural framework which prevents its participation as a neighbouring group. An example of this constraint is provided by comparison of solvolyses of the *exo*- and *endo*-norbornyl brosylate with an oxygen atom at the 7-position (**9**) with the corresponding substrate lacking an oxygen. This leads to a rate retardation of 2000- fold for the *exo*-isomers and 6000 fold for the *endo* [14] which is comparable to the differences we observed and, indeed, is similar to the effect of oxygen reported for the monocyclic tetrahydrofuranyl ring of **10** which solvolyses 1030 times more slowly than cyclopentyl brosylate [15].

These effects are much larger than that of oxygen in the 3-position of the tetrahydropyranyl brosylate (**11**), which slows the rate only by a factor of 18. However, in this case, participation of oxygen as a neighbouring group is well established [15]. Participation by oxygen in a six-membered ring is excluded for solvolysis of *endo* (although not *exo*) norbornyl brosylate substituted with oxygen at the 4-position (**12**). Comparison with the carbocyclic substrate in this case shows a rate retardation of 80,000 [16]. This value has been considered exceptionally large and an additional rate-retarding effect has been attributed to ring strain induced by the presence of oxygen in the six-

Table 2: Solvolysis reactions: oxygen substituent effects on reactivity[a].

	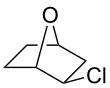	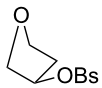		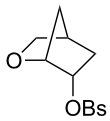
	9	**10**	**11**	**12**
k_{CH2}/k_O	2000	1030	18	80000
Temp	85 °C	85 °C	85 °C	25 °C
Solvent	20% aq EtOH	AcOH	AcOH	AcOH

[a]data from [14-16].

membered ring of the bicyclic carbocation. Surprisingly, while the solvolysis of *trans*-2-methoxycyclohexyl tosylate has been well studied [17], there appear to have been no measurements reported for its *cis* isomer.

We cannot compare these rate ratios directly with those for the solvolyses of *cis*- and *trans*-1-trichloroacetoxy-2-methoxydihydronaphthalenes (**3**) because, as noted in the introduction, the parent 1-trichloroacetoxy-1,2-dihydronaphthalene is too reactive to allow isolation and kinetic measurements. However, rate constants have been measured for the acid-catalysed reactions of *cis* and *trans*-naphthalene 1,2-dihydrodiols **13**-*cis* and **13**-*trans* (reacting at the 1-position) and may be compared with the corresponding alcohol lacking a β-hydroxy substituent, namely the 1-hydroxy-1,2-dihydronaphthalene (**14**) [3], as shown in Figure 5.

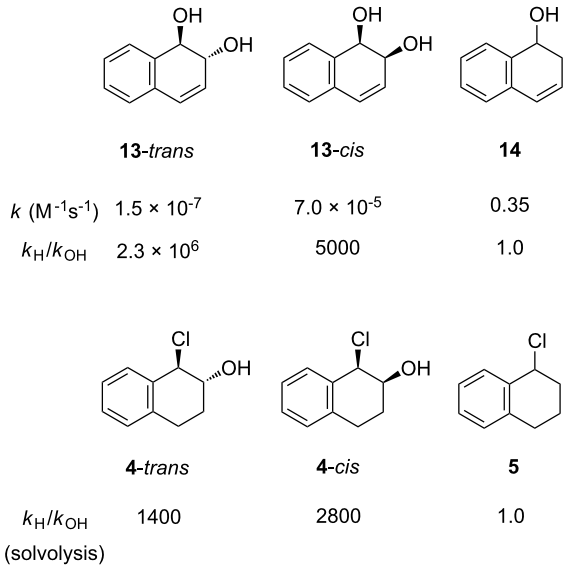

Figure 5: Comparison of the effect of a β-hydroxy group on the reactivity of *cis* and *trans* di- and tetrahdronaphthalene substrates.

It can be seen from this figure that a β-hydroxy substituent has similar effects on the reactivity of *cis*-dihydro and tetrahydro substrates, with a rate retarding effect of 5000 for **13**-*cis* in Figure 5, compared with 2800 for solvolysis of the *cis* β-hydroxychlorotetrahydronaphthalene **4**. In contrast, the effect is much greater in the dihydro case for the *trans*-substituent, i.e., 2.3×10^6 for **13**-*trans* compared with 1400 for solvolysis ot **4**-*trans*. Measurements for benzene and phenanthrene dihydrodiols confirm that, whereas the ratio of *cis*-rate constants to those of the corresponding alcohols, which lack a β-hydroxy group, remains roughly constant, those for the *trans*-dihydrodiols increase sharply as the aromaticity of the double bond increases [18].

These comparisons suggest that that the rate of reaction of the *cis*-dihydrodiol is 'normal' while that of its *trans* isomer is abnormally slow. This is consistent with the interpretation already given for the difference in reactivities between the *cis* and *trans* isomers **3**, namely that the arenium ion intermediates are strongly stabilised by hyperconjugation between the carbocationic charge centre and a β-C–H bond, and that this effect is amplified by the contribution of an aromatic structure to the no-bond resonance form (**15b**) of the valence bond representation of this interaction **15a**↔**15b** in Scheme 4 [3].

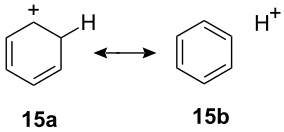

Scheme 4: 'Aromatic' hyperconjugation for the benzenium ion.

The interaction operates effectively for arenium ion intermediates formed from alcohols (arene hydrates) and *cis*-dihydrodiols or their derivatives which, as illustrated in Scheme 5, can be formed in a conformation in which an axial C–H bond bond is positioned for hyperconjugation with the positive charge.

This is a consequence of a stereochemical constraint requiring that the leaving group departs from an axial position to facilitate delocalisation of the carbocationic charge. However, for the *trans*-dihydrodiols, or the *trans*-1-trichloroacetoxy-2-methoxy-1,2-dihydronaphthol **3**-*trans*, the same constraint forces the β-OH group into an axial position. Although delocalisation of the charge appears to be highly effective when this position is occupied by a β-hydrogen atom (C–H bond), the interaction becomes very much less favourable when occupied by a β-OH group (C–OH bond).

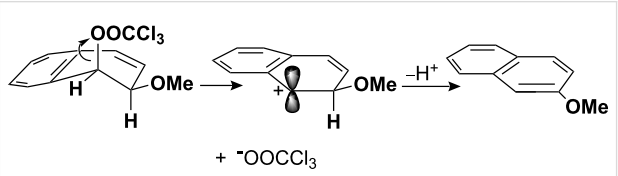

Scheme 5: Stereochemistry of carbocation formation from solvolysis of *cis*-1-trichloroacetoxy-2-hydroxy-1,2-dihydronaphthalene.

The work describing these favourable and unfavourable hyperconjugative interactions has hitherto been based largely on carbocation formation involving an H_2O leaving group characteristic of acid-catalysed dehydration of alcohols and *cis* and *trans* dihydrodiols of aromatic and aliphatic carbon–carbon double bonds (**3**). The purpose of the present study was to determine whether the same dependence on stereochemistry of a β-hydroxy group would be observed for solvolytic reactions. Our conclusion, that it is, is based on a comparison of measurements of absolute and relative reactivities of *cis* and *trans* isomers in conventional solvolytic reactions with chloride ion as a leaving group (yielding a carbocation not corresponding to a protonated aromatic molecule) with the solvolytic formation of naphthalenium ions in which the leaving group is a trichloroacetate anion. The only noteworthy difference between the two classes of reactions (i.e., dehydrations and solvolyses) is a slightly larger difference in reactivity between *cis* and *trans* methoxy groups for the solvolytically generated arenium ions (2000 compared with 415) which perhaps represents a more product-like transition for the poorer trichloroacetate than the H_2O leaving group. In sum, the influence of an enhanced hyperconjugation identified in the reactions of arene dihydrodiols is fully corroborated by the present study of β-hydroxy carbocation-forming solvolysis reactions.

Experimental

Purchased reagents were generally used without purification. *Cis*-naphthalene dihydrodiol (*cis*-1,2-dihydroxy-1,2-dihydronaphthalene) was prepared by oxidative fermentation of naphthalene [19] and was kindly provided by D. R. Boyd of the Queen's University of Belfast. Naphthalene oxide and *trans*-1-hydroxy-2-methoxy-1,2-dihydronaphthalene (**6**-*trans*) were prepared as described by Jerina and co-workers [20]. *Trans*-1,2-dihydroxy-1,2-dihydronaphthalene was prepared by the method of Platt and Oesch [21]. *Cis*- and *trans*-1,2-dihydroxy-1,2,3,4-tetrahydronaphthalene [22-24], the corresponding *trans*-1-chloro-2-hydroxy-1,2,3,4-tetrahydronaphthalene [25,26] and 1-chloro-1,2,3,4-tetrahydronaphthalene [25] were also prepared by literature methods.

***cis*-1-Hydroxy-2-methoxy-1,2-dihydronaphthalene (6-*cis*).** To a solution of *cis*-1,2-dihydroxy-1,2-dihydronaphthalene (0.5 g, 3.1 mmol) in DMF (20 mL), was added sodium hydride as a 60% dispersion on mineral oil (0.15 g, 6.2 mmol) followed over 10 min by dimethyl sulfate (0.77 g, 6.18 mmol). The mixture was stirred at room temperature for 20 h, quenched with 1 mL of acetic acid and diluted with water (50 mL). It was then extracted with diethyl ether (2 × 50 mL) and the combined ether layers washed with water (2 × 50 mL) and dried over sodium sulfate. The solvent was removed under reduced pressure to yield a residue consisting of two regioisomeric monomethylated products and the dimethylated product (*cis*-1,2-dimethoxy-1,2-dihydronaphthalene). Purification by chromatography allowed separation of the dimethylated product but the monomethylated products were obtained as a three to one mixture of the desired product with its regioisomer (0.08 g, 15%) (R_f 0.65, 20% ethyl acetate in pentane). NMR data for the principal isomer and analytical data for the mixture were as follows.

^{1}H NMR ($CDCl_3$) δ 2.6 (bs, 1H, OH), 3.45 (s, 3H), 4.0 (t, J = 4.4 Hz, 1H), 4.78 (bs, 1H), 6.08 (dd, J = 9.6, 3.9 Hz, 1H), 6.59 (dd, J = 9.6 Hz, 1H), 7.1–7.54 (m, 4H); *m/z* GC-MS) 156 (M-H_2O); (Found C 74.3, H 7.0; $C_{11}H_{12}O_2$ requires C 75.0, H 6.9).

***cis*-1-Trichloracetoxy-2-methoxy-1,2-dihydronaphthalene (3-*cis*).** To a 3:1 mixture (0.1 g, 0.56 mmol) of *cis*-1-hydroxy-2-methoxy-1,2-dihydronaphthalene (**6**-*cis*) and its regioisomer (see above) in dichloromethane (10 mL), were added pyridine (45 mg, 0.57 mmol), DMAP (7 mg 0.05 mmol) and trichloroacetic anhydride (0.21 g, 0.68 mmol) and the solution was stirred at room temperature for 2 h. Evaporation of the solvent gave a crude product mixture from which the desired product was separated by flash chromatography (R_f 0.61, 10% ethyl acetate in pentane) to give a light yellow oil (0.08g, 73%). ^{1}H NMR ($CDCl_3$) δ 3.4 (s, 3H), 4.31 (m, 1H), 6.05 (dd, J = 9.91, 2.39 Hz, 1H), 6.11 (d, J = 4.35 Hz, 1H), 6.58 (dd, J = 9.81, 1.81 Hz, 1H) 7.15–7.31 (m, 4H).

***trans*-1-Trichloracetoxy-2-methoxy-1,2-dihydronaphthalene (3-*trans*).** To a solution of *trans*-1-hydroxy-2-methoxy-1,2-dihydronaphthalene (**6**-*trans)* (0.1 g, 0.56 mmol) in

dichloromethane (10 mL), pyridine (45mg, 0.57 mmol) and DMAP (7 mg, 0.05 mmol) were added. The mixture was stirred for 5 min and trichloroacetic anhydride (0.21g, 0.68 mmol) was added over 5 min followed by stirring for 2 h at room temperature. Evaporation of the solvent gave a crude product which was purified by preparative TLC (5% ether in pentane) to yield the desired product as a light yellow-coloured liquid (0.14 g 77%); (R_f 0.73 10% ether in hexane); ^{1}H NMR ($CDCl_3$) δ 3.4 (s, 3H), 4.29 (ddd, J = 7.53, 3.24, 1.48 Hz, 1H), 6.09 (dd, J = 9.87, 3.32 Hz, 1H), 6.28 (d, J = 7.55 Hz, 1H), 6.59 (dd, J = 9.89, 1.00 Hz, 1H) 7.15–7.31 (m, 4H); m/z (GC-MS) 158.1 (321.5 $-Cl_3CCOOH$).

***cis*-1-Chloro-2-hydroxy-1,2,3,4-tetrahydronaphthalene.** A solution containing 0.05 mL of 4 M HCl in anhydrous dioxane and 0.2 mL of anhydrous THF was added dropwise to a solution of tetrahydronaphthalene-1,2-oxide (100 mg, 0.68 mmol) in anhydrous THF (2 mL) and the mixture allowed to stand at room temperature for 10 min. The solvent and excess HCl were then removed under reduced pressure to yield a crude product which was purified by TLC (10% ether in pentane) to give a colourless liquid (40 mg, 32%); ^{1}H NMR ($CDCl_3$) δ 1.96 (m, 1H), 2.09 (m, 2H), 2.91 (m, 2H), 3.1 (m, 1H), 4.12 (m, 2H), 5.33 (d, J = 3.0 Hz, 1H), 7.11–7.37 (m, 4H); ^{13}C NMR ($CDCl_3$) 26.56, 27.82, 65.55, 69.14,126.44, 128.85, 128.87, 130.71, 134.56, 135.57; m/z (GC-MS) 182.5.

Kinetic measurements and product ratios. In general, rate constants for solvolysis reactions were measured by injecting 20–25 μL of a ~0.01 M solution of substrate in acetonitrile into 2 mL of water or aqueous acetonitrile in a cuvette and monitoring the reaction from the change in the UV spectrum. For 1-chloro-1,2,3,4-tetrahydronaphthalene rate constants (s^{-1}) were measured for the following acetonitrile water solvent mixtures: 50% MeCN, 0.0320; 60% MeCN, 0.0106; 70% MeCN, 0.00335; 80% MeCN, 0.00082. A plot of log k versus Y_{OTs} and extrapolation gave a rate constant of ~2.3 s^{-1} for pure water.

For both the trichloroacetate esters of 2-methoxy-1,2-dihydro-1-naphthol and the *cis*-and *trans*-chlorohydrins of 1,2-dihydronaphthalene product analyses were carried out by HPLC. In a typical procedure 25 μL of ~0.01M solution of the substrate in acetonitrile were injected into 150 μL of water or aqueous acetonitrile mixture. After allowing time for completion of the reaction, the products were analysed by reverse phase HPLC on a C18 column with a flow rate of 0.25 mL/min and detection at 270 nm. For the trichoroacetic esters, the product proportions were required to partition measured rate constants between contributions from pathways for solvolysis and hydrolysis.

Supporting Information

Supporting Information File 1

Experimental part.
[http://www.beilstein-journals.org/bjoc/content/supplementary/1860-5397-6-118-S1.pdf]

Acknowledgements

This work was supported by The Science Foundation Ireland (Grant No. 04/IN3/B581). We thank A. Cagney for assistance with the kinetic measurements.

References

1. Boyd, D. R.; Bugg, T. D. *Org. Biomol. Chem.* **2006,** *4,* 181–192. doi:10.1039/b513226f
2. Boyd, D. R.; Blacker, J.; Briege, B.; Dalton, H.; Hand, M. V.; Kelly, S. C.; More O'Ferrall, R. A.; Rao, S. N.; Sharma, N. D.; Sheldrake, G. N. *J. Chem. Soc., Chem. Commun.* **1994,** 313–314. doi:10.1039/C39940000313
3. Boyd, D. R.; Coyne, D.; Keeffe, J. R.; Kudavalli, J. S.; Lawlor, D. A.; MacCormac, A. C.; More O'Ferrall, R. A.; Rao, S. N.; Sharma, N. D. *Org. Lett.*, in press.
4. Bentley, T. W.; Llewellyn, G. Y_x Scales of Solvent Ionizing Power. In *Prog. Phys. Org. Chem.;* Taft, R. W., Ed.; John Wiley & Sons, Inc.: Hoboken, NJ, USA, 1990; Vol. 17, pp 121–158. doi:10.1002/9780470171967.ch5
5. Bunton, C. A.; Mhala, M. M.; Moffatt, J. R. *J. Org. Chem.* **1984,** *49,* 3637–3639. doi:10.1021/jo00193a036
6. Pirinccioglu, N.; Thibblin, A. *J. Am. Chem. Soc.* **1998,** *120,* 6512–6517. doi:10.1021/ja9807800
7. Lawlor, D. A.; More O'Ferrall, R. A.; Rao, S. N. *J. Am. Chem. Soc.* **2008,** *130,* 17997–18007. doi:10.1021/ja806899d
8. Kudavalli, J. S.; More O'Ferrall, R. A. Unpublished results.
9. Streitwieser, A., Jr. *Solvolytic Displacement Reactions;* McGraw-Hill: New York, 1962.
10. Winstein, S.; Grunwald, E.; Ingraham, L. L. *J. Am. Chem. Soc.* **1948,** *70,* 821–828. doi:10.1021/ja01182a113
11. Winstein, S.; Grunwald, E. *J. Am. Chem. Soc.* **1948,** *70,* 828–837. doi:10.1021/ja01182a114
12. Capon, B.; McManus, S. P. *Neighbouring Group Participation;* Plenum Press: London, U. K., 1976.
13. Perst, H. *Oxonium Ions in Organic Chemistry;* Academic Press: London, U. K., 1971.
14. Martin, J. C.; Bartlett, P. D. *J. Am. Chem. Soc.* **1957,** *79,* 2533–2541. doi:10.1021/ja01567a047
15. Tarbell, D. S.; Hazen, J. R. *J. Am. Chem. Soc.* **1969,** *91,* 7657–7663. doi:10.1021/ja50001a023
16. Spurlock, L. A.; Fayter, R. G., Jr. *J. Am. Chem. Soc.* **1972,** *94,* 2707–2711. doi:10.1021/ja00763a027
17. Roberts, D. D. *J. Org. Chem.* **1997,** *62,* 1857–1859. doi:10.1021/jo961941q
18. MacCormac, A. C.; Lawlor, D. A.; More O'Ferrall, R. A. Unpublished results.
19. Jerina, D. M.; Daly, J. W.; Jeffrey, A. M.; Gibson, D. T. *Arch. Biochem. Biophys.* **1971,** *142,* 394–396. doi:10.1016/0003-9861(71)90298-0

20. Jeffrey, J. M.; Yeh, H. J. C.; Jerina, D. M.; DeMarinis, R. M.; Foster, C. H.; Piccolo, D. E.; Berchtold, G. A. *J. Am. Chem. Soc.* **1974,** *96,* 6929–6937. doi:10.1021/ja00829a020
21. Platt, K. L.; Oesch, F. *Synthesis* **1977,** 449–450. doi:10.1055/s-1977-24434
22. Orsini, F.; Sello, G.; Travaini, E.; Di Gennaro, P. *Tetrahedron: Asymmetry* **2002,** *13,* 253–259. doi:10.1016/S0957-4166(02)00098-8
23. Sukumaran, K. B.; Harvey, R. G. *J. Org. Chem.* **1980,** *45,* 4407–4413. doi:10.1021/jo01310a029
24. Boyd, D. R.; Sharma, N. D.; Kerley, N. A.; McConville, G.; Allen, C. C. R.; Blacker, A. J. *ARKIVOC* **2003,** *7,* 32–48.
25. Bartas-Yacoubou, J.-M.; Maduike, N.; Kyere, S.; Doan, L.; Whalen, D. L. *Tetrahedron Lett.* **2002,** *43,* 3781–3782. doi:10.1016/S0040-4039(02)00637-8
26. Reimann, E.; Hargasser, E. *Arch. Pharm.* **1989,** *322,* 159–164. doi:10.1002/ardp.19893220309

License and Terms

Beilstein Journal of Organic Chemistry

Kinetics and mechanism of vanadium catalysed asymmetric cyanohydrin synthesis in propylene carbonate

Michael North* and Marta Omedes-Pujol

Full Research Paper

Open Access

Address:
School of Chemistry and University Research Centre in Catalysis and Intensified Processing, Bedson Building, University of Newcastle, Newcastle upon Tyne, UK, NE1 7RU

Email:
Michael North* - michael.north@ncl.ac.uk

* Corresponding author

Keywords:
cyanohydrin; Hammett; kinetics; propylene carbonate; vanadium

Beilstein J. Org. Chem. **2010,** *6,* 1043–1055.
doi:10.3762/bjoc.6.119

Received: 12 July 2010
Accepted: 15 October 2010
Published: 03 November 2010

Guest Editor: J. Murphy

Abstract

Propylene carbonate can be used as a green solvent for the asymmetric synthesis of cyanohydrin trimethylsilyl ethers from aldehydes and trimethylsilyl cyanide catalysed by VO(salen)NCS, though reactions are slower in this solvent than the corresponding reactions carried out in dichloromethane. A mechanistic study has been undertaken, comparing the catalytic activity of VO(salen)NCS in propylene carbonate and dichloromethane. Reactions in both solvents obey overall second-order kinetics, the rate of reaction being dependent on the concentration of both the aldehyde and trimethylsilyl cyanide. The order with respect to VO(salen)NCS was determined and found to decrease from 1.2 in dichloromethane to 1.0 in propylene carbonate, indicating that in propylene carbonate, VO(salen)NCS is present only as a mononuclear species, whereas in dichloromethane dinuclear species are present which have previously been shown to be responsible for most of the catalytic activity. Evidence from ^{51}V NMR spectroscopy suggested that propylene carbonate coordinates to VO(salen)NCS, blocking the free coordination site, thus inhibiting its Lewis acidity and accounting for the reduction in catalytic activity. This explanation was further supported by a Hammett analysis study, which indicated that Lewis base catalysis made a much greater contribution to the overall catalytic activity of VO(salen)NCS in propylene carbonate than in dichloromethane.

Introduction

The last 15 years have witnessed an explosion of activity in the area of asymmetric cyanohydrin synthesis [1], mostly using trimethylsilyl cyanide (TMSCN) as the cyanide source to produce enantiomerically enriched silyl-protected cyanohydrins, which can readily be converted into other, pharmaceutically important, bifunctional units, such as α-hydroxy acids and β-amino alcohols [2] (Scheme 1). Asymmetric cyanohydrin synthesis can be achieved by the use of a suitable chiral cata-

lyst, and a wide range of catalysts have been found to catalyse this reaction including enzymes [3,4], organocatalysts [5,6] and metal-based catalysts [1]. All of the most effective catalysts for asymmetric cyanohydrin synthesis have been found to involve cooperative catalysis [7-9], in which the aldehyde is activated by an acidic group and the cyanide source is activated by a basic group. The acid and base catalysts can be present within a single catalyst unit, or can be in separate catalysts, either or both of which may be chiral.

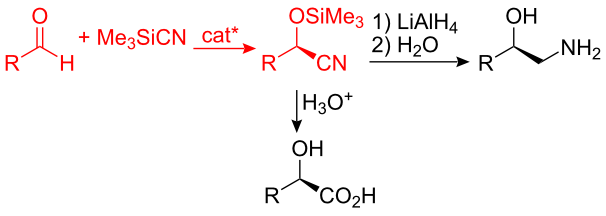

Scheme 1: Synthesis and transformation of nonracemic silyl-protected cyanohydrins.

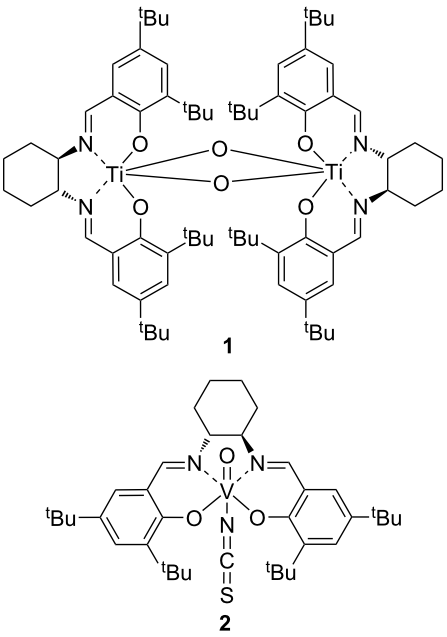

Figure 1: Highly active metal(salen) complexes for asymmetric cyanohydrin synthesis.

Whilst enzymatic catalysts (oxynitrilases) have been extensively developed [3,4] and commercialized [10], they do have the disadvantage of requiring hydrogen cyanide which is toxic and difficult to handle in a laboratory environment, and gives unprotected cyanohydrins which are prone to racemization. Pre-eminent amongst the synthetic catalysts are metal(salen) complexes, especially those based on titanium (**1**) and vanadium (**2**) [1] (Figure 1). Titanium complex **1** will catalyse the asymmetric addition of TMSCN to aromatic aldehydes with 80–90% enantiomeric excess at room temperature with just 0.1 mol % of catalyst [11]. Complex **1** also catalyses the asymmetric addition of other cyanide sources including potassium cyanide [12-15], cyanoformates [15-20] and acyl cyanides [17,19,21] to aldehydes, and will accept some ketones as substrates [22,23]. Recently, a modified version of complex **1**, in which the two salen ligands are covalently linked together has been developed which allows the amount of catalyst used to be reduced to 0.0005 mol % [24,25].

Vanadium based catalysts such as **2** also catalyse the asymmetric addition of TMSCN [26-28] and KCN [13] to aldehydes and are more enantioselective, but less reactive than the titanium based catalyst **1**. Complexes **1** and **2** have been commercialized [10,29,30], immobilized to facilitate their recycling [31-43] and used by other groups as part of synthetic studies [44-46]. Mechanistically, the mode of action of catalyst **1** is well understood [15,20,47-49], involving a bimetallic transition state in which one titanium atom acts as a Lewis acid, coordinating to the aldehyde, and the other forms a titanium–cyanide bond, thus allowing transfer of cyanide to the carbonyl to occur intramolecularly in a highly organized transition state structure. The mode of action of vanadium based catalysts such as **2** is believed to involve two parallel catalytic cycles, the slower of which involves only monometallic species, whilst the other involves bimetallic complexes [28]. Experimental evidence has shown that formation of vanadium(IV) complexes in situ is important [28,50], as is the formation of bimetallic complexes involving vanadium ions in both the +4 and +5 oxidation states [28,51]. Both Lewis acid and Lewis base catalysis are known to be involved in the catalytic cycle, the latter possibly involving the isothiocyanate counterion [52].

Despite their many favourable properties, there is one drawback associated with catalysts **1** and **2**; they exhibit highest activity and highest enantioselectivity in chlorinated solvents, optimally dichloromethane. Recently however, we showed that catalyst **2** could be used in propylene carbonate [53]. Propylene carbonate and other cyclic carbonates are starting to attract significant interest as green solvents [54-64], since they can be prepared by a 100% atom economical reaction between epoxides and CO_2 (Scheme 2) [65]. The green credentials of propylene carbonate are enhanced by the commercialization of a low temperature synthesis of propylene oxide from propene and hydrogen peroxide [66-70], by the development of a greener synthesis of hydrogen peroxide [71], and by the combination of these processes into a one-pot synthesis of propylene oxide from propene, hydrogen and oxygen [72,73]. In addition, it has

been shown that in the presence of an appropriate catalyst, the reaction between epoxides and carbon dioxide can be achieved at atmospheric pressure and room temperature [74-77], or in a gas-phase continuous flow reactor [78], thus facilitating the use of waste carbon dioxide in this process [79].

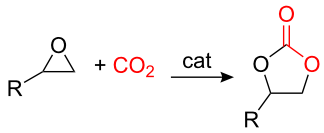

Scheme 2: Synthesis of cyclic carbonates.

In this paper we give full details of the use of catalyst **2** in propylene carbonate, and describe kinetic studies, which allow differences in the relative importance of Lewis acid and Lewis base catalysis between reactions carried out in dichloromethane and propylene carbonate to be elucidated.

Results and Discussion

Synthetic Studies

Initially, the compatibility of catalysts **1** and **2** with propylene carbonate was investigated by carrying out the asymmetric addition of TMSCN to a range of aldehydes in both dichloromethane and propylene carbonate under identical reaction conditions. These reactions were all carried out at room temperature for two hours with 0.1 mol % of catalyst, 1.1 equiv of TMSCN and a substrate concentration of 0.56 M. In each case, the enantiomeric excess of the cyanohydrin product was determined by chiral GC after conversion of the trimethylsilyl ether into the corresponding acetate by the method of Kagan [80], a process which is known to cause no racemization (Scheme 3). The results of this study are presented in Table 1.

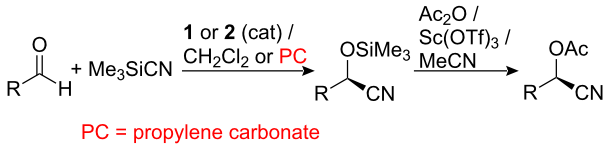

Scheme 3: Synthesis of cyanohydrin trimethylsilyl ethers and acetates.

It is apparent from Table 1, that for reactions catalysed by titanium based catalyst **1**, changing the solvent to propylene carbonate had a severely detrimental effect on the enantio-

Table 1: Influence of solvent on cyanohydrin synthesis using catalysts **1** and **2**.

Aldehyde	Solvent[a]	Catalyst **1**		Catalyst **2**	
		Conversion[b]	ee[c]	Conversion[b]	ee[c]
PhCHO	CH_2Cl_2	95	78	100	86
PhCHO	PC	33	40	73	80
4-FC_6H_4CHO	CH_2Cl_2	40	76	81	91
4-FC_6H_4CHO	PC	24	35	67	76
4-ClC_6H_4CHO	CH_2Cl_2	98	83	90	93
4-ClC_6H_4CHO	PC	20	25	73	76
3-ClC_6H_4CHO	CH_2Cl_2	83	84	83	89
3-ClC_6H_4CHO	PC	53	46	56	62
2-MeC_6H_4CHO	CH_2Cl_2	76	89	81	96
2-MeC_6H_4CHO	PC	47	36	78	73
3-MeC_6H_4CHO	CH_2Cl_2	95	97	100	99
3-MeC_6H_4CHO	PC	30	57	67	93
4-MeC_6H_4CHO	CH_2Cl_2	82	68	86	87
4-MeC_6H_4CHO	PC	16	49	56	86
$Me(CH_2)_7CHO$	CH_2Cl_2	71	73	88	83
$Me(CH_2)_7CHO$	PC	98	45	96	67
Me_3CCHO	CH_2Cl_2	93	47	100	86
Me_3CCHO	PC	100	10	99	76
CyCHO	CH_2Cl_2	100	66	100	88
CyCHO	PC	97	19	97	67

[a]PC = propylene carbonate; [b]Conversions were determined by ^1H NMR spectroscopy; [c]Enantiomeric excesses were determined by chiral GC analysis of the cyanohydrin acetates (data presented in Supporting Information File 1). The predominant cyanohydrin derivative always had the (*S*)-configuration.

selectivity of the reactions. In some cases, the enantiomeric excess of the cyanohydrin was more than halved when reactions were carried out in propylene carbonate. For aromatic aldehydes, there was also a substantial reduction in the conversion obtained from reactions carried out in propylene carbonate, though this was not apparent with the aliphatic aldehydes studied. The reason for the lower reactivity and enantioselectivity displayed by catalyst **1** in propylene carbonate can be related to the dissociation of the catalytically active bimetallic complex **1** into the catalytically inactive monometallic complex **3** (Scheme 4). The position of this equilibrium is known to be solvent dependent, with polar solvents favouring the formation of the monometallic species [15]. Propylene carbonate is a polar aprotic solvent with a dielectric constant of 65 [81], and therefore the concentration of catalytically active bimetallic complex **1** will be reduced in this solvent resulting in less effective catalysis.

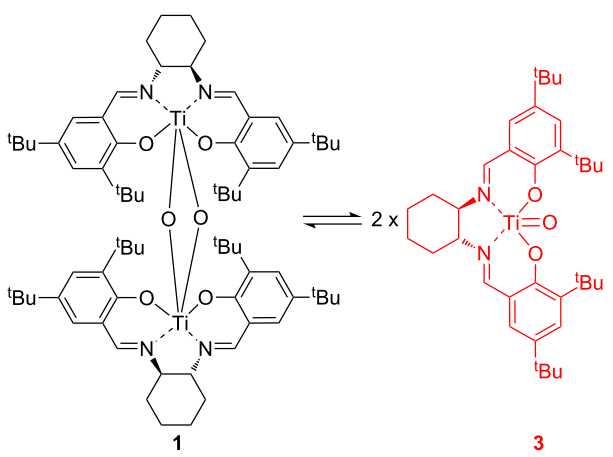

Scheme 4: Equilibrium between bimetallic and monometallic Ti(salen) complexes.

Reactions catalysed by complex **2** also proceeded more slowly and less enantioselectively in propylene carbonate than in dichloromethane (Table 1). However, the reduction in conversion and enantioselectivity was much less pronounced than for reactions catalysed by complex **1**. Therefore, attempts were made to optimize the reaction conditions for reactions catalysed by complex **2** in propylene carbonate by reducing the reaction temperature to enhance the enantioselectivity and by increasing the reaction time to optimize the conversion. The results of this study are shown in Table 2.

Reactions carried out with benzaldehyde at room temperature (entries 1 and 2) showed that increasing the reaction time increased the conversion without lowering the enantioselectivity. The conversion could also be increased by doubling the catalyst concentration (entry 3), though this did not enhance the enantioselectivity. Reducing the reaction temperature to 0 °C (entry 4) reduced the rate of reaction so that a reaction time of 18 hours was required to achieve the same conversion as could be achieved in two hours at room temperature (Table 1), but the lower temperature did restore the enantioselectivity to that observed in dichloromethane at room

Table 2: Optimization of asymmetric cyanohydrin synthesis catalysed by complex **2** in propylene carbonate.

Entry	Aldehyde	*T* (°C)	Time (h)	**2** (mol %)	Conversion[a]	ee[b]
1	PhCHO	rt	4	0.1	83	83
2	PhCHO	rt	24	0.1	92	80
3	PhCHO	rt	2	0.2	86	85
4	PhCHO	0	18	0.1	73	86
5	4-FC_6H_4CHO	0	24	0.1	88	88
6	3-ClC_6H_4CHO	0	24	0.1	89	82
7	4-ClC_6H_4CHO	0	24	0.1	86	80
8	4-MeC_6H_4CHO	0	18	0.1	63	90
9	2-MeC_6H_4CHO	rt	24	0.1	100	81
10	3-MeC_6H_4CHO	rt	24	0.1	93	89
11	4-MeC_6H_4CHO	rt	24	0.1	90	83
12	$Me(CH_2)_7CHO$	0	18	0.1	100	61
13	CyCHO	0	18	0.1	92	76
14	Me_3CCHO	0	18	0.1	100	80
15	$Me(CH_2)_7CHO$	−20	24	0.1	98	75
16	CyCHO	−20	24	0.1	88	77
17	Me_3CCHO	−20	24	0.1	100	80

[a]Conversions were determined by ^{1}H NMR spectroscopy; [b]Enantiomeric excesses were determined by chiral GC analysis of the cyanohydrin acetates (data presented in Supporting Information File 1). The predominant cyanohydrin derivative always had the (*S*)-configuration.

temperature. Electron-deficient aromatic aldehydes also gave good results at 0 °C (entries 5–7), as did 4-methylbenzaldehyde (entry 8), although in this case, whilst the enantioselectivity was higher than that obtained at room temperature in dichloromethane, the conversion was not as high. Therefore, to ensure good conversions, the optimal conditions for electron-rich aromatic aldehydes were taken as room temperature for 24 hours (entries 9–11). The three aliphatic aldehydes studied (entries 12–14) all gave high conversions at 0 °C, but the enantioselectivities were not as high as those obtained at room temperature in dichloromethane. Therefore, for these substrates, the reaction temperature was further reduced to −20 °C (entries 15–17), but this resulted in only a modest improvement in the enantioselectivity, except when nonanal was used as the substrate.

Propylene carbonate has a boiling point of 242 °C and could not be separated from the cyanohydrin trimethylsilyl ethers by distillation. Since the cyanohydrin ethers are liquids and are unstable during chromatography, it was impossible to purify the cyanohydrin trimethylsilyl ethers produced in propylene carbonate. However, one of the main applications of nonracemic cyanohydrins is in the synthesis of α-hydroxy acids [2,29,30], and (*S*)-mandelic acid could be obtained in 60% isolated yield simply by refluxing the mixture of propylene carbonate and mandelonitrile trimethylsilyl ether (81% ee) with 12 N hydrochloric acid for six hours followed by crystallization from ether/hexane. That no racemization occurred during this process was demonstrated by conversion of the mandelic acid into methyl mandelate followed analysis by chiral HPLC (data presented in Supporting Information File 1), which gave an enantiomeric excess of 81%.

Kinetic and NMR Studies using benzaldehyde

Previous work [28] has shown that the asymmetric addition of TMSCN to benzaldehyde in dichloromethane catalysed by complex **2** follows overall second-order kinetics, the reaction being first order in both benzaldehyde and TMSCN. The rate equation is then represented by Equation 1:

$$\begin{aligned} \text{Rate} &= k_2[\mathbf{2}]^{1.2}[\text{PhCHO}][\text{TMSCN}] \\ &= k_{2obs}[\text{PhCHO}][\text{TMSCN}] \end{aligned} \quad (1)$$

The order with respect to the catalyst (1.2) in Equation 1 provides information on the relative importance of mononuclear and binuclear species in the catalytic cycle [28,47]. A value greater than one implies that the catalyst exists in solution as a mixture of mononuclear and binuclear species, but that the binuclear species is predominantly responsible for the catalysis. The ability of catalyst **2** to function in propylene carbonate provided the opportunity to extend this study to a second solvent system with very different polarity to dichloromethane, and thus offered the potential to obtain a better understanding of the factors that are important for high catalyst activity.

Initially, the kinetics of reactions carried out in dichloromethane and propylene carbonate were compared. These reactions were carried out at 0 °C with 0.2 mol % of catalyst **2**, and initial concentrations of benzaldehyde and TMSCN of 0.49 M and 0.52 M, respectively. Reactions were monitored over a period of two hours by removing samples at regular intervals and monitoring the absorbance of residual benzaldehyde at 240–260 nm as previously described [28]. The reaction carried out in propylene carbonate was found neither to follow zero- nor first-order kinetics, but gave an excellent fit to second-order kinetics as shown in Figure 2, which shows the kinetic data obtained in both solvents for comparison. It is apparent from Figure 2 that the reactions in dichloromethane and propylene carbonate obey the same rate equation, but the reaction in propylene carbonate has an observed second-order rate constant a factor of four smaller than the reaction in dichloromethane, consistent with the lower conversions observed for reactions carried out in propylene carbonate (Table 1).

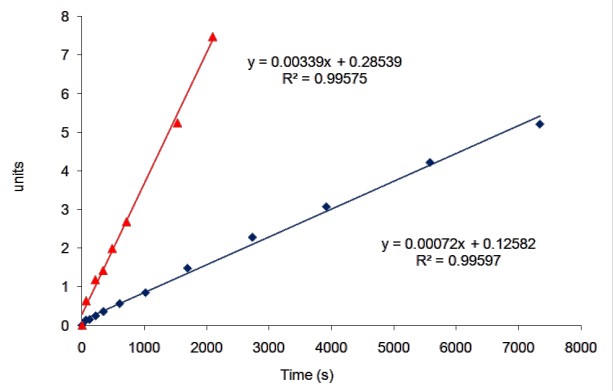

Figure 2: Second-order kinetics plot for the addition of TMSCN to benzaldehyde at 0 °C catalysed by complex **2** in dichloromethane (red) and propylene carbonate (blue). The units for the vertical scale are $\ln[(B_0A_t)/(B_tA_0)]/(A_0–B_0)$, where A = [PhCHO], B = [Me_3SiCN], and the subscripts 0 and t refer to initial concentrations and concentrations at time *t*, respectively.

To determine the order with respect to catalyst **2** and hence to investigate if changing the solvent from dichloromethane to propylene carbonate affected the aggregation state of the catalyst, reactions were carried out in propylene carbonate at 0 °C with five different concentrations of catalyst **2** (Table 3). The kinetics at each catalyst concentration were determined in triplicate, using two different batches of propylene carbonate, and the average value of the rate constant was calculated from all

Table 3: Second-order rate constants at 0 °C for the addition of TMSCN to benzaldehyde obtained at different concentrations of complex **2**.[a]

Entry	[2] (mol %)	k_{2obs1} ($M^{-1}s^{-1}$)	k_{2obs2} ($M^{-1}s^{-1}$)	k_{2obs3} ($M^{-1}s^{-1}$)	$k_{2obs\ avg}$ ($M^{-1}s^{-1}$)
1	1.13 mM (0.2)	0.00057	0.00099	0.00090	0.00083 ± 0.00016
2	1.69 mM (0.3)	0.00087	0.00116	0.00127	0.00110 ± 0.00023
3	2.25 mM (0.4)	0.00100	0.00170	0.00155	0.00142 ± 0.00042
4	3.38 mM (0.6)	0.00220	0.00205	0.00229	0.00218 ± 0.00013
5	4.50 mM (0.8)	0.00296	0.00370	0.00296	0.00321 ± 0.00049

[a]$k_{2obs1–3}$ refer to the results of three separate experiments at the specified catalyst concentration (data presented in Supporting Information File 1). $k_{2obs\ avg}$ is the average value of the three separate measurements.

three data points for each concentration. As shown in Figure 3, plots of k_{2obs} against the concentration of catalyst **2** could be fitted to a straight line, showing that in propylene carbonate the reactions are first order with respect to the concentration of the catalyst (since $k_{2obs} = k_2[\mathbf{2}]^x$ where x is the order with respect to the catalyst). This was further supported by a plot of $\log(k_{2obs})$ against log([2]), which had a slope of 0.997 (data presented in Supporting Information File 1). Thus, the order with respect to the catalyst decreases from 1.2 in dichloromethane [28] to 1.0 in propylene carbonate. This implies that in propylene carbonate, the catalyst exists only as mononuclear species and that these are exclusively responsible for the catalysis. Since it is known that catalysis by binuclear complexes formed from catalyst **2** is faster than catalysis by mononuclear complexes [28], this is therefore consistent with the reduction in reaction rate when the solvent is changed from dichloromethane to propylene carbonate. The reason for the lack of formation of bimetallic complexes in propylene carbonate is probably due to the polarity of the solvent (dielectric constant 65 [81]), which will stabilise the highly polar V=O bonds present in the mononuclear species.

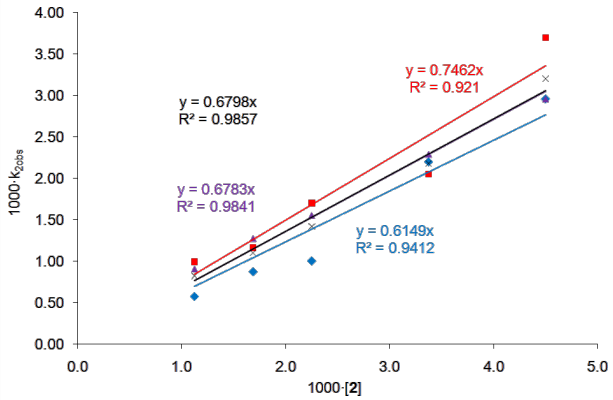

Figure 3: Plot of k_{2obs} against [2], showing that the reactions are first order with respect to the concentration of catalyst **2** (data presented in Supporting Information File 1). The red, blue and purple data and best-fit lines correspond to the three individual data sets given in Table 3. The black data and best-fit line correspond to the average data.

Having determined the order with respect to catalyst **2** in propylene carbonate, a variable temperature kinetics study was carried out to determine the activation parameters in propylene carbonate and to allow these to be compared with those previously reported for the use of catalyst **2** in dichloromethane [28]. Thus, reactions were carried out at five temperatures between 253 and 293 K. The resulting rate data are presented in Table 4. The corresponding Eyring plot is shown in Figure 4.

The Eyring equation (Equation 2) relates the rate constant for a reaction to the enthalpy and entropy of activation. Replacing the actual rate constant in Equation 2 with k_{2obs} ($k_{2obs} = k_2[\mathbf{2}]^x$) and rearranging gives Equation 3, which, after taking the logarithm of both sides, gives Equation 4. The enthalpy of activation

Table 4: Second-order rate constants at 253 K to 293 K for the addition of TMSCN to benzaldehyde.[a]

Temperature (K)	k_{2obs1} ($M^{-1}s^{-1}$)	k_{2obs2} ($M^{-1}s^{-1}$)	$k_{2obs\ avg}$ ($M^{-1}s^{-1}$)
253	0.00011	0.00006	0.00009 ± 0.00003
263	0.00029	0.00020	0.00025 ± 0.00005
273	0.00057	0.00047	0.00052 ± 0.00005
283	0.00150	0.00172	0.00161 ± 0.00011
293	0.00255	0.00325	0.00290 ± 0.00035

[a]$[PhCHO]_0$ = 0.49 M, $[Me_3SiCN]_0$ = 0.49 and [2] = 0.98 mM (data presented in Supporting Information File 1).

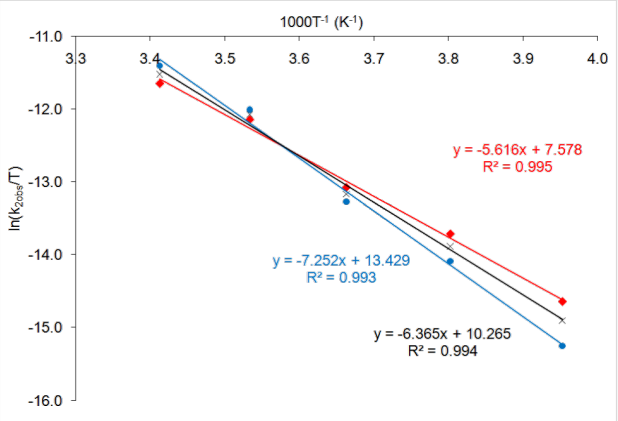

Figure 4: Eyring plot to determine the activation parameters for catalyst **2** in propylene carbonate. The red and blue data and best-fit lines correspond to the two individual data sets given in Table 4. The black data and best-fit line correspond to the average data.

($\Delta H^{\ddagger}$) can then be obtained from the slope of the best-fit line from the data plotted in Figure 4 and was found to be 67.8 (±0.2) kJ mol^{-1}. The entropy of activation ($\Delta S^{\ddagger}$) can be obtained from the y-axis intercept, once the contributions of the fundamental constants and x·ln[2] are subtracted. The latter was only possible as the reaction order with respect to catalyst **2** (x) had been determined to be 1.0 as discussed above. This gave a value for $\Delta S^{\ddagger}$ of −54 (±26) J mol^{-1} K^{-1}. The values for $\Delta H^{\ddagger}$ and $\Delta S^{\ddagger}$ are very different to those previously determined for the asymmetric addition of trimethylsilyl cyanide to benzaldehyde catalysed by complex **2** in dichloromethane [28] ($\Delta H^{\ddagger}$ = 20.4 kJ mol^{-1} and $\Delta S^{\ddagger}$ = −136 J mol^{-1} K^{-1}), though the corresponding Gibbs free energies of activation ($\Delta G^{\ddagger}$) at 273 K are similar at 53.1 and 57.5 kJ mol^{-1} for reactions carried out in propylene carbonate and dichloromethane, respectively.

$$k = \frac{k_B T}{h} \cdot \exp\left(-\frac{\Delta H^{\ddagger}}{RT}\right) \cdot \exp\left(\frac{\Delta S^{\ddagger}}{R}\right) \quad (2)$$

$$\frac{k_{2obs}}{T} = \frac{k_B}{h} \cdot [\mathbf{2}]^x \cdot \exp\left(-\frac{\Delta H^{\ddagger}}{RT}\right) \cdot \exp\left(\frac{\Delta S^{\ddagger}}{R}\right) \quad (3)$$

$$\ln\left(\frac{k_{2obs}}{T}\right) = \left(-\frac{\Delta H^{\ddagger}}{RT}\right) + \left(\frac{\Delta S^{\ddagger}}{R}\right) + \ln\left(\frac{k_B}{h}\right) + x \ln[\mathbf{2}] \quad (4)$$

(k_B = Boltzmann's constant, h = Planck's constant, R = gas constant)

Since differences in the Gibbs free energy of activation could not account for the reduction in rate constant between reactions in dichloromethane and propylene carbonate, the most likely explanation for the observed rate reduction is due to differences in the efficiency with which complex **2** is converted into species which are involved in the catalytic cycle. If propylene carbonate inhibits the conversion of complex **2** into catalytically competent species, then there will be a lower concentration of catalytically active species present in propylene carbonate than in dichloromethane, thus resulting in the observed lower rate of reaction.

Evidence to support this hypothesis came from ^{51}V NMR studies of complex **2** (Figure 5). The spectrum of complex **2** in $CDCl_3$ shows a resonance at −580 ppm (Figure 5a). It is known from X-ray crystallography that the isothiocyanate unit in complex **2** is directly bound to the vanadium ion through the nitrogen atom. Thus, the vanadium ion is six-coordinate, and is bound to three oxygen atoms and three nitrogen atoms. Addition of benzaldehyde (500 equiv) to this solution results in a change in the chemical shift of the vanadium ion to −575 ppm (Figure 5b), consistent with the formation of a complex **2**/benzaldehyde (see complex **4** in Figure 6), in which the vanadium ion is bound to four oxygen atoms and two nitrogen atoms. When the ^{51}V NMR spectrum of complex **2** is recorded in propylene carbonate, the ^{51}V NMR signal is observed at −571 ppm (Figure 5c), again indicative of formation of a species, such as **5**, in which the vanadium ion is bound to four oxygen atoms and two nitrogen atoms. The competitive formation of structure **5** would reduce the amount of complex **4** present in solution, thus reducing the concentration of catalyti-

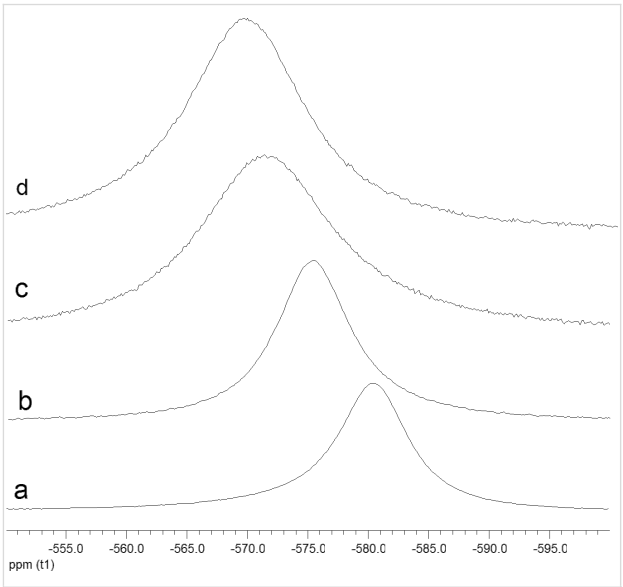

Figure 5: ^{51}V NMR spectra of complex **2** recorded at 50 °C. a) Spectrum in $CDCl_3$; b) spectrum in $CDCl_3$ with 500 equiv of PhCHO added; c) spectrum in propylene carbonate; d) spectrum in propylene carbonate with 500 equiv of PhCHO added. All spectra were recorded with a complex **2** concentration of 24 mM and for spectra b and d, the concentration of benzaldehyde was 4.8 M.

cally competent species and hence reducing the rate of asymmetric cyanohydrin synthesis in propylene carbonate compared to dichloromethane. Addition of benzaldehyde (500 equiv) to the propylene carbonate spectrum resulted in only a small additional change in the chemical shift to −569 ppm (Figure 5d).

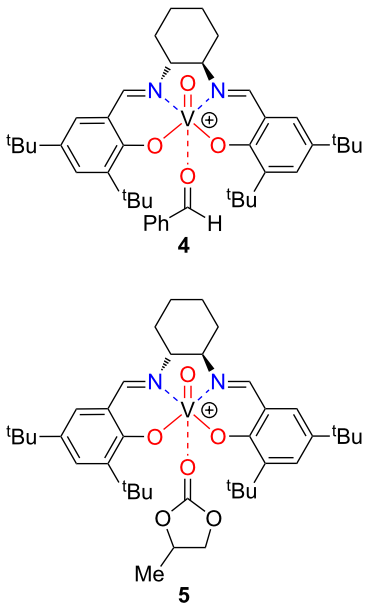

Figure 6: Structures consistent with the ^{51}V NMR spectra.

The half-widths of the signals recorded in propylene carbonate (1730 Hz and 1510 Hz for Figure 5c and Figure 5d, respectively) are much greater than the corresponding half-widths of the signals recorded in dichloromethane (930 Hz and 950 Hz for Figure 5a and Figure 5b, respectively). This is also indicative of exchange processes involving species **2**, **4** and **5** occurring in propylene carbonate.

The enthalpy of activation for the asymmetric addition of trimethylsilyl cyanide to benzaldehyde was found to be much higher in propylene carbonate than in dichloromethane, which is consistent with only one of the two reaction components (benzaldehyde or TMSCN) being activated by the mononuclear, catalytically active species present in propylene carbonate, whilst both reaction components are activated and pre-organized for reaction by the binuclear, catalytically active species present in dichloromethane [28]. The less negative value for the entropy of activation in propylene carbonate compared to that determined in dichloromethane is also consistent with a less tightly organized transition state, again consistent with only one of the reaction components interacting with the catalyst. To investigate this further, a Hammett analysis was undertaken using a range of substituted benzaldehydes.

Hammett analysis

It is well established that the asymmetric addition of TMSCN to aldehydes can be catalysed by both Lewis acids and Lewis bases [1]. A Lewis acid catalyst activates the aldehyde by formation of an aldehyde-Lewis acid complex (e.g., **4**) whilst a Lewis base catalyst activates the TMSCN through formation of a hypervalent silicon species [82] or the formation of cyanide anions. The most effective catalysts possess both Lewis acidity and Lewis basicity and so can simultaneously activate both the aldehyde and TMSCN [1].

We have recently shown [52] that a Hammett analysis correlating the rate of reaction of *meta*- and *para*-substituted benzaldehydes with their substituent constants can be used to investigate the relative importance of Lewis acid and Lewis base catalysis in a catalysed reaction. This methodology was developed using the asymmetric addition of TMSCN to aldehydes catalysed by complexes including **1, 2** and **6** (Figure 7) in dichloromethane. A reaction which is predominantly Lewis base catalysed would be expected to produce a Hammett plot with a reaction constant (ρ) close to zero, since the aldehyde is not activated in the catalytic step; so during the rate determining transition state, the negative charge will largely be located on silicon as shown in Figure 8a. This was found to be the case (ρ = +0.4) for asymmetric cyanohydrin synthesis catalysed by bimetallic aluminium(salen) complex **6** in the presence

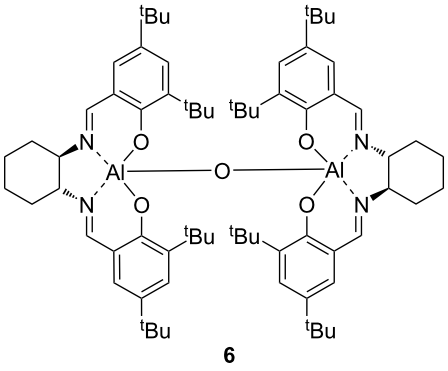

Figure 7: Bimetallic aluminium(salen) complex for asymmetric cyanohydrin synthesis.

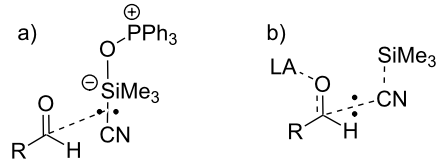

Figure 8: Rate determining transition states for asymmetric cyanohydrin synthesis: a) when Lewis base catalysis is dominant; and b) when Lewis acid catalysis is dominant.

of triphenylphosphine oxide [83,84], indicating that most of the catalysis in this case was due to activation of the TMSCN by the triphenylphosphine oxide rather than activation of the aldehyde by the metal(salen) complex. In contrast, reactions catalysed by complex **1** gave a Hammett plot with a reaction constant of +2.4, indicating that there was a significant increase in negative charge at the benzylic position of the aldehyde during the transition state, and hence that complex **1** functioned predominantly as a Lewis acid catalyst, activating the aldehyde towards attack by cyanide, and resulting in more charge transfer to the benzylic position of the aldehyde during the transition state for formation of the new carbon-carbon bond as shown in Figure 8b. Asymmetric cyanohydrin synthesis catalysed by complex **2** in dichloromethane was found to give a Hammett plot with an intermediate reaction constant of +1.6, indicating that both Lewis acid and Lewis base catalysis were operative in this case. Since the kinetic and NMR data suggested that changing the solvent to propylene carbonate was inhibiting the Lewis acidity of complex **2**, this should be reflected in a reduction in the reaction constant of a Hammett analysis. Therefore, the kinetics of the asymmetric addition of TMSCN to 12 *meta*- and *para*-substituted benzaldehydes were determined (Table 5) and used to construct a Hammett plot (Figure 9).

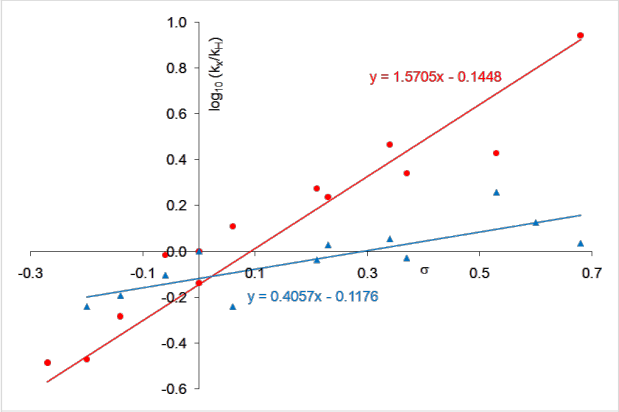

Figure 9: Hammett correlations with catalyst **2** at 0 °C. Data in red are obtained in dichloromethane [52], whilst data in blue are obtained in propylene carbonate.

All of the aldehydes included in Table 5 gave nonracemic cyanohydrin trimethylsilyl ethers, confirming that in each case the reaction was catalysed by complex **2**. In most cases the enantiomeric excess of the cyanohydrin trimethylsilyl ether was determined by chiral GC analysis after conversion to the corresponding cyanohydrin acetate [80] as discussed above. However, the cyanohydrin acetates derived from 3,4-dichlorobenzaldehyde and 3,4-dimethylbenzaldehyde were not separated by chiral GC, therefore the enantiomeric excess was determined by ^{1}H NMR analysis of the free cyanohydrin obtained by hydrolysis of the acetate [85], in the presence of (*R*)-mandelic acid and DMAP [86].

It is apparent from Figure 9 that the reaction constant for cyanohydrin synthesis catalysed by complex **2** does indeed decrease significantly (from +1.6 to +0.4) when the solvent is changed from dichloromethane to propylene carbonate. The results obtained in propylene carbonate are almost identical to those previously obtained with complex **6** and triphenylphosphine oxide as catalyst [52], and are entirely consistent with a

Table 5: Rate constants used to construct the Hammett plot.[a]

Entry	Aldehyde	$k_{(a)}$ ($M^{-1}s^{-1}$)	$k_{(b)}$ ($M^{-1}s^{-1}$)	$k_{(avg)}$ ($M^{-1}s^{-1}$)	ee[b]
1	PhCHO	0.00090	0.00090	0.00090	85
2	3,4-$Cl_2C_6H_3CHO$	0.00117	0.00124	0.00120 ± 0.00004	40[c]
3	4-ClC_6H_4CHO	0.00093	0.00099	0.00096 ± 0.00003	74
4	4-MeC_6H_4CHO	0.00058	0.00058	0.00058	77
5	4-FC_6H_4CHO	0.00056	0.00047	0.00052 ± 0.00005	84
6	3-FC_6H_4CHO	0.00104	0.00100	0.00102 ± 0.00002	72
7	3-MeC_6H_4CHO	0.00068	0.00070	0.00069 ± 0.00001	90
8	4-$F_3CC_6H_4CHO$	0.00153	0.00173	0.00163 ± 0.00010	44
9	4-BrC_6H_4CHO	0.00089	0.00076	0.00083 ± 0.00007	70
10	3,5-$F_2C_6H_3CHO$	0.00084	0.00110	0.00097 ± 0.00013	45
11	3,4-$Me_2C_6H_3CHO$	0.00055	0.00048	0.00052 ± 0.00004	85[c]
12	3-ClC_6H_4CHO	0.00078	0.00090	0.00084 ± 0.00006	57

[a]All reactions were carried out in duplicate (to give $k_{(a)}$ and $k_{(b)}$, respectively) in propylene carbonate at 0 °C with $[aldehyde]_0$ = 0.5 M, $[Me_3SiCN]_0$ = 0.55 M and [2] = 1.0 mM. [b]Enantiomeric excesses were determined by chiral GC analysis of the cyanohydrin acetates (data presented in Supporting Information File 1) unless stated otherwise. The predominant cyanohydrin derivative always had the (*S*)-configuration. [c]Determined by ^{1}H NMR spectroscopy in the presence of (*R*)-mandelic acid and DMAP.

significant reduction in the Lewis acidity of complex **2** in propylene carbonate compared to dichloromethane. This is manifested as an increase in the relative importance of Lewis base catalysis and hence a decrease in the reaction constant. It is important to note however, that complex **2** must still possess some Lewis acidity in propylene carbonate, otherwise cyanohydrin synthesis would not occur in the chiral environment around the vanadium ion and racemic cyanohydrin trimethylsilyl ethers would be obtained.

Conclusion

Asymmetric cyanohydrin synthesis catalysed by VO(salen)NCS complex **2** can be carried out in propylene carbonate, thus providing a green, alternative solvent to dichloromethane. Reactions in propylene carbonate are slower and less enantioselective than those carried out in dichloromethane; though by optimization of the reaction conditions, high enantioselectivities can still be obtained. A study of the reaction kinetics showed that complex **2** is active only as mononuclear species in propylene carbonate. Kinetic and NMR studies also showed that the propylene carbonate can coordinate to the vanadium ion of complex **2**, thus reducing its Lewis acidity and accounting for the decrease in reaction rate observed in propylene carbonate. The lower Lewis acidity of complex **2** in propylene carbonate was confirmed by a Hammett analysis using substituted benzaldehydes, which gave a reaction constant of only 0.4 in propylene carbonate compared to 1.6 in dichloromethane.

The lower enantioselectivities observed in propylene carbonate under identical reaction conditions to those used in dichloromethane can be explained in two ways. It is possible that in propylene carbonate, some addition of TMSCN to aldehydes occurs exclusively by Lewis base catalysis (using the thiocyanate anion as the Lewis base) and hence is independent of the chiral VO(salen) unit, thus forming some racemic cyanohydrin trimethylsilyl ether. Alternatively, all of the catalysis may occur within the coordination sphere of the VO(salen) unit by cooperative Lewis acid/Lewis base catalysis, but the aldehyde may be less tightly bound to the vanadium ion in the more polar propylene carbonate than in dichloromethane. This would result in the aldehyde being further from the chiral salen ligand during the key transition state and hence less effective transfer of chirality from the ligand to the newly formed stereocentre.

Experimental

General procedure for the synthesis and analysis of cyanohydrin trimethylsilyl ethers in propylene carbonate

The aldehyde (0.98 mmol) was added to a solution of catalyst **1** or **2** (0.98 μmol, 0.1 mol %) in propylene carbonate (1.75 mL) at the specified temperature. Me_3SiCN (1.12 mmol, 0.15 mL) was then added and the reaction mixture stirred for the specified time. The solution was then passed through a short silica plug eluting with CH_2Cl_2. The eluent was evaporated in vacuo to remove the CH_2Cl_2, and the residue analysed by ^1H NMR spectroscopy to determine the conversion. To determine the enantiomeric excess, Ac_2O (2.0 mmol, 0.15 mL) and $Sc(OTf)_3$ (5 mg, 0.01 mmol) were added to the stirred residue. After 20 min, the reaction mixture was passed through a short silica plug eluting with MeCN. The resulting solution was analysed by chiral GC using a Supelco Gamma DEX 120 fused silica capillary column (30 m x 0.25 mm) with hydrogen as a carrier gas. Details of the analysis of each cyanohydrin acetate are given in the Supporting Information File 1. When no separation could be achieved by chiral GC, the cyanohydrin acetate (0.985 mmol) was dissolved in ethanol (3 mL), *p*-$TsOH{\cdot}H_2O$ (187 mg, 0.985 mmol) was added, and the mixture stirred at room temperature for 2 days. The solvent was evaporated in vacuo and the residue purified by column chromatography eluting with a gradient from 1:15 EtOAc/hexane to 1:6 EtOAc/hexane to give the deprotected cyanohydrin. (*R*)-Mandelic acid (2.74 mg, 18 μmol), DMAP (1.73 mg, 18 μmol) and $CDCl_3$ (0.6 mL) were mixed in an NMR tube. The cyanohydrin (18 μmol) was then added and the solution analysed by ^1H NMR spectroscopy.

(*S*)-Mandelic acid

To a solution of mandelonitrile trimethylsilyl ether in propylene carbonate, obtained following the general procedure above, was added 12 N HCl (10 mL). The mixture was heated at reflux for 6 h, cooled to rt and basified with 10% aqueous NaOH solution. The aqueous solution was extracted with ether (3 x 10 mL), acidified with 12 N HCl and extracted again with ether (3 x 10 mL). The last three ethereal extracts were combined, dried (Na_2CO_3) and evaporated in vacuo to give a yellow solid which was recrystallised at 4 °C from ether/hexane and the resulting solid washed with hexane to give mandelic acid (91 mg, 60%) as white crystals. δ_H (300 MHz, $CDCl_3$) 5.26 (1H, s, CHO), 7.3–7.5 (5H, m, ArH).

(*S*)-Methyl mandelate

Mandelic acid (50 mg, 0.33 mmol) was suspended in toluene (10 mL), then methanol (2 mL) was added to give a homogenous solution. One drop of concentrated H_2SO_4 was added and the mixture heated at reflux for 4 h. The reaction mixture was then cooled to room temperature, the solvents were evaporated in vacuo and the residue was dissolved in water (10 mL). The aqueous solution was extracted with ether (3 x 5 mL). The ethereal extract was dried over anhydrous Na_2SO_4 and concentrated in vacuo to give methyl mandelate (28 mg, 50%) as a pale yellow solid. δ_H (300 MHz, $CDCl_3$) 3.77 (3H, s, CH_3), 5.20 (1H, s, CHO), 7.3–7.5 (5H, m, ArH).

General procedure for kinetics experiments in propylene carbonate

A solution of catalyst **2** (0.2–0.8 mol %) in freshly distilled propylene carbonate (1.75 mL) was added to a round-bottomed flask fitted with a magnetic stirrer bar and a SubaSeal stopper. The reaction temperature was adjusted by a water bath (water/ice for 0 °C) or cryostat for reactions below 0 °C; temperatures other than 0 °C were kept within a ±0.5 °C range. A 0.5 μL aliquot was taken and diluted with dry CH_2Cl_2 (3.5 mL). This solution was used for UV-baseline calibration at 240–260 nm. Freshly distilled aldehyde (0.96 mmol) was then added, and a $t = 0$ aliquot was taken and diluted as described for the baseline calibration sample. Me_3SiCN (0.15 mL, 1.125 mmol) was added, and aliquots of the reaction were taken and diluted at appropriate intervals for a period of 2 h. After completion of the kinetics analysis, the reaction mixture was passed through a short silica plug eluting with CH_2Cl_2. The solvent was evaporated and the residue converted into mandelonitrile acetate as described above to allow the enantiomeric excess of the cyanohydrin to be determined.

Supporting Information

Chiral GC traces for all chiral cyanohydrin acetates and chiral HPLC data for methyl mandelate. NMR spectra of cyanohydrins in the presence of mandelic acid. Additionally, all of the kinetic data used to determine the catalyst order, the activation parameters and construct the Hammett plot are given.

Supporting Information File 1

Analytical data for all chiral compounds.
[http://www.beilstein-journals.org/bjoc/content/supplementary/1860-5397-6-119-S1.pdf]

Acknowledgements

The authors thank the EPSRC physical organic chemistry initiative for financial support and a studentship (to MOP).

References

1. North, M.; Usanov, D. L.; Young, C. *Chem. Rev.* **2008,** *108,* 5146–5226. doi:10.1021/cr800255k
2. Brunel, J.-M.; Holmes, I. P. *Angew. Chem., Int. Ed.* **2004,** *43,* 2752–2778. doi:10.1002/anie.200300604
3. Sharma, M.; Sharma, N. N.; Bhalla, T. C. *Enzyme Microb. Technol.* **2005,** *37,* 279–294. doi:10.1016/j.enzmictec.2005.04.013
4. Purkarthofer, T.; Skranc, W.; Schuster, C.; Griengl, H. *Appl. Microbiol. Biotechnol.* **2007,** *76,* 309–320. doi:10.1007/s00253-007-1025-6
5. Davie, E. A. C.; Mennen, S. M.; Xu, Y.; Miller, S. J. *Chem. Rev.* **2007,** *107,* 5759–5812. doi:10.1021/cr068377w
6. Denmark, S. E.; Beutner, G. L. *Angew. Chem., Int. Ed.* **2008,** *47,* 1560–1638. doi:10.1002/anie.200604943
7. Schneider, C. *Angew. Chem., Int. Ed.* **2009,** *48,* 2082–2084. doi:10.1002/anie.200805542
8. Shibasaki, M.; Kanai, M.; Matsunaga, S.; Kumagai, N. *Acc. Chem. Res.* **2009,** *42,* 1117–1127. doi:10.1021/ar9000108
9. Nájera, C.; Sansano, J. M.; Saá, J. M. *Eur. J. Org. Chem.* **2009,** 2385–2400. doi:10.1002/ejoc.200801069
10. Breuer, M.; Ditrich, K.; Habicher, T.; Hauer, B.; Keßeler, M.; Stürmer, R.; Zelinski, T. *Angew. Chem., Int. Ed.* **2004,** *43,* 788–824. doi:10.1002/anie.200300599
11. Belokon, Y. N.; Caveda-Cepas, S.; Green, B.; Ikonnikov, N. S.; Khrustalev, V. N.; Larichev, V. S.; Moscalenko, M. A.; North, M.; Orizu, C.; Tararov, V. I.; Tasinazzo, M.; Timofeeva, G. I.; Yashkina, L. V. *J. Am. Chem. Soc.* **1999,** *121,* 3968–3973. doi:10.1021/ja984197v
12. Belokon, Y. N.; Gutnov, A. V.; Moskalenko, M. A.; Yashkina, L. V.; Lesovoy, D. E.; Ikonnikov, N. S.; Larichev, V. S.; North, M. *Chem. Commun.* **2002,** 244–245. doi:10.1039/b110335k
13. Belokon, Y. N.; Carta, P.; Gutnov, A. V.; Maleev, V.; Moskalenko, M. A.; Yashkina, L. V.; Ikonnikov, N. S.; Voskoboev, N. V.; Khrustalev, V. N.; North, M. *Helv. Chim. Acta* **2002,** *85,* 3301–3312. doi:10.1002/1522-2675(200210)85:10<3301::AID-HLCA3301>3.0.CO;2-2
14. Belokon, Y. N.; Carta, P.; North, M. *Lett. Org. Chem.* **2004,** *1,* 81–83. doi:10.2174/1570178043488617
15. Belokon, Y. N.; Blacker, A. J.; Carta, P.; Clutterbuck, L. A.; North, M. *Tetrahedron* **2004,** *60,* 10433–10447. doi:10.1016/j.tet.2004.07.098
16. Belokon, Y. N.; Blacker, A. J.; Clutterbuck, L. A.; North, M. *Org. Lett.* **2003,** *5,* 4505–4507. doi:10.1021/ol035828f
17. Belokon, Y. N.; Ishibashi, E.; Nomura, H.; North, M. *Chem. Commun.* **2006,** 1775–1777. doi:10.1039/b602156e
18. Lundgren, S.; Wingstrand, E.; Penhoat, M.; Moberg, C. *J. Am. Chem. Soc.* **2005,** *127,* 11592–11593. doi:10.1021/ja052804q
19. Wingstrand, E.; Lundgren, S.; Penhoat, M.; Moberg, C. *Pure Appl. Chem.* **2006,** *78,* 409–414. doi:10.1351/pac200678020409
20. Belokon, Y. N.; Clegg, W.; Harrington, R. W.; Ishibashi, E.; Nomura, H.; North, M. *Tetrahedron* **2007,** *63,* 9724–9740. doi:10.1016/j.tet.2007.07.016
21. Lundgren, S.; Wingstrand, E.; Moberg, C. *Adv. Synth. Catal.* **2007,** *349,* 364–372. doi:10.1002/adsc.200600365
22. Belokon, Y. N.; Green, B.; Ikonnikov, N. S.; North, M.; Tararov, V. I. *Tetrahedron Lett.* **1999,** *40,* 8147–8150. doi:10.1016/S0040-4039(99)01677-9
23. Belokon, Y. N.; Green, B.; Ikonnikov, N. S.; North, M.; Parsons, T.; Tararov, V. I. *Tetrahedron* **2001,** *57,* 771–779. doi:10.1016/S0040-4020(00)01053-X
24. Zhang, Z.; Wang, Z.; Zhang, R.; Ding, K. *Angew. Chem., Int. Ed.* **2010,** *49,* 6746–6750. doi:10.1002/anie.201002127
25. North, M. *Angew. Chem., Int. Ed.* **2010,** *49,* 8079–8081. doi:10.1002/anie.201003014
26. Belokon, Y. N.; North, M.; Parsons, T. *Org. Lett.* **2000,** *2,* 1617–1619. doi:10.1021/ol005893e
27. Belokon, Y. N.; Maleev, V. I.; North, M.; Usanov, D. L. *Chem. Commun.* **2006,** 4614–4616. doi:10.1039/b609591g
28. Belokon, Y. N.; Clegg, W.; Harrington, R. W.; Maleev, V. I.; North, M.; Omedes Pujol, M.; Usanov, D. L.; Young, C. *Chem.–Eur. J.* **2009,** *15,* 2148–2165. doi:10.1002/chem.200801679

29. Blacker, A. J.; North, M.; Belokon, Y. N. *Chim. Oggi* **2004,** *22* (8, Suppl. Chiral Catalysis), 30–32.
30. Blacker, J.; North, M. *Chem. Ind.* **2005,** *(issue 12: 20 June),* 22–25.
31. Baleizão, C.; Gigante, B.; Garcia, H.; Corma, A. *Green Chem.* **2002,** *4,* 272–274. doi:10.1039/b201497c
32. Kim, G.-J.; Shin, J. H. *Catal. Lett.* **1999,** *63,* 83–90. doi:10.1023/A:1019040215323
33. Baleizão, C.; Gigante, B.; Garcia, H.; Corma, A. *J. Catal.* **2003,** *215,* 199–207. doi:10.1016/S0021-9517(03)00007-1
34. Baleizão, C.; Gigante, B.; Das, D.; Alvaro, M.; Garcia, H.; Corma, A. *Chem. Commun.* **2003,** 1860–1861. doi:10.1039/b304814d
35. Baleizão, C.; Gigante, B.; Garcia, H.; Corma, A. *Tetrahedron Lett.* **2003,** *44,* 6813–6816. doi:10.1016/S0040-4039(03)01746-5
36. Baleizão, C.; Gigante, B.; Garcia, H.; Corma, A. *Tetrahedron* **2004,** *60,* 10461–10468. doi:10.1016/j.tet.2004.08.077
37. Huang, W.; Song, Y.; Wang, J.; Cao, G.; Zheng, Z. *Tetrahedron* **2004,** *60,* 10469–10477. doi:10.1016/j.tet.2004.08.078
38. Baleizão, C.; Gigante, B.; Garcia, H.; Corma, A. *J. Catal.* **2004,** *221,* 77–84. doi:10.1016/j.jcat.2003.08.016
39. Baleizão, C.; Gigante, B.; Das, D.; Álvaro, M.; Garcia, H.; Corma, A. *J. Catal.* **2004,** *223,* 106–113. doi:10.1016/j.jcat.2004.01.016
40. Kim, J. H.; Kim, G. J. *Catal. Lett.* **2004,** *92,* 123–130. doi:10.1023/B:CATL.0000014334.73726.d3
41. Huang, W.; Song, Y.; Bai, C.; Cao, G.; Zheng, Z. *Tetrahedron Lett.* **2004,** *45,* 4763–4767. doi:10.1016/j.tetlet.2004.04.086
42. Khan, N. H.; Agrawal, S.; Kureshy, R. I.; Abdi, S. H. R.; Mayani, V. J.; Jasra, R. V. *Eur. J. Org. Chem.* **2006,** 3175–3180. doi:10.1002/ejoc.200600208
43. Khan, N. H.; Agrawal, S.; Kureshy, R. I.; Abdi, S. H. R.; Mayani, V. J.; Jasra, R. V. *Tetrahedron: Asymmetry* **2006,** *17,* 2659–2666. doi:10.1016/j.tetasy.2006.09.024
44. Lu, S.-F.; Herbert, B.; Haufe, G.; Laue, K. W.; Padgett, W. L.; Oshunlei, O.; Daly, J. W.; Kirk, K. L. *J. Med. Chem.* **2000,** *43,* 1611–1619. doi:10.1021/jm990599h
45. Dong, L.-C.; Crowe, M.; West, J.; Ammann, J. R. *Tetrahedron Lett.* **2004,** *45,* 2731–2733. doi:10.1016/j.tetlet.2004.02.040
46. Lloyd-Jones, G. C.; Wall, P. D.; Slaughter, J. L.; Parker, A. J.; Laffan, D. P. *Tetrahedron* **2006,** *62,* 11402–11412. doi:10.1016/j.tet.2006.05.003
47. Belokon, Y. N.; Green, B.; Ikonnikov, N. S.; Larichev, V. S.; Lokshin, B. V.; Moscalenko, M. A.; North, M.; Orizu, C.; Peregudov, A. S.; Timofeeva, G. I. *Eur. J. Org. Chem.* **2000,** 2655–2661. doi:10.1002/1099-0690(200007)2000:14<2655::AID-EJOC2655>3.0.CO;2-O
48. Belokon, Y. N.; North, M.; Maleev, V. I.; Voskoboev, N. V.; Moskalenko, M. A.; Peregudov, A. S.; Dmitriev, A. V.; Ikonnikov, N. S.; Kagan, H. B. *Angew. Chem., Int. Ed.* **2004,** *43,* 4085–4089. doi:10.1002/anie.200454031
49. Belokon, Y. N.; Clegg, W.; Harrington, R. W.; Young, C.; North, M. *Tetrahedron* **2007,** *63,* 5287–5299. doi:10.1016/j.tet.2007.03.140
50. Chechik, V.; Conte, M.; Dransfield, T.; North, M.; Omedes-Pujol, M. *Chem. Commun.* **2010,** *46,* 3372–3374. doi:10.1039/c001703e
51. Belokon', Y. N.; Clegg, W.; Harrington, R. W.; North, M.; Young, C. *Inorg. Chem.* **2008,** *47,* 3801–3814. doi:10.1021/ic702451a
52. North, M.; Omedes-Pujol, M.; Williamson, C. *Chem.–Eur. J.* **2010,** *16,* 11367–11375. doi:10.1002/chem.201001078
53. North, M.; Omedes-Pujol, M. *Tetrahedron Lett.* **2009,** *50,* 4452–4454. doi:10.1016/j.tetlet.2009.05.052
54. Reetz, M. T.; Lohmer, G. *Chem. Commun.* **1996,** 1921–1922. doi:10.1039/cc9960001921
55. Behr, A.; Naendrup, F.; Obst, D. *Adv. Synth. Catal.* **2002,** *344,* 1142–1145. doi:10.1002/1615-4169(200212)344:10<1142::AID-ADSC1142>3.0.CO;2-P
56. Behr, A.; Naendrup, F.; Obst, D. *Eur. J. Lipid Sci. Technol.* **2002,** *104,* 161–166. doi:10.1002/1438-9312(200203)104:3<161::AID-EJLT161>3.0.CO;2-N
57. Bayardon, J.; Holz, J.; Schäffner, B.; Andrushko, V.; Verevkin, S.; Preetz, A.; Börner, A. *Angew. Chem., Int. Ed.* **2007,** *46,* 5971–5974. doi:10.1002/anie.200700990
58. Preetz, A.; Drexler, H.-J.; Fischer, C.; Dai, Z.; Börner, A.; Baumann, W.; Spannenberg, A.; Thede, R.; Heller, D. *Chem.–Eur. J.* **2008,** *14,* 1445–1451. doi:10.1002/chem.200701150
59. Schäffner, B.; Holz, J.; Verevkin, S. P.; Börner, A. *Tetrahedron Lett.* **2008,** *49,* 768–771. doi:10.1016/j.tetlet.2007.11.199
60. Schäffner, B.; Andrushko, V.; Holz, J.; Verevkin, S. P.; Börner, A. *ChemSusChem* **2008,** *1,* 934–940. doi:10.1002/cssc.200800157
61. Schnäffner, B.; Holz, J.; Verevkin, S. P.; Börner, A. *ChemSusChem* **2008,** *1,* 249–253. doi:10.1002/cssc.200700142
62. North, M.; Pizzato, F.; Villuendas, P. *ChemSusChem* **2009,** *2,* 862–865. doi:10.1002/cssc.200900144
63. Clegg, W.; Harrington, R. W.; North, M.; Pizzato, F.; Villuendas, P. *Tetrahedron: Asymmetry* **2010,** *21,* 1262–1271. doi:10.1016/j.tetasy.2010.03.051
64. North, M.; Villuendas, P. *Org. Lett.* **2010,** *12,* 2378–2381. doi:10.1021/ol1007313
65. North, M.; Pasquale, R.; Young, C. *Green Chem.* **2010,** *12,* 1514–1539. doi:10.1039/c0gc00065e
66. Tullo, A. H.; Short, P. L. *Chem. Eng. News* **2006,** *84* (41), 22–23.
67. Meiers, R.; Dingerdissen, U.; Hölderich, W. F. *J. Catal.* **1998,** *176,* 376–386. doi:10.1006/jcat.1998.2036
68. Jenzer, G.; Mallat, T.; Maciejewski, M.; Eigenmann, F.; Baiker, A. *Appl. Catal., A* **2001,** *208,* 125–133. doi:10.1016/S0926-860X(00)00689-X
69. Li, G.; Wang, X.; Yan, H.; Chen, Y.; Su, Q. *Appl. Catal., A* **2001,** *218,* 31–38. doi:10.1016/S0926-860X(01)00607-X
70. Taylor, B.; Lauterbach, J.; Blau, G. E.; Delgass, W. N. *J. Catal.* **2006,** *242,* 142–152. doi:10.1016/j.jcat.2006.06.007
71. Chen, Q.; Beckman, E. J. *Green Chem.* **2007,** *9,* 802–808. doi:10.1039/b618934b
72. Chen, Q.; Beckman, E. J. *Green Chem.* **2008,** *10,* 934–938. doi:10.1039/b803847c
73. Sheldon, R. A. *Chem. Commun.* **2008,** 3352–3365. doi:10.1039/b803584a
74. Melendez, J.; North, M.; Pasquale, R. *Eur. J. Inorg. Chem.* **2007,** 3323–3326. doi:10.1002/ejic.200700521
75. North, M.; Pasquale, R. *Angew. Chem., Int. Ed.* **2009,** *48,* 2946–2948. doi:10.1002/anie.200805451
76. Meléndez, J.; North, M.; Villuendas, P. *Chem. Commun.* **2009,** 2577–2579. doi:10.1039/b900180h
77. Clegg, W.; Harrington, R. W.; North, M.; Pasquale, R. *Chem.–Eur. J.* **2010,** *16,* 6828–6843. doi:10.1002/chem.201000030
78. North, M.; Villuendas, P.; Young, C. *Chem.–Eur. J.* **2009,** *15,* 11454–11457. doi:10.1002/chem.200902436
79. Metcalfe, I. S.; North, M.; Pasquale, R.; Thursfield, A. *Energy Environ. Sci.* **2010,** *3,* 212–215. doi:10.1039/B918417A
80. Norsikan, S.; Holmes, I.; Lagasse, F.; Kagan, H. B. *Tetrahedron Lett.* **2002,** *43,* 5715–5717. doi:10.1016/S0040-4039(02)01200-5

81. Silva, L. B.; Freitas, L. C. G. *THEOCHEM* **2007,** *806,* 23–34. doi:10.1016/j.theochem.2006.10.014
82. Chuit, C.; Corriu, R. J. P.; Reye, C.; Young, J. C. *Chem. Rev.* **1993,** *93,* 1371–1448. doi:10.1021/cr00020a003
83. North, M.; Williamson, C. *Tetrahedron Lett.* **2009,** *50,* 3249–3252. doi:10.1016/j.tetlet.2009.02.028
84. North, M.; Villuendas, P.; Williamson, C. *Tetrahedron* **2010,** *66,* 1915–1924. doi:10.1016/j.tet.2010.01.004
85. Sakai, T.; Wang, K.; Ema, T. *Tetrahedron* **2008,** *64,* 2178–2183. doi:10.1016/j.tet.2007.12.030
86. Moon, L. S.; Jolly, R. S.; Kasetti, Y.; Bharatam, P. V. *Chem. Commun.* **2009,** 1067–1069. doi:10.1039/b817800c

License and Terms

Beilstein Journal of Organic Chemistry

Intramolecular hydroxycarbene C–H-insertion: The curious case of (*o*-methoxyphenyl)hydroxycarbene

Dennis Gerbig, David Ley, Hans Peter Reisenauer and Peter R. Schreiner*

Full Research Paper

Open Access

Address:
Institut für Organische Chemie, Justus-Liebig University Giessen, Heinrich-Buff-Ring 58, 35392 Giessen, Germany

Email:
Dennis Gerbig - Dennis.Gerbig@org.chemie.uni-giessen.de;
David Ley - David.Ley@org.chemie.uni-giessen.de;
Hans Peter Reisenauer - Hans.P.Reisenauer@org.chemie.uni-giessen.de;
Peter R. Schreiner* - prs@org.chemie.uni-giessen.de

* Corresponding author

Keywords:
benzofuran; C–H-insertion; hydroxycarbene; singlet carbene; tunneling

Beilstein J. Org. Chem. **2010,** *6,* 1061–1069.
doi:10.3762/bjoc.6.121

Received: 07 August 2010
Accepted: 21 October 2010
Published: 11 November 2010

Guest Editor: J. Murphy

Abstract

The first C–H insertion of a hydroxycarbene species in the gas phase has been observed experimentally by means of high vacuum flash pyrolysis (HVFP) and subsequent matrix isolation: (*o*-Methoxyphenyl)glyoxylic acid gives non-isolable (*o*-methoxyphenyl)hydroxycarbene upon pyrolysis at 600 °C, which rapidly inserts into the methyl C–H bond. The insertion product, 2,3-dihydrobenzofuran-3-ol, was trapped in an excess of Ar at 11 K and characterized by infrared spectroscopy. The insertion process kinetically outruns the alternative [1,2]H-tunneling reaction to *o*-anisaldehyde, a type of reaction observed for other hydroxycarbenes. Traces of the dehydration product, benzo[*b*]furan, were also detected. The potential energy hypersurface including the insertion and hydrogen migration processes was computed at the all-electron coupled-cluster level of theory encompassing single and double substitutions and perturbatively included triple excitations [AE-CCSD(T)] in conjunction with a correlation-consistent double-ζ basis set (cc-pVDZ) by utilizing density functional theory (DFT) optimized geometries (M06-2X/cc-pVDZ) with zero-point vibrational energy (ZPVE) corrections. Exchange of the methoxy for a trifluoromethoxy group successfully prevents insertion and (*o*-trifluoromethoxy)benzaldehyde is produced instead; however, the carbene cannot be observed under these conditions. Thermal decomposition of (*o*-methoxyphenyl)glyoxylic acid in refluxing xylenes does not give the insertion product but yields *o*-anisaldehyde. This unanticipated outcome can be rationalized by protonation of the hydroxycarbene intermediate leading to the tautomeric formyl group. Thermochemical computations at M06-2X/cc-pVDZ in conjunction with a self-consistent solvent reaction field model support this suggested reaction pathway.

Introduction

Hydroxycarbenes have been the subject of many theoretical and experimental studies since the early years of last century, however, these proved to be elusive for a long time [1]. Whilst a large variety of hydroxycarbene ligands have been prepared as fairly stable Fischer-type carbene–metal complexes with group VI, VII, VIII, and X elements [2-12] it was only very recently that free hydroxycarbenes were generated by high vacuum flash pyrolysis (HVFP) followed by immediate matrix isolation and thoroughly characterized by means of IR- and UV-spectroscopy [13-15]. Very surprisingly, several hydroxycarbenes exhibit remarkable [1,2]H-tunneling under cryogenic conditions in solid noble gas matrices, even at temperatures as low as 11 K: Hydroxymethylene (**1**) [13] and phenylhydroxycarbene (**3**) [14] yield formaldehyde (**2**) and benzaldehyde (**4**), respectively, as a result of facile [1,2]hydrogen tunneling from the hydroxy group to the carbene center. Dihydroxycarbene (**a**) [15] and methoxyhydroxycarbene (**c**) [15], however, do not undergo [1,2]H-tunneling under the same conditions: Their respective products, formic acid (**b**) and methyl formate (**d**) were not detected in matrix isolation experiments (Scheme 1).

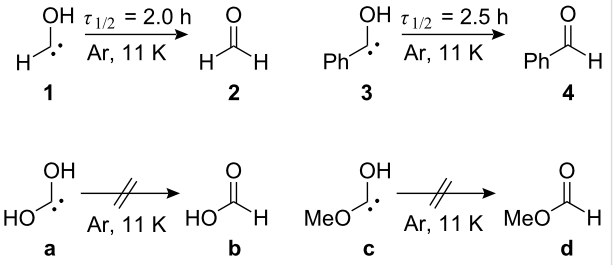

Scheme 1: Unimolecular reactivity of hydroxycarbenes under cryogenic conditions: [1,2]H-Tunneling of **1** and **3** ($\tau_{1/2}$: half-life).

Ring insertions characteristic for other singlet phenylcarbenes, i. e., phenylmethylcarbene [16] and phenylchlorocarbene [17], were not experimentally observed for **3**, and we report herein the first C–H-bond insertion reaction of a hydroxycarbene that is akin to other heterocarbenes [18-20] (Scheme 2). (*o*-Methoxyphenyl)hydroxycarbene (**5**) serves as the model compound for studying the intramolecular carbene C–H-bond insertion both under matrix isolation and solution conditions (Scheme 3). The generation of such carbenes in solution in high-boiling solvents would also provide convenient preparative access to dihydrobenzofuranols from readily accessible α-keto acids as the starting materials. Our results were rationalized by quantum chemical computations.

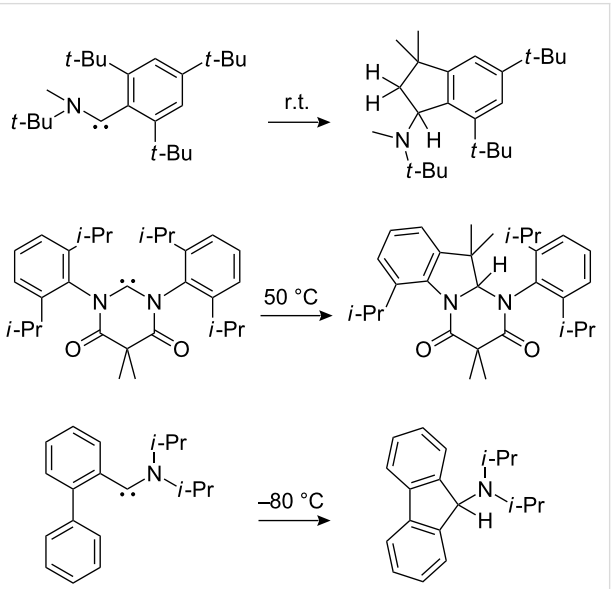

Scheme 2: A selection of heterocarbenes that undergo intramolecular C–H insertions.

Results and Discussion

Matrix isolation studies on (*o*-methoxyphenyl)hydroxycarbene

In the course of our ongoing investigations regarding the nature of the fascinating [1,2]H-tunneling mechanism in phenylhydroxycarbenes (with parent **3**, Scheme 1), we sought to study the behavior of derivatives of **3** in Ar matrices at temperatures as low as 11 K. We attempted to generate novel *o*-methoxy-substituted carbene **5** by extrusion of carbon dioxide from (*o*-methoxyphenyl)glyoxylic acid (**6**) by HVFP and subsequent condensation and isolation of the pyrolysis products in an excess of Ar (Scheme 3). However, neither **5** nor its tunneling

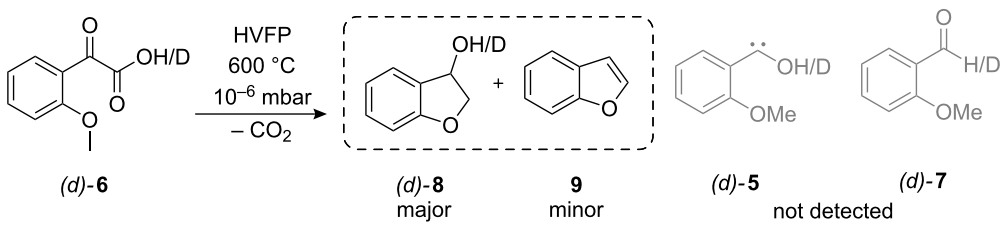

Scheme 3: Attempted generation of **5** and *d*-**5** as well as their corresponding insertion products.

product, *o*-anisaldehyde (**7**), could be detected: Comparison with an authentic spectrum of matrix-isolated **7** showed that this compound was not present among the pyrolysis products. Even after more than 12 h in the dark at 11 K, the IR spectrum was unchanged, indicating that there is no compound among the pyrolysis products that is susceptible to a tunneling decay mechanism. The TD-DFT (B3LYP/cc-pVDZ) absorption maximum of **5** lies at 591 nm [21,22]. To rule out the existence of a persistent, non-tunneling carbene, irradiation experiments were conducted: Subsequent irradiation with a high-pressure Hg-lamp at λ = 577 nm, 546 nm, and 313 nm did not lead either to the appearance of new or the disappearance of existing signals, thereby verifying the complete absence of **5**.

Analysis of the IR spectrum showed that **8** was the main product instead. To confirm the C–H-insertion into the neighboring methyl group, to yield 2,3-dihydrobenzofuran-3-ol (**8**), a sample of **8** was prepared by the reduction of commercially available 3-coumaranone and subjected to matrix isolation studies. All intense signals in the original pyrolysis spectrum of **6** could be shown to originate from **8**. As a side product, traces of the dehydration product of **8**, benzo[*b*]furan (**9**), were found and identified by comparison with an authentic spectrum of matrix-isolated **9** (Scheme 3 and Scheme 4).

The [1,2]H-tunneling reactions in hydroxycarbenes can be suppressed by an exchange of hydrogen for deuterium. Hence, carbene signals can readily be identified by prolonged irradiation at or near the maximum absorption wavelength of the carbene. Thus, the pyrolysis experiment was repeated with the mono-deuterated acid *d*-**6** (*o*-MeOC$_6$H$_4$COCOOD) to yield *d*-**8** (OD). Again minor amounts of **9** (without any deuterium incorporation) were formed. In accordance with prior results, neither *d*-**5** nor *d*-**7** could be detected after irradiation. A proposed mechanism for the formation of the insertion product **8** is presented in Scheme 4. Matrix isolation spectra of both pyrolyses (**6** and *d*-**6**, respectively) are presented in Figure 1 and Figure 2, along with an assignment of all signals. A collection of all the matrix spectra is contained in Supporting Information File 1.

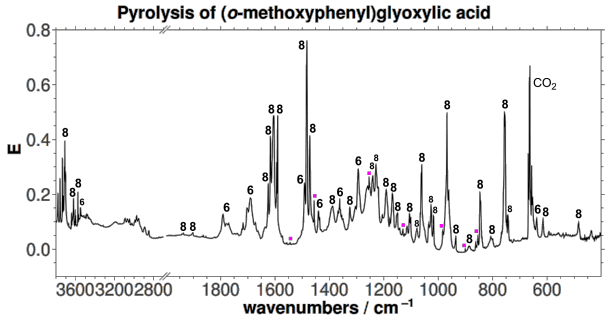

Figure 1: Unmodified matrix IR spectrum (Ar, 11 K) of the pyrolysis (600 °C) of **5**. Traces of **9** are indicated by magenta dots.

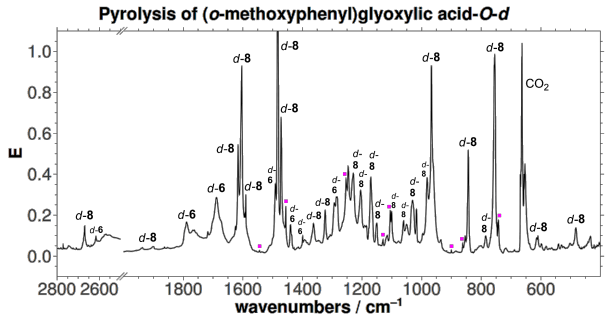

Figure 2: Unmodified matrix IR spectrum (Ar, 11 K) of the pyrolysis (600 °C) of *d*-**5**. Traces of **9** are indicated by magenta dots.

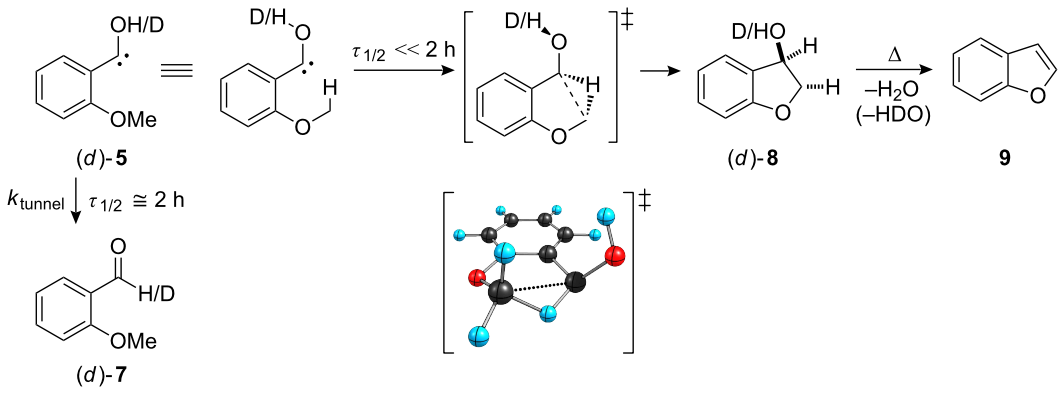

Scheme 4: Proposed mechanism for the generation of **8** and **9**. The [1,2]H-tunneling process apparently cannot compete with C–H-insertion ($\tau_{1/2}$: half-life).

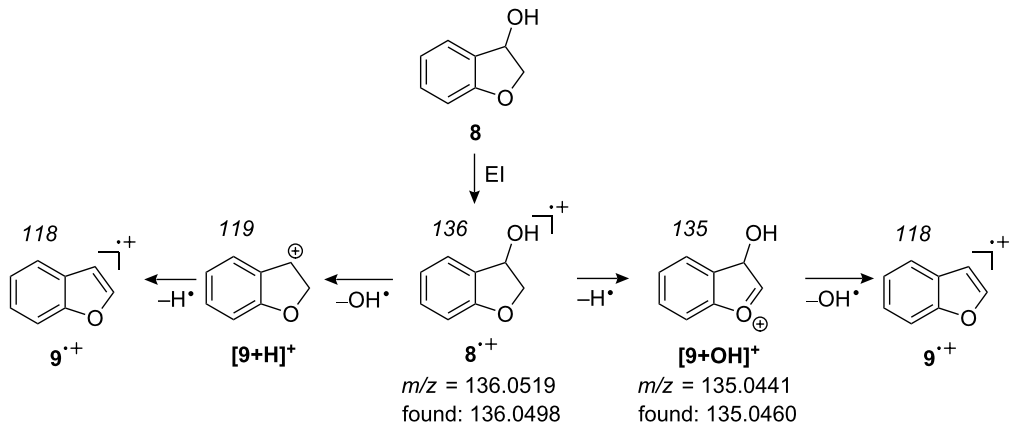

Scheme 5: Decay of the 2,3-dihydrobenzofuran-3-ol molecular radical cation ($8^{+\bullet}$).

After warming of the matrix to room temperature, a sample of the pyrolysis products of **6** was collected from the matrix window. The molecular ions of **8** and **9** were found in the corresponding electron-impact mass spectrum, most probably generated through the decay mechanism proposed by Florêncio et al. [23] (Scheme 5).

Matrix isolation studies on [(*o*-trifluoromethoxy)phenyl]hydroxycarbene

Exchanging the methoxy group for a trifluoromethoxy moiety should prohibit the insertion reaction due to the much stronger carbon–fluorine bond compared to the carbon–hydrogen bond. HVFP of [(*o*-trifluoromethoxy)phenyl]glyoxylic acid (**10**) at 600 °C (500 °C, 800 °C) and subsequent matrix isolation gave (*o*-trifluoromethoxy)benzaldehyde (**11**); as expected, no insertion product (**13**) was detected (Scheme 6).

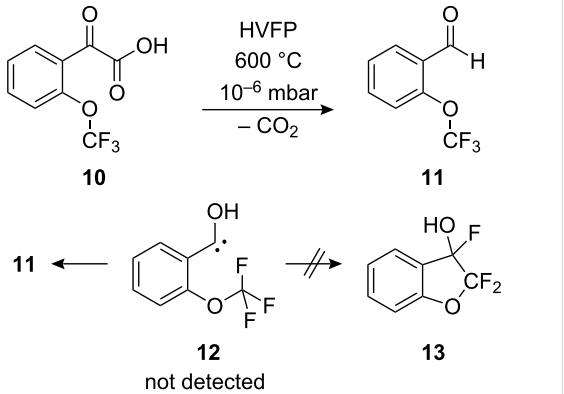

Scheme 6: Attempted generation of **12** and the actual pyrolysis product **11**.

Contrary to our findings on hydroxycarbenes, [(*o*-trifluoromethoxy)phenyl]hydroxycarbene (**12**) was not detected. Instead, only the substituted anisaldehyde **11** could be identified. On repeating the experiment with deuterated acid (OD) *d*-**10**, no deutero-carbene *d*-**12** was likewise produced, as verified by subsequent irradiation (577 nm, 313 nm). The computed [1,2]H-tunneling half-lives of **5** and **12**, based on a) an Eckart barrier approach, and b) the Wentzel–Kramers–Brillouin (WKB) approximation (see Computational methods for details), are summarized in Table 1, together with the computed half-life of **3** for comparison.

Table 1: Computed half-lives (*unscaled*) for the [1,2]H-tunneling reaction in carbenes **3**, **5**, and **12** at 11 K. The measured half-life of **3** is 2.5 h at 11 K. The thermal barrier for the [1,2]H-shift was computed at AE-CCSD(T)/cc-pVDZ // M06-2X/cc-pVDZ; (cf. Computational methods).

	$\Delta H^{\ddagger}$ for [1,2]H-shift [kcal mol^{-1}]	Eckart [h]	WKB [h]
PhCOH (**3**)	28.9	3.7	4.8
o-$MeOC_6H_4COH$ (**5**)	27.1	0.6	0.5
o-$F_3COC_6H_4COH$ (**12**)	29.3	1.2	1.1

Based on the computed tunneling half-lives, **12** should be observable in matrix-isolation experiments if it survives the formation conditions in the gas phase. The same holds true for *d*-**12**.

Pyrolysis of (*o*-methoxyphenyl)glyoxylic acid (6) in solution

Surprisingly, the reactivity of **5** in solution is quite different from that in our matrix isolation experiments as *o*-anisaldehyde **7** forms instead of **8** upon refluxing **6** in xylenes (bp 139–140 °C) for 12 h in almost quantitative yield (Scheme 7). This unanticipated outcome is in stark contrast to the reactions of other heterocarbenes that have been shown to insert into comparable methyl C–H bonds in solution with ease [24]. When

the reaction was carried out in an even higher boiling solvent, i.e., nitrobenzene (bp 211 °C), a complicated mixture of decomposition products resulted.

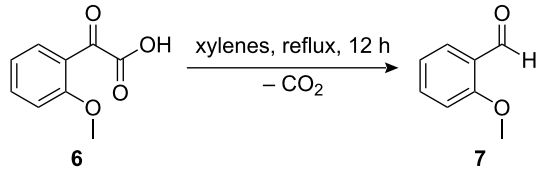

Scheme 7: Unanticipated reaction of **6** upon heating in xylenes.

In order to probe for a chemical connection between **7** and **8**, insertion product **8** was also refluxed in xylenes for 12 h. However, only pure **8** was recovered. As expected on thermodynamic and kinetics grounds, the direct interconversion of **7** and **8** can therefore be excluded.

Computational considerations

AE-CCSD(T)/cc-pVDZ single point computations (with DFT ZPVEs; Scheme 8, for computational details see Computational Methods below) on M06-2X/cc-pVDZ geometries do not indicate a thermodynamic preference for either **7** or **8**. The thermal barrier for the reaction of **5** via conformer **5i** leading to **8** is lower (18 kcal mol^{-1}, via **TS3**) than that leading to **7** (27 kcal mol^{-1}, via **TS1**). These results help rationalize the observed reactivity under HVFP conditions. The thermal barrier for the dehydration of **7** is quite high (in excess of 60 kcal mol^{-1}, via **TS4**), which was confirmed by HVFP of **7** at 600 °C and subsequent matrix isolation of the products: While **8** was more abundant at this temperature than in the pyrolysis of **6**, **7** was for the most part unchanged. In order to assess the condensed phase reactivity of **5**, M06-2X/cc-pVDZ computations including a solvent model were performed. These indicate a thermodynamic preference of −12 kcal mol^{-1} for the insertion product **8** over the aldehyde **7** as well as a 5 kcal mol^{-1} lower activation energy for the formation of **8**.

Based on this potential energy hypersurface, it seems surprising that **7** is produced by pyrolysis of **6** in the condensed phase as **8** is both favored both thermodynamically and kinetically due to a lower thermal barrier. As a result, another mechanism must be implicated for the transformation of **6** to **7**. A possibly alternative pathway, involving an acid-catalyzed formation of the aldehyde, is presented in Scheme 9: Protonation of **5** at the carbene center by **6** leads to a carbonyl-protonated aldehyde **[7+H]**$^+$, which is then deprotonated at the oxygen atom in the follow-up reaction, regenerating **6** and producing **7**. As the proton affinity E_{pa} of **5** was computed to be 262 kcal mol^{-1}, which is comparable to those of alkali metal hydroxides, this seems a viable possibility.

Conclusion

The formation of a 2,3-dihydrobenzofuran derivative from carbene **5** in the gas phase is the first C–H insertion reaction observed for a hydroxycarbene derivative. Hence, the general reactivity pattern of **5** under HVFP conditions is similar to that of other hetereocarbenes. However, synthetic access to substituted 2,3-dihydrobenzofuran derivatives through the in situ generation of various (*o*-methoxyphenyl)hydroxycarbenes from (*o*-methoxyphenyl)glyoxylic acids in high-boiling solvents is not possible, because an *o*-anisaldehyde derivatives are formed. We suggest that this dichotomy in reactivity between the high-temperature HVFP and the high-temperature solution experi-

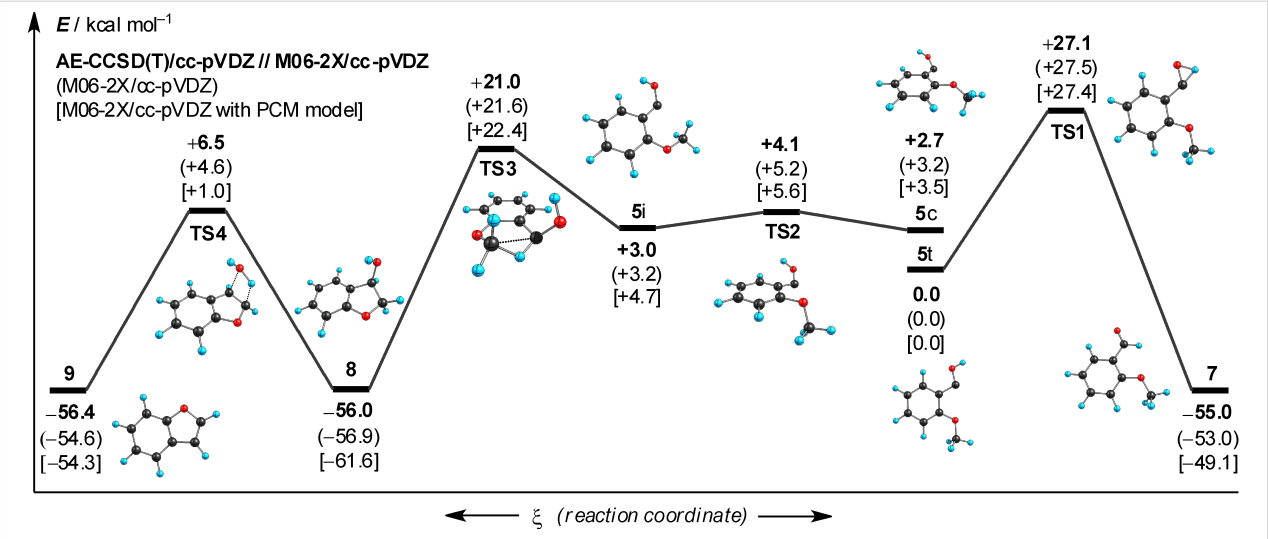

Scheme 8: Potential energy hypersurface of (*o*-methoxyphenyl)hydroxycarbene (**5**) (not drawn to scale; ZPVE included); *legend*: **5c**: carbene, *cis* conformation; **5t**: carbene, *trans* conformation; **5i**: conformer that undergoes insertion.

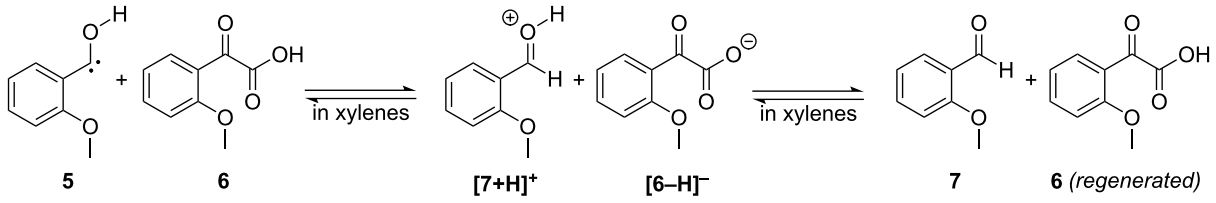

Scheme 9: Acid-catalyzed generation of **7** by unreacted **6**.

ments derives from protonation of the intermediate hydroxycarbene by the starting material in solution; this inevitably leads to the aldehyde upon deprotonation. Although preliminary tunneling computations indicate that carbene **12** should be observable, it has not yet been detected experimentally.

Experimental

Matrix-isolation studies. An APD Cryogenics HC-2 closed-cycle cryostat system with an inner CsI window was used for IR measurements. Spectra were recorded with a Bruker IFS 55 FT-IR spectrometer (4500–300 cm^{-1} spectral range with a resolution of 0.7 cm^{-1}). For the combination of high-vacuum flash pyrolysis with matrix isolation, a small, custom-built, water-cooled oven was used, which was directly connected to the vacuum shroud of the cryostat. The pyrolysis zone consisted of an empty quartz tube with an internal diameter of 8 mm and a length of the heating zone of 50 mm, which was resistively heated by a coax wire. The temperature was controlled with a Ni/CrNi thermocouple. (*o*-Methoxyphenyl)glyoxylic acid (**6**) was evaporated at room temperature from a small storage tube into the pyrolysis tube. All pyrolysis products were immediately co-condensed with a large excess of argon (typically 30 to 80 mbar from a 2000 mL storage bulb) on the surface of the 11 K matrix window at a distance of approximately 50 mm. A high-pressure mercury lamp (HBO 200, Osram) with a monochromator (Bausch & Lomb) was used for irradiation. Experiments with deuterated acid were conducted accordingly.

(*o*-Methoxyphenyl)glyoxylic acid (6) [25]. To a solution of 3.00 g (20.0 mmol) *o*-methoxyacetophenone in absolute pyridine, was added 3.33 g (30.0 mmol) of selenium dioxide. The mixture was stirred at 80 °C for 4 h. After filtration, concentration of the solution gave a brown oil that was dissolved in 5% sodium hydroxide solution and washed three times with small portions of diethyl ether. The aqueous layer was acidified with dilute hydrochloric acid and extracted with ethyl acetate. The organic layer was then dried over sodium sulfate. Filtration and concentration gave a brown oil, which crystallized on standing. (*o*-Methoxyphenyl)glyoxylic acid (3.30 g,18.4 mmol) was obtained as a brown solid. Sublimation in vacuo afforded the pure title compound as a white to yellowish powder in 60% yield.

^{1}H NMR (400 MHz, d_6-DMSO): δ = 3.85 (s, 3H, –OMe), 7.13 (t, 1H, ^3J = 7.5 Hz, *p*-H to –OMe), 7.24 (d, 1H, ^3J = 8.4 Hz, *o*-H to –OMe), 7.66–7.78 (m, 2H), 14.01 (s, 1H, acid-H); ^{13}C NMR (100 MHz, d_6-DMSO): δ = 56.2 (–OMe), 113.1 (*o*-C to –OMe), 121.2 (*p*-C to –OMe), 122.2 (*ipso*-C to –COCOOH), 126.1 (*o*-C to –COCOOH), 136.6 (*p*-C to –COCOOH), 160.0 (*ipso*-C to –OMe), 166.8 (–CO*C*OOH), 188.1 (–*C*OCOOH).

(*o*-Methoxyphenyl)glyoxylic acid-*O-d* (*d*-**6**) was obtained by repeated dissolution of (*o*-methoxyphenyl)glyoxylic acid in excess deuterium oxide followed by evaporation of the solvent in vacuo.

2,3-Dihydrobenzofuran-3-ol (8) [26]. To a solution of 1.96 g (5 mmol) 3-coumaranone in 40 mL of absolute methanol, sodium borohydride was added in small portions at –10 °C until the solution solidified. After the succession of hydrogen evolution, 20 mL of 0.2 N hydrochloric acid was added to the reaction mixture. The mixture was then extracted with chloroform. The combined organic layers were washed with brine and dried over anhydrous sodium carbonate. Filtration and removal of the solvent gave a brown oily liquid that was immediately purified by flash chromatography on a short column of silica gel with *tert*-butyl methyl ether as the eluent. The purified product was obtained as the second fraction ($R_f \approx 0.6$) in 30% yield.

^{1}H NMR (400 MHz, $CDCl_3$): δ = 1.91 (s, 1H, –OH), 4.35 (dd, 1H, ^2J = 10.6 Hz, ^3J = 2.5 Hz, –O–CH_2–), 4.44 (dd, 1H, ^2J = 10.6 Hz, ^3J = 6.5 Hz, –O–CH_2–), 5.26 (dd, 1H, ^3J = 6.5 Hz, 2.5 Hz,–C*H*OH–), 6.81 (d, 1H, ^3J = 8.1, *o*-H to –O–CH_2–), 6.87 (t, 1H, ^3J = 7.04, *p*-H to –O–CH_2–), 7.17-7.23 (m, 1H, *p*-H to –CHOH–), 7.34 (d, 1H, ^3J = 7.5 Hz, *o*-H to –CHOH–); ^{13}C NMR (100 MHz, $CDCl_3$): δ = 106.5 (–O–CH_2–), 111.4 (–CHOH–), 121.4 (*o*-C to –O–CH_2–, *m*-C to –CHOH–), 122.7 (*p*-C to –O–CH_2),124.2 (*o*-C to –CHOH–, *m*-C to –O–CH_2–), 127.4 (*ipso*-C –CHOH–), 144.9 (*p*-C to –CHOH–), 154.9 (*ipso*-C –O–CH_2–).

2,3-Dihydrobenzofuran-3-ol-*O-d*. H–D-exchange with D_2O proved to be unsuccessful on the preparative scale. As a consequence, the deuterated compound was prepared in the same way as its protium analogue: To a solution of 0.55 g (1.3 mmol) of

3-coumaranone in 20 mL of methanol-*O*-*d*, sodium borohydride was added in small portions at −10 °C until the solution solidified. After the succession of hydrogen evolution, 10 mL of D_2O were added to the reaction mixture. The mixture was then extracted with $CDCl_3$. The combined organic layers were washed with brine and dried over anhydrous sodium carbonate. Filtration and removal of the solvent gave a yellow liquid in 60% yield.

^{1}H NMR (400 MHz, $CDCl_3$): δ = 4.35 (dd, 1H, ^2J = 10.6 Hz, ^3J = 2.5 Hz, –O–C*H*$_2$–), 4.44 (dd, 1H, ^{2}J = 10.6 Hz, ^3J = 6.5 Hz, –O–C*H*$_2$–), 5.26 (dd, 1H, ^3J = 6.5 Hz, 2.5 Hz, –C*H*OH–), 6.81 (d, 1H, ^3J = 8.1, *o*-H to –O–CH_2–), 6.87 (t, 1H, ^3J = 7.04, *p*-H to –O–CH_2–), 7.17–7.23 (m, 1H, *p*-H to –CHOH–), 7.34 (d, 1H, ^3J = 7.5 Hz, *o*-H to –CHOH–).

Benzo[*b*]furan was purchased from Sigma–Aldrich and used without further purification. For matrix isolation studies, the sample was cooled to −35 °C to reduce its vapor pressure.

Computational methods

All computations were performed with the Gaussian09 [27] or Cfour suite [28] of programs. All structures were computed employing the M06 density functional [29,30] with doubled (50%) HF-exchange (M06-2X), developed by Truhlar and co-workers, in conjunction with a Dunning-type correlation-consistent double-ζ (zeta) basis set [31] (cc-pVDZ). Single point energies of the DFT structures were evaluated with the coupled cluster method, incorporating singles and doubles as well as perturbative triples and taking into account both valence and core electrons [32-34]. Again, cc-pVDZ was used as the basis set (AE-CCSD(T)/cc-pVDZ). For the elucidation of solvent effects, M06-2X/cc-pVDZ-computations with the Polarization Continuum Model [35] (PCM) were performed, containing radii based on the United Atom Topological Model as implemented in Gaussian09. Tunneling half-lives $\tau_{1/2}$ of carbenes **5** and **12** were estimated employing a) a simple Eckart barrier methodology [36,37], and b) the one-dimensional Wentzel–Kramers–Brillouin approximation [13,14,37,38].

Eckart-barrier approach

For evaluation of the rate constant *k*, the activation barriers of the forward and back reaction, V_f and V_b, were computed, along with the imaginary frequency ν_i of the transition state and the frequency ν_ξ, corresponding to the reaction coordinate. All energies were vibrationally zero-point corrected, excluding ν_i and ν_ξ. The transmission probability *P* was computed as

$$P = \frac{\cosh(\alpha+\beta)-\cosh(\alpha-\beta)}{\cosh(\alpha+\beta)+\cosh\delta}$$, with the three parameters being

$$\alpha = \frac{4\pi}{h\nu_i}\left(\frac{1}{\sqrt{V_f}}+\frac{1}{\sqrt{V_r}}\right)^{-1}\sqrt{\frac{1}{2}h\nu_\xi}\,,$$

$$\beta = \frac{4\pi}{h\nu_i}\left(\frac{1}{\sqrt{V_f}}+\frac{1}{\sqrt{V_r}}\right)^{-1}\sqrt{\frac{1}{2}h\nu_\xi - V_f + V_r}$$ and

$$\delta = 4\pi\sqrt{\frac{V_f V_r}{(h\nu_i)}-\frac{1}{16}}\,.$$

The half-life $\tau_{1/2}$ was obtained by employing the rate law of first-order kinetics:

$$\tau_{1/2} = \ln 2 / \left[\nu_\xi P\right].$$

Computations at B3PW91/cc-pVDZ were found to produce reasonable half-lives for PhCOH [21,39,40], for which experimental data are available.

Wentzel–Kramers–Brillouin approximation

The intrinsic reaction path, IRP [41], (or minimum energy path, MEP) for each molecule was established at M06-2X/6-311++G(d,p) using the Hessian-based predictor-corrector algorithm [42] as implemented in Gaussian09, with tight convergence criteria. An augmented triple-ζ basis is necessary to achieve an IRP as accurate as possible (as far as the system size permits). The single point energies along the reaction path were vibrationally zero-point corrected by adding the energy contribution of the projected frequencies along the path, i.e., a zero-point correction excluding the frequency ν_ξ, corresponding to the reaction coordinate. The thus obtained corrected potential along the reaction coordinate ξ was then characterized by an interpolating function $V(\xi)$. The attempt frequency of barrier penetration, ν_ξ, was identified by comparing the starting material's frequencies and the projected frequencies [43] along the IRC. The barrier penetration integral σ between the classical turning points $s_{1,2}$, where $V(\xi) = \varepsilon$ and

$\varepsilon = \frac{1}{2}h\tilde{\nu}_\xi$, was then computed as

$$\sigma = \frac{1}{\hbar}\mathrm{Re}\int_{S_1}^{S_2}\sqrt{2\left(V\left(\xi\right)-\varepsilon\right)}d\xi\,.$$

With σ at hand, the transition probability *P* could be computed as

$$P = 1/\left[1+e^{2\sigma}\right].$$

The half-life $\tau_{1/2}$ was again obtained by employing the rate law of first-order kinetics:

$$\tau_{1/2} = \ln 2 / \left[\nu_\xi P\right].$$

All mathematical operations were carried out with the Mathematica software package [44].

Supporting Information

Supporting Information File 1

Full matrix isolation spectra.
[http://www.beilstein-journals.org/bjoc/content/supplementary/1860-5397-6-121-S1.pdf]

References

1. Sodeau, J. R.; Lee, E. K. C. *Chem. Phys. Lett.* **1978,** *57,* 71–74. doi:10.1016/0009-2614(78)80353-4
2. Fischer, E. O.; Riedel, A. *Chem. Ber.* **1968,** *101,* 156–161. doi:10.1002/cber.19681010120
3. Moss, J. R.; Green, M.; Stone, F. G. A. *J. Chem. Soc., Dalton Trans.* **1973,** 975–977.
4. Fischer, E. O.; Kreis, G.; Kreissl, F. R. *J. Organomet. Chem.* **1973,** *56,* C37–C40. doi:10.1016/S0022-328X(00)89948-9
5. Fischer, E. O.; Weiß, K.; Kreiter, C. G. *Chem. Ber.* **1974,** *107,* 3554–3561. doi:10.1002/cber.19741071110
6. Weiß, K.; Fischer, E. O. *Chem. Ber.* **1976,** *109,* 1120–1127. doi:10.1002/cber.19761090334
7. McKinney, R. J.; Stone, F. G. A. *Inorg. Chim. Acta* **1980,** *44,* L227–L228. doi:10.1016/S0020-1693(00)91015-6
8. Chatt, J.; Jeffery Leigh, G.; Pickett, C. J.; Stanley, D. R. *J. Organomet. Chem.* **1980,** *184,* C64–C66. doi:10.1016/S0022-328X(00)93774-4
9. Fischer, E. O.; Kleine, W. *J. Organomet. Chem.* **1981,** *208,* C27–C30. doi:10.1016/S0022-328X(00)82684-4
10. Powell, J.; Farrar, D. H.; Smith, S. J. *Inorg. Chim. Acta* **1984,** *85,* L23–L25. doi:10.1016/S0020-1693(00)81013-0
11. Steinborn, D.; Gerisch, M.; Bruhn, C.; Davies, J. A. *Inorg. Chem.* **1999,** *38,* 680–683. doi:10.1021/ic9805170
12. Bennett, M. A.; Byrnes, M. J.; Kováčik, I. *J. Organomet. Chem.* **2004,** *689,* 4463–4474. doi:10.1016/j.jorganchem.2004.07.027
13. Schreiner, P. R.; Reisenauer, H. P.; Pickard, F. C.; Simmonett, A. C.; Allen, W. D.; Mátyus, E.; Császár, A. G. *Nature* **2008,** *453,* 906–909. doi:10.1038/nature07010
14. Gerbig, D.; Reisenauer, H. P.; Wu, C.-H.; Ley, D.; Allen, W. D.; Schreiner, P. R. *J. Am. Chem. Soc.* **2010,** *132,* 7273–7275. doi:10.1021/ja9107885
15. Schreiner, P. R.; Reisenauer, H. P. *Angew. Chem., Int. Ed. Engl.* **2008,** *47,* 7071–7074. doi:10.1002/anie.200802105
16. Matzinger, S.; Bally, T. *J. Phys. Chem. A* **2000,** *104,* 3544–3552. doi:10.1021/jp993496j
17. Sander, W. *Spectrochim. Acta, Part A* **1987,** *43,* 637–646. doi:10.1016/0584-8539(87)80146-0
18. Solé, S.; Gornitzka, H.; Schoeller, W. W.; Bourissou, D.; Bertrand, G. *Science* **2001,** *292,* 1901–1903. doi:10.1126/science.292.5523.1901
19. Vignolle, J.; Asay, M.; Miqueu, K.; Bourissou, D.; Bertrand, G. *Org. Lett.* **2008,** *10,* 4299–4302. doi:10.1021/ol801670z
20. Hudnall, T. W.; Bielawski, C. W. *J. Am. Chem. Soc.* **2009,** *131,* 16039–16041. doi:10.1021/ja907481w
21. Becke, A. D. *J. Chem. Phys.* **1993,** *98,* 5648–5652.
22. Lee, C.; Yang, W.; Parr, R. G. *Phys. Rev. B* **1988,** *37,* 785–789. doi:10.1103/PhysRevB.37.785
23. Florênico, H.; Heerma, W. *Org. Mass Spectrom.* **1978,** *13,* 368–370. doi:10.1002/oms.1210130614
24. Holdroyd, R. S.; Page, M. J.; Warren, M. R.; Whittlesey, M. K. *Tetrahedron Lett.* **2010,** *51,* 557–559. doi:10.1016/j.tetlet.2009.11.090
25. Domagala, J. M.; Haskell, T. H. *J. Org. Chem.* **1981,** *46,* 134–140. doi:10.1021/jo00314a029
26. Ghosh, S.; Datta, I.; Chakraborty, R.; Das, T. K.; Sengupta, J.; Sarkar, D. C. *Tetrahedron* **1989,** *45,* 1441–1446. doi:10.1016/0040-4020(89)80142-5
27. *Gaussian 09,* Revision A.02; Gaussian, Inc.: Wallingford CT, 2009.
28. *CFOUR;* , http://www.cfour.de. *Coupled-Cluster techniques for Computational Chemistry;* quantum-chemical program package.
29. Zhao, Y.; Truhlar, D. G. *Theor. Chem. Acc.* **2008,** *120,* 215–241. doi:10.1007/s00214-007-0310-x
30. Zhao, Y.; Truhlar, D. G. *Acc. Chem. Res.* **2008,** *41,* 157–167. doi:10.1021/ar700111a
31. Dunning, T. H., Jr. *J. Chem. Phys.* **1989,** *90,* 1007–1023. doi:10.1063/1.456153
32. Bartlett, R. J.; Purvis, G. D. *Int. J. Quantum Chem.* **1978,** *14,* 561–581. doi:10.1002/qua.560140504
33. Pople, J. A.; Krishnan, R.; Schlegel, H. B.; Binkley, J. S. *Int. J. Quantum Chem.* **1978,** *14,* 545–560. doi:10.1002/qua.560140503
34. Pople, J. A.; Head-Gordon, M.; Raghavachari, K. *J. Chem. Phys.* **1987,** *87,* 5968–5975.
35. Scalmani, G.; Frisch, M. J. *J. Chem. Phys.* **2010,** *132,* 114110–114115.
36. Eckart, C. *Phys. Rev.* **1930,** *35,* 1303–1309. doi:10.1103/PhysRev.35.1303
37. Kiselev, V. G.; Swinnen, S.; Nguyen, V. S.; Gritsan, N. P.; Nguyen, M. T. *J. Phys. Chem. A* **2010,** *114,* 5573–5579. doi:10.1021/jp911655a
38. Hou, H.; Li, Y.; Wang, B. *J. Phys. Chem. A* **2006,** *110,* 13163–13171. doi:10.1021/jp065346w
39. Perdew, J. P.; Chevary, J. A.; Vosko, S. H.; Jackson, K. A.; Pederson, M. R.; Singh, D. J.; Fiolhais, C. *Phys. Rev. B* **1992,** *46,* 6671–6687. doi:10.1103/PhysRevB.46.6671
40. Perdew, J. P.; Chevary, J. A.; Vosko, S. H.; Jackson, K. A.; Pederson, M. R.; Singh, D. J.; Fiolhais, C. *Phys. Rev. B* **1993,** *48,* 4978. doi:10.1103/PhysRevB.48.4978.2
41. Fukui, K. *J. Phys. Chem.* **1970,** *74,* 4161–4163. doi:10.1021/j100717a029
42. Hratchian, H. P.; Schlegel, H. B. *J. Chem. Phys.* **2004,** *120,* 9918–9924.
43. Baboul, A. G.; Schlegel, H. B. *J. Chem. Phys.* **1997,** *107,* 9413–9417.
44. *Mathematica,* Version 7.0.1; Wolfram Research Inc., http://www.wolfram.com.

Beilstein Journal of Organic Chemistry

Accuracy in determining interproton distances using Nuclear Overhauser Effect data from a flexible molecule

Catharine R. Jones, Craig P. Butts* and Jeremy N. Harvey

Full Research Paper

Open Access

Address:
Department of Chemistry, University of Bristol, Cantock's Close, Bristol, BS8 1TS, United Kingdom

Email:
Catharine R. Jones - chcrj@bris.ac.uk; Craig P. Butts* - craig.butts@bris.ac.uk; Jeremy N. Harvey - Jeremy.Harvey@bristol.ac.uk

* Corresponding author

Keywords:
conformation; internuclear distances; NMR spectroscopy; NOE

Beilstein J. Org. Chem. **2011,** *7,* 145–150.
doi:10.3762/bjoc.7.20

Received: 03 November 2010
Accepted: 10 December 2010
Published: 01 February 2011

Guest Editor: J. Murphy

Abstract

The determination of accurate NOE-derived interproton distances and confirmation/prediction of relative populations in multi-conformer, flexible small molecules was investigated with the model compound 4-propylaniline. The low accuracy assumed for semi-quantitative NOE distance restraints is typically taken to suggest that large numbers of constraints need to be used in the dynamical analysis of flexible molecules, and this requires, for example, the measurement and Karplus-type analysis of scalar coupling constants ($^3J_{CH}$ and $^3J_{HH}$). Herein we demonstrate that, contrary to this common perception, NOE measurements alone are accurate enough to establish interproton distances, and hence conformational detail, in flexible molecules to within a few percent of their ensemble-averaged values, hence reducing the demand for additional restraints in such dynamic analyses.

Introduction

Information obtained from Nuclear Overhauser Effect (NOE) experiments in NMR spectroscopy is widely employed in the determination of stereochemical and conformational details [1]. It is traditionally used in a qualitative or semi-quantitative manner to establish gross differences between conformers. However, the quantitative use of NOEs is often discounted or at least considered to be only approximately accurate. This perceived inaccuracy in NOE-distance relationships arises because many factors may perturb NOE intensities, including spin diffusion, selective polarisation transfer, variation in τ_c between spins, accuracy of signal integration and conformational flexibility [1]. Despite this, we have recently shown that surprisingly accurate NOE-derived distances can be obtained in small organic molecules, and that many of the perturbing factors do not contribute significantly to NOE intensities when the molecule of interest is in the fast tumbling regime and measurements are made within the Initial Rate Approximation limits [2]. In this previous report we observed mean errors of ~3% in distances obtained from 1D NOESY experiments on the rigid molecule strychnine in d_6-benzene (as

compared to their computationally-derived values [3]). With accurate distances obtained in a rigid organic molecule, it seems sensible to examine whether this approach can be extended more generally to multi-conformational systems with similar accuracy. Further, it is likely that the accurate interproton distance-assessments from NOE will allow accurate modelling of conformer populations in solution with fewer NOE constraints, or indeed improvements in the accuracy of modelling with the same number of NOE constraints.

If flexible systems exhibiting multiple conformations in solution are interconverting rapidly on the NMR time-scale, then conformational exchange will lead to ensemble-averaging of the observed NOEs for each corresponding interproton distance in each contributing conformer. One approach to analysing such ensemble-averaged NOEs is to assume the molecule will occupy a number of distinct low-energy conformations with particular populations in solution. The ensemble-averaged NOE-determined distances can thus be used, along with computations of conformer geometries, to confirm the structures and energies/populations of contributing conformers. An excellent description of the advantages and disadvantages of such an approach was made by Kozerski et al., using conformational ensemble fitting to NOE data from 2,3-dihydrobenzofuran derivatives to determine stereochemical and conformational information [4]. Critically, they highlight the challenge in fitting multi-conformer, multi-isomeric models, which require large numbers of NOE contacts in order to extract the best-fit to these loose data. On the other hand, with more accurate distances available, we suggest it will be possible to identify not only geometry, but also fit conformation populations to within reasonable errors.

Method

The determination of interproton distances from NOE data previously described by us is based on comparison of relative NOE intensities for pairs of spins in 1D transient NOESY experiments [2]. Assuming that the molecule of interest is in the fast tumbling regime and that the Initial Rate Approximation holds true, the normalised NOE intensity between two spins *I* and *S*, η_{IS}, is proportional to the cross-relaxation rate, σ_{IS}, between these spins and the mixing time, τ_m, of the experiment (Equation 1). In turn, the cross-relaxation rate, σ_{IS}, between spins *I* and *S* is proportional to the internuclear distance between spins I and S (r_{IS}^{-6}) as described in Equation 2. A more complete description of these equations and their use in determining interproton distances can be found in references [1] and [2].

$$\eta_{IS} = \sigma_{IS}\tau_m \tag{1}$$

$$\sigma_{IS} = kr_{IS}^{-6} \tag{2}$$

where

$$k = \left(\frac{\mu_0}{4\pi}\right)\frac{\hbar^2\gamma^4}{10}\left(\frac{6\tau_c}{1+4\omega^2\tau_c^2} - \tau_c\right)$$

Assuming that the values defining *k* (ω-Larmor frequency, τ_c-rotational correlation time, γ-magnetogyric ratio) remain constant for *each spin pair in a given selective inversion experiment*, the ratio of intensities of a pair of NOE signals, η_{I1S}:η_{I2S}, *within that experiment* can thus be assumed to be proportional to the ratio of their internuclear distances (Equation 3). Thus, by comparing η_{I1S} and η_{I2S} *within the same selective inversion experiment*, we only need to know one distance, e.g., r_{I1S}, in order to calculate the second distance, r_{I2S}.

$$\frac{\eta_{I1S}}{\eta_{I2S}} = \frac{r_{I1S}^{-6}}{r_{I2S}^{-6}} \tag{3}$$

As outlined above, when there are multiple conformations describing a flexible molecular system, the matter of internuclear distance determination becomes more challenging. A general outline of the treatment of flexible small molecules using NOE experiments for both conformational and population analysis can be found in reference [1]. Larger flexible systems with multiple conformations such as peptides and proteins have been investigated using NOE-derived data, where techniques such as ensemble-averaged full relaxation matrix approaches are used to simulate NOEs [5-7]. The relative proportions of the various conformations contributing to the ensemble are then iteratively adjusted to derive the best fit to the experimentally measured NOEs. Accurate determination of populations in these analyses has always been limited by the inherently low accuracy of the NOE-derived restraints used, resulting in a broad range of conformer populations fitting the observed NOE restraints.

On the other hand, with the high accuracy provided by the NOE-distance analysis we employ, we have recently identified and quantified a previously unrecognised conformer of strychnine through a relatively minor deviation in a single measured NOE-derived interproton distance across the seven-membered ring of strychnine [8]. This intra-ring distance was observed to be ~0.6 Å (15%) shorter than expected by X-ray crystallography [9] and DFT [3], which would traditionally be considered an acceptable 'experimental error' for NOE-derived interproton distances. However, given that the average errors for NOE-

derived distances in our earlier study [2] were ~3%, this was identified as significantly anomalous. In the event, a second low-energy conformer was identified with a population of ~2.2% compared to the major conformer. By incorporating this second conformer, the error for the problematic distance was reduced from 15% to 3%, while no other significant changes in the NOE-derived distances arose.

We now sought to investigate the conformer populations of a flexible molecule where conformational exchange causes the perturbation of more than one distance, and hence more than one NOE intensity. Herein, we report that the high accuracy reported for relatively rigid molecules is maintained for multiple NOE-derived distances arising from conformationally flexible molecules when compared to their time-averaged computationally-derived distances in the alkyl chain of a small molecule – 4-propylaniline. These NOE-derived distances can thus be applied to modelling the populations (and hence energy differences) of the conformers, again with good accuracy when compared to their calculated values.

Results and Discussion

A B3LYP/6-31G* conformational search of 4-propylaniline leads not surprisingly to four non-degenerate low-energy conformers, with the propyl chain either in an anti, **1a** and **1b**, or a gauche, **2a** and **2b**, conformation (Figure 1). The anti conformers, **1a** and **1b**, differ from each other only in the opposite pyramidalisation of the amino group: The gauche conformers **2a** and **2b** are similarly related, with two further degenerate gauche conformers of **2a** and **2b** arising by rotation of 120° around the C5–C6 bond. In each case, the isomer '**a**' is the one in which the aniline H atoms are on the same side of the benzene ring as the carbon chain. The optimised H–H distances in **1a** are very similar to those found in **1b**, and likewise for **2a** and **2b**.

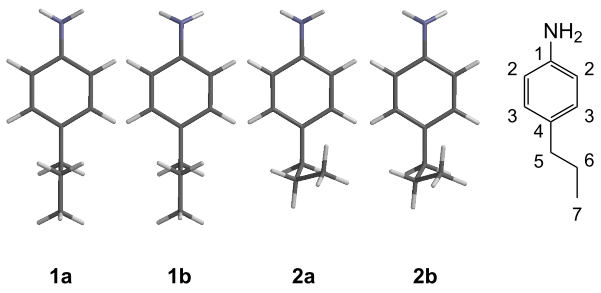

Figure 1: Four low energy conformations of 4-propylaniline obtained from B3LYP/6-31G* conformational search and labelled 2D structure (**1a**/**2a** differ from **1b**/**2b** in the pyramidalization at the amine nitrogen, see main text for details).

The calculated energies of conformers **1a** and **1b** differ by less than 0.01 kJ/mol from each other, and lie only 1.99 and 1.94 kJ/mol lower than **2a** and **2b**. After correction for zero-point energy and thermal and entropic corrections, the relative calculated ΔG at 298 K for conformers **1a**, **1b**, **2a** and **2b** were 0.09, 0.00, 3.20 and 3.14 kJ/mol, respectively. Finally, on including the solvation free energies (in $CDCl_3$) for all species, this leads to corresponding predicted free energies of 0.10, 0.00, 3.55 and 3.39 kJ/mol, respectively. As the B3LYP relative electronic energies are not expected to be highly accurate, single-point calculations using two very accurate local correlated methods were used to refine the gas phase relative energies. At the LCCSD(T0) level of theory, relative electronic energies of 0.07, 0.03, 0.09 and 0.00 kJ/mol, respectively, are obtained. The better description of dispersion interactions stabilises the more compact gauche conformers as expected. LPNO-CEPA-1/cc-pVTZ calculations, yield relative energies of 0.03, 0.00, 0.20 and 0.14 kJ/mol, very close to the coupled-cluster values, suggesting that these quantities are reliable to ± 0.5 kJ/mol and perhaps better.

Including the corrections for zero-point energy, thermal and entropic corrections, and solvation, these correlated ab initio calculations lead to predicted relative free energies in solution for the four conformers of 0.15, 0.00, 1.63 and 1.43 kJ/mol based on the LCCSD(T0) calculations, and very similar values of 0.14, 0.00, 1.76 and 1.60 kJ/mol based on the CEPA calculations. Taking into account the two-fold degeneracy of each of the gauche conformers **2a** and **2b**, this gives expected equilibrium populations of 23, 24, 25 and 27% or 24, 25, 25 and 26%, respectively. As the distances in each pair of conformers are so similar, this can be described more concisely as being predicted populations of **1 (a + b)** and **2 (a + b)** of 47% and 53% or 49% and 51%.

Experimentally, a selection of interproton distances: H3–H5, H3–H6, H3–H7, H5–H7, was determined using NOE intensities from 1D NOESY experiments. The intensities of the measured NOE signals were first corrected for the chemical equivalence/symmetry in each group by dividing the NOE intensity between signals I and S, η_{IS}, by $n_I n_S$, where n_I and n_S are the number of chemically equivalent spins in the groups giving rise to signals I and S respectively [1]. In order to convert the corrected NOE intensities into physically realistic interproton distances, vide supra, they need to be scaled against a single fixed reference distance for which an NOE has also been measured [1,2]. The obvious candidate distance, between the fixed aromatic H2 and H3 protons, could not be used as the experimental NOE signal between these two protons showed strong coupling artefacts that obscured the NOE intensity. Instead, the NOE data were internally calibrated from the

conformationally averaged H3–H5 NOE, assuming a reference distance for this proton pair of 2.77 Å (which is the calculated ensemble-average using the populations for **1a/b** and **2a/b** as determined above). The relative NOE intensities were then converted to ensemble-averaged internuclear distances, r_{NOE}, by applying the r^{-6} analysis vide supra. Where the same ensemble-averaged interproton distance was measured by two NOE experiments, e.g., *H3*–H6, *H6*–H3 (where the labels in italics are the inverted proton respectively) the experimental distance, H3–H6, was taken as the average of the pair and the results are presented in Table 1.

Table 1: NOE-derived and ensemble-averaged interproton distances.

	r_{NOE} (Å)	r_{calc} (Å)	% error
H3–H5 (ref)	2.77	2.77	-
H3–H6	3.21	3.34	3.83
H3–H7	4.16	4.05	2.54
H5–H7	3.13	3.08	1.67

To calculate the effective interproton distances, r_{calc}, for the conformationally averaged molecule, i.e., those distances which theoretically should be determined by the NOE experiments, each interproton distance, r_{IS}, as determined in the B3LYP/6-31G* structural optimisation for the conformers **1a**, **1b**, **2a** and **2b** was converted into a corresponding NOE intensity for each conformer using the r^{-6} relationship ($\eta_{IS} = r_{IS}^{-6}$). The measured NOEs all involve protons in chemically equivalent groups, e.g., H3 and H3' or H6 and H6', so the effective distances were obtained from the calculated structures (and thus relative NOE values determined) for *all* the contributing chemically equivalent pairs in each case, e.g., the H3–H6 NOE derived from $r_{H3–H6}$, $r_{H3–H6'}$, $r_{H3'–H6}$ and $r_{H3'–H6'}$, which were combined with $\langle r_{IS}^{-6} \rangle = (\Sigma r_{IS}^{-6})/(n_I n_S)$, where n_I and n_S are the number of equivalent spins in the groups *I* and *S*, respectively. These individual NOE intensities for each of the six conformers were then weighted using the calculated Boltzmann populations from above, to convert them into effective distances.

A comparison of the resulting NOE-derived distances, r_{NOE}, and ensemble-averaged distances, r_{calc}, from calculations for H3–H6, H3–H7 and H5–H7 are shown in Table 1. The observed errors for these distances derived from a free-rotating group are in the range of 1–4% (mean 2.68%) and this compares very well with the observations in our previous work on the rigid strychnine system, which gave mean errors of ~3% in d_6-benzene and ~4% in $CDCl_3$ [2,3].

An alternative method of data analysis might assume that the NOE measurements and the DFT conformer structures are accurate, but that the computed free energies (and hence the populations) are not. Thus, one might use the NOE and geometry data to model the conformer populations and hence the relative energies. In theory, there are too many conformers (four non-degenerate) to model their populations against the measured NOEs. However, if one assumes the degeneracy of **1a/b** and also **2a/b**, on near-symmetry grounds, then the relative populations of conformers **1a** and **1b** would be equal, (**x**), as would **2a** and **2b**, (1−**x**), reducing the problem to a single unknown with three NOE restraints. Figure 2 shows the plot of the average errors, compared to experiment, arising from weighting the calculated NOE intensities (vide supra) for each conformer by a range of populations (**x**) of **1a/b**. The best fit to experiment is obtained at ~55% **1a/b**, (and thus ~45% **2a/b**), corresponding to a free energy difference of ca. 2.1–2.2 kJ/mol between conformers **1a/b** and **2a/b**. This compares extremely well with the highest level calculations, which suggest a corresponding free energy difference of ca. 1.5 kJ/mol. This remarkable match in populations and energies supports the proposition that fitting populations of conformers from the NOE-derived distances is an inherently accurate approach when the geometries of the contributing conformers can be accurately described.

Figure 2 also demonstrates the requirement for the relatively accurate determination of internuclear distances in order to fit conformationally flexible systems. Assuming a mean 3% error in the interproton distances determined by NOEs (black line in Figure 2), the experimental results are consistent with a population of **1a/b** lying in the range 40 to 65%. However, typical semi-quantitative NOE studies are assumed to lead to much larger errors in distances, in the order of ± 10% (red line in Figure 2), or even assign distance-ranges to NOE intensities such as strong (2–3 Å), medium (3–4 Å) and weak (> 4 Å). The entire population range of conformers **1a/b** falls below the red line in Figure 2, showing that such loose assumptions of NOE accuracy would effectively allow *any* population of **1a/b** and **2a/b** to be fitted acceptably to the experimental data, requiring other constraints to be invoked in order to model even this simple system.

In summary, these results suggest that the methods we have previously described for extracting accurate interproton distances from NOE data in rigid systems can be extended with little, or no, loss of accuracy to relatively flexible small molecules. The high accuracy of this distance data allows it to be applied to assessing/confirming the relative populations of contributing conformers in small, flexible molecules with reasonable certainty, even where very few restraints are available – succeeding where traditional semi-quantitative NOE analysis would not.

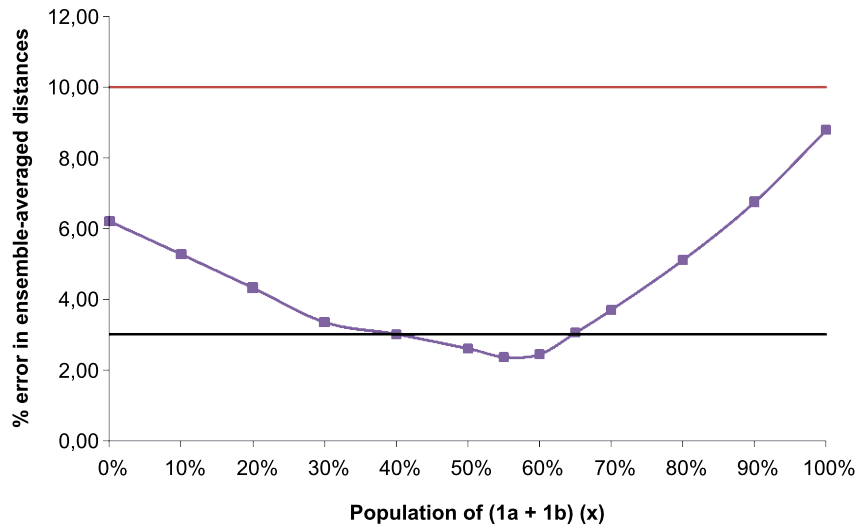

Figure 2: Plot of the mean calculated error arising from fitting the population distribution of conformers **1a/b** (**x**) and **2a/b** (1−**x**) to the experimental NOE-derived interproton distances. Exemplar error thresholds are represented at 3% (black line) and 10% (red line).

Experimental

NMR samples were prepared in 5 mm tubes with 0.7 ml $CDCl_3$ and ~10 mg 4-propylaniline, in air without degassing. NMR data were all collected on a 500 MHz Varian VNMRS Direct-Drive spectrometer equipped with an indirect observe probe. 1D selective transient NOESY spectra (64 k data points, 8 kHz spectral width, 500 ms mixing time, 4.096 sec. acquisition time, 1 s relaxation delay, 512 scans (45 minutes/irradiation)) were obtained using the Varian Chempack NOESY1D sequence which is based on the DPFGSENOE (double-pulse field gradient spin-echo NOE) excitation sculpted selective sequence reported by Stott et al. [10] and incorporates a zero-quantum filter element [11]. NOE build-up curves were obtained with mixing times up to 900 ms and the critical constancy of relative NOE intensities within each irradiation was confirmed (as well as the linearity of absolute NOE intensities).

Geometry optimisation at the B3LYP/6-31G* level was carried out using the Gaussian 03 package and frequencies were computed to characterise the minima and derive statistical mechanical corrections to the electronic energies. Gas-phase single point energies were then calculated at the four minima in Gaussian, with B3LYP/6-31G* and a polarisable continuum model (IEF-PCM, parameters for chloroform solvent, $\varepsilon = 4.9$). The LCCSD(T0)/cc-pVTZ calculations [12,13] were performed as implemented in the MOLPRO2008 package [14]. Inspection of the orbital domains for the different conformers show that a consistent set is obtained for all, hence the domain error on relative energies should be small. The LPNO CEPA-1/cc-pVTZ calculations [15] were performed using the implementation in the ORCA 2.8 package [16].

Acknowledgements

We thank the University of Bristol for funding for CRJ and the EPSRC (EP/F013515/1) and BBSRC (BB/F011539/1) for instrumentation funding. We thank Frank Neese for providing the ORCA program package.

References

1. Neuhaus, D.; Williamson, M. P. *The Nuclear Overhauser Effect in Structural and Conformational Analysis,* 2nd ed.; John Wiley & Sons, Inc.: New York, 2000.
2. Butts, C. P.; Jones, C. R.; Towers, E. C.; Flynn, J. L.; Appleby, L.; Barron, N. J. *Org. Biomol. Chem.* **2011,** *9,* 177–184. doi:10.1039/C0OB00479K
3. Bagno, A.; Rastrelli, F.; Saielli, G. *Chem.–Eur. J.* **2006,** *12,* 5514–5525. doi:10.1002/chem.200501583
4. Kozerski, L.; Krajewski, P.; Pupek, K.; Blackwell, P. G.; Williamson, M. P. *J. Chem. Soc., Perkin Trans. 2* **1997,** 1811–1818. doi:10.1039/a700149e
5. Bonvin, A. M. J. J.; Brünger, A. T. *J. Biomol. NMR* **1996,** *7,* 72–76.
6. Xu, Q.; Gitti, R.; Bush, C. A. *Glycobiology* **1996,** *6,* 281–288. doi:10.1093/glycob/6.3.281
7. Wang, J.; Hodges, R. S.; Sykes, B. D. *J. Am. Chem. Soc.* **1995,** *117,* 8627–8634. doi:10.1021/ja00138a019
8. Butts, C. P.; Jones, C. R.; Harvey, J. N. *Chem. Commun.* **2011,** *47,* 1193–1195. doi:10.1039/C0CC04114A
9. Messerschmidt, M.; Scheins, S.; Luger, P. *Acta Crystallogr., Sect. B: Struct. Sci.* **2005,** *61,* 115–121. doi:10.1107/S0108768104032781
10. Stott, K.; Keeler, J.; Van, Q. N.; Shaka, A. J. *J. Magn. Reson.* **1997,** *125,* 302–324. doi:10.1006/jmre.1997.1110
11. Thrippleton, M. J.; Keeler, J. *Angew. Chem.* **2003,** *42,* 3938–3941. doi:10.1002/anie.200351947
12. Schütz, M. *J. Chem. Phys.* **2000,** *113,* 9986–10001. doi:10.1063/1.1323265

13. Schütz, M.; Manby, F. R. *Phys. Chem. Chem. Phys.* **2003,** *5,* 3349–3358. doi:10.1039/b304550a
14. *MOLPRO,* Version 2010.1, a package of *ab initio programs*, Werner, H. J.; Knowles, P. J.; Lindh, R.; Manby, F. R.; Schütz, M. and others, see http://www.molpro.net.
15. Neese, F.; Wennmohs, F.; Hansen, A. *J. Chem. Phys.* **2009,** *130,* No. 114108. doi:10.1063/1.3086717
16. *ORCA,* Version 2.8; Neese, F.; Wennmohs, F.: Bonn, 2010.

License and Terms

Beilstein Journal of Organic Chemistry

Anion–π interactions influence pK_a values

Christopher J. Cadman and Anna K. Croft*

Full Research Paper

Open Access

Address:
School of Chemistry, University of Wales Bangor, Bangor, Gwynedd, LL57 2UW, United Kingdom. Fax: +44 1248 370 528. Tel: +44 1248 382 375

Email:
Anna K. Croft* - a.k.croft@bangor.ac.uk

* Corresponding author

Keywords:
anion–π; DFT; intramolecular interaction; LFER; pK_a

Beilstein J. Org. Chem. **2011,** *7,* 320–328.
doi:10.3762/bjoc.7.42

Received: 01 December 2010
Accepted: 23 February 2011
Published: 17 March 2011

Guest Editor: J. Murphy

Abstract

Five 8-(4-R-phenyl)-1-naphthol derivatives were prepared by $PdCl_2$-catalysed electrophilic aromatic substitution. The pK_a' values for these 1,8-disubstituted arene naphthols have been measured in acetonitrile/water (R = NO_2, 8.42; R = Cl, 8.52; R = H, 8.56; R = Me 8.68; and R = OMe, 8.71) and indicate a correlation with the electronic nature of the arene substituent, as determined through LFER analysis. Contributions to the relative pK_a' values have been interpreted, using M06-2X DFT calculations, as consisting of two components: A small contribution from initial OH–π bonding in the starting materials and a larger contribution from anion–π interactions in the products. Such effects have implications for a range of other systems.

Introduction

There are numerous examples in nature of interactions involving aromatic systems and these interactions underpin many modern supramolecular binding agents, with clear applications in biological, medical and environmental chemistry [1]. Cation–π and π–π interactions are perhaps the best known of these non-covalent forces and are driven by attractions between the quadrupole moments of the aromatic species in question, with either a cation or other aromatic, respectively. In a similar fashion, CH–π interactions and anion–π interactions have been identified as influencing binding in a number of systems. Since key computational investigations have indicated that anion–π interactions might be very important [2-4], which is also supported by strong circumstantial evidence from crystal-structure mining [5-7], there has been a resurgence of work in this area.

One prime focus has been on anion–π interactions as a means to design selective supramolecular anion receptors and template-directed synthesis of macrocyclic complexes has also been achieved [8-17]. The magnitude of the anion–π interaction varies with the size of the aromatic quadrupole and the polarisability of the system. Recent quantitative measurements of chloride binding to calixarenes in solution estimate these interactions to be as much as 4.6 kJ·mol^{-1} [18].

Moreover, computational models suggest that these interactions can be further enhanced through co-operative interactions [19,20].

In addition to guiding binding interactions, aromatic groups are also able to direct reaction outcomes. This has been well established in the field of cation–π interactions, where early experiments by Cram indicated that aromatics in close proximity to an incipient carbocation could accelerate tosylation reactions by up to 1800-fold [21]. Similarly, neighbouring aromatics have been shown to have an effect on radical reactions proceeding through a polarised transition state [22]. Clearly there is excellent potential, therefore, for aromatic interactions to mediate reactions involving anions [23], and it is likely that these types of interactions will be extremely relevant in catalysis, particularly in biological systems [24].

To probe this possibility in more detail, we have prepared a selection of simple model systems **1**–**5**, based on 1,8-disubstituted naphthalene (Figure 1). Such model systems have already been utilised to great effect by Cozzi and co-workers to probe π–π interactions [25,26]. Related models have also proven effective in exploring neighbouring group interactions in reactive systems, such as phosphate hydrolysis [27,28]. In order to analyse any effects of the aromatic system on the pK_a value of the naphthols **1**–**5** in a complementary fashion, density functional calculations using the M06-2X functional [29], and atoms in molecules (AIM) [30], analyses have been used.

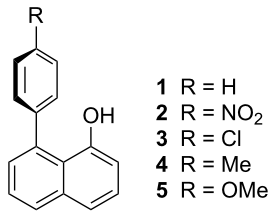

Figure 1: 1,8-disubstituted naphthalene model systems.

Results

Preparation of the 1,8-disubstituted naphthalenes **1**–**5** was carried out following literature procedures [31]. 1-Naphthol (**6**) was reacted with an 1-iodo-4-R-benzene **7** [R = (a) H, (b) NO_2, (c) Cl, (d) Me, (e) OMe] in the presence of a $PdCl_2$ catalyst and Cs_2CO_3 in DMF at 110 °C for 19–43 h, under Schlenk conditions (Scheme 1). Reactions were continued until all the starting material was consumed, as determined by TLC. It was noted that iodobenzenes with larger substituents [(d) Me, (b) NO_2 and (e) OMe] took longer to react, suggesting steric, rather than electronic, limitations in the rate-determining step of the reaction.

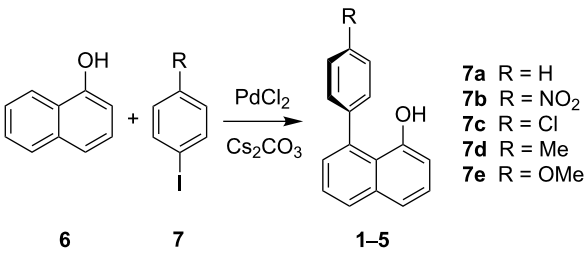

Scheme 1: The general reaction for the preparation of the 1,8-disubstituted naphthol derivatives **1**–**5** [31].

The five different substituents were chosen to span the range of electronic effects that could be invoked as a neighbouring effect. The identity of the products **2**–**5** was confirmed through melting point, ^{1}H and ^{13}C NMR spectral data, IR and MS (Supporting Information File 2). The 8-(4-methylphenyl)-1-naphthol derivative **4** was also crystallised and an X-ray crystal structure obtained, confirming the structure (Figure 2). Details are supplied in the Supporting Information Files 4–6.

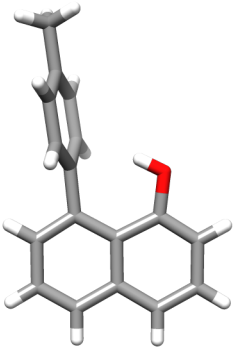

Figure 2: X-ray structure of 8-(4-methylphenyl)-1-naphthol derivative **4**.

The acid dissociation constants (K_a'), and hence the pK_a' values of each of the five derivatives **1**–**5**, were measured by potentiometric titration in 50:50 mixtures of acetonitrile/water with tetrabutylammonium hydroxide (TBAH) as the base. As an example, the plot obtained for compound **1** with TBAH is shown in Figure 3.

The derived pK_a' values, along with the Hammett σ_p-constant for each R-substituent are presented in Table 1. The method was validated with 1-naphthol, for which the experimental pK_a value is reported as 9.30 [32,33].

Gas phase calculations for the H, NO_2 and OMe substituted derivatives **1**–**5**, respectively, and their corresponding anions,

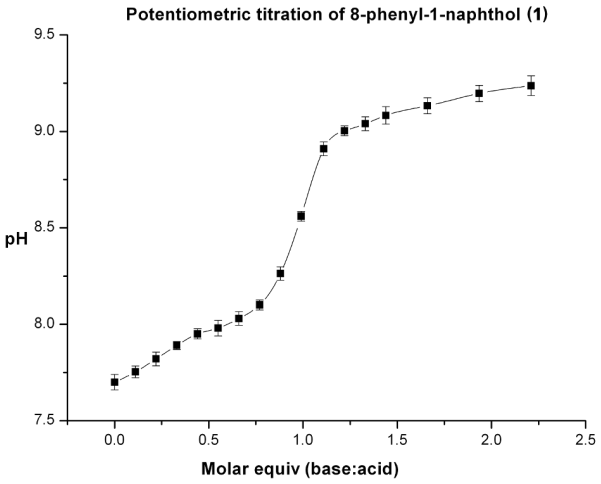

Figure 3: Potentiometric titration data for compound **1** and TBAH.

Table 1: pK_a' Values of 1-naphthol and the derivatives **1**–**5**, along with the corresponding σ_p values. Errors calculated on the basis of standard deviations from triplicate measurements.

Derivative	pK_a' Value	σ_p Value [34]
6 (1-Naphthol)	9.31 ± 0.04	n/a
5 (OMe)	8.71 ± 0.05	−0.29
4 (Me)	8.68 ± 0.04	−0.17
1 (H)	8.56 ± 0.03	0.00
3 (Cl)	8.52 ± 0.05	0.22
2 (NO_2)	8.42 ± 0.04	0.77

8–**12**, were carried out to delineate the factors contributing to the experimental pK_a' values. These were carried out using the M06-2X functional [29] with the 6-31+G(d,p) basis set. This parameterised functional has been shown to provide reliable values for intermolecular interactions, including hydrogen-bonding interactions [35]. For the acid, two minima were identified; one with the hydrogen atom pointing into the neighbouring aromatic ring (a) and one with the hydrogen atom pointing away from the ring (b) (Figure 4). The relative energies for each derivative and its corresponding anion are presented in Table 2. Structures are supplied in the Supporting Information File 1.

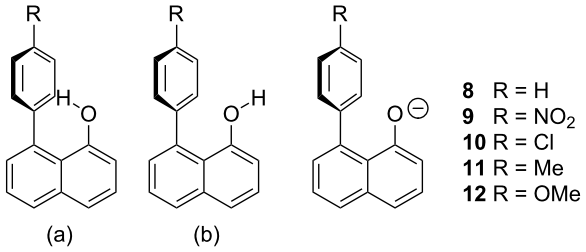

Figure 4: Structures (a) with the hydrogen atom pointing into the ring, as seen in the crystal structure of **4**, and (b) with the hydrogen atom pointing away from the ring and the anions **8**–**12**.

Discussion

Intermolecular effects on molecules are widely recognised as being important in both binding and reactions, with solvent effects being the classic example of the latter. The effects of solvation on reactive intermediates can change the outcome of a reaction, primarily by modifying the rate. In these cases, interactions with the reactive intermediate or with the starting material can serve to accelerate a process, for example, by stabilisation of the intermediate or by activation of the starting material, or decelerate it in an analogous fashion. In restricted model systems and in enzyme active sites, in which the interacting species are brought in close proximity to one another, these effects are often amplified because of the reduction of the contribution of entropic factors. This is recognised as a proximity effect and can be measured by an effective molarity [37]. As such, we chose the 1,8-disubstituted naphthalenes as model

Table 2: Relative energies (kJ·mol^{-1}) of protonated species **1**–**5** and their corresponding anions **8**–**12**, relative to 1-napthol (**6**), calculated with the M06-2X DFT method. Mean standard error (MSE) for mixed systems with M06-2X/6-31+G(d,p) has been reported as −1.0 kJ·mol^{-1} [35].

Species	H-in (a)		H-out (b)[a]	Anion[b]	
	6-31+G(d,p)	6-311+G(3df,2p)		6-31+G(d,p)	6-311+G(3df,2p)
1 (H)	−9.7	−10.2	0	−5.6	−7.5
2 (NO_2)	−0.2	−1.6	0	−41.5	−42.6
3 (Cl)	−6.1	−7.1	0	−19.7	−21.3
4 (CH_3)	−11.7	−12.3	0	−4.6	−6.4
5 (OCH_3)	−11.5	−12.3	0	−3.8	−5.7

All values included zero point corrections, scaled to 0.967 [36]. [a]Set arbitrarily at zero for comparison across each row. Either smaller or more negative numbers denote more stable species. [b]Calculated from the isodesmic reaction with naphthol **6** to afford the corresponding anion, using H-out (b) as the neutral. Larger negative values indicate anions relatively more stable with respect to naphtholate.

systems to examine the effect of a neighbouring aromatic ring on one of the simplest reactions, the removal of a proton from an acid to generate an anion. Cozzi and co-workers examined related models extensively in the study of arene–arene interactions [25,26]. These models were utilised because rotation to generate a conjugated biphenyl system is aggravated by steric interactions [38] and contributions from para-substitution towards generating such a conjugated system are very small [39]. The lack of conjugation is corroborated in the solid state by the X-ray crystal structure of compound **4**, which shows the structure as having the substituted aromatic ring roughly perpendicular to the naphthalene rings. These factors render the structures **1**–**5** suitable for the current study.

Compounds **1**–**5** were titrated with TBAH to generate the corresponding anions **8**–**12** (Scheme 2). Potentiometric titrations of acidic compounds are normally conducted by adding aliquots of a base to an acid in an aqueous solution. However, all five derivatives **1**–**5**, as well as naphth-1-ol (**6**) itself, are insoluble in water. A substitute was therefore required with similar properties to water that would enable the calculation of the appropriate relative pK_a values. There has been a substantial amount of literature produced on potentiometric titrations in binary solvent systems of a 50:50 mix of water and a solvent that dissolves the relevant compound [40,41].

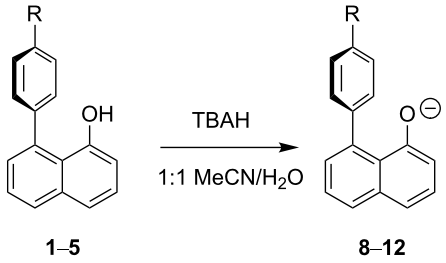

Scheme 2: Titration of the acids **1**–**5** to generate the corresponding anions **8**–**12**, respectively.

Acetonitrile has been shown to be the most suitable solvent for the pK_a' determination as it has the closest properties to water [42], therefore the titrations were carried out in a 50:50 mix of water and acetonitrile, with the pH meter calibrated against standard calibrants fully dissolved in this solvent mixture. Solvent effects will nevertheless impact upon the pK_a calculated, therefore pK_a values derived from compounds in binary solvent systems are represented with a prime symbol (') indicating the pK_a values are not measured in pure water.

Solvents can affect the properties of acids in three ways; firstly, protic solvents encourage ionisation of the acid via hydrogen bonding. However, acetonitrile is non-protic, which means this does not need to be considered. Secondly, the basicity of the solvent affects the acidity of a compound; the more basic a solvent, the more an acid dissociates. Acetonitrile and water have very similar donor numbers of 14.1 and 18, respectively [43], therefore the pK_a value of each of the acids **1**–**5** will be barely affected through this effect. The final effect that may influence the pK_a value of an acid is through homoconjugation, where the conjugate base hydrogen bonds to the parent acid. This does not occur to a significant extent in water, as the water forms strong hydrogen bonds with itself. The extent of homoconjugation that may occur can be gauged by the dielectric constant (ε) of the solvent, where a lower dielectric constant corresponds to a higher extent of homoconjugation, which increases the acidity and lowers the pK_a value of an acid. Acetonitrile and water have dielectric constants of 36 and 81.7 [42,44], respectively. As a consequence of the difference in the dielectric constants, there may be a slight difference in the measured pK_a' value and the actual pK_a. It is worth remembering, however, that the resulting pK_a' value of every derivative is relative to the others and therefore any effects of the R-substituents are likely to be preserved.

The pK_a' values correlate linearly with the corresponding Hammett σ_p-constants for the R-substituents, affording a correlation constant (R^2) of 0.916. The linear dependence is illustrated in Figure 5. The slope of the Hammett plot confirms that the intermediate or product is stabilised by electron deficient groups, consistent with deprotonation. The magnitude of the slope is relatively small (−0.27), as might be expected for a through-space effect, and may also be indicative of solvation reducing the apparent localised charge.

For a better interpretation of the factors contributing to the changes in measured pK_a' values, M06-2X density functional calculations of both the starting materials **1**–**5** and the corresponding anions **8**–**12** were carried out. Such calculations

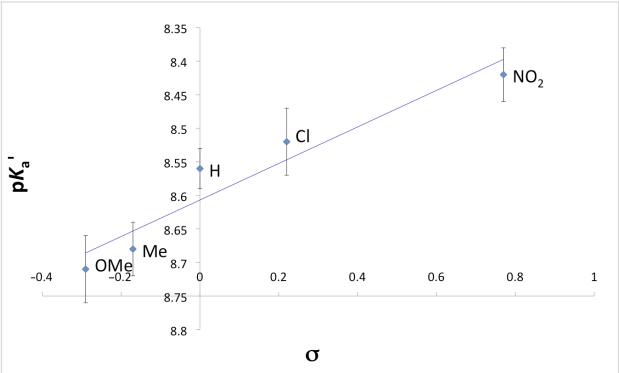

Figure 5: Plot of pK_a' values for compounds **1**–**5** versus the corresponding R-substituent σ_p Hammett parameter. The linear correlation has R^2 of 0.916.

generate both energetic information and structural information, which may be otherwise difficult to obtain for the anion intermediates. These calculations indicate that the nature of the differences in pK_a' values are two-fold. In the first instance, there is a small contribution from differences in binding of the naphtholic hydrogen atom to the neighbouring ring (Figure 4a), measured relative to the alternative minimum-energy orientation (Figure 4b). This interaction is tightest for the electron-rich ring of the methoxy-substituted acid **5**, and would result in more difficult abstraction of the proton, relative to less electron-rich acids, such as **2**. In fact, for the acid **2**, the difference is negligible, suggesting that this could be a simple electrostatic interaction. The nature of this interaction was confirmed by AIM analysis of **1**(a)–**5**(a) and the ρ values for relevant critical points, for these molecules and anions **8**–**12**, are included in Table 3. For these derivatives, a non-covalent bonding interaction is detected as a bond critical point between the naphthol proton and the quaternary (1') carbon of the 8-substituent and is accompanied by a ring critical point from the 6-membered ring made from the additional atoms of the naphthalene moiety. The ρ value is, as can be surmised from the lower interaction energy, lower for the bond critical point between H and C for **2**(a) (0.0193 e·bohr^{-3}) than for that between H and C for **1**(a) (0.0223 e·bohr^{-3}). Molecular graphs are supplied in the Supporting Information File 3.

The second component that is likely to contribute to the measured pK_a' values is the interaction between the anion and the neighbouring aromatic ring. Because of the difference in the system from the starting materials, namely one less bond and thus calculation through an isodesmic procedure, the values are best compared within the series. This interaction is again least strong for the nitro derivative **2**, indicating either a less unfavourable interaction [18] or a more favourable one. In addition, this latter effect seems to reach saturation with electron-rich rings, consistent with the argument that the differences in anion–π interaction are primarily a result of quadrupole interactions.

The two effects observed act together, and are thus consistent with the trend observed for the pK_a' values. It is worth noting that, relative to gas-phase calculations, the measured experimental effect is likely to be attenuated by hydrogen-bonding interactions with solvent. Such an interaction with solvent may not, however, be relevant in some enzyme and supramolecular systems.

The minimised structures for each of the anions illustrate an interesting feature. There is consistently an increased twist from the perpendicular plane of the naphthalene, such that the angle is around 130°, rather than the ca. 120° of the starting material. This, however, is not enough to bring the substituted ring into conjugation with the anion, as indicated by the distribution of the HOMO, which is confined to the naphthol portion of each molecule, and is in fact principally located on the phenolic ring (illustrated for **8** in Figure 6). This may, however, bring the oxyanion closer to the more positively charged periphery of the neighbouring aromatic ring.

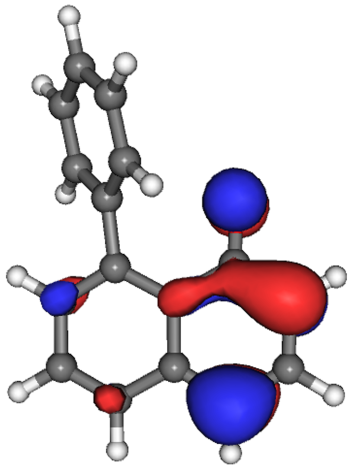

Figure 6: Anion density (HOMO) for the phenyl-derivative **8**, illustrating no conjugation of the anion with the neighbouring aromatic.

Table 3: Electronic densitites (ρ) (e·bohr^{-3}) and Laplacian (Lp) values $\nabla^2\rho$ (e·bohr^{-5}) of the identified bond critical points for protonated (OH-C1') and deprotonated (O-C1') species **1**–**5** and their corresponding anions **8–12**, as determined from AIM analysis.

Species	H-in (a)		Anion	
	ρ	Lp ρ	ρ	Lp ρ
1 (H)	0.0223	−0.0175	0.0163	−0.0155
2 (NO_2)	0.0193	−0.0162	0.0176	−0.0167
3 (Cl)	0.0215	−0.0171	0.0167	−0.0162
4 (CH_3)	0.0227	−0.0176	0.0162	−0.0155
5 (OCH_3)	0.0230	−0.0176	0.0164	−0.0158

AIM analysis of the anions revealed a bond critical point between the oxygen and the C1' carbon (Figure 7) with positive ρ of 0.0163. This indicates that the interaction between the ring and the anion is not just one of proximity, but does indeed constitute a 'bond' that can, in principle, be classified as a true anion–π interaction.

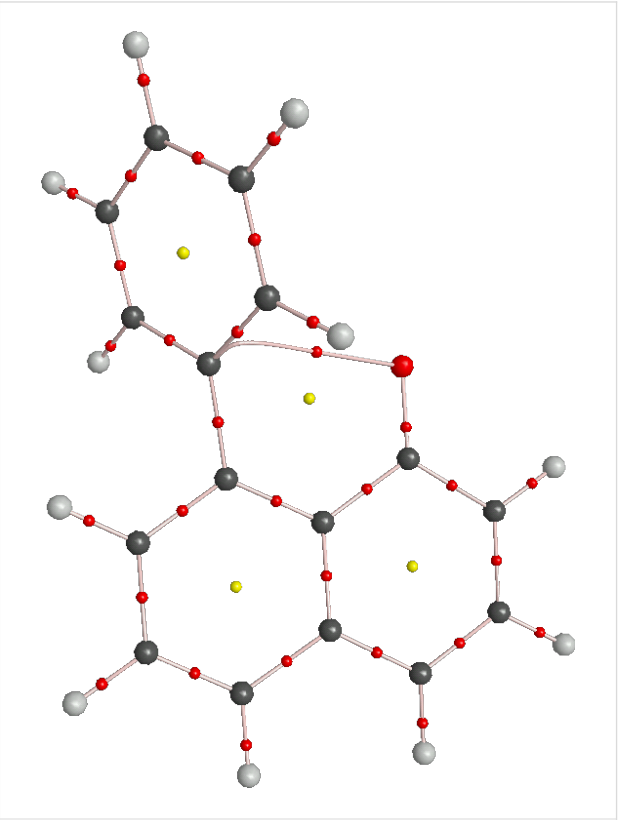

Figure 7: Bond critical points (red), ring critical points (yellow) and bond paths illustrated for the anion **8**, generated by AIM2000.

Conclusion

The effects of proximal aromatic residues on anions have been described in the literature extensively in the context of binding studies. We have examined one of the simplest reactions, proton abstraction, with the five 8-(4-R-phenyl)-1-naphthol derivatives **1**–**5**. These derivatives exhibit changes in their pK_a' values consistent with the changing electronic nature of R substituent, suggesting an anion–π effect in modulating the hydrogen abstraction process. Density functional calculations indicate that the change in reactivity is likely to be dependent on two factors: a stronger OH-C1' interaction with more electron-rich character, making the hydrogen more difficult to abstract, and an increased stability of the anion with electron-poor substituents, relative to electron-rich aromatics. AIM analysis revealed bond critical points that suggest that the OH-C1' interaction can indeed be classified as a bond, as well as an anion–π interaction between the anion oxygen and C1'. Such interactions are likely to have an impact on related reactions where anions are formed in close proximity to an aromatic ring and indicate that anion–π interactions could be used in supramolecular architectures to modulate reactivity. Likewise, interactions of this type may play a guiding role in some enzyme reactions.

Experimental

General

The ^{1}H and ^{13}C NMR spectra were recorded on a Bruker Avance 500 Digital NMR spectrometer at 500 MHz in $CDCl_3$. GC-MS spectra were recorded on an Agilent Technologies 6890N network GC system. All IR spectra were recorded on a Perkin Elmer 100 FT-IR spectrometer. The UV–vis spectra were recorded on a Unicam UV–vis spectrometer UV 4.

Pure 1-naphthol **6** was required to increase the yield of the desired product. Once exposed to air, over time, 1-naphthol **6** degrades to form impurities and the crystals change colour from white to dark grey. Crystals that were not white were purified by the following method [45]: 1-Naphthol (**6**) (3–4 g) was placed in the bottom of a purpose-built sublimator. Water pumps were attached to the sublimator and chilled water was run through the system. The system was then connected to a vacuum. The solid was then heated in an oil bath to 90 °C (just below the melting point of 1-naphthol of 95.5–96.0 °C); care was taken not to heat the oil bath above the melting point of naphthol. After 2 h the solid was removed from the heat and left to cool. Pale yellow crystals had formed on the cold finger. These crystals were placed in a round-bottomed flask (50 cm^3) and dissolved in hot 25% aq ethanol (5 cm^3). After the crystals had dissolved, they were left to cool in an ice bath and then filtered using a Buchner funnel. The crystals were washed with deionised water and dried for 24 h in a vacuum desiccator with P_2O_5 as the drying agent.

The DMF used for the reactions must be dry, as water must not enter the system while the reaction is taking place. Dry DMF was prepared by the following method:

DMF was run over silica gel and the run off collected in a round-bottomed flask. The flask was placed on a rotary evaporator and 10% of the liquid evaporated to remove any low boiling impurities (DMF has a high boiling point of 153 °C so any low boiling material can be considered as unwanted impurities). The dry DMF was stored over molecular sieves (3 Å) in a dark bottle below 5 °C. The DMF stayed dry for three weeks under these conditions. Before using the DMF the bottle was removed from the fridge and left to warm up to room temperature. If the bottle was opened whilst cold, condensation formed on the walls of the bottle and contaminated the DMF.

All other chemicals were used as supplied, with ^{1}H NMR spectra and either the melting points or boiling points of all materials recorded to confirm identity and purity.

Arylation of 1-naphthol

Cs_2CO_3 (10 mmol) was placed in a two-necked round-bottomed flask (100 cm^3) and dried in vacuo (150 °C, 2 h). $PdCl_2$ (0.125 mmol), 1-iodo-4-R-benzene **7** (6 mmol), naphthol **6** (5 mmol) and DMF (25 cm^3) were added to the pre-dried base. Upon addition of the reactants, the mixture turned dark green/black. The reaction mixture was stirred under a nitrogen atmosphere and heated (110 °C, 19–43 h, Table 4) then left to cool and extracted twice with diethyl ether (25 cm^3) and water (25 cm^3), and once with brine (25 cm^3). The extracts were dried with magnesium sulfate. The products (**1**–**5**) were isolated by column chromatography on silica gel with hexane/ethyl acetate as the eluent.

Table 4: Time taken for reaction to occur for each of the five derivaties of **1**–**5**.

Product	Reaction time (h)	Isolated yield (%)
1	19	81
4	39	45
3	21	68
5	43	46
2	42	77

8-phenyl-1-naphthol (1): Oil; ^{1}H NMR δ = 5.29 (s, 1H), 6.78 (d, 1H, *J* = 6.3 Hz), 7.05 (d, 1H, *J* = 6.9 Hz), 7.24 (t, 1H, *J* = 7.9 Hz), 7.28 (t, 1H, *J* = 8.2 Hz), 7.28–7.36 (m, 6H), 7.71 (d, 1H, *J* = 6.5 Hz) ppm; ^{13}C NMR δ = 111.9, 121.3, 125.0, 127.0, 128.7, 129.1, 135.9, 141.5, 153.2 ppm.

8-(4-nitrophenyl)-1-naphthol (2): mp 135–135.5 °C; ^{1}H NMR δ = 7.02 (d, 2H, *J* = 9.15 Hz), 7.17 (s, 1H), 7.50 (m, 3H), 7.79 (d, 1H, *J* = 8.5 Hz), 7.93 (d, 2H, *J* = 9.15 Hz), 8.20 (d, 2H, *J* = 9.45 Hz) ppm; ^{13}C NMR δ = 116.6, 121.6, 125.8, 125.9, 126.1, 126.7, 126.9, 127.0, 128.2, 135.2, 150.4 ppm; IR (nujol mull) ν: 2000–1650, 1592, 1507, 1488, 1342, 1244 cm^{-1}; MS *m*/*z* 265 (M$^+$).

8-(4-chlorophenyl)-1-naphthol (3): mp 44–46 °C; ^{1}H NMR δ = 5.20 (s, 1H), 6.92 (dd, 1H, *J* = 0.95, 7.55 Hz), 7.18 (dd, 1H, *J* = 0.95, 6.95 Hz), 7.39–7.46 (m, 7H), 7.86 (dd, 1H, *J* = 0.95, 8.2 Hz) ppm; ^{13}C NMR δ = 112.1, 121.4, 125.1, 127.0, 128.9, 130.9, 134.7, 135.9, 140.2, 152.8 ppm; IR (nujol mull) ν: 3548, 2000–1650, 1526, 1488, 1457 cm^{-1}; MS *m*/*z* 254 (M$^+$).

8-(4-methylphenyl)-1-naphthol (4): mp 77–79 °C; ^{1}H NMR δ = 2.46 (s, 3H), 5.56 (s, 1H), 6.91 (dd, 1H, *J* = 1.25, 6.3 Hz), 7.18 (dd, 1H, *J* = 1.25, 6.9 Hz), 7.41 (d, 2H, *J* = 7.85 Hz), 7.42–7.49 (m, 5H), 7.85 (dd, 1H, *J* = 1.25, 7.25 Hz) ppm; ^{13}C NMR δ = 21.4, 111.8, 121.4, 125.0, 127.0, 128.6, 136.3, 138.3, 138.8, 153.3 ppm; IR (nujol mull) ν: 3532, 1582, 1262, 822; MS *m*/*z* 234 (M$^+$).

8-(4-methoxyphenyl)-1-naphthol (5): mp 167–168 °C; ^{1}H NMR δ = 1.60 (s, 3H), 3.90 (s, 1H), 5.26 (dd, 1H, *J* = 0.95, 8.85 Hz), 6.81–7.33 (m, 7H), 7.81 (dd, 1H, *J* = 0.95, 9.45 Hz), 8.18 (dd, 1H, *J* = 0.95, 9.15 Hz) ppm; ^{13}C NMR δ = 55.5, 108.7, 111.8, 114.6, 120.8, 121.7, 124.5, 125.4, 127.8, 134.9 ppm; IR (nujol mull) ν: 3516, 2000–1650, 1539, 1464, 1377 cm^{-1}; MS *m*/*z* 250 (M$^+$).

Measurement of pK_a values

The pK_a values for the derivatives **1**–**5** dissolved in 50:50 water/acetonitrile solution were determined by potentiometric titration using a PHM210 Standard lab pH meter that had been calibrated against standards (pH 4 and pH 7). The electrode was first placed in 50 ml of a known concentration of an acid **1**–**5** and the solution was constantly stirred to ensure equilibration. To this sample of **1**–**5**, 20 μL aliquots of TBAH (0.034 mol·L^{-1}, 50:50 water/acetonitrile) were added. The solution was allowed to equilibrate for 30 s after each addition, and the pH was recorded. This process was repeated until three millilitres of base had been added, which corresponded to a molar ratio of base to acid of approximately 3:1, depending on the acid. This ratio was more than sufficient to fully deprotonate the acid as the half way neutralisation point (HNP) occurs when the ratio is 1:1. This process was carried out in triplicate for all of the derivatives and the results were averaged out over all three titrations.

The action of TBAH was confirmed through UV–vis spectroscopy. First the molar absorption coefficient (ε) for each acid **1**–**5** was determined by producing standard curves from known acid concentrations ranging from 4 × 10^{-4} to 1 × 10^{-4} by applying the Beer–Lambert law. The UV–vis spectra of all five derivatives of **1**–**5** showed a shift in the λ_{max} value upon addition of TBAH. This shift and the corresponding molar absorption coefficients are presented in Table 5.

Calculation of 1,8-disubstituted naphthols 1–5 and their corresponding anions **8**–**12**

DFT calculations were performed using the Gaussian 09 package [46]. The parameterised functional M06-2X with the 6-31+G(d,p) basis set was used for geometry optimisations. All optimised structures are local minima, as confirmed by frequency calculations. The minimum energy conformers of all molecules examined have C_1 symmetry. Vibrational frequen-

Table 5: Table indicating the standard concentrations to use for the titrations along with the relevant UV–vis spectral data.

Derivative	Concentration ($\times 10^{-4}$ mol·L^{-1})	λ_{max} of acid (nm)	ε of acid (mol·L^{-1}·cm^{-1})	λ_{max} of deprotonated acid (nm)	ε of deprotonated acid (mol·L^{-1}·cm^{-1})
6	3	296	7640	332	38660
1	2.5	308	6753	332	4265
2	1.5	292	34240	304	2069
3	2	348	1298	308	19790
4	2	316	6242	304	10720
5	4	292	2324	296	3595

cies and zero point energies were calculated by the M06-2X method, and scaled by 0.9670 [36]. AIM analyses were performed using XAim on Gaussian wfn output to examine densities and laplacians [47], and AIM2000 to identify critical points [48]. To generate the wfn files, M06-2X/6-311+G(3df,2p) single point energies were calculated.

Supporting Information

Supporting Information File 1

Structural data for compounds **1**–**6** and **8**–**12** optimised at M06-2X/6-31+G(d,p).
[http://www.beilstein-journals.org/bjoc/content/supplementary/1860-5397-7-42-S1.doc]

Supporting Information File 2

Original spectral data for compounds **1**–**5**.
[http://www.beilstein-journals.org/bjoc/content/supplementary/1860-5397-7-42-S2.pdf]

Supporting Information File 3

Molecular graphs for molecules **1**(a)-**5**(a) and **8**-**12**.
[http://www.beilstein-journals.org/bjoc/content/supplementary/1860-5397-7-42-S3.pdf]

Supporting Information File 4

Crystal information file for compound **4**.
[http://www.beilstein-journals.org/bjoc/content/supplementary/1860-5397-7-42-S4.cif]

Supporting Information File 5

Crystal information data file for compound **4**.
[http://www.beilstein-journals.org/bjoc/content/supplementary/1860-5397-7-42-S5.cif]

Supporting Information File 6

Crystal structure refinement details for compound **4**.
[http://www.beilstein-journals.org/bjoc/content/supplementary/1860-5397-7-42-S6.pdf]

Acknowledgements

The authors wish to thank the European Union (COST CM0603) for financial support and the award of an STSM to CJC. The authors would also like to thank Richard Grainger, Chris Hunter and Jason Harper for useful discussions and Greg Chass for assistance with AIM2000. This research was also supported in part by the National Science Foundation through TeraGrid resources provided by NCSA under grant number TG-MCB100077. The X-ray crystallographic structure of **4** was provided by Graham Tizzard of the EPSRC National Crystallographic Service at Southampton.

References

1. Meyer, E. A.; Castellano, R. K.; Diederich, F. *Angew. Chem., Int. Ed. Engl.* **2003,** *42,* 1210. doi:10.1002/anie.200390319
2. Quiñonero, D.; Garau, C.; Rotger, C.; Frontera, A.; Ballester, P.; Costa, A.; Deyà, P. M. *Angew. Chem., Int. Ed. Engl.* **2002,** *41,* 3389. doi:10.1002/1521-3773(20020916)41:18<3389::AID-ANIE3389>3.0.CO;2-S
3. Quiñonero, D.; Garau, C.; Frontera, A.; Ballester, P.; Costa, A.; Deyà, P. M. *Chem. Phys. Lett.* **2002,** *359,* 486. doi:10.1016/S0009-2614(02)00709-1
4. Mascal, M.; Armstrong, A.; Bartberger, M. D. *J. Am. Chem. Soc.* **2002,** *124,* 6274. doi:10.1021/ja017449s
5. Ahuja, R.; Samuelson, A. G. *CrystEngComm* **2003,** *5,* 395. doi:10.1039/b311000a
6. Casellas, H.; Massera, C.; Buda, F.; Gamez, P.; Reedijk, J. *New J. Chem.* **2006,** *30,* 1561. doi:10.1039/b608172j
7. Frontera, A.; Saczewski, F.; Gdaniec, M.; Dziemidowicz-Borys, E.; Kurland, A.; Deyà, P. M.; Quiñonero, D.; Garau, C. *Chem.–Eur. J.* **2005,** *11,* 6560. doi:10.1002/chem.200500783
8. Gamez, P.; Mooibroek, T. J.; Teat, S. J.; Reedijk, J. *Acc. Chem. Res.* **2007,** *40,* 435. doi:10.1021/ar7000099
9. Black, C. A.; Hanton, L. R.; Spicer, M. D. *Chem. Commun.* **2007,** 3171. doi:10.1039/b703522e
10. Rosokha, Y. S.; Lindeman, S. V.; Rosokha, S. V.; Kochi, J. K. *Angew. Chem., Int. Ed. Engl.* **2004,** *43,* 4650. doi:10.1002/anie.200460337
11. Ilioudis, C. A.; Tocher, D. A.; Steed, J. W. *J. Am. Chem. Soc.* **2004,** *126,* 12395. doi:10.1021/ja047070g
12. Das, A.; Choudhury, S. R.; Dey, B.; Yalamanchili, S. K.; Helliwell, M.; Gamez, P.; Mukhopadhyay, S.; Estarellas, C.; Frontera, A. *J. Phys. Chem. B* **2010,** *114,* 4998. doi:10.1021/jp911884x

13. Hung, C.-Y.; Singh, A. S.; Chen, C.-W.; Wen, Y.-S.; Sun, S.-S. *Chem. Commun.* **2009,** 1511. doi:10.1039/b820234f
14. Gural'skiy, I. A.; Escudero, D.; Frontera, A.; Solntsev, P. V.; Rusanov, E. B.; Chernega, A. N.; Krautscheid, H.; Domasevitch, K. V. *Dalton Trans.* **2009,** 2856. doi:10.1039/b818125j
15. Manzano, B. R.; Jalón, F. A.; Ortiz, I. M.; Soriano, M. L.; de la Torre, F. G.; Elguero, J.; Maestro, M. A.; Mereiter, K.; Claridge, T. D. *Inorg. Chem.* **2008,** *47,* 413. doi:10.1021/ic701117a
16. Zuo, C.-S.; Quan, J.-M.; Wu, Y.-D. *Org. Lett.* **2007,** *9,* 4219. doi:10.1021/ol701740p
17. Mascal, M.; Yakovlev, I.; Nikitin, E. B.; Fettinger, J. C. *Angew. Chem., Int. Ed. Engl.* **2007,** *46,* 8782. doi:10.1002/anie.200704005
18. Gil-Ramírez, G.; Escudero-Adán, E. C.; Benet-Buchholz, J.; Ballester, P. *Angew. Chem., Int. Ed. Engl.* **2008,** *47,* 4114. doi:10.1002/anie.200800636
19. Quiñonero, D.; Deyà, P. M.; Carranza, M. P.; Rodríguez, A. M.; Jalón, F. A.; Manzano, B. R. *Dalton Trans.* **2010,** *39,* 794. doi:10.1039/b915794h
20. Lucas, X.; Estarellas, C.; Escudero, D.; Frontera, A.; Quiñonero, D.; Deyà, P. M. *ChemPhysChem* **2009,** *10,* 2256. doi:10.1002/cphc.200900157
21. Cram, D. J.; Goldstein, M. *J. Am. Chem. Soc.* **1963,** *85,* 1063. doi:10.1021/ja00891a009
22. Cabellero, A. G.; Croft, A. K.; Nalli, S. M. *Tetrahedron Lett.* **2008,** *49,* 3613. doi:10.1016/j.tetlet.2008.04.009
23. Jones, S. G.; Yau, H. M.; Davies, E.; Hook, J. M.; Youngs, T. G. A.; Harper, J. B.; Croft, A. K. *Phys. Chem. Chem. Phys.* **2010,** *12,* 1873. doi:10.1039/b919831h
24. Estarellas, C.; Frontera, A.; Quiñonero, D.; Deyà, P. M. *Angew. Chem., Int. Ed. Engl.* **2011,** *50,* 415. doi:10.1002/anie.201005635
25. Cozzi, F.; Cinquini, M.; Annuziata, R.; Siegel, J. S. *J. Am. Chem. Soc.* **1993,** *115,* 5330. doi:10.1021/ja00065a069
26. Cozzi, F.; Cinquini, M.; Annunziata, R.; Dwyer, T.; Siegel, J. S. *J. Am. Chem. Soc.* **1992,** *114,* 5729. doi:10.1021/ja00040a036
27. Asaad, N.; Davies, J. E.; Hodgson, D. R. W.; Kirby, A. J.; van Vliet, L.; Ottavi, L. *J. Phys. Org. Chem.* **2005,** *18,* 101. doi:10.1002/poc.858
28. Asaad, N.; Kirby, A. J. *J. Chem. Soc., Perkin Trans. 2* **2002,** 1708. doi:10.1039/b204609a
29. Zhao, Y.; Truhlar, D. G. *Theor. Chem. Acc.* **2008,** *120,* 215. doi:10.1007/s00214-007-0310-x
30. Bader, R. *Atoms in molecules: a quantum theory;* Clarendon Press, 1994.
31. Satoh, T.; Inoh, J.-i.; Kawamura, Y.; Kawamura, Y.; Miura, M.; Nomura, M. *Bull. Chem. Soc. Jpn.* **1998,** *71,* 2239. doi:10.1246/bcsj.71.2239
32. Cruces Blanco, C.; Garcia Sanchez, F. *J. Photochem. Photobiol., A: Chem.* **1988,** *42,* 357. doi:10.1016/1010-6030(88)80079-0
33. Bhattacharyya, K. In *Reviews in Fluorescence 2005;* Geddes, C. D.; Lakowicz, J. R., Eds.; Springer: New York, NY, 2005; Vol. 2005, pp 1 ff. doi:10.1007/0-387-23690-2_1
34. Hansch, C.; Leo, A.; Taft, R. W. *Chem. Rev.* **1991,** *91,* 165. doi:10.1021/cr00002a004
35. Riley, K. E.; Pitoňák, M.; Jurečka, P.; Hobza, P. *Chem. Rev.* **2010,** *110,* 5023. doi:10.1021/cr1000173
36. Alecu, I. M.; Zheng, J.; Zhao, Y.; Truhlar, D. G. *J. Chem. Theory Comput.* **2010,** *6,* 2872. doi:10.1021/ct100326h
37. Kirby, A. J. In *Adv. Phys. Org. Chem.;* Gold, V.; Bethell, D., Eds.; Academic Press, 1981; Vol. 17, pp 183 ff.
38. Adams, R.; Yuan, H. C. *Chem. Rev.* **1933,** *12,* 261. doi:10.1021/cr60042a003
39. Oki, M.; Iwamura, H.; Yamamoto, G. *Bull. Chem. Soc. Jpn.* **1971,** *44,* 262. doi:10.1246/bcsj.44.262
40. Ruiz, R.; Rosés, M.; Ràfols, C.; Bosch, E. *Anal. Chim. Acta* **2005,** *550,* 210. doi:10.1016/j.aca.2005.06.058
41. Wróbel, R.; Chmurzyński, L. *Anal. Chim. Acta* **2000,** *405,* 303. doi:10.1016/S0003-2670(99)00737-0
42. Serin, S.; Kurtoğlu, M. *Analyst* **1994,** *119,* 2213. doi:10.1039/an9941902213
43. *CRC Handbook of Chemistry and Physics,* 85th ed.; CRC Press: Cleveland; Ohio, 2004.
44. Coetzee, J. F.; Padmanabhan, G. R. *J. Am. Chem. Soc.* **1965,** *87,* 5005. doi:10.1021/ja00950a006
45. Perrin, D. D.; Armarego, W. L. F. *Purification of laboratory chemicals,* 3rd ed.; Pergamon Press: New York, 1988.
46. *Gaussian 09,* Revision A.02; Gaussian, Inc.: Wallingford, CT, 2009.
47. *XAim;* Tarragona, Spain, 2010.
48. *AIM2000;* Büro für Innovative Software: Bielefeld, Germany, 2002.

License and Terms

Beilstein Journal of Organic Chemistry

Molecular rearrangements of superelectrophiles

Douglas A. Klumpp

Review

Open Access

Address:
Department of Chemistry and Biochemistry, Northern Illinois University, DeKalb, Il 60115

Email:
Douglas A. Klumpp - dklumpp@niu.edu

Keywords:
dication; rearrangement; superacid; superelectrophile

Beilstein J. Org. Chem. **2011,** *7,* 346–363.
doi:10.3762/bjoc.7.45

Received: 15 December 2010
Accepted: 02 March 2011
Published: 23 March 2011

This article is part of the Thematic Series "Physical organic chemistry".

Guest Editor: J. Murphy

Abstract

Superelectrophiles are multiply charged cationic species (dications, trications, etc.) which are characterized by their reactions with weak nucleophiles. These reactive intermediates may also undergo a wide variety of rearrangement-type reactions. Superelectrophilic rearrangements are often driven by charge–charge repulsive effects, as these densely charged ions react so as to maximize the distances between charge centers. These rearrangements involve reaction steps similar to monocationic rearrangements, such as alkyl group shifts, Wagner–Meerwein shifts, hydride shifts, ring opening reactions, and other skeletal rearrangements. This review will describe these types of superelectrophilic reactions.

Introduction

The Knorr cyclization is a classical method for preparing quinol-2-ones from β-ketoamides [1]. In 1964, Staskin published a report describing his studies of the Knorr cyclization and noted that the conversion works best with more than 1.0 equiv of Brønsted or Lewis acids [2]. To explain this observation, he suggested a mechanism involving the double protonation of the β-ketoamide to form a dicationic electrophile. A similar mechanism was proposed in which two molecules of Lewis acid were complexed to the β-ketoamide. This manuscript suggested the importance of dicationic intermediates in organic reactions. Other classical conversions, such as the Grewe cyclization [3], clearly involved reactive dicationic intermediates, but until recently there was little or no recognition of these intermediates.

During the 1970s, Brouwer and Kiffin reported [4-6] the reactions of branched alkanes with acetyl cation (CH_3CO^+) salts in $HF{\cdot}BF_3$. These studies showed that acetyl cation (CH_3CO^+) salts were capable of abstracting hydride from the isoalkanes when the reactions were performed in superacdic media. Studies by Olah and coworkers had shown [7] that acetyl cation salts do not react with isoalkanes in aprotic solvents (SO_2, SO_2ClF, or CH_2Cl_2). To account for the observed increasing electrophilic reactivities, Olah proposed the concept of superelectrophilic activation [7]. It was suggested that the superacidic media interacts with the non-bonding electron pairs of the acetyl cation (**1**), to generate a protosolvated superelectrophile (**2** or **3**, Scheme 1). Protosolvation of the acetyl cation produces an electrophile with increasing dicationic character and conse-

quently superelectrophilic reactivity. Since Olah's proposal of superelectrophilic activation, the role of dicationic intermediates has become more widely appreciated and it is shown to involve both Brønsted and Lewis acids [8]. Moreover, superelectrophiles have been utilized in many synthetic conversions. While these reactions are often carried out in superacids, less acidic media (CF_3CO_2H, H_2SO_4, $BF_3{\cdot}H_2O$, and solid acids) have also been shown to produce superelectrophiles [9-11].

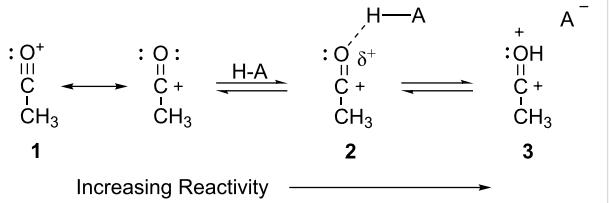

Scheme 1: Superelectrophilic activation of the acetyl cation.

Olah has proposed [8] categories for superelectrophiles, organized according to their structures and the approximate distance between the charge centers (Table 1).

The two basic categories are the *gitionic* and *distonic* superelectrophiles. Gitionic (close) superelectrophiles are characterized by the charge centers being separated by no more than one carbon atom or heteroatom. They are further distinguished by the distance between charges: *Geminal* systems (**4** and **5**) have the charges located around a single atom whilst *vicinal* systems (**6** and **7**) are represented as 1,2-dications. The 1,3-dicationic systems (**8** and **9**) are also considered gitionic superelectrophiles. It is understood that various factors (including charge delocalization) makes such a classification approximate. Distonic (distant) superelectrophiles are characterized by structures having charges separated by 2 or more carbon atoms or heteroatoms (i.e., **10** and **11**). The distonic superelectrophiles are distinguished from other types of onium dications, those in which the onium charge centers are isolated electrophilic sites. In such cases, the onium dications exhibit chemistry that is little different than monocationic electrophiles. Superelectrophiles may also involve hypervalent species, such as protosolvated *tert*-butyl cation (**7**).

Superelectrophiles are characterized by several types of reactions [8]. As very powerful electrophiles, they are best known for their reactions with weak nucleophiles, such as arenes and alkanes. This has led to the development of several new synthetic transformations leading to the functionalization of alkanes. Moreover, superelectrophiles have been used to prepare a wide variety of functionalized arenes. Many types of Friedel–Crafts type reactions have been developed. Among the useful Friedel–Crafts reactions, a large number of cyclizations have been developed, including efficient routes to heterocyclic systems [12]. Several reports have also described superelectrophiles participating in concerted reactions, such as the Nazarov cyclization [13]. Because superelectrophiles are often densely charged species, they are also known for their tendencies to undergo rearrangement and charge migration reactions. These types of conversions will be examined in this review article, including ring opening reactions, carbon–carbon bond shifts, skeletal rearrangements, and charge migrations or hydride shifts. Simple Friedel–Crafts type reactions and cyclizations will not be covered.

Review

Ring opening reactions

Several types of superelectrophiles are known to undergo ring opening reactions. The ring opening reaction step can be followed by the reaction with a nucleophile. For example, 2-oxazolines were shown [14] to form products with arenes and a mechanism was proposed involving ring opening of the superelectrophile (**13**, Scheme 2).

Table 1: Representative examples and categories of superelectrophiles.

gitionic superelectrophiles			distonic superelectrophiles
geminal	*vicinal*	1,3-dicationic	
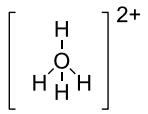	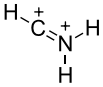	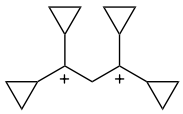	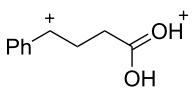
4	**6**	**8**	**10**
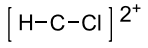	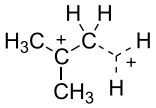	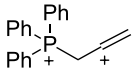	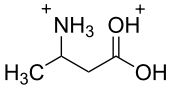
5	**7**	**9**	**11**

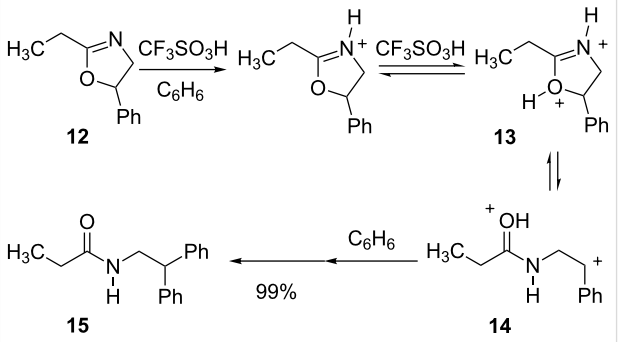

Scheme 2: Ring opening of diprotonated 2-oxazolines.

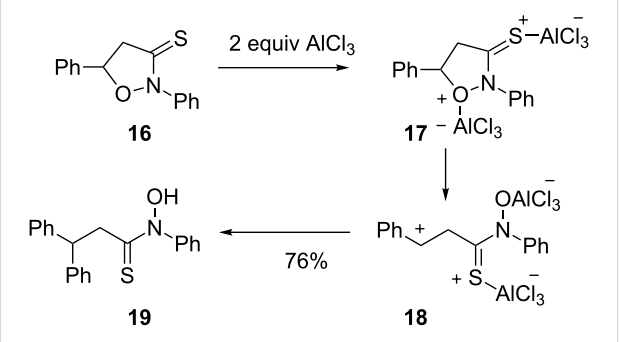

Scheme 3: $AlCl_3$-promoted ring opening of isoxaolidine **16**.

The ring opening step effectively separates the positive charge centers, as the superelectrophile isomerizes from a 1,3-dication **13** to a 1,5-dication **14**. Subsequent reaction with benzene yields the final product. Using the same chemistry, a chiral 2-oxazoline was shown to give a Friedel–Crafts product in modest diastereoselectivity. A similar reaction was reported [15] in the $AlCl_3$-catalyzed reactions of isoxazolidines (Scheme 3). Product conversion required excess amounts of acid, suggesting a mechanism involving superelectrophile **17**. Ring opening to give **18** followed by reaction with benzene afforded **19** in good yield.

In a similar respect, 2-phenylcyclopropanecarboxylic acid (**20**) undergoes diprotonation with ring opening to form the distonic superelectrophile **22** (Scheme 4) [16]. Initial protonation is assumed to occur at the carboxylic acid group to produce **21** followed by protonation of the cyclopropyl ring to give **22**. Protonation at the C1–C2 bond produces a dicationic species with the largest possible charge separation (1,5-dication). Reaction with benzene and cyclization affords the final product **23**. Interestingly, a similar reaction with *trans*-2- phenylcyclopropylamine hydrochloride **24** leads to cleavage of the C2–C3 bond and formation of the 1,3-dication **25** [17]. Protonation of the C1–C2 bond would provide the 1,4-dication **27**, however, this is not observed. It is proposed that the adjacent ammonium group decreases the basicity of the C1–C2 bond in **24**, leading to protonation at the more distant C2–C3 bond. The final product is formed by reaction of benzene at the carbocation site.

A number of superelectrophilic ring opening reactions are followed by ring closure steps. For example, ninhydrin (**28**) was shown [18] to give condensation products with arenes in acid-

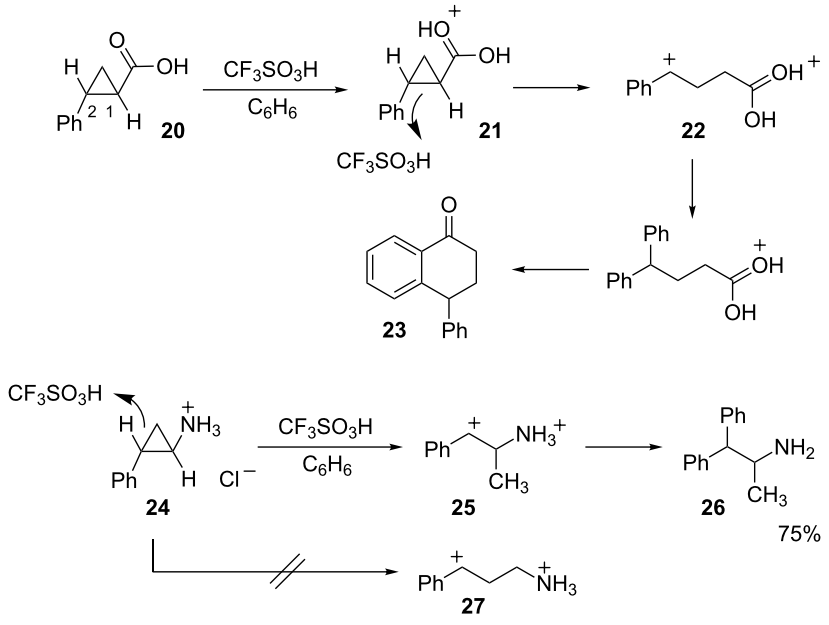

Scheme 4: Ring-opening reactions of cyclopropyl derivatives.

promoted reactions. In H_2SO_4, the product **29** is obtained via a simple condensation reaction at the C-2 *gem*-diol group (Scheme 5). When superacidic CF_3SO_3H is used, ninhydrin yields 3-(diphenylmethylene)isobenzofuranone (**30**). If product **29** is isolated and then treated with superacid, **30** is obtained as the sole reaction product.

A mechanism for this conversion is proposed which involves the formation of the *O*,*O*-diprotonated superelectrophile **32** with subsequent ring opening and closing reaction steps (Scheme 6). The mechanism can be understood as a consequence of maximizing charge separation and enabling the charge to have resonance stabilization (i.e., **33**) with two phenyl rings.

Succinic anhydride (**33**) reacts in FSO_3H-SbF_5-SO_2ClF solution (Scheme 7) to give the acylium–carboxonium dication **34** which is a stable species at –80 °C [19]. Warming the solution leads to an equilibration between acylium–carboxonium dications and the bis-carboxonium dication.

A similar degenerate rearrangement has also been described for glutaric anhydride in superacid. Phthalic acid (**36**) also undergoes a dicationic rearrangement via the anhydride (Scheme 8) [20]. Diprotonated phthalic acid **37** is observed by low temperature ^1H and ^{13}C NMR. When the solution of **37** is warmed, new signals appear which have been assigned to the cleavage product, the acylium–carboxonium dication **38**. NMR evidence suggests the degenerate rearrangement proceeds via the anhydride derivative **39**.

Carbon migrations and other skeletal rearrangements

Among the reactions of superelectrophiles, a significant number involve the migration of carbon atoms or heteroatoms. For

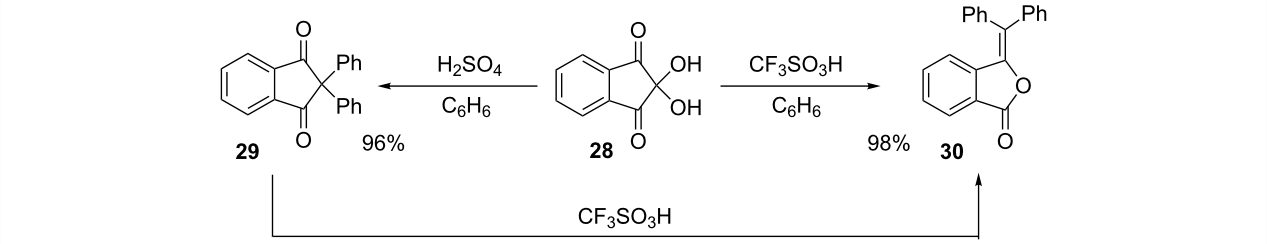

Scheme 5: Condensations of ninhydrin (**28**) with benzene.

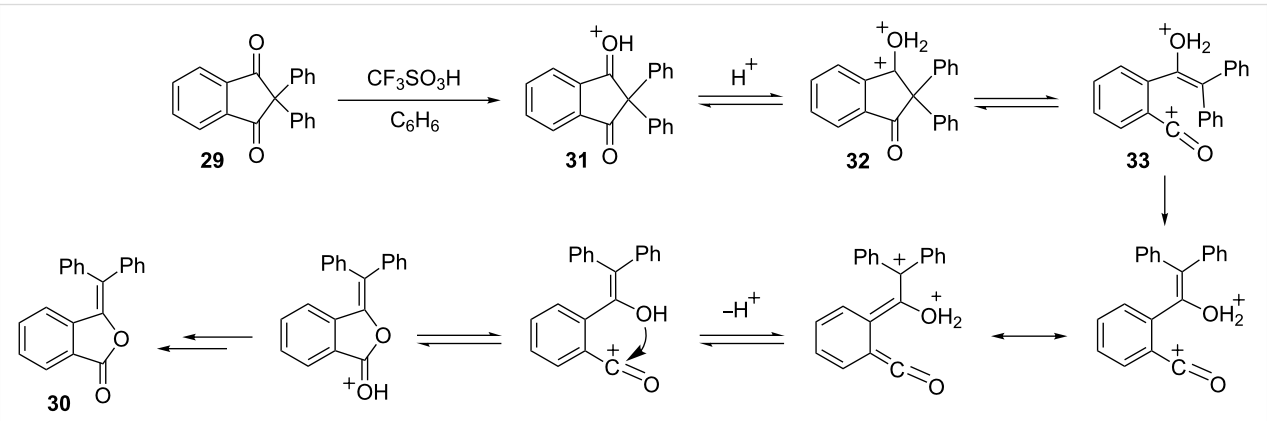

Scheme 6: Rearrangement of **29** to **30**.

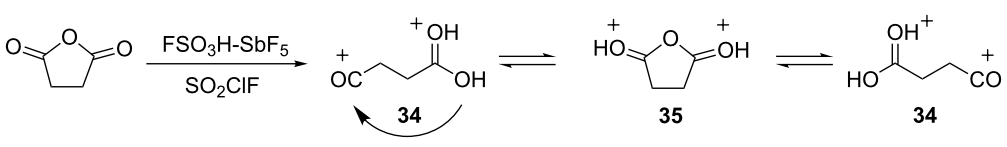

Scheme 7: Superacid promoted ring opening of succinic anhydride (**33**).

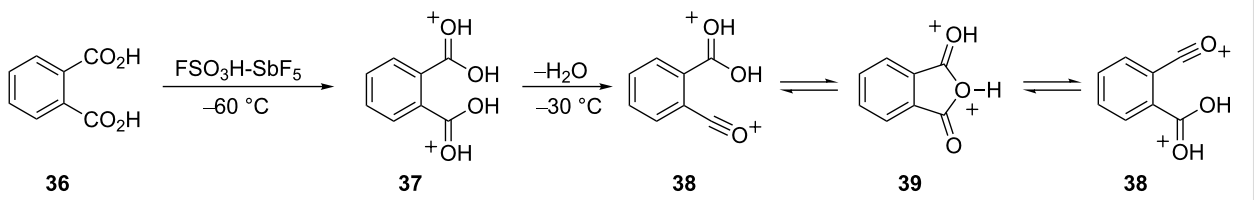

Scheme 8: Reaction of phthalic acid (**36**) in FSO_3H-SbF_5.

example, ring expansions reactions have been reported for superelectrophiles. In the synthesis of the analgesic drug butorphanol (**40**) [21], a key step involves the ring expansion of dication **42** to dication **43** (Scheme 9). Interestingly, the ring expansion step moves the carbocationic site away from a benzylic position, but also transforms it from a 1,4-dication to a 1,5-dication. This suggests charge–charge repulsive effects in this system.

When camphor (**44**) is reacted with HF-SbF_5, three products are isolated (Scheme 10) [22]. A mechanism is proposed for conversion of ketone **45** to enone **47**. Initially, the carboxonium ion **45a** is formed by protonation of the carbonyl oxygen. A second protonation occurs in the superacid to produce the carboxonium-carbonium dication **45b** and this species isomerizes to the *tertiary*-carbenium ion by a Wagner–Meerwein shift. Although this isomerization converts a 1,5-dication to a 1,4-dication, the decreasing charge separation is compensated by the formation of a *tertiary*-carbenium ion **45c** which ultimately leads to the stable enone structure **47**.

When 2-cyclohexen-1-one (**47**) is reacted with HF-SbF_5, a ring contraction occurs to give 3-methyl-2-cyclopenten-1-one (**50**, Scheme 11) [23]. This conversion involves diprotonation of **48** to give a superelectrophile, which undergoes rearrangement via the protonated cyclopropyl derivative **49**. Final reaction steps include a hydride shift and deprotonations to give **50**.

Jacquesy and coworkers [24] have investigated the chemistry of polycyclic ketones in HF-SbF_5-CCl_4, a powerful reagent combination for dehydrogenation. For example, 2-decalone (**51**) (primarily *trans*) was reacted with HF-SbF_5-CCl_4 at 0 °C to give products **52** and **53** in 25% and 12% yields, respectively (Scheme 12). The proposed mechanism involves protonation and hydride abstraction to give superelectrophile **54**. It is notable that the carbocation forms in the 6- or 7-position on the decalone ring, as this provides maximum separation of the cationic centers. In accord with other carbocation rearrangements, the superelectrophile **54** (a 2° carbocation) isomerizes to **56** (a 3° carbocation). This likely occurs through the ring-fused, protonated cyclopropane **55**. Subsequent deprotonation and hydride abstractions steps give the final product **52**. A similar series of reactions affords the isomeric product **53**.

An interesting rearrangement and cyclization of an acyl dication has been reported [25]. Ionization of the acid chloride **57** in superacid (FSO_3H-SbF_5 or HF-SbF_5) leads to formation of two ions, **60** and **63**, which are observable by NMR spectroscopy

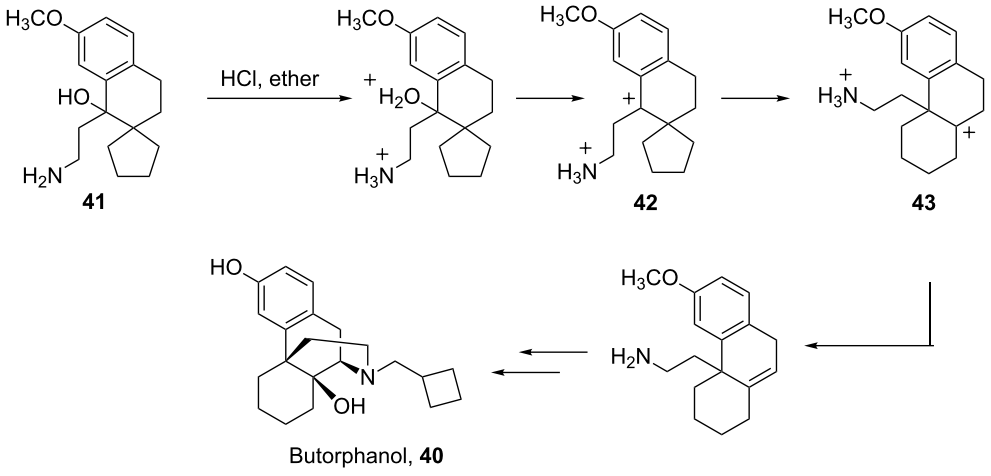

Scheme 9: Ring expansion of superelectrophile **42**.

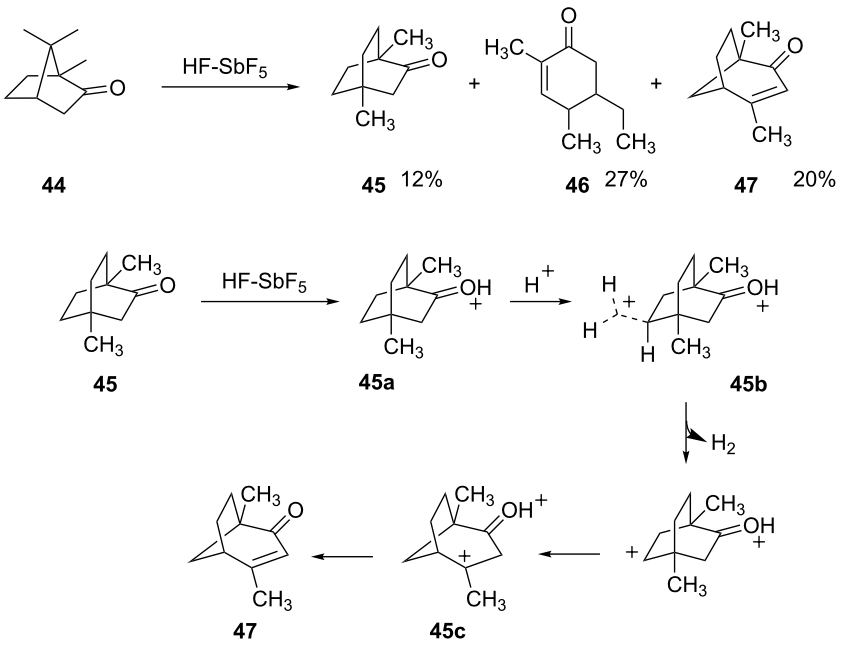

Scheme 10: Reaction of camphor (**44**) in superacid.

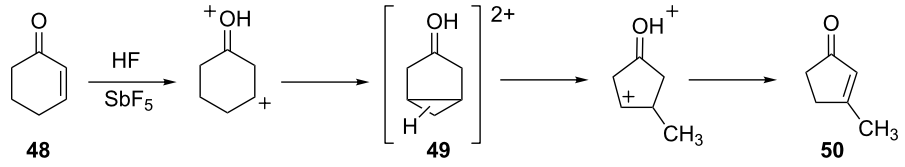

Scheme 11: Isomerization of 2-cyclohexen-1-one (**48**).

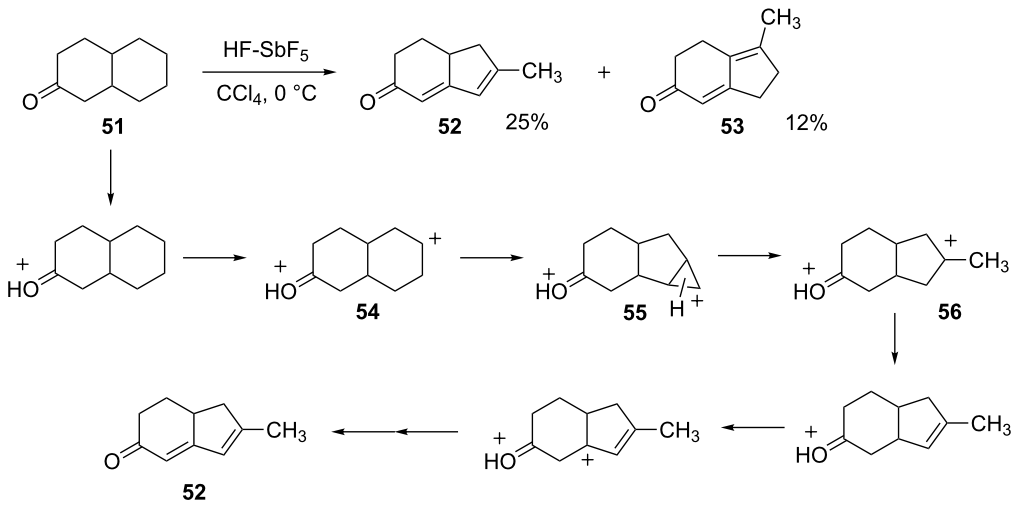

Scheme 12: Isomerization of 2-decalone (**51**).

(Scheme 13). It was proposed that these ions are formed via superelectrophile **58** by competing hydride and methyl shifts. Following the methyl shift, the acyl cations **61** and **62** are formed. Cyclization then gives the cyclopentenone derivative **63**.

Carbonylation of superelectrophiles has been shown to give acids and esters in good yields [26]. A rearrangement was described in the carbonylations of dialkyl ketones in HF-SbF_5 (Scheme 14). Thus, ketone **64** reacts at 20 °C to give **65–67** as products of carbonylation. At this temperature, the rearrangement product **67** is the major product, whilst at −20 °C compound **65** is the major product. The formation of these products can be understood to be the result of two reactions with the superacid: Protonation of the carbonyl group and protolysis of C–H σ-bonds. As a relatively strong base site, the ketone is completely protonated in the superacid to give the carboxonium ion **68**. In the protolysis steps, there is a strong preference to generate the second cationic charge at a site distant from the carboxonium center. Protolysis of the methyl group C–H σ-bonds (i.e., **69**) yields superelectrophile **70** by migration of the methyl group. Protolysis also occurs at the methine position (**72**) which leads directly to superelectrophile **73**. Ions **70** and **73** react with carbon monoxide to give products **66** and **65**, respectively, on aqueous workup. The major product **67** evidently arises from hydride migration in **70** to give dication **71**. This step should be favorable because it increases the distance between charge centers. Although a hydride shift is the most direct route from **70** to **71**, this isomerization may also occur through deprotonation and reprotonation steps. As noted by the authors of this study, protolysis steps with alkanes often leads to β-scission reactions (cleavage of the alkane-based carbocations). This reaction path is not observed with superelectrophiles **70**, **71**, or **73**, because these types of cleavage reactions would generate dicationic species with the cationic charges in closer proximity. Consequently, the carboxonium ion has two interesting effects in this superelectrophilic chemistry. It directs protolysis to the most distant site(s) and it "protects" the alkyl chain from cleavage in the superacid.

A series of ozone-based oxidation-rearrangements have been reported by Olah and coworkers some of which involve superelectrophiles [27]. In the presence of Brønsted superacids, ozone is protonated and the resulting ion (O_3H^+) is a highly reactive electrophilic species, capable of inserting into C–C and

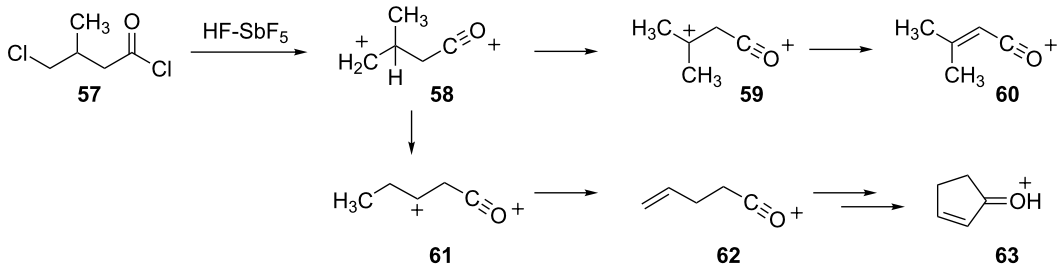

Scheme 13: Rearrangement of the acyl-dication **58**.

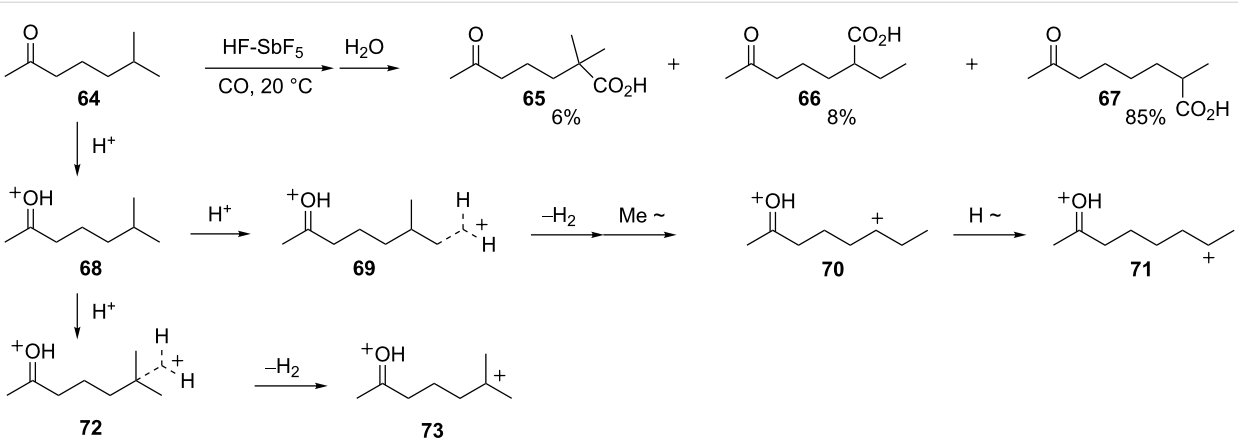

Scheme 14: Reaction of dialkylketone **64**.

C–H σ-bonds in alkanes or alkyl groups. With another ionizable group present in the substrate, dicationic species can be produced. For example, the pentan-1-ol derivative **74** reacts with ozone in magic acid to yield dication **75** quantitatively (Scheme 15). This conversion involves protonation of the hydroxy group to give the oxonium ion **76** and reaction of O_3H^+ at the methine center of **76**. The loss of hydrogen peroxide affords the oxygen-centered cation **78** and subsequent migration of the adjacent group gives dication **75**.

Whittaker and Carr have described a series of superacid-promoted reactions to prepare bicyclic lactones [28]. Several of the conversions involve superelectrophilic rearrangements. Ionization of the 1-hydroxy-2-methylcyclohexane carboxylic acid (**79**) in FSO_3H-SO_3 at –20 °C leads to a mixture of three ions **80**–**82** (Scheme 16). For ion **80**, a mechanism was proposed which involves initial formation of superelectrophile **83** followed by methyl group migration to produce dication **84** and successive hydride shifts to give **85** which on ring closure affords the protonated lactone **80**.

A novel isomerization of a bicyclic ring system was described [29] for the 1,5-manxyl dication (**87,** Scheme 17). Ionization of the dichloride **86** in SbF_5-SO_2ClF gave the 1,5-manxyl dication (**87**) which was found to be stable at −105 °C. However, upon warming to −60 °C, the 3,7-dimethylbicyclo[3.3.1]nona-3,7-diyl dication (**88**) was formed.

This isomerization is thought to occur through a series of hydride shifts, Wagner–Meerwein shifts, ring contractions, and

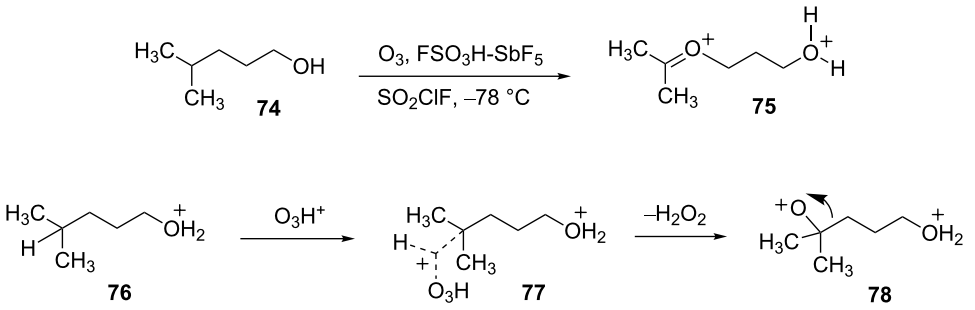

Scheme 15: Ozonolysis in superacid.

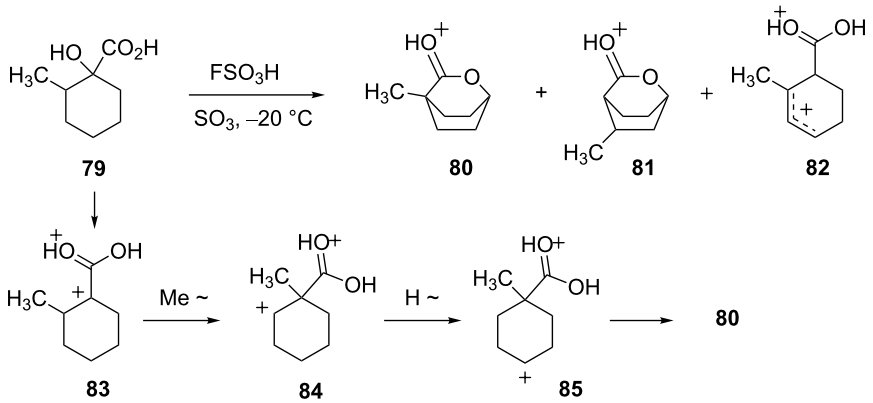

Scheme 16: Rearrangement of 1-hydroxy-2-methylcyclohexane carboxylic acid (**79**) in superacid.

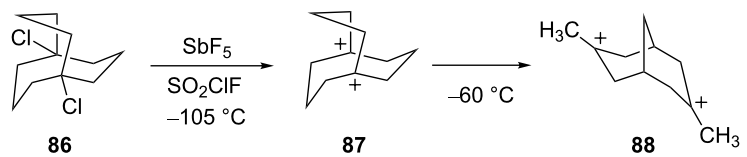

Scheme 17: Isomerization of the 1,5-manxyl dication **87**.

methyl shifts (Scheme 18). Ab initio calculations were performed and revealed that the isomerization lowers the energy of the dication by about 26 kcal/mol. Moreover, isomerization increased the distance between the carbocation sites from 2.80 Å in **87** to 3.58 Å in **88**.

Olah and coworkers have described [30] an attempt to generate the 1,4-dication **90** from the disubstituted 1,4-cyclohexanediol (**89**, Scheme 19). The 1,4-dication was not stable and instead isomerized to the 1,8-dication **91**.

Superelectrophilic carboxonium ions are also known to undergo rearrangements by carbon migrations [31]. For example, Olah and Prakash have described the superacid-promoted isomerization of pivaldehyde (**92**) to methyl isopropyl ketone (**98**, Scheme 20).

The rearrangement is best carried out in strong or superacidic media (Table 2). Since the carbonyl group is monoprotonated under less acidic conditions, it suggests the involvement of the *O,O*-diprotonated species **93**. Migration of the methyl group

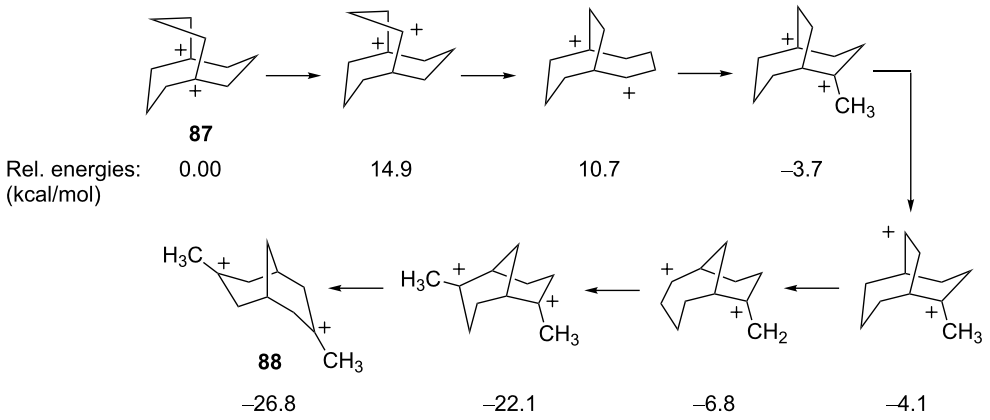

Scheme 18: Energetics of isomerization.

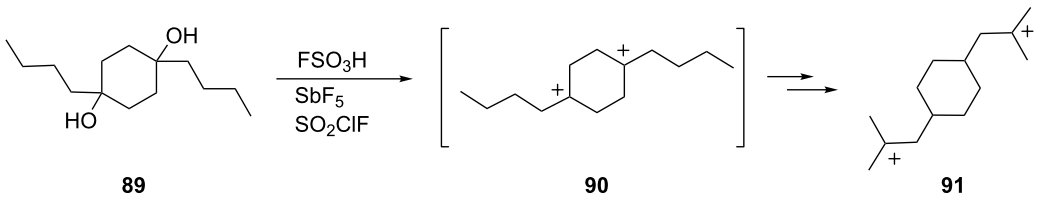

Scheme 19: Rearrangement of dication **90**.

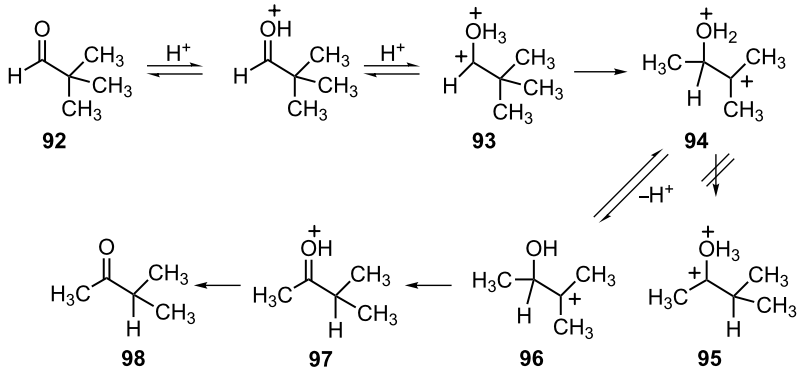

Scheme 20: Superacid promoted rearrangement of pivaldehyde (**92**).

leads to separation of the charge centers and the formation of dication **94**. Theoretical calculations show that hydride shift for the dications (**94** → **95**) is energetically unfavorable, presumably due to the closer proximity of the charges. In the final steps, the monocation **96** undergoes a hydride shift to form the carboxonium ion **97** which leads to ketone **98** on deprotonation. Methyl isopropyl ketone (**98**) is known [32] to be an excellent gasoline oxygenate. Since pivaldehyde can be made from carbon monoxide and isobutane (in superacid), this superelectrophilic rearrangement may have significant commercial value. Other isoalkanes have shown similar chemistry. For example, 3-methylpentane reacts with carbon monoxide to give the isomeric C_7 ketones.

Table 2: Isomerization of pivaldehyde in CF_3SO_3H:CF_3CO_2H solutions[a].

H_0	acid system, w/w	pivaldehyde	methyl isopropyl ketone
−10.9	26.9% CF_3SO_3H	0%	100%
−9.7	11.4% CF_3SO_3H	17%	83%
−9.4	8.0% CF_3SO_3H	29%	71%
−8.4	3.1% CF_3SO_3H	68%	32%
−7.7	0.9% CF_3SO_3H	83%	17%
−2.7	100% CF_3SO_3H	100%	0%

[a]Reaction conditions: 2 h, 25 °C, 1:5 pivaldehyde:acid.

A retro-pinacol rearrangement is triggered by the superelectrophilic carboxonium **100** and subsequent dehydration leads to the efficient formation of the phenanthrene condensation product **102** (Scheme 21) [33]. The key step involves phenyl migration to the carboxonium carbon. This effectively separates and further stabilizes the carbocationic center. Formation of the 1,2-ethylene dication **101** then gives the cyclization product **102**. When dication **101** is generated by other routes, 9,10-diphenylphenanthrene is also formed.

Superelectrophiles are also thought to be involved in some of the classical rearrangements of nitrogen-containing functional groups. For example, Olah and co-workers have studied [34] the Wallach rearrangement and the dicationic intermediates involved were directly observed by low temperature NMR (Scheme 22). Azoxybenzene (**103**) is shown to form the monoprotonated species **104** in FSO_3H at low temperature, while the dicationic species **105** and **106** are directly observable by NMR in HF-SbF_5 at low temperature. In the Wallach rearrangement,

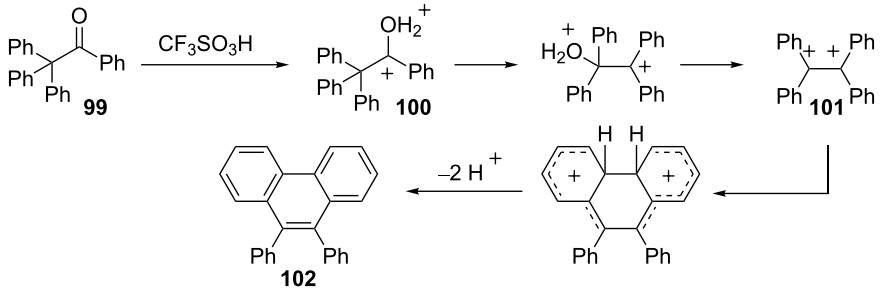

Scheme 21: Rearrangement of a superelectrophilic carboxonium ion **100**.

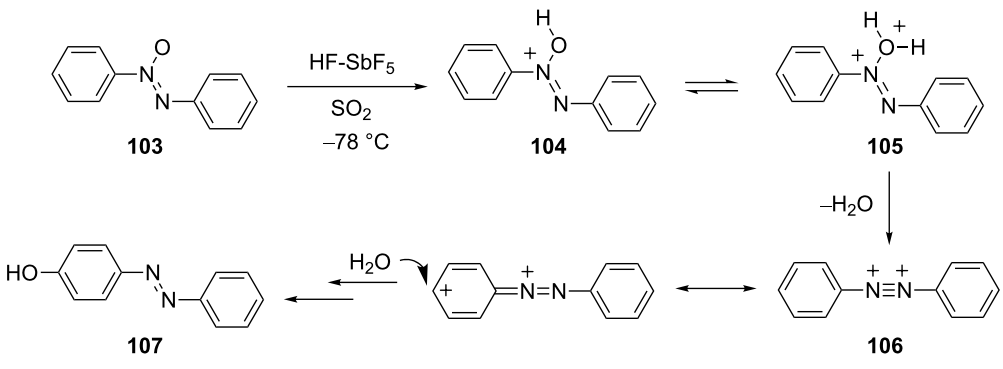

Scheme 22: Proposed mechanism for the Wallach rearrangement.

delocalization of the positive charges is followed by nucleophilic attack by water at a ring carbon during the aqueous workup of the reaction.

An interesting example of the Wallach rearrangement was studied by Buncel and coworkers [35]. In a series of reports, they described the reactions of azoxypyridines in sulfuric acid media. The relative reactivities of the α- and β-isomers **108** and **109** were correlated to stabilization of a developing cationic charge center (Scheme 23). Thus, the α-isomer **108** ionizes in 100% H_2SO_4 to give the tricationic species **110** and subsequent nucleophilic attack gives the product **114**. When the β-isomer **104** is reacted under similar conditions, no rearrangement product was obtained. These observations are understood by recognizing that the loss of water from the trications **110** and **115** leads to the development of a positive charge on the adjacent nitrogen atom. In the case of α-isomer **108**, the developing azonium cation may be stabilized by resonance interaction with the phenyl group of **111**. However, with the β-isomer **109** the developing azonium cation is located next to the pyridinium ring **116**. Evidently, structure **116** is destabilized by the unfavorable interactions of cationic charges and the reaction does not occur at a significant rate.

The benzidine rearrangement is another rearrangement that – depending on the reaction conditions – may involve superelectrophiles [36]. In the reaction of 1,2-diphenylhydrazine (**117**), the diprotonated species **118** is formed in strong acid and a 5,5-sigmatropic bond migration occurs (Scheme 24). This step involves the isomerization of the 1,2-dication **118** to the 1,10-dication **119**, a conversion driven to some extent by charge–charge repulsion. The final deprotonation steps give benzidine **121**. Yamabe recently studied the benzidine rearrangement using DFT calculations [37]. The results were in general agreement with the above mechanism: Dication **119** was estimated to be about 9 kcal·mol^{-1} more stable than dication **118** (calculated ions included 12 molecules of water in their structures). Similarly, Olah and coworkers studied this reaction by low temperature NMR and showed clean conversion of hydrazobenzene to the stable ion **119** in FSO_3H-SO_3 at –78 °C [34].

Jacquesy and coworkers have examined the chemistry of natural products in superacids and found several unusual rearrangements of multiply-protonated species. For example, quinine (**122**) gives product **123** in 89% yield from reaction with HF-SbF_5 at −30 °C (Scheme 25) [38]. The conversion is thought to involve the di- and triprotonated derivatives of quinine **124** and **125**. Hydride and Wagner–Meerwein (WM) shifts lead to formation of trication **127**. Hydride shift gives trication **128**, which undergoes cyclization with the neighboring hydroxy group. This isomerization is somewhat surprising because the 1,4-dicationic system **127** produces a 1,3-dicationic system **128** – generally an energetically unfavorable transformation. This superacid-promoted isomerization of quinine reveals several interesting aspects of the chemistry of

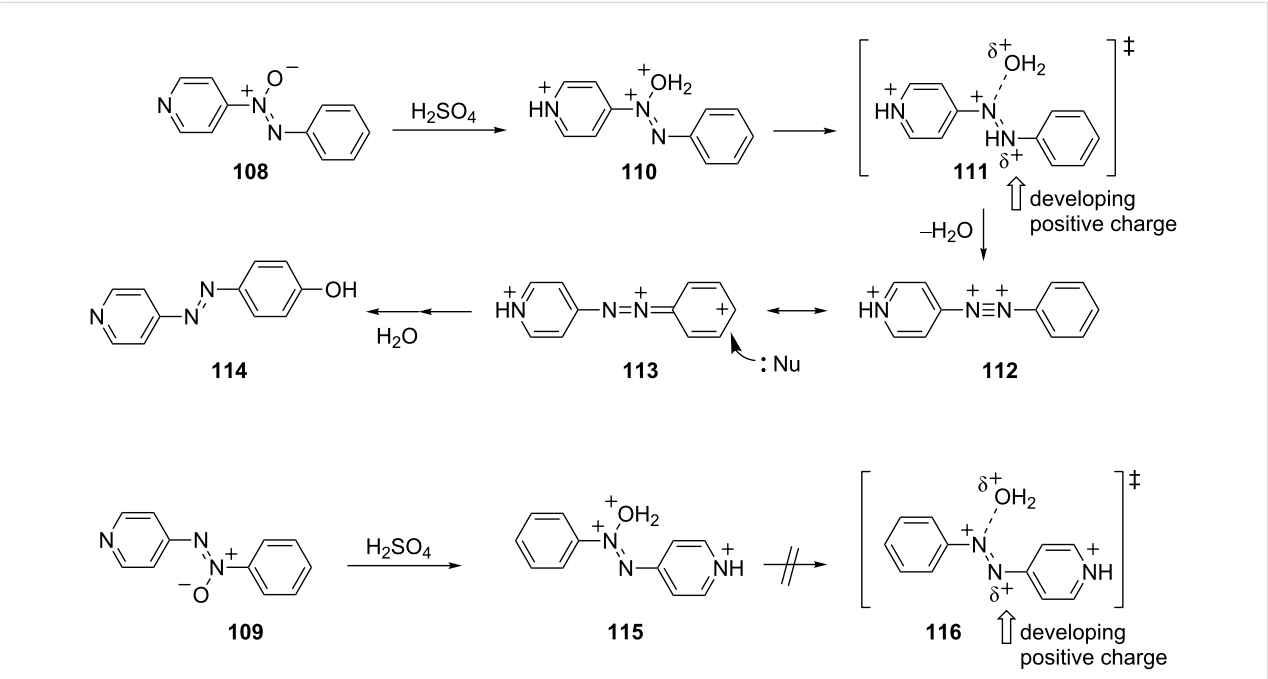

Scheme 23: Wallach rearrangement of azoxypyridines **108** and **109**.

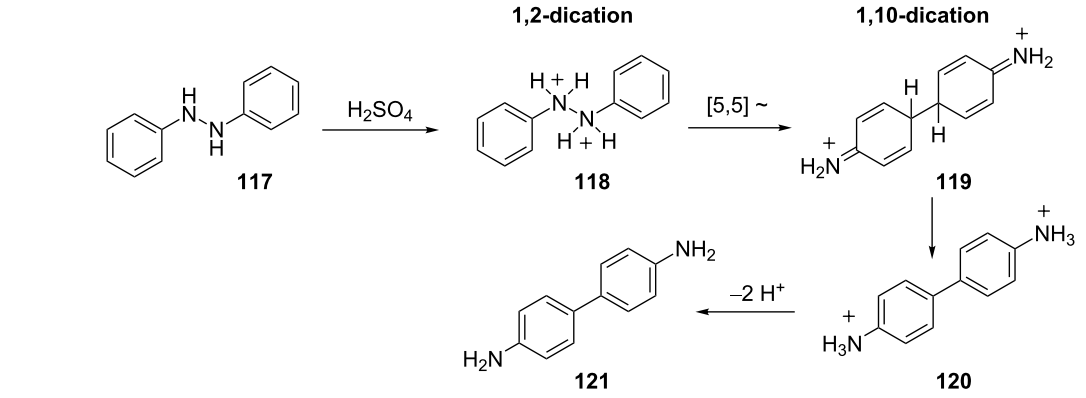

Scheme 24: Proposed mechanism of the benzidine rearrangement.

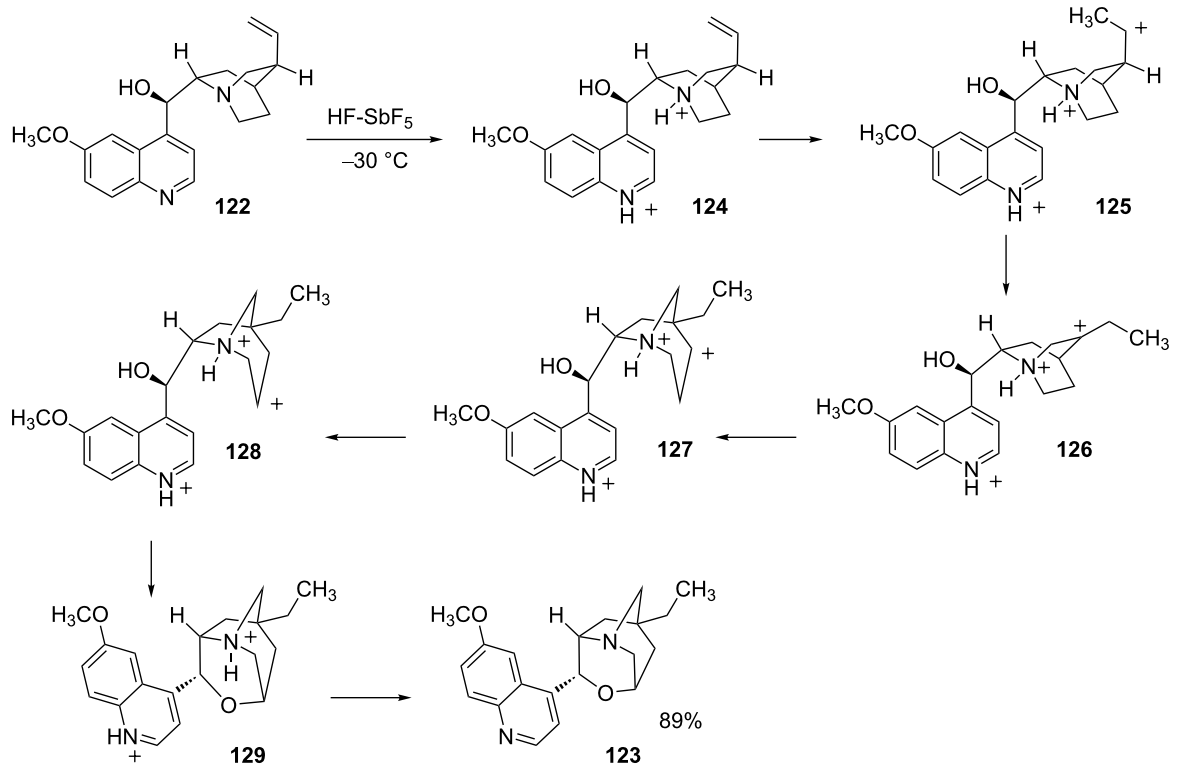

Scheme 25: Superacid-promoted reaction of quinine (**122**).

structurally complex superelectrophiles. First, protonation of the nitrogen base sites occurs readily and the cationic site may influence the reactivities of adjacent functional groups. This prevents ionization of the hydroxy group and cleavage of the methoxy group, despite being in a superacidic media. Secondly, this example illustrates the challenges in predicting the course of a reaction involving a superelectrophile with a complex structure. There is a very complex interplay of charge–charge repulsions, neighboring group interactions, and other effects.

A similar type of rearrangement and cyclization was described [39] for the vindoline derivative **130** in HF-SbF_5 (Scheme 26). Initial protonation is assumed to occur at the relative strong base sites – the nitrogen atoms and the ester group – to give trication **131**. Further protonation of the double bond leads to carbocation **132**. This intermediate then undergoes an alkyl group shift and deprotonation to give the rearranged alkene **133**. Protonation and charge migration gives ion **135**, which cyclizes to afford **136** as a mixture of diastereomers in 18% yield. Like

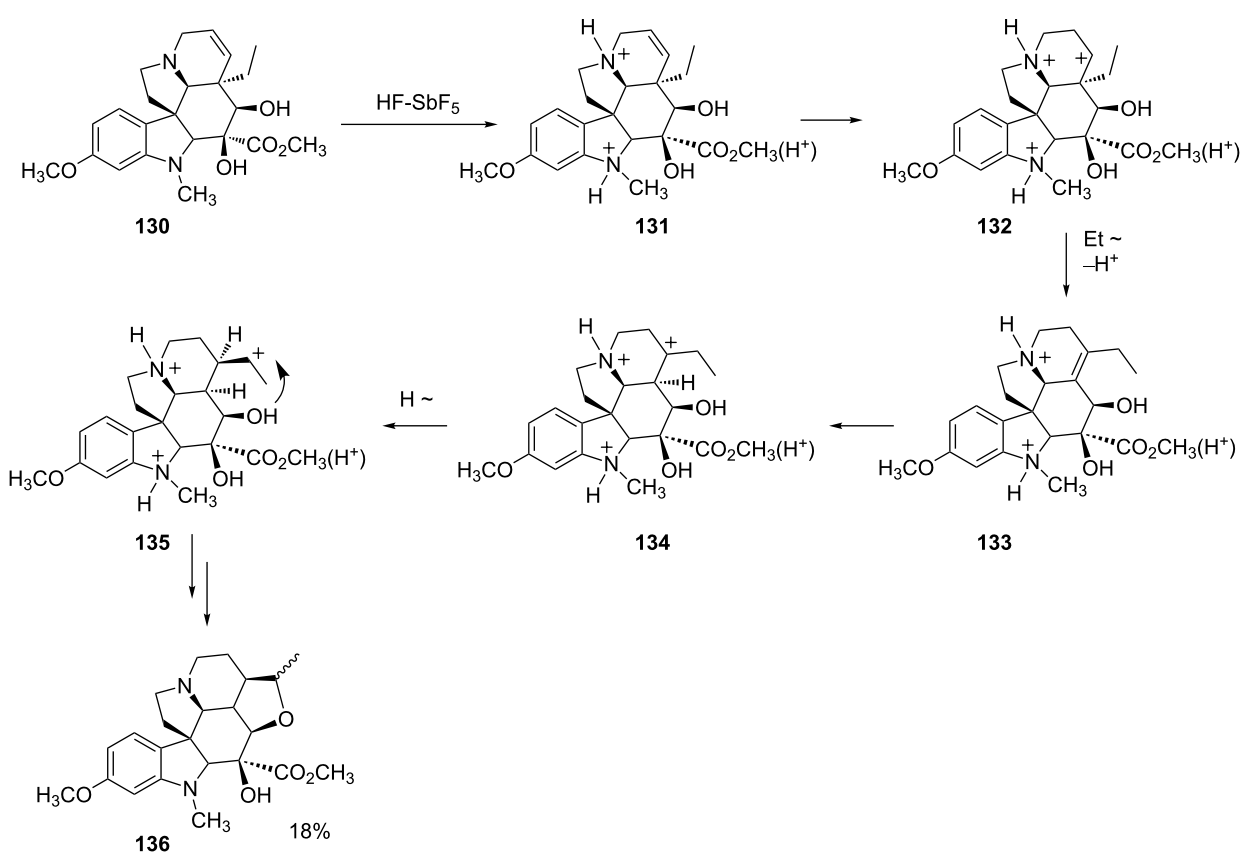

Scheme 26: Superacid-promoted reaction of vindoline derivative **130**.

the rearrangement and cyclization of quinine, this reaction of the vindoline derivative **130** involves a series of structurally complex superelectrophiles. Other superacid-promoted reactions of natural products have been described in recent reviews [40,41].

Charge migration or hydride shifts

In the previous section, there were a number of rearrangements that involved both the migration of carbon-centered groups and hydride shifts. The migration of hydride is a common reaction step in carbocation chemistry. Not surprisingly, it also appears to be involved in the chemistry of superelectrophilic systems. There are two means by which charge can migrate in superelectrophiles with the involvement of hydrogen. Charge migration can occur by a direct hydride shift or by deprotonation and protonation steps (Scheme 27). It should be noted that a variety of dicationic superelectrophiles have been shown to exhibit extreme levels of carbon acidity, even undergoing rapid deprotonation in the strongest superacids [42-44]. In general, (di- or tricationic) superelectrophiles tend to favor reactions in which positive charge becomes be more widely dispersed and separated. Reactions are also favored when positive charge can be removed from the structure. Deprotonation can be a means for reducing the overall charge on the superelectrophile. Consequently, the deprotonation–reprotonation may be one of the most common means by which charge migrates in superelectrophiles.

Several studies have examined this question using deuterium-labeled superelectrophiles. Reaction of 1-hydroxycyclohexanecarboxylic acid (**137**) in FSO_3H and SO_3 at −70 °C, followed by warming to 0 °C, gives a clean conversion to the protonated bicyclic lactone **140** (Scheme 28) [28]. A mechanism is proposed which involves ionization to the superelectrophile

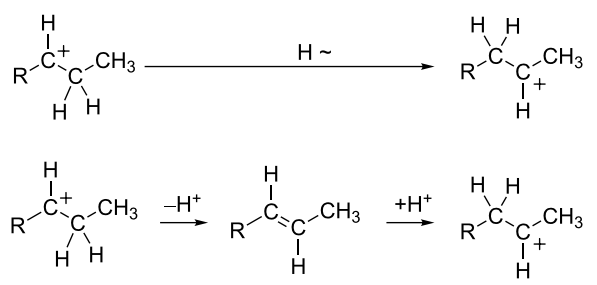

Scheme 27: Charge migration by hydride shift and acid–base chemistry.

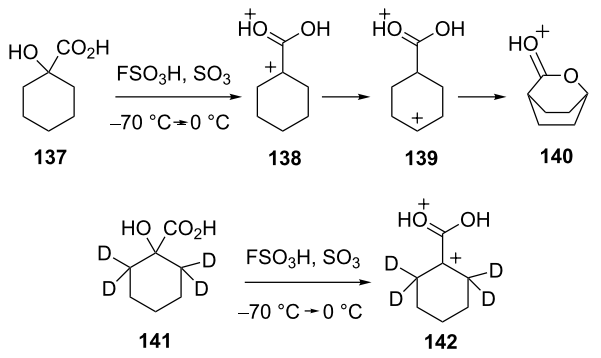

Scheme 28: Reactions of 1-hydroxycyclohexanecarboxylic acid (**137**).

138, followed by successive hydride shifts to give the charge separated dication **139**. Cyclization then leads to the lactone derivative **140**. In order to further probe this conversion, the deuterium labeled compound **141** was prepared and reacted under similar conditions. Interestingly, a lactone derivative was not formed and only the dicationic species **142** was observed by low temperature NMR. It was proposed that the deuterium atoms slow the initial 1,2-hydride (deuteride) shift and charge migration is inhibited.

In another study, the heterocyclic alcohol **143** ionizes in superacid to give the 1,4-dication **144** (Scheme 29) [45]. Further reaction steps lead to the 1,5-dication **146** and ultimately to product **147** in 90% yield. With only one deuterium in the final product, this indicates that charge migration has not occurred by hydride (deuteride) shift, but rather via acid–base chemistry. In this case, the acid–base chemistry may be aided by the formation of a conjugated π-system in **145**.

When cationic charges are in close proximity, it is energetically favorable for the charge centers to be further separated. DFT calculations have performed on several systems and charge separation can result in at least 10–20 kcal·mol^{-1} stabilization. For example, the thiazole derivative **148** was reacted with CF_3SO_3H and then benzene to give two products (**151** and **152**, Scheme 30) [42]. When the two precursor superelectrophiles are studied computationally (B3LYP 6-311(d,p) level), the charge separated 1,4-dication **150** is estimated to be about 16 kcal·mol^{-1} more stable than the 1,3-dication **149**. However, since **151** is the major product, this conversion is assumed to be a kinetically controlled reaction. Indeed, compound **152** may be formed exclusively by reacting alcohol **148** in superacid for 1 h, followed by addition of benzene. The initial reaction period enables the superelectrophile to equilibrate and form the more stable charge-separated ion **150**. The addition of benzene then forms **152**.

Another recent study included calculations with the solution-phase model MPW1/6-311G(d)//PCMsp and the solvation was found to narrow the energy gap between a superelectrophile and its charge-separated species (Table 3) [45]. By incorporating the solution-phase into the model, the energy gap between the two ions is decreased by between 3–11 kcal·mol^{-1} compared to gas-phase structures. This result suggests that solvation effects (and almost certainly counter ion effects) are increasingly important in stabilizing superelectrophiles as the ions become more densely charged or the charges are in closer proximity.

Charge migration and hydride shifts have been involved in several synthetic methods involving superelectrophiles. A useful route to aza-polycyclic aromatic compounds has been

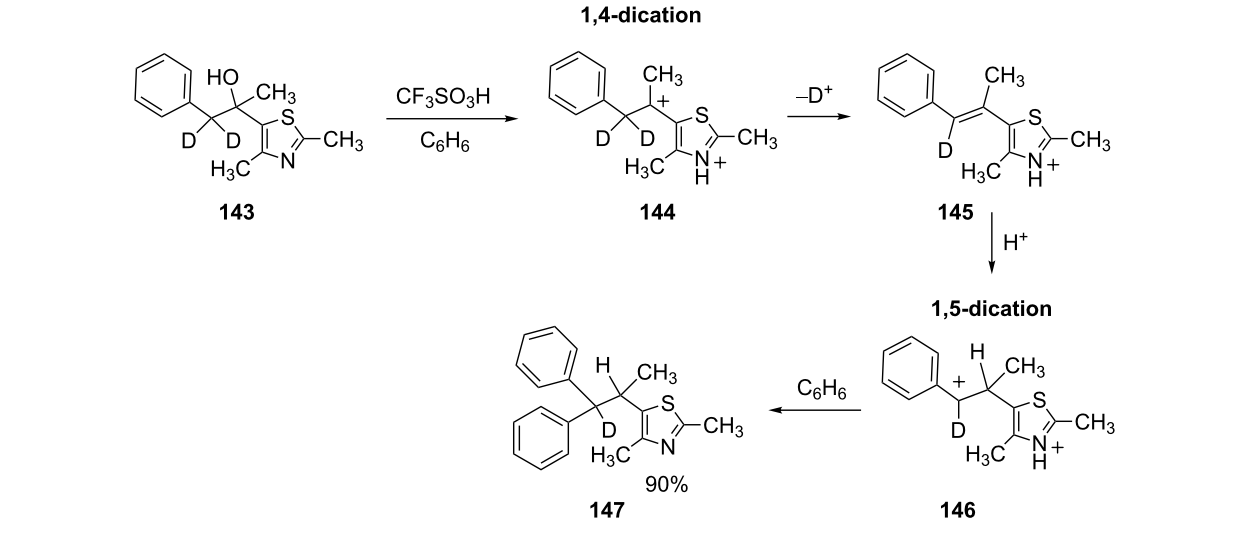

Scheme 29: Reaction of alcohol **143** with benzene in superacid.

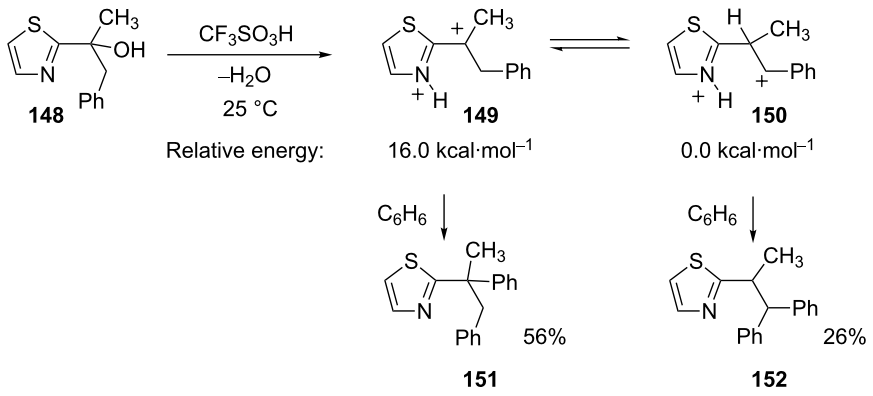

Scheme 30: Reaction of alcohol **148** in superacid with benzene.

Table 3: Calculated energies of dications **153** and **154**.

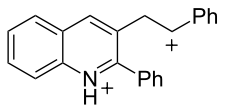

153

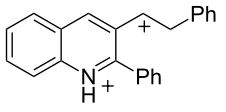

154

Level of theory	Relative energy, kcal·mol^{-1}	
	153	**154**
HF/6-311G (d)	0.0	18.0
B3LYP/6-311G (d)	0.0	14.9
PBE/6-311G (d)	0.0	10.0
MP2/6-311G (d)	0.0	10.3
IPCMsp//MPW1/6-311G (d)	0.0	7.4

developed utilizing charge migration [42,45]. For example, alcohol **155** reacts in superacid to give 5-methylbenzo-[*f*]isoquinoline (**158**, Scheme 31) in good yield. This conversion involves formation of the 1,4-dication **156**, which then undergoes charge migration to the 1,5-dication **157**. Intramolecular cyclization and benzene elimination gives the benzo-[*f*]isoquinoline system **158**.

Olah and coworkers have described a series of reactions involving glycols and related substrates in superacids [46]. These substrates are found to give protonated aldehydes and hydride shifts are thought to be involved. In superacidic media, substrates such as ethylene glycol (**159**) are diprotonated and form the bis-oxonium ions, i.e., **160** as a stable species at −80 °C. When the solution is warmed to 25 °C, protonated acetaldehyde (**162**) is formed (Scheme 32). The conversion may occur by one of several routes: by dehydration of **160** with formation of the gitionic superelectrophile **161** and hydride shift/proton loss; by a concerted reaction involving loss of hydronium ion and hydride shift via **163**; dehydration and proton loss with isomerization of the monocationic species **164**. A similar conversion was observed with other substrates such as 1,3-propanediol (**165**) (Scheme 33) and for alkoxy alcohols, i.e., **169**. Both reactions are thought to involve hydride shifts.

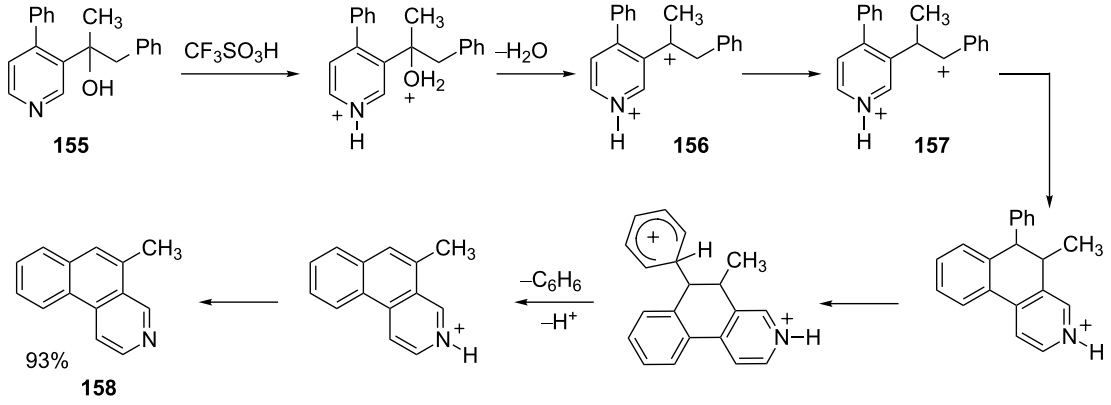

Scheme 31: Mechanism of aza-polycyclic aromatic compound formation.

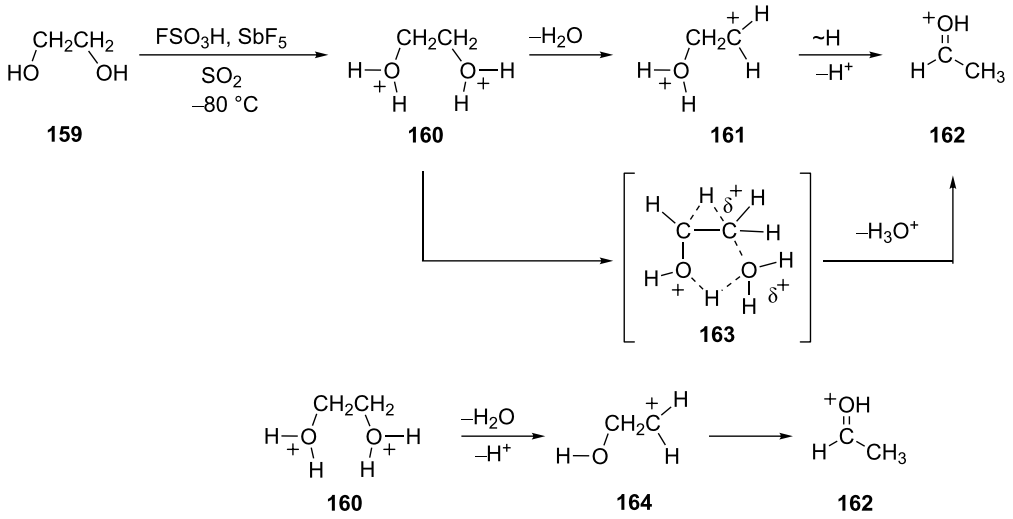

Scheme 32: Superacid-promoted reaction of ethylene glycol (**159**).

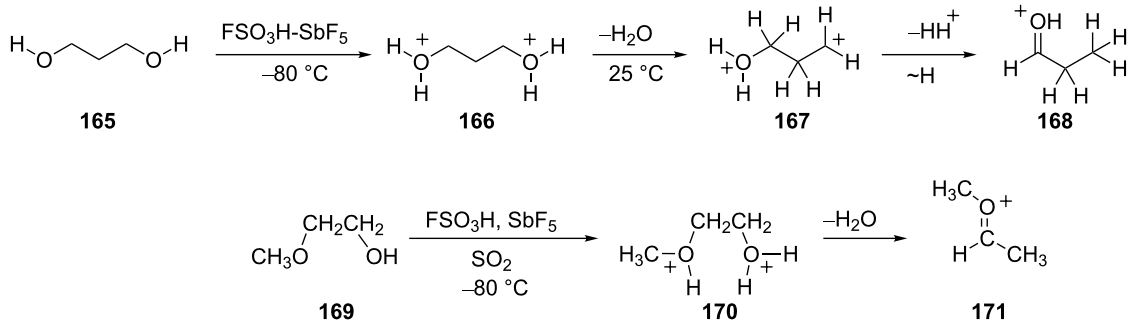

Scheme 33: Reactions of 1,3-propanediol (**165**) and 2-methoxyethanol (**169**).

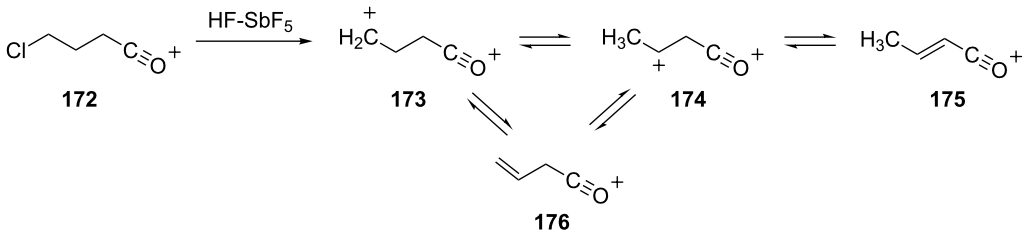

Scheme 34: Rearrangement of superelelctrophilic acyl dication **173**.

Reaction of the 4-chlorobutanoyl cation **172** in superacidic HF-SbF_5 or HSO_3F-SbF_5 leads to formation of the 2-butenoyl cation (**175**, Scheme 34) [47]. One of the proposed intermediates in this transformation is the superelectrophilic species **174**, which undergoes deprotonation to give the 2-butenoyl cation **176**. Presumably, **174** is formed by rapid charge migration involving **173**. Further evidence for the superelectrophile **174** is obtained from experiments in which the 2-butenoyl cation **175** is generated in DSO_3F-SbF_5. Significant deuterium incorporation is found at the α and γ positions, suggesting equilibria involving **173–176**.

Conclusion

As a result of their high charge densities, superelectrophiles can exhibit very high reactivities. Superelectrophilic reactivity extends beyond the realm of chemistry with weak nucleophiles.

Superelectrophiles may undergo a variety of rearrangement reactions in order to form more stable structures or to lose positive charge. Typically, stabilized structures are characterized by greater separation of cationic charge centers. Superelectrophiles may also undergo structural rearrangements that lead to favorable deprotonation steps. This gives ions with reduced positive charge. Superelectrophiles have been shown to undergo ring opening reactions, alkyl group shifts, Wagner–Meerwein shifts, and hydride shifts. Thus, superelectrophiles tend to rearrange by reaction steps similar to monocationic rearrangements.

Acknowledgements

We gratefully acknowledge the support of the National Science Foundation (CHE-0749907).

References

1. Knorr, L. *Justus Liebigs Ann. Chem.* **1886,** *236,* 69–115. doi:10.1002/jlac.18862360105
2. Staskun, B. *J. Org. Chem.* **1964,** *29,* 1153–1157. doi:10.1021/jo01028a038
3. Palmer, D. C.; Strauss, M. J. *Chem. Rev.* **1977,** *77,* 1–36. doi:10.1021/cr60305a003
4. Brouwer, D. M.; Kiffen, A. A. *Recl. Trav. Chim. Pays-Bas* **1973,** *92,* 689–697. doi:10.1002/recl.19730920617
5. Brouwer, D. M.; Kiffen, A. A. *Recl. Trav. Chim. Pays-Bas* **1973,** *92,* 809–813. doi:10.1002/recl.19730920716
6. Brouwer, D. M.; Kiffen, A. A. *Recl. Trav. Chim. Pays-Bas* **1973,** *92,* 906–914. doi:10.1002/recl.19730920812
7. Olah, G. A.; Germain, A.; Lin, H. C.; Forsyth, D. A. *J. Am. Chem. Soc.* **1975,** *97,* 2928–2929. doi:10.1021/ja00843a067
8. Olah, G. A.; Klumpp, D. A. *Superelectrophiles and Their Chemistry;* Wiley: NY, 2008.
9. Prakash, G. K. S.; Mathew, T.; Hoole, D.; Esteves, P. M.; Wang, Q.; Rasul, G.; Olah, G. A. *J. Am. Chem. Soc.* **2004,** *126,* 15770–15776. doi:10.1021/ja0465247
10. Koltunov, K. Y.; Walspurger, S.; Sommer, J. *Chem. Commun.* **2004,** 1754–1755. doi:10.1039/b404074k
11. Klumpp, D. A.; Zhang, Y.; O'Connor, M. J.; Esteves, P. M.; de Almeida, L. S. *Org. Lett.* **2007,** *9,* 3085–3088. doi:10.1021/ol0711570
12. Klumpp, D. A. *ARKIVOC* **2009,** Part (i) 63–80.
13. Suzuki, T.; Ohwada, T.; Shudo, K. *J. Am. Chem. Soc.* **1997,** *119,* 6774–6780. doi:10.1021/ja971100g
14. Klumpp, D. A.; Rendy, R.; McElrea, A. *Tetrahedron Lett.* **2004,** *45,* 7959–7961. doi:10.1016/j.tetlet.2004.08.109
15. Seo, Y.; Kim, K. *Bull. Korean Chem. Soc.* **1995,** *16,* 356–359.
16. Rendy, R.; Zhang, Y.; McElrea, A.; Gomez, A.; Klumpp, D. A. *J. Org. Chem.* **2004,** *69,* 2340–2347. doi:10.1021/jo030327t
17. Unpublished results.
18. Klumpp, D. A.; Fredrick, S.; Lau, S.; Jin, K. K.; Bau, R.; Prakash, G. K. S.; Olah, G. A. *J. Org. Chem.* **1999,** *64,* 5152–5155. doi:10.1021/jo990197h
19. Olah, G. A.; White, A. M. *J. Am. Chem. Soc.* **1967,** *89,* 4752–4756. doi:10.1021/ja00994a032
20. Bruck, D.; Rabinovitz, M. *J. Am. Chem. Soc.* **1977,** *99,* 240–241. doi:10.1021/ja00443a041
21. Kleemann, A.; Engel, J.; Kutscher, B.; Reichert, D. *Pharmaceutical Substances,* 4th ed.; Thieme: Stuttgart, 2001; p 308.
22. Jacquesy, J.-C.; Jacquesy, R.; Patoiseau, J.-F. *Tetrahedron* **1976,** *32,* 1699–1704. doi:10.1016/0040-4020(76)85161-7
23. Brouwer, D. M.; van Doorn, J. A. *Recl. Trav. Chim. Pays-Bas* **1971,** *90,* 1010–1026. doi:10.1002/recl.19710900908
24. Martin, A.; Jouannetaud, M.-P.; Jacquesy, J.-C. *Tetrahedron Lett.* **1996,** *37,* 7731–7734. doi:10.1016/0040-4039(96)01736-4
25. Fărcaşiu, D.; Miller, G.; Sharma, S. *J. Phys. Org. Chem.* **1990,** *3,* 639–642. doi:10.1002/poc.610031004
26. Yoneda, N.; Sato, H.; Fukuhara, T.; Takahashi, Y.; Suzuki, A. *Chem. Lett.* **1983,** 19–20. doi:10.1246/cl.1983.19
27. Olah, G. A.; Yoneda, N.; Ohnishi, R. *J. Am. Chem. Soc.* **1976,** *98,* 7341–7345. doi:10.1021/ja00439a038
28. Carr, G.; Whittaker, D. *J. Chem. Soc., Perkin Trans. 2* **1987,** 1877–1880. doi:10.1039/p29870001877
29. Taeschler, C.; Sorensen, T. S. *Tetrahedron Lett.* **2001,** *42,* 5339–5341. doi:10.1016/S0040-4039(01)01032-2
30. Olah, G. A.; Prakash, G. K. S.; Rawdah, T. N. *J. Am. Chem. Soc.* **1980,** *102,* 6127–6130. doi:10.1021/ja00539a026
31. Olah, G. A.; Mathew, T.; Marinez, E. R.; Esteves, P. M.; Etzkorn, M.; Rasul, G.; Prakash, G. K. S. *J. Am. Chem. Soc.* **2001,** *123,* 11556–11561. doi:10.1021/ja011253a
32. Temple, R. G.; Gribble, N. R. *Prepr. Pap. - Am. Chem. Soc., Div. Fuel Chem.* **1992,** *37,* 1829–1835.
33. Klumpp, D. A.; Baek, D. N.; Prakash, G. K. S.; Olah, G. A. *J. Org. Chem.* **1997,** *62,* 6666–6671. doi:10.1021/jo970293n
34. Olah, G. A.; Dunne, K.; Kelly, D. P.; Mo, Y. K. *J. Am. Chem. Soc.* **1972,** *94,* 7438–7447. doi:10.1021/ja00776a029
35. Buncel, E. *Can. J. Chem.* **2000,** *78,* 1251–1271. doi:10.1139/cjc-78-10-1251
36. Smith, M. B.; March, J. *March's Advanced Organic Chemistry,* 6th ed.; Wiley: NY, 2007; pp 1678–1680.
37. Yamabe, S.; Nakata, H.; Yamazaki, S. *Org. Biomol. Chem.* **2009,** *7,* 4631–4640. doi:10.1039/b909313c
38. Thibaudeau, S.; Violeau, B.; Martin-Mingot, A.; Jouannetaud, M.-P.; Jacquesy, J.-C. *Tetrahedron Lett.* **2002,** *43,* 8773–8775. doi:10.1016/S0040-4039(02)02068-3
39. Lafitte, C.; Jouannetaud, M.-P.; Jacquesy, J.-C.; Duflos, A. *Tetrahedron* **1999,** *55,* 1989–2000. doi:10.1016/S0040-4020(98)01223-X
40. Jacquesy, J.-C. In *Stable Carbocation Chemistry;* Prakash, G. K. S.; Schleyer, P. v. R., Eds.; Wiley: NY, 1997; pp 549–574.
41. Jacquesy, J.-C. In *Stable Carbocation Chemistry;* Olah, G. A.; Prakash, G. K. S., Eds.; Wiley: NY, 2004; pp 359–376.
42. Li, A.; Kindelin, P. J.; Klumpp, D. A. *Org. Lett.* **2006,** *8,* 1233–1236. doi:10.1021/ol060125u
43. Olah, G. A.; Grant, J. L.; Spear, R. J.; Bollinger, J. M.; Serianz, A.; Sipos, G. *J. Am. Chem. Soc.* **1976,** *98,* 2501–2507. doi:10.1021/ja00425a018
44. Farcasiu, D.; Ghenciu, A. *J. Org. Chem.* **1991,** *56,* 6050–6052. doi:10.1021/jo00021a017
45. Li, A.; Gilbert, T. M.; Klumpp, D. A. *J. Org. Chem.* **2008,** *73,* 3654–3657. doi:10.1021/jo8003474
46. Olah, G. A.; Sommer, J. *J. Am. Chem. Soc.* **1968,** *90,* 927–933. doi:10.1021/ja01006a016
47. Farcasiu, D.; Miller, G. *J. Org. Chem.* **1989,** *54,* 5423–5424. doi:10.1021/jo00284a008

Beilstein Journal of Organic Chemistry

Predicting the UV–vis spectra of oxazine dyes

Scott Fleming, Andrew Mills and Tell Tuttle*

Full Research Paper

Open Access

Address:
WestCHEM, Department of Pure and Applied Chemistry, University of Strathclyde, 295 Cathedral Street, Glasgow G1 1XL, UK

Email:
Andrew Mills - a.mills@strath.ac.uk; Tell Tuttle* - tell.tuttle@strath.ac.uk

* Corresponding author

Keywords:
DFT; dyes; oxazine; TD-DFT; UV–vis

Beilstein J. Org. Chem. **2011,** *7,* 432–441.
doi:10.3762/bjoc.7.56

Received: 08 November 2010
Accepted: 23 March 2011
Published: 15 April 2011

This article is part of the Thematic Series "Physical organic chemistry".

Guest Editor: J. Murphy

Abstract

In the current work we have investigated the ability of time-dependent density functional theory (TD-DFT) to predict the absorption spectra of a series of oxazine dyes and the effect of solvent on the accuracy of these predictions. Based on the results of this study, it is clear that for the series of oxazine dyes an accurate prediction of the excitation energy requires the inclusion of solvent. Implicit solvent included via a polarizable continuum approach was found to be sufficient in reproducing the excitation energies accurately in the majority of cases. Moreover, we found that the SMD *s*olvent *m*odel, which is dependent on the full electron *d*ensity of the solute without partitioning into partial charges, gave more reliable results for our systems relative to the conductor-like polarizable continuum model (CPCM), as implemented in Gaussian 09. In all cases the inclusion of solvent reduces the error in the predicted excitation energy to <0.3 eV and in the majority of cases to <0.1 eV.

Introduction

Oxazine dyes are a subclass of quinone imines, which are all based upon the *p*-benzoquinone imine or -diimine scaffold. Other important subclasses within the quinone imines include, the azine dyes and thiazine dyes. The structural relationships described are illustrated in Figure 1 for clarity.

All the dyes are based on an anthracene skeleton in which one carbon is replaced by a nitrogen atom and another by an additional heteroatom such as N, O, or S in the central ring. Although azine dyes have been found to demonstrate solvatochromism [1-3], and many thiazine dyes are metachromatic [4,5], this investigation is limited to the study of oxazine dyes.

Oxazine dyes are useful partly because they exhibit solvatochromism, this makes them sensitive to their surrounding environment, and hence they have been utilized in various applications as molecular probes [6-8]. In the current investigation we focus on the ten oxazine dyes shown in Figure 2,

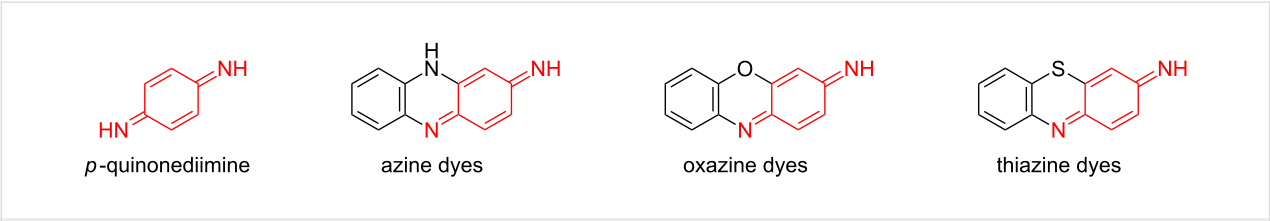

Figure 1: Quinone imine structural relationships.

which are readily soluble in aqueous solution, in order to determine the ability of computational methodology to describe the solvent dependence on the absorption maxima.

Solvatochromism in oxazine dyes has been observed and the mechanism(s) explored in previous studies by various authors [9-11]. Most of these investigations have involved measuring experimentally the spectroscopic features of oxazine dyes, upon varying the solvent polarity. However, some attempt has been made to rationalize these observations by a computational study of the solvatochromism of the oxazine dye Nile red [12]. In the investigation, TD-DFT was applied in order to try and explore the contributing factors in the solvatochromism observed with Nile red, upon gradually increasing the solvent polarity from benzene to acetonitrile. A computational approach such as this is advantageous, because it allows consideration of the individual molecular orbital transitions involved – a feat difficult to achieve via experiment alone.

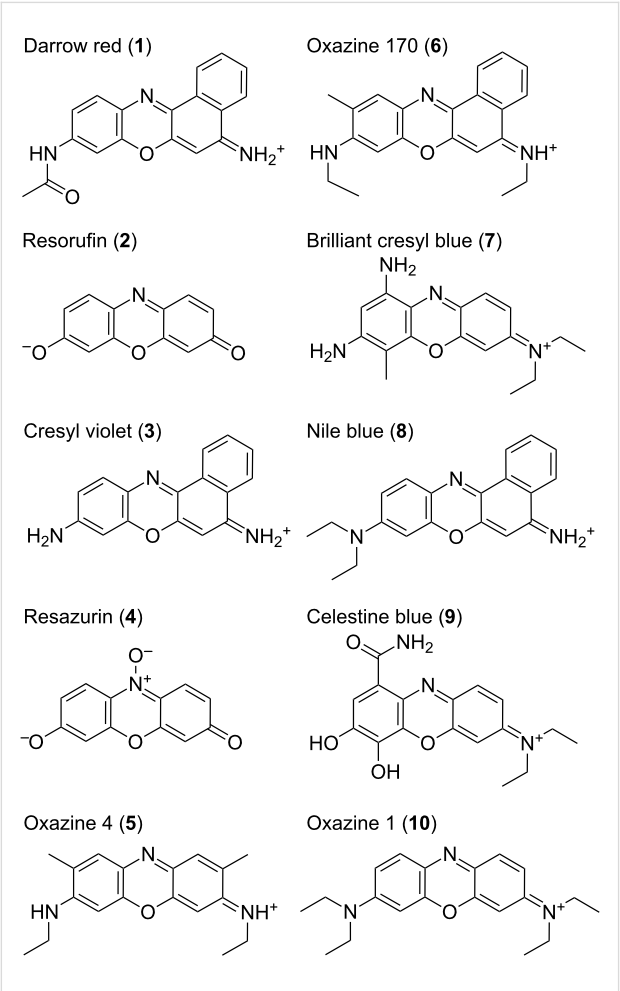

Figure 2: Numbering and structure of oxazine dyes studied in this work (counterions not shown).

TD-DFT has become the modern day workhorse for the determination of electronic excited states in medium sized systems (up to 100 atoms) [13-17]. This method performs particularly well for predicting the excitation energies of local excitations and Rydberg states (although in the case of Rydberg states the choice of functional is particularly important with accurate excitation energies for these states requiring large amounts of exact exchange), while its performance in predicting charge-transfer (CT) states is more questionable [18-23]. A number of studies have demonstrated the failures of TD-DFT in predicting CT excitation energies accurately [24-29], while one can also find within the literature examples where TD-DFT performs well for such states [30]. As such in the current work we explore the ability of various density functionals to predict the excitation energies of the intramolecular CT states in a series of oxazine dyes and the effect of solvent models on the accuracy of these predictions. The assessment of these functionals was carried out against the experimental λ_{max} for the absorption of each dye, which was determined experimentally.

Results and Discussion

Role of the solvent

The gas-phase optimized geometries of the dyes were used as the basis for the single point excited state calculations. The six lowest singlet vertical excitation energies and oscillator strengths from the TD-DFT calculations were used to predict the UV–vis spectrum for each dye through the fitting of a Gaussian (with the GaussView default parameters for half-width) centered at the computed excitation energies. The predicted UV–vis spectra in the gas-phase, gas//CPCM, and gas//SMD were plotted for each dye, and the λ_{max} values in each case are summarized in Table 1.

Table 1: Calculated λ_{max} values and the shift resulting from the different solvent models.[a]

Dye	λ_{max}			Shift	
	Gas[b]	CPCM[c]	SMD[d]	CPCM[c]	SMD[d]
1	485	548	566	62	81
2	458	546	571	88	113
3	481	563	587	82	106
4	486	570	596	84	110
5	468	558	588	90	120
6	505	597	626	92	121
7	470	596	616	129	146
8	512	597	625	85	113
9	476	560	584	86	108
10	492	584	617	92	125

[a]λ_{max} and the shift are reported in nm. The shifts are reported relative to the gas-phase λ_{max}. [b]Gas refers to the gas-phase. [c]CPCM refers to the TD-DFT single point calculations using the CPCM solvent model on the gas-phase optimized structures. [d]SMD refers to the TD-DFT single point calculations using the SMD solvent model on the gas-phase optimized structures.

Table 2: Magnitudes of dipole and transition moments in Debye.[a]

Dye	Dipole		Transition	
	Gas	CPCM	Gas	CPCM
1	8.35	12.44	3.41	4.75
2	3.72	5.21	3.28	4.66
3	3.99	5.81	3.17	4.65
4	3.16	4.40	3.07	4.34
5	2.27	3.10	3.69	4.91
6	3.13	4.65	3.74	5.06
7	2.74	3.79	3.11	3.55
8	3.24	4.94	3.59	4.98
9	11.82	16.61	3.21	4.51
10	2.16	2.99	4.00	5.19

[a]Gas refers to the gas-phase. B3LYP TD-DFT calculations and CPCM refers to the solvent phase CPCM/B3LYP TD-DFT calculations. All TD-DFT calculations were carried out on the gas-phase B3LYP/6-311++G(d,p) optimized geometries.

The results in Table 1 indicate a red shift of about 60–130 nm upon moving from the gas-phase to the CPCM solvent description. Upon moving from the CPCM to the SMD description of the solvent we observe a further red shift in the λ_{max} value relative to the gas-phase calculated spectra. This result is consistent with a narrowing of the energy gap between ground and excited states, due to an increased stabilization of the more polarizable excited state by polar solvents. Clearly, the SMD description of the solvent provides greater stabilization of the excited state with the red shift increased on average by 20–30 nm relative to the spectra obtained within the CPCM solvent model.

The absorbance spectra for oxazine dyes are often described as occurring through CT excitations. Therefore, it is also helpful to examine the dipole moments, and corresponding transition dipole moments in the gas-phase and in the solvent phase. In each case, the transition moments chosen relates to the most significant excited state (vida infra). In the first instance an examination of the dipole and transition moment magnitudes, shows a increase upon moving to the solvated species (Table 2).

The observed increases in magnitude are indicative of polarization by the solvent field. It is also possible to examine the x, y, and z components associated with the corresponding dipole and transition moments (Figure 3a and Figure 3b). It should be noted, that the direction associated with each molecule does not change significantly between gaseous and solvated phases, and hence plots are only shown for the latter.

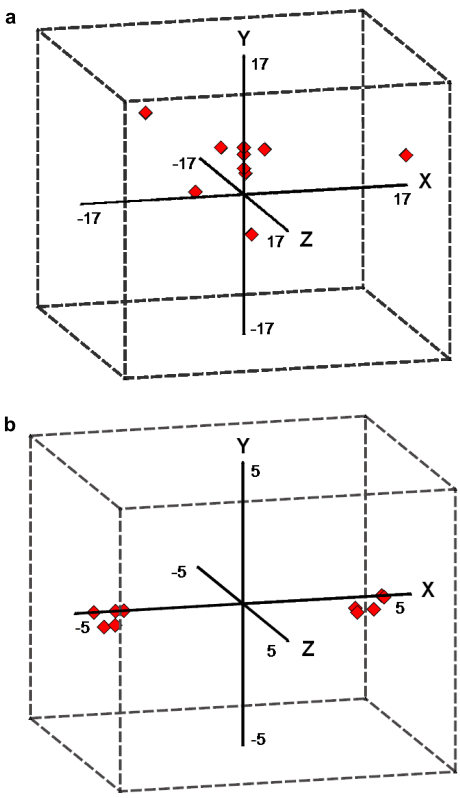

Figure 3: Directions of solvated (a) dipole moments and (b) transition moments from origin (0,0,0).

In the above representation the molecule lies in the xy plane, and is elongated along the x-axis, hence the z component only makes a very slight contribution towards the overall direction. In the case of the ground state dipole moments (Figure 3a), the observed vector differs depending upon the substituents present. For instance, Oxazine 1 (**10**), Oxazine 4 (**5**), Resazurin (**4**), and

Resorufin (**2**) have symmetry in the yz plane, and thus have vectors based almost exclusively on the y-axis. In more complex examples, the direction of dipole moment vector is predominately dictated by the positions of the amines/imines, which possess a partial positive charge due to electron donation to the aromatic system. In contrast the transition dipole moments (Figure 3b) show very little variation in the magnitude and direction associated with the transition moment. The only significant contribution lies along the x-axis, and in each case the magnitude is consistently 3–4 Debye. This is indicative of CT along the extended aromatic system and consistent with the classical description of these excitations.

Performance of functionals and solvent models

The TD-DFT calculations were carried out using the selection of functionals and solvation methods described in the computational methods. The accuracy of the calculated λ_{max} values was assessed against the values obtained experimentally (Table 3).

The data presented in Table 3 clearly shows the important role of the solvent in attaining a realistic description of the excited state. The gas-phase calculated λ_{max} values are all strongly blue shifted relative to the experimental data with an average error of 123 nm (0.51 eV). The inclusion of the solvent using either of the continuum models (i.e., either the CPCM or SMD model) corrects this error to a large degree with the mean unsigned error (MUE) decreased to 43 nm (0.15 eV) with the CPCM solvent model and 22 nm (0.08 eV) within the SMD solvent model at the B3LYP level of theory. Given the large transition dipole moments for the transitions corresponding to the λ_{max} excitations (Table 2), we examined whether a number of functionals that have been shown to perform well for CT states could improve upon the TD-B3LYP calculated excitation energies.

Within the SMD solvent model, TD-B3LYP performs well across all of the dyes. However, the largest errors in the calculated λ_{max} values are found for dyes **1** (Darrow red), which is overestimated by 64 nm (−0.28 eV); and **9** (Celestine blue), which is underestimated by 62 nm (0.20 eV). In the case of **1** the best performing functional is M06-2X, which still overestimates the value of λ_{max} (30 nm; −0.14 eV) but to a lesser extent relative to B3LYP. However, across the series of dyes, M06-2X is the worst performing functional with an MUE of 33 nm (0.11 eV) and has the largest error for **9** (89 nm; 0.31 eV). In contrast, the M06-L functional provides the most accurate representation of **9**, underestimating the λ_{max} excitation by 40 nm (0.13 eV), however, offers no improvement in the prediction of the λ_{max} value of **1** (M06-L error: 69 nm; −0.30 eV). Surprisingly, the gas-phase calculated value of λ_{max} for **1** is relatively accurate. The gas-phase B3LYP calculation of **1** underestimates the value of λ_{max} by only 16 nm (0.08 eV), although this appears to be a fortuitous error cancellation as the solvent calculations systematically result in a strong red shift, which leads to the overestimation mentioned above.

Despite the difficulties associated with predicting the excitation energies of **1** and **9**, the range of different functionals that were tested perform remarkably well once the effect of solvent is taken into account. This is clearly seen in the plot of the errors for the various methodological combinations (Figure 4). Given the non-linear relationship between the observed wavelength

Table 3: Comparison between the experimental and calculated λ_{max} values at different levels of theory.[a]

Dye	Exp.	B3LYP[b]	B3LYP[c]	B3LYP[d]	CAM-B3LYP[d]	M06[d]	M06-L[d]	M06-2X[d]
1	502	486	548	566	535	565	571	532
2	572	458	546	571	581	578	554	578
3	588	481	563	587	573	591	582	570
4	602	486	570	596	591	601	578	583
5	616	468	558	588	580	592	579	576
6	620	505	597	626	610	629	622	607
7	624	467	596	616	592	613	625	590
8	636	512	597	625	608	625	621	607
9	646	474	560	584	560	586	606	557
10	654	492	584	617	606	616	606	606
MSE		−123	−34	−8	−22	−6	−12	−25
MUE		123	43	22	31	23	26	33

[a]All wavelengths are given in nm. MSE is the mean signed error and MUE is the mean unsigned error relative to the experimental λ_{max}. [b]Gas-phase TD-B3LYP/6-311++G(d,p). [c]CPCM/TD-B3LYP/6-311++G(d,p). [d]SMD/TD-DFT/6-311++G(d,p). All single point TD-DFT calculations employed the gas-phase optimized structures.

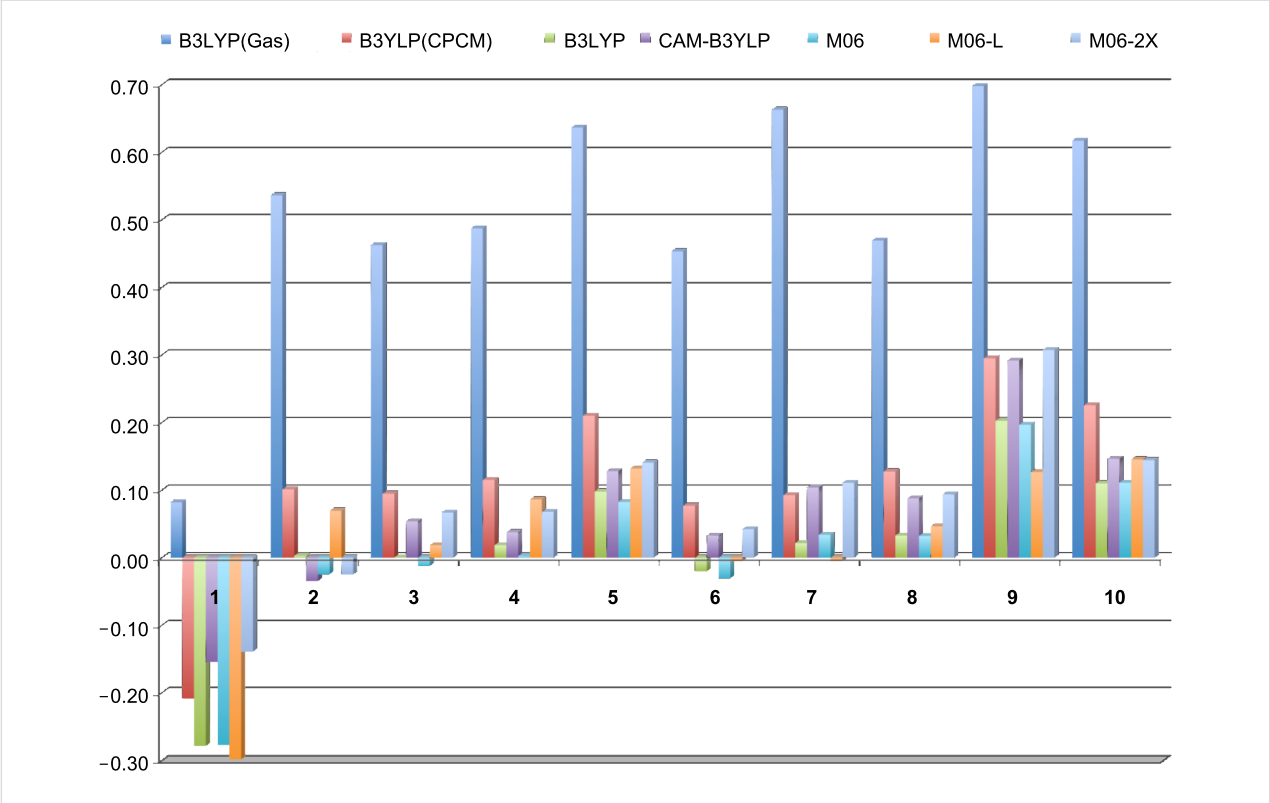

Figure 4: Error between experimental and calculated λ_{max} values for each dye at the different levels of theory investigated. All errors are reported in eV. All structures were optimized in the gas-phase at the B3LYP/6-311++G(d,p) level of theory. B3LYP(Gas) refers to the TD-B3LYP calculation in the gas-phase. B3LYP(CPCM) refers to the TD-B3LYP calculation within the CPCM solvent model. All other TD-DFT calculations were carried out using the SMD solvent model as described in the computational methods.

and the excitation energy (i.e., an error at a high excitation energy will have a lesser impact on the calculated λ_{max} than an equally sized error at a lower excitation energy), the errors associated with the computed excitation energies at the various levels of theory, shown in Figure 4, are in eV. Increasing the percentage of HF exchange is considered beneficial for low-lying excited states that have an ionic character and as such suffer, to a greater extent, from a self-interaction error. This error can be corrected to some extent by increasing the percentage of HF exchange [19]. However, in our dyes, this was not observed, as both the CAM-B3LYP (greater HF exchange at long range) and M06-2X functionals produce larger errors (Figure 4). Clearly in the series of dyes examined, the increased HF exchange leads to a slight over-correction, which has also been observed by others [22].

The calculated transition dipole moments for the various dyes are consistent with a CT nature of the excitation. Moreover, the largest errors are obtained for **1** and **9**, which also have significantly larger ground state dipole moments, relative to the other dyes. TD-DFT is well-known to fail in a variety of CT excitations, which is in contrast to the results obtained for the other eight dyes. Therefore, we employed the Tozer diagnostic to examine whether the calculated excitation energies indeed correspond to CT excitations from an orbital overlap perspective.

Orbital overlap

Within the literature there are conflicting cases as to the accuracy of TD-DFT in predicting CT states [24-30]. In some cases, TD-DFT methods appear to perform reasonably well, whereas in other cases – generally long-range CT – TD-DFT significantly underestimates the excitation energy. In an effort to help identify those excitations where TD-DFT is likely to fail, Tozer and co-workers have recently introduced the use of an orbital overlap diagnostic which utilizes the spatial overlap of the unperturbed ground state orbitals in order to assess the likelihood of an accurate TD-DFT excitation energy, for local, Rydberg and intramolecular CT excitations between those orbitals.

The diagnostic, Λ, considers the spatial overlap between the orbitals involved in the excitation. Where more than one set of orbitals contribute to the excitation (as commonly occurs in TD-DFT calculations) the orbital overlaps are scaled by the contribution (κ) from each pair. In the following, we

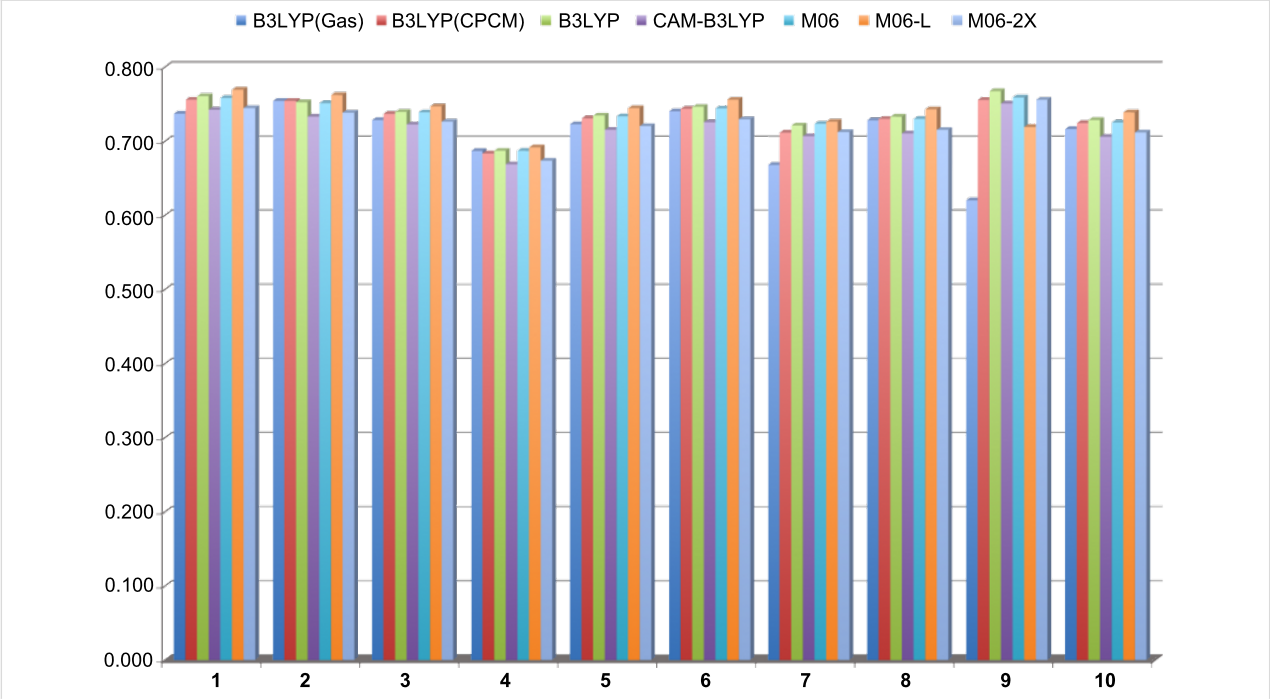

Figure 5: The orbital overlaps (Λ) for each dye at the different levels of theory investigated. All structures were optimized in the gas-phase at the B3LYP/6-311++G(d,p) level of theory. B3LYP(Gas) refers to the TD-B3LYP calculation in the gas-phase. B3LYP(CPCM) refers to the TD-B3LYP calculation within the CPCM solvent model. All other TD-DFT calculations were carried out using the SMD solvent model as described in the computational methods.

have employed the same form of Λ as that introduced by Tozer to investigate the spatial overlap between our orbital pair, namely:

$$\Lambda = \frac{\sum_{i,a} \kappa_{ia}^2 O_{ia}}{\sum_{i,a} \kappa_{ia}^2} \quad (1)$$

where the spatial overlap (O_{ia}) between the occupied orbital (φ_i) and the virtual orbital (φ_a) is given by the inner product of the moduli of the two orbitals:

$$O_{ia} = \int |\varphi_i(r)||\varphi_a(r)| dr \quad (2)$$

and κ_{ia} is the largest coefficient in the CI expansion for each orbital pair.

The resulting overlaps calculated at the various level of theory for each dye are plotted in Figure 5. The value of Λ is largely conserved across the different methods for each dye. In the case of **9**, where there is some variation between the values of Λ calculated in either the gas or solvent phase, this is due primarily to the difference in the two orbital pairs that contribute to the λ_{max} excitation. For the primary excitation in **9**, the κ_{ia} value for the minor contributing orbital pair (HOMO-3–LUMO in the gas-phase and HOMO-1–LUMO in the solvent phase) varies between 0.4–0.6, while the major contribution (HOMO–LUMO) remains constant across the series, resulting in the slight variation in the Λ values observed for this dye. Figure 5 illustrates that the orbital overlap for the solvent phase calculations is largely unaffected by the choice of functional. This is due primarily to the fact that the predominant contribution to the excitation energy and the nature and overlap of the orbital pair (HOMO–LUMO) is conserved across the different methods. In the gas-phase TD-DFT calculations the number of orbital pairs contributing towards the λ_{max} excitation varies with respect to the solvent calculations – two orbital pairs contribute in the gas-phase calculations for **2**, **3**, **5**, **7**, **9**, and **10** – however, a comparable Λ value is obtained in most cases due to the dominance of the HOMO–LUMO contribution in these excitations as well.

The strong overlap between the occupied and virtual orbital can intuitively be seen by visualizing the orbitals. Given the consistency of the calculated overlaps the orbital contributions to the λ_{max} for each dye across the series of functionals, only the orbitals calculated at the CPCM/B3LYP level of theory are displayed in Table 4.

Tozer and co-workers suggest that an overlap of $\Lambda \leq 0.3$, indicates that TD-DFT will struggle to predict correctly the excita-

Table 4: Orbital pairs involved in the λ_{max} excitation for each dye.[a]

Dye	Occupied MO(s)	Virtual MO(s)
1	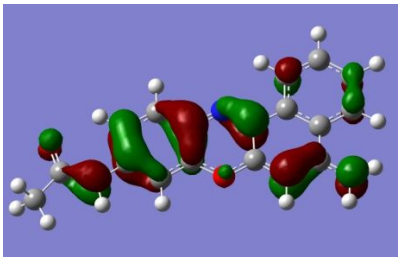	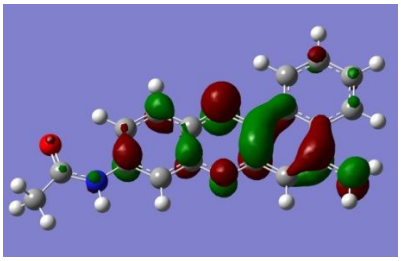
2	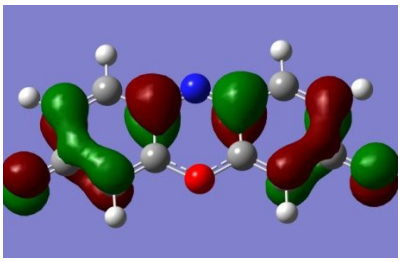	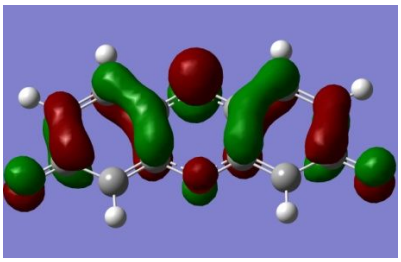
3	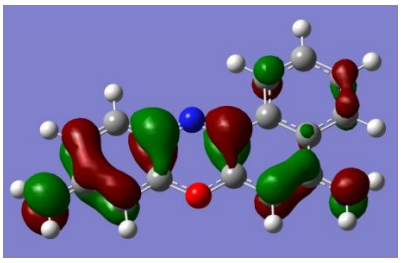	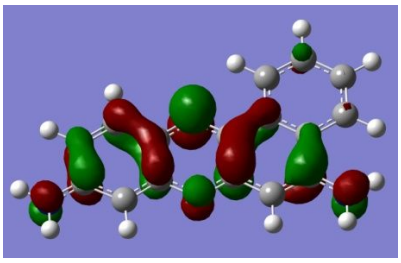
4	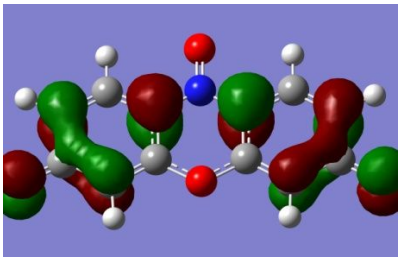	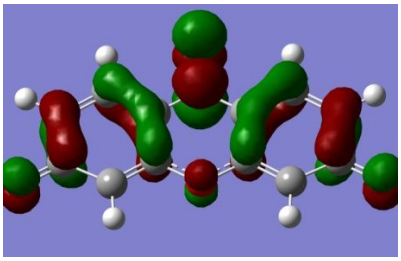
5	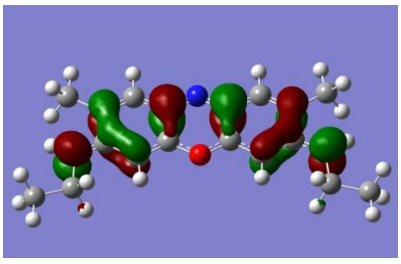	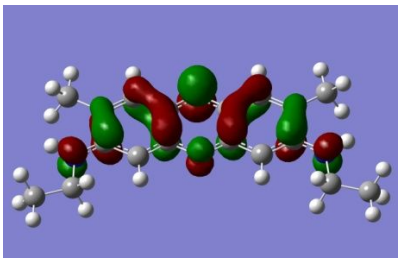
6	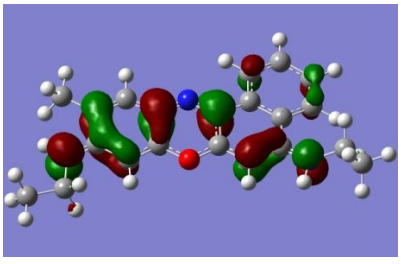	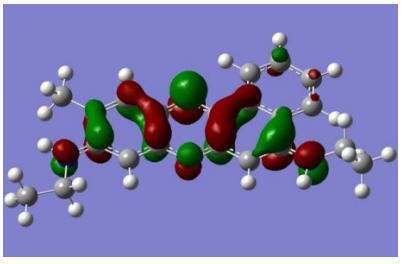

Table 4: Orbital pairs involved in the λ_{max} excitation for each dye.[a] (continued)

7	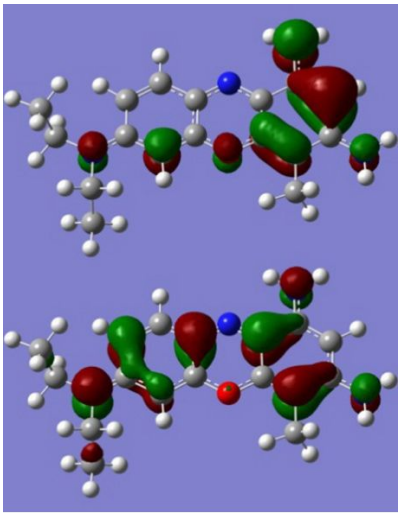	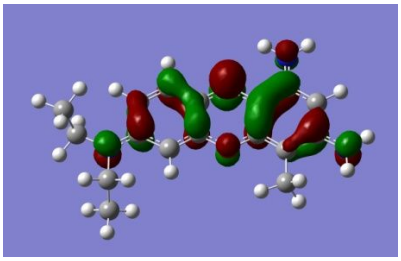
8	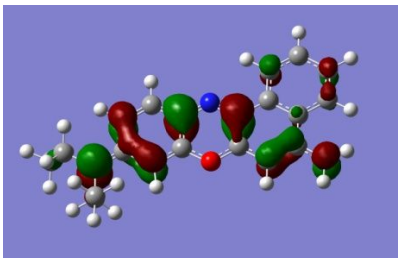	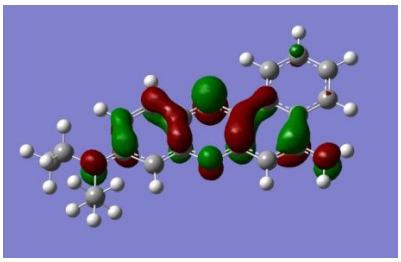
9	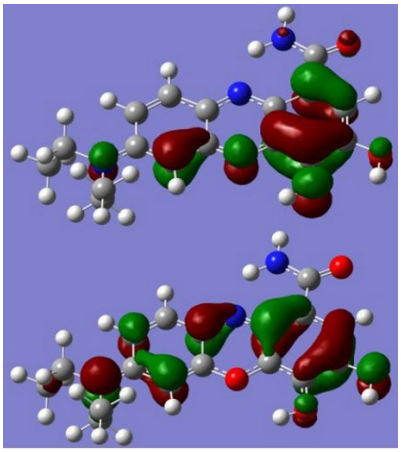	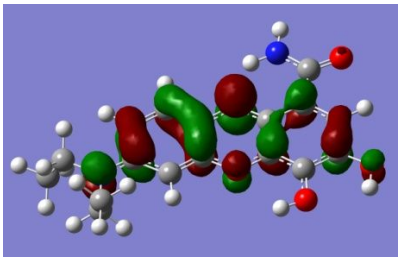
10	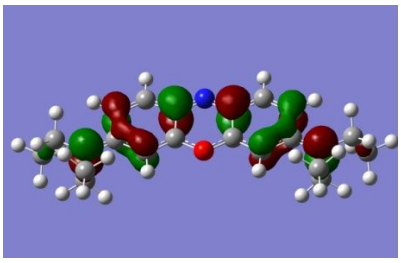	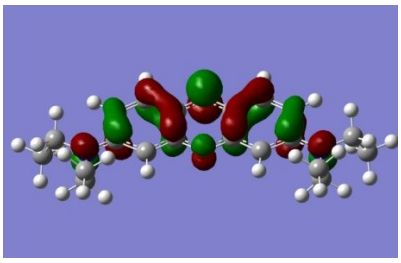

[a]All orbitals are taken from the CPCM/B3LYP/6-311++G(d,p) single point calculation. Isovalue for surface = 0.04.

tion energy in such cases which can be classified as problematic CT states. The calculated orbital overlaps in our series of oxazine dyes are all above the cut-off value, which is consistent with the general accuracy of the calculated excitation energies and suggests that the excitations do not fall into the category of being CT states. However, it is interesting to note that the

overlap diagnostic does not cover all cases where TD-DFT fails to predict accurately the λ_{max}. The most striking example of this is **1**, which has strong orbital overlap and the largest error. However, as the authors of the diagnostic point out, "the test just states that low Λ implies large errors, it does not preclude the possibility that high Λ can also have large errors" [31].

Conclusion

In the current work we have investigated the ability of TD-DFT to predict the absorption spectra of a series of oxazine dyes and the effect of solvent on the accuracy of these predictions. Based on the results of this study, it is clear that for the series of oxazine dyes and accurate prediction of the excitation energy requires the inclusion of solvent. Implicit solvent included via a polarizable continuum approach was found to be sufficient in reproducing the excitation energies accurately in the majority of cases. Moreover, we found that the SMD solvent model gave more reliable results for our systems relative to the CPCM model, as implemented in Gaussian 09.

This study has also illustrated that for the oxazine dyes studied the principal excitation can be classified as an intramolecular CT excitation, based on the transition dipole moments of the excitations. Nonetheless, in all cases the inclusion of solvent reduces the error in the predicted excitation energy to <0.3 eV and in the majority of cases to <0.1 eV.

Experimental

The commercially available oxazine dyes were used as supplied from Aldrich. Depending upon the solubility of the dye, deionized water was used as the solvent for all dyes. Counterions varied as summarized in Table 5. All absorption spectra were obtained using 1 cm cuvettes in a Cary 50 UV–vis spectrophotometer, scanning within the 200–800 nm range. Solutions of 10^{-4} mol dm^{-3} were prepared in a 100 cm^3 volumetric flask, and, if required, subsequently diluted by a factor of ten so as to obtain a maximum absorbance of less than 1.

Table 5: Counterions of each oxazine dye.

Dye	Counterion
Nile blue	SO_4^{2-}
Brilliant cresyl blue	$ZnCl_4^{2-}$
Cresyl violet	$MeCOO^-$
Oxazine 1	ClO_4^-
Oxazine 4	ClO_4^-
Oxazine 170	ClO_4^-
Celestine blue	Cl^-
Darrow red	Cl^-
Resazurin	Na^+
Resorufin	Na^+

Computational methods

All structures were optimized in the gas-phase. For geometry optimizations, the B3LYP [32-37] level of theory with the 6-311++G(d,p) basis set [38,39] was employed and no symmetry constraints were imposed. Time dependent density functional theory [13-17] (TD-DFT) single-point calculations were performed on the optimized structures to obtain the calculated λ_{max} values. The TD-DFT calculations were carried out in both the gas-phase and the aqueous phase. In order to evaluate the effect of the description of the solvent on the calculated spectra, both the conductor-like polarizable continuum model [40,41] (CPCM) and SMD [42] (Truhlar's new solvent model, which is dependent on the full electron density of the solute without partitioning into partial charges) solvent models were employed within the TD-DFT calculations. The ability of different density functionals to accurately describe the excited states of the oxazine dye series was investigated by varying the functional employed in the single point TD-DFT calculations using the B3LYP optimized geometry of the molecule. The series of functionals investigated in this way includes B3LYP, CAM-B3LYP [43] (the coulomb attenuated version of the B3LYP functional which has been shown to provide a better description of CT states) [28], M06 [44], M06-L [45], and M06-2X [44] as the M06 suite of functionals have been shown to perform generally well for a range of molecular properties [46]. The M06-2X functional was included to examine the effect of an increased percentage of HF exchange on the ability of the functional to predict accurately the excitation energies as this has been shown to be beneficial in some cases [19]. All calculations were done within the Gaussian 09 program [47]. Finally, we have also employed the orbital overlap diagnostic of Tozer et al. in order to assess the CT character in the principal excited states [27].

Acknowledgements

TT thanks the Glasgow Centre of Physical Organic Chemistry for funding.

References

1. Mills, A.; Hazafy, D.; Parkinson, J.; Tuttle, T.; Hutchings, M. G. *Dyes Pigm.* **2011,** *88,* 149. doi:10.1016/j.dyepig.2010.05.015
2. Mills, A.; Hazafy, D.; Parkinson, J. A.; Tuttle, T.; Hutchings, M. G. *J. Phys. Chem. A* **2009,** *113,* 9575. doi:10.1021/jp9030927
3. Singh, M. K.; Pal, H.; Bhasikuttan, A. C.; Sapre, A. V. *Photochem. Photobiol.* **1998,** *68,* 32. doi:10.1111/j.1751-1097.1998.tb03249.x
4. Levine, A.; Schubert, M. *J. Am. Chem. Soc.* **1952,** *74,* 91. doi:10.1021/ja01121a021
5. Taylor, K. B. *Stain Technol.* **1961,** *36,* 73. doi:10.3109/10520296109113247

6. Hintersteiner, M.; Enz, A.; Frey, P.; Jaton, A.-L.; Kinzy, W.; Kneuer, R.; Neumann, U.; Rudin, M.; Staufenbiel, M.; Stoeckli, M.; Wiederhold, K.-H.; Gremlich, H.-U. *Nat. Biotechnol.* **2005,** *23,* 577. doi:10.1038/nbt1085
7. Knemeyer, J.-P.; Marmé, N.; Sauer, M. *Anal. Chem.* **2000,** *72,* 3717. doi:10.1021/ac000024o
8. Vogelsang, J.; Cordes, T.; Forthmann, C.; Steinhauer, C.; Tinnefeld, P. *Proc. Natl. Acad. Sci. U. S. A.* **2009,** *106,* 8107. doi:10.1073/pnas.0811875106
9. Deye, J. F.; Berger, T. A.; Anderson, A. G. *Anal. Chem.* **1990,** *62,* 615. doi:10.1021/ac00205a015
10. Ghanadzadeh, A.; Zeini, A.; Kashef, A.; Moghadam, M. *Spectrochim. Acta, Part A: Mol. Biomol. Spectrosc.* **2009,** *73,* 324. doi:10.1016/j.saa.2009.02.029
11. Tajalli, H.; Gilani, A. G.; Zakerhamidi, M. S.; Tajalli, P. *Dyes Pigm.* **2008,** *78,* 15. doi:10.1016/j.dyepig.2007.10.002
12. Tuck, P. O.; Mawhinney, R. C.; Rappon, M. *Phys. Chem. Chem. Phys.* **2009,** *11,* 4471. doi:10.1039/b902528f
13. Bauernschmitt, R.; Ahlrichs, R. *Chem. Phys. Lett.* **1996,** *256,* 454. doi:10.1016/0009-2614(96)00440-X
14. Casida, M. E.; Jamorski, C.; Casida, K. C.; Salahub, D. R. *J. Chem. Phys.* **1998,** *108,* 4439. doi:10.1063/1.475855
15. Marques, M. A. L.; Gross, E. K. U. *Annu. Rev. Phys. Chem.* **2004,** *55,* 427. doi:10.1146/annurev.physchem.55.091602.094449
16. Runge, E.; Gross, E. K. U. *Phys. Rev. Lett.* **1984,** *52,* 997. doi:10.1103/PhysRevLett.52.997
17. Stratmann, R. E.; Scuseria, G. E.; Frisch, M. J. *J. Chem. Phys.* **1998,** *109,* 8218. doi:10.1063/1.477483
18. Tozer, D. J.; Handy, N. C. *J. Chem. Phys.* **1998,** *109,* 10180. doi:10.1063/1.477711
19. Goerigk, L.; Grimme, S. *J. Chem. Phys.* **2010,** *132,* 184103. doi:10.1063/1.3418614
20. Goerigk, L.; Moellmann, J.; Grimme, S. *Phys. Chem. Chem. Phys.* **2009,** *11,* 4611. doi:10.1039/b902315a
21. Jacquemin, D.; Perpète, E. A.; Ciofini, I.; Adamo, C.; Valero, R.; Zhao, Y.; Truhlar, D. G. *J. Chem. Theory Comput.* **2010,** *6,* 2071. doi:10.1021/ct100119e
22. Jacquemin, D.; Wathelet, V.; Perpète, E. A.; Adamo, C. *J. Chem. Theory Comput.* **2009,** *5,* 2420. doi:10.1021/ct900298e
23. Silva, M. R.; Schreiber, M.; Sauer, S. P. A.; Thiel, W. *J. Chem. Phys.* **2008,** *129,* 104103. doi:10.1063/1.2973541
24. Anand, S.; Schlegel, H. B. *Mol. Phys.* **2006,** *104,* 933. doi:10.1080/00268970500418042
25. Dreuw, A.; Fleming, G. R.; Head-Gordon, M. *J. Phys. Chem. B* **2003,** *107,* 6500. doi:10.1021/jp034562r
26. Fabian, J. *Theor. Chem. Acc.* **2001,** *106,* 199. doi:10.1007/s002140100250
27. Peach, M. J. G.; Benfield, P.; Helgaker, T.; Tozer, D. J. *J. Chem. Phys.* **2008,** *128,* 044118. doi:10.1063/1.2831900
28. Peach, M. J. G.; Helgaker, T.; Sałek, P.; Keal, T. W.; Lutnæs, O. B.; Tozer, D. J.; Handy, N. C. *Phys. Chem. Chem. Phys.* **2006,** *8,* 558. doi:10.1039/b511865d
29. Tozer, D. J.; Amos, R. D.; Handy, N. C.; Roos, B. O.; Serrano-Andres, L. *Mol. Phys.* **1999,** *97,* 859. doi:10.1080/00268979909482888
30. Jamorski, C.; Foresman, J. B.; Thilgen, C.; Lüthi, H.-P. *J. Chem. Phys.* **2002,** *116,* 8761. doi:10.1063/1.1465404
31. Peach, M. J. G.; Le Sueur, C. R.; Ruud, K.; Guillaume, M.; Tozer, D. J. *Phys. Chem. Chem. Phys.* **2009,** *11,* 4465. doi:10.1039/b822941d
32. Becke, A. D. *Phys. Rev. A* **1988,** *38,* 3098. doi:10.1103/PhysRevA.38.3098
33. Becke, A. D. *J. Chem. Phys.* **1993,** *98,* 5648. doi:10.1063/1.464913
34. Hertwig, R. H.; Koch, W. *Chem. Phys. Lett.* **1997,** *268,* 345. doi:10.1016/S0009-2614(97)00207-8
35. Lee, C. T.; Yang, W. T.; Parr, R. G. *Phys. Rev. B* **1988,** *37,* 785. doi:10.1103/PhysRevB.37.785
36. Stephens, P. J.; Devlin, F. J.; Chabalowski, C. F.; Frisch, M. J. *J. Phys. Chem.* **1994,** *98,* 11623. doi:10.1021/j100096a001
37. Vosko, S. H.; Wilk, L.; Nusair, M. *Can. J. Phys.* **1980,** *58,* 1200. doi:10.1139/p80-159
38. Hariharan, P. C.; Pople, J. A. *Theor. Chim. Acta* **1973,** *28,* 213. doi:10.1007/BF00533485
39. Krishnan, R.; Binkley, J. S.; Seeger, R.; Pople, J. A. *J. Chem. Phys.* **1980,** *72,* 650. doi:10.1063/1.438955
40. Barone, V.; Cossi, M. *J. Phys. Chem. A* **1998,** *102,* 1995. doi:10.1021/jp9716997
41. Cossi, M.; Rega, N.; Scalmani, G.; Barone, V. *J. Comput. Chem.* **2003,** *24,* 669. doi:10.1002/jcc.10189
42. Marenich, A. V.; Cramer, C. J.; Truhlar, D. G. *J. Phys. Chem. B* **2009,** *113,* 6378. doi:10.1021/jp810292n
43. Yanai, T.; Tew, D. P.; Handy, N. C. *Chem. Phys. Lett.* **2004,** *393,* 51. doi:10.1016/j.cplett.2004.06.011
44. Zhao, Y.; Truhlar, D. G. *Theor. Chem. Acc.* **2008,** *120,* 215. doi:10.1007/s00214-007-0310-x
45. Zhao, Y.; Truhlar, D. G. *J. Chem. Phys.* **2006,** *125,* 194101. doi:10.1063/1.2370993
46. Zhao, Y.; Truhlar, D. G. *Acc. Chem. Res.* **2008,** *41,* 157. doi:10.1021/ar700111a
47. *Gaussian 09,* A.02; Gaussian, Inc.: Wallingford, CT, 2009.

License and Terms

Beilstein Journal of Organic Chemistry

Kinetic evaluation of the solvolysis of isobutyl chloro- and chlorothioformate esters

Malcolm J. D'Souza*[1], Matthew J. McAneny[1], Dennis N. Kevill*[2], Jin Burm Kyong*[3] and Song Hee Choi[3]

Full Research Paper

Open Access

Address:
[1]Department of Chemistry, Wesley College, 120 N. State Street, Dover, DE 19901-3875, USA, [2]Department of Chemistry and Biochemistry, Northern Illinois University, DeKalb, IL 60115-2862, USA and [3]Department of Chemistry & Applied Chemistry, Hanyang University, Ansan-si, Gyeonggi-do, 426-791, Korea

Email:
Malcolm J. D'Souza* - dsouzama@wesley.edu; Dennis N. Kevill* - dkevill@niu.edu; Jin Burm Kyong* - jbkyong@hanyang.ac.kr

* Corresponding author

Keywords:
addition–elimination; Grunwald–Winstein equations; ionization; isobutyl chloroformate; isobutyl chlorothioformate; solvolysis

Beilstein J. Org. Chem. **2011,** *7,* 543–552.
doi:10.3762/bjoc.7.62

Received: 07 February 2011
Accepted: 13 April 2011
Published: 29 April 2011

Guest Editor: J. Murphy

Abstract

The specific rates of solvolysis of isobutyl chloroformate (**1**) are reported at 40.0 °C and those for isobutyl chlorothioformate (**2**) are reported at 25.0 °C, in a variety of pure and binary aqueous organic mixtures with wide ranging nucleophilicity and ionizing power. For **1**, we also report the first-order rate constants determined at different temperatures in pure ethanol (EtOH), methanol (MeOH), 80% EtOH, and in both 97% and 70% 2,2,2-trifluoroethanol (TFE). The enthalpy ($\Delta H^{\neq}$) and entropy ($\Delta S^{\neq}$) of activation values obtained from Arrhenius plots for **1** in these five solvents are reported. The specific rates of solvolysis were analyzed using the extended Grunwald–Winstein equation. Results obtained from correlation analysis using this linear free energy relationship (LFER) reinforce our previous suggestion that side-by-side addition–elimination and ionization mechanisms operate, and the relative importance is dependent on the type of chloro- or chlorothioformate substrate and the solvent.

Introduction

Alkyl chloro- and chlorothioformate esters are frequently used precursors [1-4] in the synthesis of pharmaceutical intermediates. Hence, it is important to comprehend the correlations between their chemical structure, chemical reactivity, and solvent effects. This knowledge can then be applied to the development of compounds that are designed to either stimulate or block other chemicals from interacting with targeted receptors. The effects of solvent variation upon the available specific rates of solvolysis of adamantyl [5,6], methyl [7], ethyl [8], 2,2,2-trichloro-1,1-dimethylethyl [9], *n*-propyl [10], iso-

propyl [11,12], *n*-octyl [13], and neopentyl [14] chloroformate esters, and those of methyl [15], ethyl [8], and isopropyl [16] chlorothioformate esters have been successfully analyzed using the extended [17-19] Grunwald–Winstein equation (Equation 1). In Equation 1, k and k_0 are the specific rates of solvolysis in a given solvent and in the standard solvent (80% ethanol), respectively, l estimates the sensitivity to changes in solvent nucleophilicity (N_T), m represents the sensitivity to changes in the solvent ionizing power Y_{Cl}, and c is a constant (residual) term.

$$\log(k/k_0) = lN_T + mY_{Cl} + c \quad (1)$$

Kevill and Anderson developed N_T scales based on the solvolyses of the *S*-methyldibenzothiophenium ion [20,21] for considerations of solvent nucleophilicity, and Bentley et al. have recommended Y_{Cl} scales [22-25] based on the solvolyses of adamantyl derivatives for estimating the sensitivity to solvent ionizing power.

In reactions where the reaction center is adjacent to a π-system, or in α-haloalkyl aryl compounds that proceed via anchimeric assistance (k_Δ), Kevill and D'Souza proposed the addition of an aromatic ring parameter (hI) term [26-28] to Equation 1 to give Equation 2. In Equation 2, h represents the sensitivity of solvolyses to changes in the aromatic ring parameter I.

$$\log(k/k_0) = lN_T + mY_{Cl} + hI + c \quad (2)$$

Lee [29], Bentley [30] and others [3,31-38], used computational and experimental evidence to show that the chloroformate and chlorothioformate esters always exist in a *syn* conformation where the halogen atom is in a *trans* position with respect to the alkyl group. In Figure 1, the molecular structures for *syn*-isobutyl chloroformate (**1**), *syn*-isobutyl chlorothioformate (**2**), phenyl chloroformate (**3**), phenyl chlorodithioformate (**4**), and isopropyl chloroformate (**5**), and their corresponding 3-D structures **1'**, **2'**, **3'**, **4'** and **5'** are shown in the most stable geometries for RXCXCl (where X = S or O) which exist in a conformation where the C=X is *syn* with respect to R.

In a recent review [17], commemorating the 60th anniversary of the Grunwald–Winstein equation, we previously published reported analyses [5-8,10,11,13,39-49] that were obtained using Equation 1, with examples of several alkyl and aryl chloro-, chlorothio-, chlorothiono-, and dithiochloroformate esters. For these esters, we proposed [17] side-by-side addition–elimination ($A_N + D_N$) and ionization (S_N1) solvolytic mechanisms, with proportions that were dependent on the type of RXCXCl (X = O or S) substrate, solvent nucleophilicity, and the ionizing ability of the solvents studied.

At one extreme when R = Ph in phenyl chloroformate (PhOCOCl, **3**), due to the presence of two electronegative oxygen atoms and the planarity of the phenoxy group (**3'**), compound **3** [17,39,40] was found to solvolyze in all of the 49 solvents studied solely by an addition–elimination ($A_N + D_N$) pathway (Scheme 1) with formation of the tetrahedral intermediate as the rate-determining step. When both oxygens are replaced by the more polarizable sulfur as in phenyl chlorodithioformate (PhSCSCl, **4**) [17,40,45], the mechanism of reaction was found to completely switch over to an ionization (S_N1) pathway (Scheme 2) in all of the pure and binary aqueous organic mixtures studied. This tendency to follow an ionization process in such sulfur-for-oxygen substitutions occurs primarily as a result of the formation of a more favored resonance-stabilized transition-state (Scheme 2) [40,45].

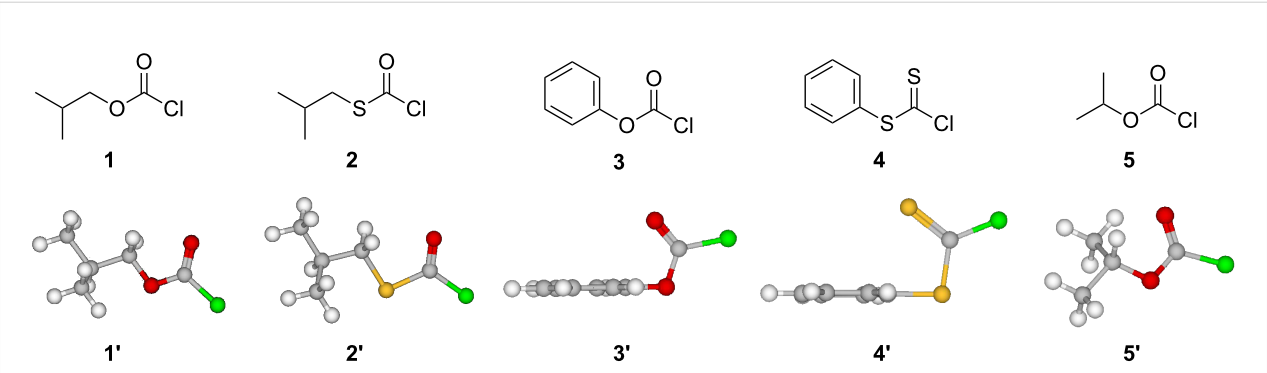

Figure 1: Molecular structures of *syn*-isobutyl chloroformate (**1**), *syn*-isobutyl chlorothioformate (**2**), phenyl chloroformate (**3**), phenyl chlorodithioformate (**4**), and isopropyl chloroformate (**5**). The 3-D images for *syn*-isobutyl chloroformate (**1'**), *syn*-isobutyl chlorothioformate (**2'**), phenyl chloroformate (**3'**), phenyl chlorodithioformate (**4'**), and isopropyl chloroformate (**5'**) are also shown.

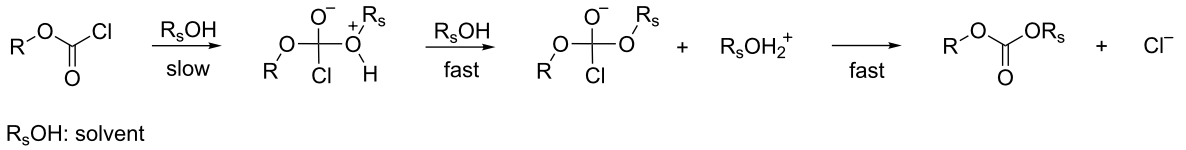

Scheme 1: Stepwise addition–elimination mechanism through a tetrahedral intermediate for solvolysis of chloroformate esters.

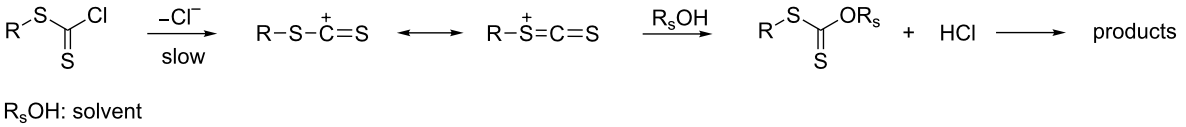

Scheme 2: Unimolecular solvolytic pathway for the dithioformate esters.

We have since recommended [17] that the *l* (1.66) and *m* (0.56) values obtained by using Equation 1 for the solvolyses of **3**, and values of *l* (0.69) and *m* (0.95) obtained for the solvolyses of **4**, be taken as appropriate standards for the bimolecular addition–elimination and unimolecular ionization (without fragmentation) pathways, respectively. The appreciable sensitivity to solvent nucleophilicity (0.69) seen in the ionization–solvolysis of **4**, points to strong rear-side nucleophilic solvation of the developing resonance-stabilized carbocation. Another useful tool for mechanistic studies is the *l*/*m* ratio. We have found [17] that values >2.7 are typical of solvolytic mechanisms proceeding by an addition–elimination pathway with the addition-step being rate-determining (Scheme 1). Ratios between 0.5 and 1.0 signify a unimolecular ionization mechanism with strong rear-side nucleophilic solvation of the developing resonance-stabilized transition-state, while *l*/*m* values <<0.5 are indicative of an ionization–fragmentation process.

Early studies by other groups favored competing S_N1 and S_N2 pathways for the alkyl chloro-, chlorothio-, chlorothiono-, and dithiochloroformates [50-59]. Upon evaluating the rates of hydrolysis in aqueous solvents, Queen [54,55] suggested that with increasing electron donation to the chlorocarbonyl group in alkyl chloro- and chlorothioformates, the positive entropies and low solvent isotope effects pointed to a mechanism involving a unimolecular acyl–halogen bond fission. More recent studies on alkyl and aryl chlorothio-, chlorodithio-, and chlorothionoformate esters favor a stepwise mechanism via a zwitterionic tetrahedral intermediate [60-65].

Isobutyl chloroformate (**1**) and isobutyl chlorothioformate (**2**) have found use as specific precursors in novel synthetic routes for the preparation of peptidyl carbamate and thiocarbamate inhibitors of the enzyme elastase [66]. In Figure 1, the 3-D images of isobutyl chloroformate (**1'**) and isobutyl chlorothioformate (**2'**) are presented. In these figures, it is clear that the isopropyl group is pushed out of the plane due the presence of a carbon atom next to the ether or thioether atom in **1'** and **2'**. This could have an impact on any potential steric or electronic effects, due to presence of the isobutyl group, on the specific rates of reaction.

In this article we present determinations of the specific rates of reaction for isobutyl chloroformate (iBuOCOCl, **1**) at 40.0 °C and of isobutyl chlorothioformate (iBuSCOCl, **2**) at 25.0 °C in a variety of pure and binary aqueous organic solvents with wide ranging nucleophilicity and ionizing power values. Using Equation 1, we analyze in detail values for *l* and *m* obtained for **1** and **2** compared to those of the recommended standards (**3** and **4**) for such substrates, and also in comparison to the *l* and *m* values of other previously reported alkyl chloro- and chlorothioformate esters. We will also seek evidence for any changes in mechanism due to the presence of the isobutyl group. For **1**, we report studies at additional temperatures in five organic solvents to determine the corresponding values of the enthalpy ($\Delta H^{\neq}$) and entropy ($\Delta S^{\neq}$) of activation.

Results and Discussion

The specific rates of solvolysis of **1** at 40.0 °C and of **2** at 25.0 °C, are reported in Table 1. Also presented in Table 1 are the N_T and Y_{Cl} values needed for the multiple correlation analysis of the assembled data using Equation 1.

For **1**, we report in Table 2 the first-order rate constants determined at different temperatures in pure ethanol (EtOH), methanol (MeOH), 80% EtOH, 97% 2,2,2-trifluoroethanol

Table 1: Specific rates of solvolysis (k) of isobutyl chloroformate (**1**) and isobutyl chlorothioformate (**2**), in several binary solvents and literature values for N_T and Y_{Cl}.

Solvent[a]	**1** at 40.0 °C 10^4 k (s^{-1})[b]	**2** at 25.0 °C 10^5 k (s^{-1})[b]	N_T[c]	Y_{Cl}[d]
100% MeOH	3.28 ± 0.04	2.27 ± 0.14	0.17	−1.2
90% MeOH	6.25 ± 0.03	4.63 ± 0.22	−0.01	−0.20
80% MeOH	8.74 ± 0.08	7.57 ± 0.19	−0.06	0.67
70% MeOH	11.6 ± 0.2		−0.40	1.46
100% EtOH	0.848 ± 0.053	1.01 ± 0.09	0.37	−2.50
90% EtOH	1.97 ± 0.05	1.22 ± 0.10	0.16	−0.90
80% EtOH	2.65 ± 0.02	2.99 ± 0.13	0.00	0.00
70% EtOH	3.28 ± 0.02		−0.20	0.78
60% EtOH	4.19 ± 0.05		−0.38	1.38
50% EtOH	5.12 ± 0.05		−0.58	2.02
90% Acetone	0.113 ± 0.027		−0.35	−2.39
80% Acetone	0.316 ± 0.002	0.201 ± 0.015	−0.37	−0.80
70% Acetone	0.652 ± 0.004	1.06 ± 0.09	−0.42	0.17
60% Acetone	1.02 ± 0.02		−0.52	1.00
97% TFE (w/w)	0.0511 ± 0.0007	6.01 ± 0.10	−3.30	2.83
90% TFE (w/w)	0.0690 ± 0.0004	11.7 ± 0.8	−2.55	2.85
70% TFE (w/w)	0.263 ± 0.005	40.8 ± 2.3	−1.98	2.96
50% TFE (w/w)	0.775 ± 0.002		−1.73	3.16
80% T-20% E	0.0289 ± 0.0005	1.47 ± 0.09	−1.76	1.89
60% T-40% E	0.106 ± 0.001	0.688 ± 0.007	−0.94	0.63
50% T-50% E		0.299 ± 0.021	−0.64	0.60
40% T-60% E	0.283 ± 0.008	0.465 ± 0.016	−0.34	−0.48
20% T-80% E	0.561 ± 0.006	0.521 ± 0.027	0.08	−1.42
97% HFIP (w/w)		66.0 ± 2.9	−5.26	5.17
90% HFIP (w/w)		48.2 ± 1.6	−3.84	4.41
70% HFIP (w/w)		78.4 ± 2.0	−2.94	3.83

[a]Substrate concentration of ca. 0.0052 M; binary solvents on a volume–volume basis at 25.0 °C, except for TFE-H_2O and HFIP-H_2O (1,1,1,3,3,3-hexafluoro-2-propanol/water) solvents which are on a weight–weight basis. T-E are TFE-ethanol mixtures. [b]With associated standard deviation. [c]References [20,21]. [d]References [22-25].

(TFE) and 70% TFE. The corresponding enthalpy ($\Delta H^{\neq}$) and entropy ($\Delta S^{\neq}$) of activation values obtained from Arrhenius plots for **1** in these five mixtures are also reported in Table 2.

The l, m, and c values obtained for **1** and **2**, together with the multiple correlation coefficients (R) and the F-test values are reported in Table 3, together with corresponding values from the literature for solvolyses of other chloroformate and chlorothioformate esters.

As can be seen in Table 1, the pseudo first-order rate constants for **1** and **2** gradually increase as the amount of water is increased in the binary aqueous–organic solvents. This observation holds true even in the highly ionizing fluoroalcohols and can be attributed to solute–solvent interactions in the transition-state where both nucleophilicity and ionizing power play an important role. The very negative entropies of activation observed for **1** in the aqueous alcohols are typical for substrates that undergo solvolysis by a bimolecular process. The negative entropies of activation (−28.6 to −30.4 cal mol^{-1} K^{-1}) in EtOH, MeOH and 80% EtOH are similar to those observed for the simplest primary alkyl chloroformate, methyl chloroformate (MeOCOCl) [67], where attack at the acyl carbon in an addition–elimination ($A_N + D_N$) process was indicated as the rate-determining step. In order to evaluate the details of the interactions at the transition-state for **1**, we statistically analyzed (using Equation 1) the rates of reaction using multiple regression analysis. In all 22 solvents we obtained l = 1.11 ± 0.14, m = 0.43 ± 0.08, R = 0.886, F-test = 35, and c = 0.01 ± 0.10. The poor correlation coefficient and rather low F-test value was a strong indication of the possibility of superimposed dual mechanisms occurring within the range of solvent systems studied.

Table 2: Specific rates for solvolysis of isobutyl chloroformate (**1**) at various temperatures and the enthalpies and entropies of activation.

Solvent[a]	Temp. (°C)	10^4 k (s^{-1})	$\Delta H^{\neq}$ (kcal mol^{-1})[b]	$\Delta S^{\neq}$ (cal $mol^{-1}K^{-1}$)[b]
100% MeOH	40.0	3.27 ± 0.05	14.1 ± 0.3	−29.6 ± 0.9
	45.0	4.63 ± 0.04		
	50.0	6.85 ± 0.06		
	55.0	9.54 ± 0.07		
100% EtOH	40.0	0.848 ± 0.005	15.2 ± 0.05	−28.6 ± 0.2
	45.0	1.27 ± 0.01		
	50.0	1.89 ± 0.02		
	55.0	2.71 ± 0.02		
80% EtOH	40.0	2.65 ± 0.02	14.0 ± 0.1	−30.4 ± 0.3
	45.0	3.85 ± 0.05		
	50.0	5.53 ± 0.05		
	55.0	7.732 ± 0.08		
70% TFE	40.0	0.263 ± 0.006	20.6 ± 0.4	−13.8 ± 1.3
	45.0	0.468 ± 0.004		
	50.0	0.775 ± 0.004		
	55.0	1.26 ± 0.01		
97% TFE	40.0	0.0511 ± 0.0007	21.5 ± 0.2	−14.3 ± 0.6
	55.0	0.266 ± 0.003		
	60.0	0.429 ± 0.009		
	65.0	0.704 ± 0.006		

[a]Volume–volume basis at 25.0 °C. [b]With associated standard error.

As mentioned in the introduction, PhOCOCl (**3**) was shown to solvolyze in all of the 49 solvents studied by the addition–elimination process with a rate-determining addition step [39,40]. Using the similarity model concept [68], a plot of log (k/k_0) for iBuOCOCl (**1**) in the 22 solvents studied against log (k/k_0) for PhOCOCl (**3**) is shown in Figure 2. This plot results in a weak correlation with R = 0.913, F-test = 101, slope = 0.62 ± 0.06, and c = −0.08 ± 0.08. It is further observed in Figure 2 that the four aqueous TFE mixtures clearly lie above the line of best fit. Removal of these four points significantly improves the correlation analyses between **1** and **3** with results of R = 0.988, F-test = 659, slope = 0.947 ± 0.04 and c = −0.02 ± 0.03. This indicates that the mechanism of reaction for **1** and **3** in the remaining 18 pure and binary solvents (no aqueous TFE solvents) are identical.

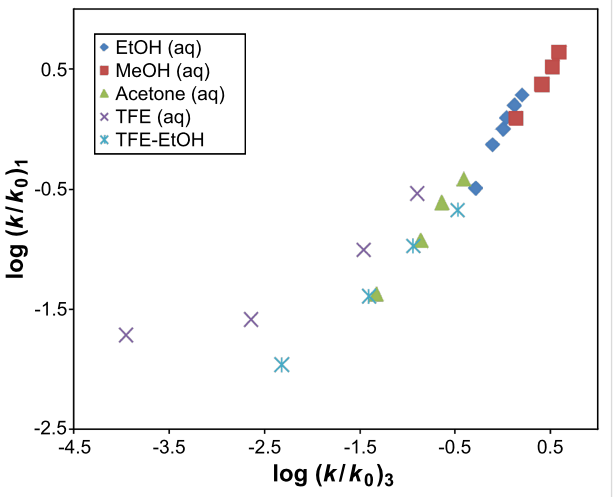

Figure 2: The plot of log (k/k_0) for iBuOCOCl (**1**) against log (k/k_0) for PhOCOCl (**3**).

For **1**, analysis was performed for 18 solvents (no aqueous TFE) using Equation 1, and we obtained (reported in Table 3) l = 1.82 ± 0.15, m = 0.53 ± 0.05, R = 0.957, F-test = 82, and c = 0.18 ± 0.07. Such improvements seen in the correlation coefficient and F-test values for solvolyses of **1** on removal of the four aqueous TFE mixtures indicate that the data is now robust (Figure 3). The l/m ratio of 3.43 falls within the range (shown in Table 3) observed for the other alkyl chloroformate esters in the more nucleophilic solvents.

Previous solvolytic studies with primary alkyl chloroformates such as methyl chloroformate (MeOCOCl) [7], ethyl chloroformate (EtOCOCl) [8], and n-propyl chloroformate (n-PrOCOCl) [10] provided evidence that a bimolecular association–dissocia-

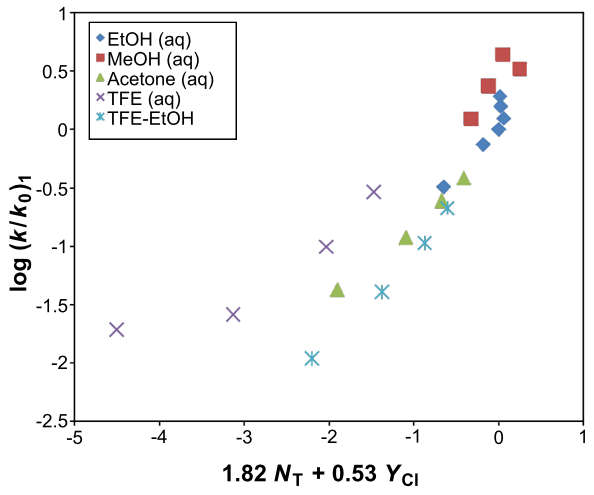

Figure 3: The plot of log (k/k_0) for isobutyl chloroformate (**1**) against 1.82 N_T + 0.53 Y_{Cl} in eighteen pure and binary solvents. The points for the four aqueous TFE values were not included in the correlation. They are added here to show the extent of their deviation.

tion (addition–elimination) process was favored in the more nucleophilic solvents, while an ionization pathway was dominant in the highly ionizing solvents, including the fluoroalcohols with high fluoroalcohol content [7,8,10]. The *l*/*m* ratios for these three substrates in the more nucleophilic solvents (listed in Table 3) are almost identical in value (2.74, 2.84, and 2.79, respectively) and are very similar to the value of 2.94 observed for **3**.

The only two branched alkyl chloroformates that have been studied in detail using a Grunwald–Winstein analysis are isopropyl chloroformate (iPrOCOCl) [11,12] and neopentyl chloroformate (neoPenOCOCl) [14]. The secondary alkyl chloroformate, iPrOCOCl (**5**) [11,12], was found to solvolyze in a majority of the solvents studied by a mechanism similar to that proposed for the tertiary 1- or 2-adamantyl chloroformates [5,6]. This pathway included a unimolecular fragmentation–ionization process with loss of carbon dioxide [5,6,11,12]. For **5**, in nine of the more nucleophilic solvents the *l*/*m* ratio of 3.38 (Table 3) was a typical value for an addition–elimination (association–dissociation) mechanism [12].

We have proposed that neopentyl chloroformate (neoPenOCOCl) [14] solvolyzes in the HFIP rich mixtures with a Wagner–Meerwein 1,2-methyl shift leading to the formation of a tertiary pentyl cation. In 13 of the more nucleophilic solvents the *l*/*m* ratio of 3.67 (Table 3) for neoPenOCOCl was found to be typical of a bimolecular $A_N + D_N$ process [14].

Table 3: Correlation of the specific rates of solvolysis of iBuOCOCl and iBuSCOCl (this study) and several other chloroformate and chlorothioformate esters (values from the literature), using the extended Grunwald–Winstein equation (Equation 1).

Substrate	n[a]	l[b]	m[b]	c[b]	l/m	R[c]	F[d]	Mechanism
PhOCOCl[g]	49	1.66 ± 0.05	0.56 ± 0.03	0.15 ± 0.07	2.95	0.980	568	A–E[e]
2-AdOCOCl[g]	19	0.03 ± 0.07	0.48 ± 0.04	−0.10 ± 0.09	0.06	0.971	130	I[f]
1-AdOCOCl[g]	11	0.08 ± 0.20	0.59 ± 0.05	0.06 ± 0.08	0.14	0.985	133	I[f]
MeOCOCl[g]	19	1.59 ± 0.09	0.58 ± 0.05	0.16 ± 0.07	2.74	0.977	171	A–E
EtOCOCl[g]	28	1.56 ± 0.09	0.55 ± 0.03	0.19 ± 0.24	2.84	0.967	179	A–E
	7	0.69 ± 0.13	0.82 ± 0.16	−2.40 ± 0.27	0.84	0.946	17	S_N1
n-PrOCOCl[g]	22	1.57 ± 0.12	0.56 ± 0.06	0.15 ± 0.08	2.79	0.947	83	A–E
	6	0.40 ± 0.12	0.64 ± 0.13	−2.45 ± 0.27	0.63	0.942	11	S_N1
iPrOCOCl[g]	9	1.35 ± 0.22	0.40 ± 0.05	0.18 ± 0.07	3.38	0.960	35	A–E
	16	0.28 ± 0.04	0.59 ± 0.04	−0.32 ± 0.06	0.47	0.982	176	I[f]
iBuOCOCl[h]	18	1.82 ± 0.15	0.53 ± 0.05	0.18 ± 0.07	3.43	0.957	82	A–E
neoPenOCOCl[g]	13	1.76 ± 0.14	0.48 ± 0.06	0.14 ± 0.08	3.67	0.977	226	A–E
	8	0.36 ± 0.10	0.81 ± 0.14	−2.79 ± 0.33	0.44	0.938	18	S_N1
PhSCSCl[g]	31	0.69 ± 0.05	0.95 ± 0.03	0.18 ± 0.05	0.72	0.987	521	S_N1
MeSCOCl[g]	12	1.48 ± 0.18	0.44 ± 0.06	0.08 ± 0.08	3.36	0.949	40	A–E
	8	0.79 ± 0.06	0.85 ± 0.07	−0.27 ± 0.18	0.93	0.987	95	S_N1
EtSCOCl[g]	19	0.66 ± 0.08	0.93 ± 0.07	−0.16 ± 0.31	0.71	0.961	96	S_N1
iPrSCOCl[g]	19	0.38 ± 0.11	0.72 ± 0.09	−0.28 ± 0.10	0.53	0.961	97	S_N1
iBuSCOCl[i]	15	0.42 ± 0.13	0.73 ± 0.09	−0.37 ± 0.13	0.58	0.961	73	S_N1
PhSCOCl[g]	16	1.74 ± 0.17	0.48 ± 0.07	0.19 ± 0.23	3.63	0.946	55	A–E
	6	0.62 ± 0.08	0.92 ± 0.11	−2.29 ± 0.13	0.67	0.983	44	S_N1

[a]*n* is the number of solvents. [b]With associated standard error. [c]Multiple Correlation Coefficient. [d]*F*-test value. [e]Addition–elimination. [f]Ionization–fragmentation. [g]See text for references giving the source of this data. [h]No 97–50% TFE. [i]No 100%, 90% EtOH and MeOH, no 20% T-80% E.

The higher errors associated with the *l* values, and the higher *l*/*m* ratios observed for iBuOCOCl (**1**), iPrOCOCl (**5**), and neoPenOCOCl, in the more nucleophilic solvents (3.43, 3.38, and 3.67, respectively) when compared to the *l*/*m* ratio obtained for **3** (2.95), is due to a limited range of solvents in which the $A_N + D_N$ mechanism is operative. This view is supported by the multiple regression analysis of **3** in the same 18 solvents used for **1**, where an $A_N + D_N$ mechanism is proposed, which yields $l = 1.96 \pm 0.14$, $m = 0.49 \pm 0.05$, $R = 0.965$, F-test = 101, and $c = 0.23 \pm 0.07$ such that the *l*/*m* ratio for **3** is 4.00.

As shown in Table 1, the nucleophilicity (N_T) values for the four aqueous TFE solvents range from a very low value of −3.30 in 97% TFE (w/w), to −1.73 in 50% TFE (w/w), while the ionizing power values (Y_{Cl}) vary only slightly (2.83–3.16). A plot of log $(k/k_0)_1$ against N_T in these four solvents results in a slope (l) = 0.72 ± 0.22 (0.08 probability that the term is statistically insignificant), R = 0.919, F-test = 11, and $c = 0.51 \pm 0.54$. This l value is within the magnitude seen in aqueous fluoroalcohols for other alkyl chloroformate esters that undergo an ionization mechanism with strong rear-side solvation of the resonance-stabilized intermediate (Table 3).

In Table 4, the methanolysis and ethanolysis specifc rate order is shown to be $k_{MeOCOCl} > k_{EtOCOCl} \approx k_{n\text{-}PrOCOCl} \approx k_{iBuOCOCl} \approx k_{OctOCOCl} > k_{iPrOCOCl}$. As previously pointed out and shown in Figure 1, the presence of an additional carbon in the 3-D image of iBuOCOCl (**1'**), pushs the isopropyl group out of the plane of the ether oxygen. As a result, access to the carbonyl carbon in iBuOCOCl (**1'**) is not hindered by the presence of a branching alkyl group (**1'**, Figure 1), and the observed rate order in EtOH and MeOH (Table 4) suggests that any steric or inductive or hyperconjugative effect due to the presence of the isobutyl group in **1** is, at best, negligible. On the other hand, the inductive effect and competing hyperconjugative release of the isopropyl group in **5** does have an impact on its rates of ethanolysis and methanolysis.

Grunwald–Winstein analysis using Equation 1 for isobutyl chlorothioformate (**2**) in all 20 solvents studied (Table 1) resulted in $l = 0.34 \pm 0.18$, $m = 0.57 \pm 0.13$, $R = 0.873$, F-test = 27, and $c = -0.11 \pm 0.17$. This scatter can be resolved by excluding the rate data for **2** in 100% EtOH, 90% EtOH, 100% MeOH, 90% MeOH, and 20% T-80% E. In the remaining 15 solvents, the correlation coefficient (R) improves significantly to 0.961, the F-test value rises to 73, $l = 0.42 \pm 0.13$, $m = 0.73 \pm 0.09$, and $c = -0.37 \pm 0.13$ (Table 3). A plot of log (k/k_0) for isobutyl chlorothioformate (**2**) against 0.42 N_T + 0.73 Y_{Cl} is shown in Figure 4 with the five deviating points included.

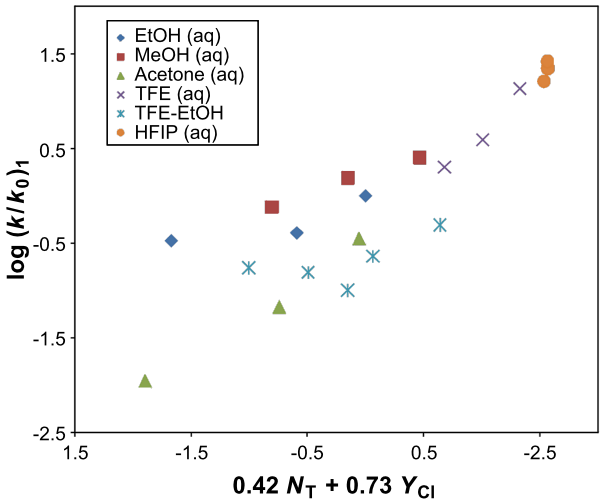

Figure 4: The plot of log (k/k_0) for isobutyl chlorothioformate (**2**) against 0.42 N_T + 0.73 Y_{Cl} in 15 pure and binary solvents. The points for the 100% EtOH, 90% EtOH, 100% MeOH, 90% MeOH, and 20% T-80% E were not included in the correlation. They are added to show the extent of their deviation.

The *l*/*m* ratio of 0.58 obtained for **2** in these 15 solvents is similar in magnitude to the previously observed ratios for methyl- (MeSCOCl) [15], ethyl- (EtSCOCl) [8], isopropyl- (iPrSCOCl) [16], and phenyl- (PhSCOCl) chlorothioformates

Table 4: A comparison of the specific rates of solvolysis of MeOCOCl, EtOCOCl, *n*-PrOCOCl, iPrOCOCl, iBuOCOCl, and *n*-OctOCOCl in common solvents at 25.0 °C.

Solvent	MeOCOCl $10^5\ k\ (s^{-1})$[a]	EtOCOCl $10^5\ k\ (s^{-1})$[b]	*n*-PrOCOCl $10^5\ k\ (s^{-1})$[c]	iPrOCOCl $10^5\ k\ (s^{-1})$[d]	iBuOCOCl $10^5\ k\ (s^{-1})$[e]	*n*-OctOCOCl $10^5\ k\ (s^{-1})$[f]
100% MeOH	15.6	8.24	8.88	4.19	9.89	8.51
100% EtOH	3.51	2.26	2.20	1.09	2.36	2.39
80% EtOH	17.2	7.31	7.92	3.92	8.17	7.37
97% TFE		0.023	0.062	12.3	0.086	
70% TFE	0.857	0.611	0.591	19.7	0.481	

[a]Value obtained using Arrhenius plots with the values reported at different temperatures in reference [67]. [b]Rates are reported at 24.2 °C in reference [8]. [c]Reference [10]. [d]Reference [12]. [e]Extrapolated value obtained using Arrhenius plots with the values reported at different temperatures in Table 2. [f]Reference [13].

[40,46,47] in solvents where an S_N1 mechanism was said to be operative. The range of the *l*/*m* ratios, from 0.53 to 0.93, for these chlorothioformate esters (Table 3) is similar to the *l*/*m* ratio of 0.73 obtained for phenyl dithiochloroformate (**4**), the recommended standard for understanding ionization mechanisms in acyl containing systems.

Hence we suggest that in these 15 solvents, **2** solvolyzes by a dominant unimolecular ionization process with significant rear-side solvation of the developing acylium ion intermediate. For the five solvents (100% EtOH, 90% EtOH, 100% MeOH, 90% MeOH, and 20% T-80% E) whose data points lie above the regression line (Figure 4), a dominant superimposed addition–elimination mechanism ($A_N + D_N$) is proposed. The rate order shown in Table 5, of $k_{MeSCOCl} \approx k_{EtSCOCl} \approx k_{iPrSCOCl} \approx k_{iBuSCOCl}$, is for the methanolysis and ethanolysis of these alkyl chlorothioformate esters at 25.0 °C. In pure methanol and ethanol a dominant association–dissociation (addition–elimination) mechanism, with rate-limiting addition, is believed to be effective in all four substrates. This rate order indicates that the inductive ability of the alkyl thioether group is almost independent of the type of alkyl group present. In Table 5, for solvolysis in the least nucleophilic and most highly ionizing solvent, 97% HFIP (w/w), a rate order of $k_{MeSCOCl} << k_{EtSCOCl} < k_{iBuSCOCl} << k_{iPrSCOCl}$ is observed. This demonstrates that the hyperconjugative release during the formation of the developing resonance-stabilized carbocation intermediate is more efficient for isopropyl chlorothioformate (**5**) when compared to **2**, as the presence of the additional carbon pushes the isopropyl group out of the plane of the thioether atom in **2'** (Figure 1). This opinion is supported by an increase seen in the *l*/*m* ratio in the order of $k_{MeSCOCl} < k_{EtSCOCl} < k_{iBuSCOCl} < k_{iPrSCOCl}$.

As shown from Table 4 and Table 5, the $k_{iBuSCOCl} < k_{iBuOCOCl}$ rate order applies in methanol and ethanol where the addition–elimination mechanism is dominant. This is due to the inductive ability of the isobutoxy group being much greater than that of the corresponding sulfur analog. The observed rate order is completely reversed in 97% TFE (aqueous) to $k_{iBuSCOCl} >> k_{iBuOCOCl}$, where **2** is a 100-fold faster than **1**. In the highly ionizing fluoroalcohols an ionization mechanism (S_N1) is proposed to prevail for both substrates: This rate order signifies that the hyperconjugative release from the sulfur atom in **2** to the developing acylium ion is the dominant factor.

Conclusion

Correlation analysis of the solvolysis of isobutyl chloroformate (**1**) and isobutyl chlorothioformate (**2**) in a variety of pure and binary aqueous organic solvents was successfully analyzed using the extended Grunwald–Winstein equation (Equation 1). In both compounds side-by-side addition–elimination (with a rate-determining addition step) and unimolecular S_N1 type mechanisms are believed to be possible.

In a majority of the solvents studied it is proposed that **1** solvolyzes by a bimolecular addition–elimination ($A_N + D_N$) process due to the inductive ability of the isobutoxy group, whereas in the four aqueous TFE mixtures a predominant unimolecular S_N1 mechanism with rear-side solvation of the developing carbocation is suggested.

For **2**, due to a more proficient hyperconjugative release, a dominant unimolecular ionization (S_N1) mechanism with strong rear-side nucleophilic solvation is proposed for all solvents except 100% EtOH, 90% EtOH, 100% MeOH, 90% MeOH, and 20% T-80% E. In these five solvents an $A_N + D_N$ process is believed to dominate.

Experimental

The isobutyl chloroformate (98%, Sigma-Aldrich) and isobutyl chlorothioformate (96%, Sigma-Aldrich) were used as received. Solvents were purified and the kinetic runs carried out as previ-

Table 5: A comparison of the rates of solvolysis of MeSCOCl, EtSCOCl, iPrSCOCl, and iBuSCOCl, in selected common solvents at 25.0 °C.

Solvent	MeSCOCl $10^5\ k\ (s^{-1})$[a]	EtSCOCl $10^5\ k\ (s^{-1})$[b]	iPrSCOCl $10^5\ k\ (s^{-1})$[c]	iBuSCOCl $10^5\ k\ (s^{-1})$[d]
100% MeOH	2.00	2.15	1.99	2.27
100% EtOH	0.884	0.430	1.21	1.01
80% EtOH	2.44	2.68	13.7	2.99
97% TFE	0.986	5.98	49.8	6.01
90% TFE	1.92	10.2	69.5	11.7
70% TFE	13.9	54.3	212	40.8
97% HFIP	3.21	39.2	376	66.0
90% HFIP	3.48	36.1	437	48.2
70% HFIP	13.9	81.3	659	78.4

[a]Reference [15]. [b]Rates are reported at 24.2 °C in reference [8]. [c]Reference [16]. [d]See Table 1.

ously described [5,39]. A substrate concentration of approximately 0.005 M in a variety of solvents was employed. The specific rates and associated standard deviations, as presented in Table 1, were obtained by averaging all of the values from duplicate runs.

Multiple regression analyses were carried out using the Excel 2007 package from the Microsoft Corporation. The 3-D-views presented in Figure 1, were generated using the KnowItAll® Informatics System, ADME/Tox Edition, from BioRad Laboratories, Philadelphia, PA.

Acknowledgements

The research in the USA was supported by grant number 2 P2O RR016472-010 from the National Center for Research Resources (NCRR), a component of the National Institutes of Health (NIH). This IDeA Network of Biomedical Research Excellence (INBRE) grant to the state of Delaware (DE) was obtained under the leadership of the University of Delaware, and the authors sincerely appreciate their efforts. Matthew J. McAneny completed a part of this research under the direction of Dr. Malcolm J. D'Souza as an undergraduate research assistant in the DE-INBRE sponsored Wesley College Directed Research Program.

References

1. Qiu, Y.-L.; Phan, T.; Liu, T.; Chen, Z.; Or, S. Bicyclic Macrolide Derivatives. U.S. Patent 6,790,835 B1, Sept 14, 2004.
2. Jones, J. *The Chemical Synthesis of Peptides;* Oxford University Press: Oxford, 1991.
3. Kevill, D. N. Chloroformate Esters and Related Compounds. In *The Chemistry of the Functional Groups: The Chemistry of Acyl Halides;* Patai, S., Ed.; Wiley: New York, NY, USA, 1972; pp 381–453.
4. Matzner, M.; Kurkjy, R. P.; Cotter, R. J. *Chem. Rev.* **1964,** *64,* 645–687. doi:10.1021/cr60232a004
5. Kevill, D. N.; Kyong, J. B.; Weitl, F. L. *J. Org. Chem.* **1990,** *55,* 4304–4311. doi:10.1021/jo00301a019
6. Kyong, J. B.; Suk, Y. J.; Kevill, D. N. *J. Org. Chem.* **2003,** *68,* 3425–3432. doi:10.1021/jo0207426
7. Kevill, D. N.; Kim, J. C.; Kyong, J. B. *J. Chem. Res., Synop.* **1999,** 150–151. doi:10.1039/A808929I
8. Kevill, D. N.; D'Souza, M. J. *J. Org. Chem.* **1998,** *63,* 2120–2124. doi:10.1021/jo9714270
9. Koh, H. J.; Kang, S. J.; Kevill, D. N. *Bull. Korean Chem. Soc.* **2010,** *31,* 835–839. doi:10.5012/bkcs.2010.31.04.835
10. Kyong, J. B.; Won, H.; Kevill, D. N. *Int. J. Mol. Sci.* **2005,** *6,* 87–96. doi:10.3390/i6010087
11. Kyong, J. B.; Kim, Y.-G.; Kim, D. K.; Kevill, D. N. *Bull. Korean Chem. Soc.* **2000,** *21,* 662–664.
12. D'Souza, M. J.; Reed, D. N.; Erdman, K. J.; Kevill, D. N. *Int. J. Mol. Sci.* **2009,** *10,* 862–879. doi:10.3390/ijms10030862
13. Kevill, D. N.; D'Souza, M. J. *J. Chem. Soc., Perkin Trans. 2* **2002,** 240–243. doi:10.1039/b109169g
14. D'Souza, M. J.; Carter, S. E.; Kevill, D. N. *Int. J. Mol. Sci.* **2011,** *12,* 1161–1174. doi:10.3390/ijms12021161
15. D'Souza, M. J.; Hailey, S. M.; Kevill, D. N. *Int. J. Mol. Sci.* **2010,** *11,* 2253–2266. doi:10.3390/ijms11052253
16. D'Souza, M. J.; Mahon, B. P.; Kevill, D. N. *Int. J. Mol. Sci.* **2010,** *11,* 2597–2611. doi:10.3390/ijms11072597
17. Kevill, D. N.; D'Souza, M. J. *J. Chem. Res.* **2008,** 61–66. doi:10.3184/030823408X293189
18. Winstein, S.; Grunwald, E.; Jones, H. W. *J. Am. Chem. Soc.* **1951,** *73,* 2700–2707. doi:10.1021/ja01150a078
19. Grunwald, E.; Winstein, S. *J. Am. Chem. Soc.* **1948,** *70,* 846–854. doi:10.1021/ja01182a117
20. Kevill, D. N.; Anderson, S. W. *J. Org. Chem.* **1991,** *56,* 1845–1850. doi:10.1021/jo00005a034
21. Kevill, D. N. Development and Uses of Scales of Solvent Nucleophilicity. In *Advances in Quantitative Structure-Property Relationships;* Charton, M., Ed.; JAI Press: Greenwich, CT, USA, 1996; Vol. 1, pp 81–115.
22. Bentley, T. W.; Carter, G. E. *J. Am. Chem. Soc.* **1982,** *104,* 5741–5747. doi:10.1021/ja00385a031
23. Bentley, T. W.; Llewellyn, G. *Prog. Phys. Org. Chem.* **1990,** *17,* 121–158. doi:10.1002/9780470171967.ch5
24. Kevill, D. N.; D'Souza, M. J. *J. Chem. Res., Synop.* **1993,** 174–175.
25. Kevill, D. N.; Ryu, Z. H. *Int. J. Mol. Sci.* **2006,** *7,* 451–455. doi:10.3390/i7100451
26. Kevill, D. N.; Ismail, N. H.; D'Souza, M. J. *J. Org. Chem.* **1994,** *59,* 6303–6312. doi:10.1021/jo00100a036
27. D'Souza, M. J.; Darrington, A. M.; Kevill, D. N. *Org. Chem. Int.* **2010,** No. 130506. doi:10.1155/2010/130506
28. Kevill, D. N.; D'Souza, M. J. *Curr. Org. Chem.* **2010,** *14,* 1037–1049.
29. Lee, I. *J. Korean Chem. Soc.* **1972,** *16,* 334–340.
30. Bentley, T. W. *J. Org. Chem.* **2008,** *73,* 6251–6257. doi:10.1021/jo800841g
31. Silvia, C. J.; True, N. S.; Bohn, R. K. *J. Phys. Chem.* **1978,** *82,* 483–488. doi:10.1021/j100493a023
32. Shen, Q.; Krisak, R.; Hagen, K. *J. Mol. Struct.* **1995,** *346,* 13–19. doi:10.1016/0022-2860(94)08420-M
33. Gobbato, K. I.; Della Védova, C. O.; Mack, H.-G.; Oberhammer, H. *Inorg. Chem.* **1996,** *35,* 6152–6157. doi:10.1021/ic960536e
34. So, S. P. *J. Mol. Struct. Theochem.* **1998,** *168,* 217–225. doi:10.1016/0166-1280(88)80356-7
35. Ulic, S. E.; Coyanis, E. M.; Romano, R. M.; Della Védova, C. O. *Spectrochim. Acta, Part A* **1998,** *54,* 695–705. doi:10.1016/S1386-1425(98)00002-X
36. Romano, R. M.; Della Védova, C. O.; Downs, A. J.; Parsons, S.; Smith, S. *New J. Chem.* **2003,** *27,* 514–519. doi:10.1039/b209005h
37. Erben, M. F.; Della Védova, C. O.; Boese, R.; Willner, H.; Oberhammer, H. *J. Phys. Chem. A* **2004,** *108,* 699–706. doi:10.1021/jp036966p
38. Silvia, C. J.; True, N. S.; Bohn, R. K. *J. Mol. Struct.* **1979,** *51,* 163–170. doi:10.1016/0022-2860(79)80290-2
39. Kevill, D. N.; D'Souza, M. J. *J. Chem. Soc., Perkin Trans. 2* **1997,** 1721–1724. doi:10.1039/a701140g
40. Kevill, D. N.; Koyoshi, F.; D'Souza, M. J. *Int. J. Mol. Sci.* **2007,** *8,* 346–362. doi:10.3390/i8040346
41. D'Souza, M. J.; Reed, D.; Koyoshi, F.; Kevill, D. N. *Int. J. Mol. Sci.* **2007,** *8,* 788–796. doi:10.3390/i8080788
42. D'Souza, M. J.; Shuman, K. E.; Carter, S. E.; Kevill, D. N. *Int. J. Mol. Sci.* **2008,** *9,* 2231–2242. doi:10.3390/ijms9112231
43. Park, K. H.; Kyong, J. B.; Kevill, D. N. *Bull. Korean Chem. Soc.* **2000,** *21,* 1267–1270.

44. Kyong, J. B.; Park, B.-C.; Kim, C.-B.; Kevill, D. N. *J. Org. Chem.* **2000,** *65,* 8051–8058. doi:10.1021/jo005630y
45. Kevill, D. N.; D'Souza, M. J. *Can. J. Chem.* **1999,** *77,* 1118–1122.
46. Kevill, D. N.; Hailey, S. M.; Mahon, B. P.; D'Souza, M. J. Mechanistic Trends Observed with Sulfur-for-Oxygen Substitution in Chloroformate Esters. *Faraday Discussion 145: Frontiers in Physical Organic Chemistry*; Royal Society of Chemistry: Cardiff, 2009; pp 563 ff.
47. Kevill, D. N.; Bond, M. W.; D'Souza, M. J. *J. Org. Chem.* **1997,** *62,* 7869–7871. doi:10.1021/jo970657b
48. Koo, I. S.; Yang, K.; Kang, D. H.; Park, H. J.; Kang, K.; Lee, I. *Bull. Korean Chem. Soc.* **1999,** *20,* 577–580.
49. An, S. K.; Yang, J. S.; Cho, J. M.; Yang, K.; Lee, J. P.; Bentley, T. W.; Lee, I.; Koo, I. S. *Bull. Korean Chem. Soc.* **2002,** *23,* 1445–1450. doi:10.5012/bkcs.2002.23.10.1445
50. Leimu, R. *Chem. Ber.* **1937,** *70 B,* 1040–1053.
51. Crunden, E. W.; Hudson, R. F. *J. Chem. Soc.* **1961,** 3748–3755. doi:10.1039/jr9610003748
52. Hudson, R. F.; Green, M. *J. Chem. Soc.* **1962,** 1055–1061. doi:10.1039/jr9620001055
53. Green, M.; Hudson, R. F. *J. Chem. Soc.* **1962,** 1076–1080. doi:10.1039/jr9620001076
54. Queen, A. *Can. J. Chem.* **1967,** *45,* 1619–1629.
55. Queen, A.; Nour, T. A.; Paddon-Row, M. N.; Preston, K. *Can. J. Chem.* **1970,** *48,* 522–527.
56. McKinnon, D. M.; Queen, A. *Can. J. Chem.* **1972,** *50,* 1401–1406.
57. La, S.; Koh, K. S.; Lee, I. *J. Korean Chem. Soc.* **1980,** *24,* 1–7.
58. La, S.; Koh, K. S.; Lee, I. *J. Korean Chem. Soc.* **1980,** *24,* 8–14.
59. Orlov, S. I.; Chimishkyan, A. L.; Grabarnik, M. S. *J. Org. Chem. USSR (Engl. Transl.)* **1983,** *19,* 1981–1987.
60. Castro, E. A. *Chem. Rev.* **1999,** *99,* 3505–3524. doi:10.1021/cr990001d
61. Castro, E. A.; Cubillos, M.; Santos, J. G. *J. Org. Chem.* **2004,** *69,* 4802–4807. doi:10.1021/jo049559y
62. Castro, E. A.; Aliaga, M.; Gazitúa, M.; Santos, J. G. *Tetrahedron* **2006,** *62,* 4863–4869. doi:10.1016/j.tet.2006.03.013
63. Castro, E. A. *J. Sulfur Chem.* **2007,** *28,* 401–429. doi:10.1080/17415990701415718
64. Castro, E. A.; Aliaga, M.; Campodonico, P. R.; Leis, J. R.; García-Río, L.; Santos, J. G. *J. Phys. Org. Chem.* **2008,** *21,* 102–107. doi:10.1002/poc.1286
65. Castro, E. A.; Gazitúa, M.; Santos, J. G. *J. Phys. Org. Chem.* **2009,** *22,* 1030–1037. doi:10.1002/poc.1555
66. Digenis, G. A.; Agha, B. J.; Tsuji, K.; Kato, M.; Shinogi, M. *J. Med. Chem.* **1986,** *29,* 1468–1476. doi:10.1021/jm00158a025
67. Seong, M. H.; Choi, S. H.; Lee, Y.-W.; Kyong, J. B.; Kim, D. K.; Kevill, D. N. *Bull. Korean Chem. Soc.* **2009,** *30,* 2408–2412. doi:10.5012/bkcs.2009.30.10.2408
68. Bentley, T. W.; Harris, H. C.; Zoon, H.-R.; Gui, T. L.; Dae, D. S.; Szajda, S. R. *J. Org. Chem.* **2005,** *70,* 8963–8970. doi:10.1021/jo0514366

License and Terms